

TECHNICAL
LIBRARY

ARMY MATERIEL SYSTEMS ANALYSIS ACTIVITY

PROCEEDINGS
SECOND MEETING OF THE COORDINATING GROUP
ON MODERN CONTROL THEORY

PART I

10-11 DECEMBER 1980

ABERDEEN PROVING GROUND, MD 21005

Approved for public release;
distribution unlimited.

19971103 126

DTIC QUALITY INSPECTED 3

U S ARMY MATERIEL SYSTEMS ANALYSIS ACTIVITY
ABERDEEN PROVING GROUND, MARYLAND 21005

DISPOSITION

Destroy this report when no longer needed. Do not return it to the originator.

DISCLAIMER

The findings in this report are not to be construed as an official Department of the Army position unless so specified by other official documentation.

WARNING

Information and data contained in this document are based on the input available at the time of preparation. The results may be subject to change and should not be construed as representing the DARCOM position unless so specified.

TRADE NAMES

The use of trade names in this report does not constitute an official endorsement or approval of the use of such commercial hardware or software. The report may not be cited for purposes of advertisement.

UNCLASSIFIED

SECURITY CLASSIFICATION OF THIS PAGE (When Data Entered)

REPORT DOCUMENTATION PAGE		READ INSTRUCTIONS BEFORE COMPLETING FORM
1. REPORT NUMBER	2. GOVT ACCESSION NO.	3. RECIPIENT'S CATALOG NUMBER
4. TITLE (and Subtitle) Proceedings of the Second Meeting of the Coordinating Group on Modern Control Theory (10-11 Dec 1980) Aberdeen Proving Ground, MD 21005		5. TYPE OF REPORT & PERIOD COVERED Conference
7. AUTHOR(s) H. Cohen (Chairman)		6. PERFORMING ORG. REPORT NUMBER
9. PERFORMING ORGANIZATION NAME AND ADDRESS Director US Army Materiel Systems Analysis Activity Aberdeen Proving Ground, MD 21005		8. CONTRACT OR GRANT NUMBER(s)
11. CONTROLLING OFFICE NAME AND ADDRESS Director US Army Materiel Systems Analysis Activity ATTN: DRXSY-MP, Aberdeen Proving Ground, MD 21005		10. PROGRAM ELEMENT, PROJECT, TASK AREA & WORK UNIT NUMBERS DA Project No. 1R665706M541
14. MONITORING AGENCY NAME & ADDRESS (if different from Controlling Office) Cdr, US Army Materiel Development & Readiness Comd, 5001 Eisenhower Avenue, Alexandria, VA 22333		12. REPORT DATE April 1981
		13. NUMBER OF PAGES 255
		15. SECURITY CLASS. (of this report) UNCLASSIFIED
		15a. DECLASSIFICATION/DOWNGRADING SCHEDULE
16. DISTRIBUTION STATEMENT (of this Report) Approved for public release; distribution unlimited.		
17. DISTRIBUTION STATEMENT (of the abstract entered in Block 20, if different from Report)		
18. SUPPLEMENTARY NOTES		
19. KEY WORDS (Continue on reverse side if necessary and identify by block number) Control Theory, Kalman Filtering, Man-Model, Maneuvering Target, Fire Control, Missile Guidance and Control		
20. ABSTRACT (Continue on reverse side if necessary and identify by block number) Report documents papers presented at second meeting of the coordinating group on modern control theory with emphasis on military systems and recommendations of participants.		

TABLE OF CONTENTS

PART I - UNCLASSIFIED PORTION

	<u>PAGE NO.</u>
AGENDA	i
DISCUSSION AND SUMMARY	v
DOCUMENTATION/ACKNOWLEDGEMENT.	vii
APPLICATION OF MODERN CONTROL THEORY TO THE DESIGN OF A HELICOPTER TURRET CONTROL SYSTEM	1
SUB-OPTIMAL STATE ESTIMATION AS RELATED TO PREDICTIVE FIRE CONTROL SYSTEM DESIGN . .	21
NON-LINEAR LEAST CHI-SQUARE ALGORITHM AN IMPROVEMENT ON NON-LINEAR LEAST SQUARES . .	37
APPLICATIONS OF MODERN CONTROL AND ESTIMATION THEORY TO THE GUIDANCE OF TACTICAL AIR-TO-AIR MISSILES	59
DELAYED-MEASUREMENT OBSERVERS FOR DISCRETE-TIME LINEAR SYSTEMS	71
ON-LINE IDENTIFICATION METHODS	87
A MULTIPLE MODEL LEAD PREDICTION ALGORITHM FOR MANEUVERING TARGET ENGAGEMENT	97
MULTIPLE MODEL ADAPTIVE CONTROL	103
A DESIGN METHODOLOGY FOR ESTIMATORS AND PREDICTION IN FIRE CONTROL SYSTEMS	113
OPTIMAL CONTROL AND ESTIMATION FOR STRAPDOWN SEEKER GUIDANCE OF TACTICAL MISSILES. .	123
PREDICTION OF AIRCRAFT MOTION BASED ON MULTISENSOR INTEGRATION	133
AN ADAPTIVE AUTOMATIC CONTROL SYSTEM FOR REDUCTION OF HELICOPTER VIBRATION	137
ON CONTROL IN PERIODIC SYSTEMS	151
MIRROR TRACK ANTENNA--AN APPLICATION OF TIME-OPTIMAL CONTROL	155
OPTIMAL UTILIZATION OF GRAVITY IN A HOMING MISSILE PROBLEM	177
EVALUATION OF GUNNER STATION CONFIGURATIONS FOR FIRING-ON-THE-MOVE	193
DYNAMIC GUN TUBE BENDING ANALYSIS	213
ANALYSIS OF UNIVERSAL TURRET SUBSYSTEM (UTS) IN THE AH-1S MODERNIZED COBRA	225
DISTRIBUTION LIST	251

SECOND MEETING

COORDINATING GROUP ON MODERN CONTROL THEORY

10-11 DECEMBER 1980

Dickson Hall
APG, MD 21005

AGENDA

SESSION I: Control Theory & Applications I

(Chairman - Herbert E. Cohen - AMSAA)

- 1 WELCOMING STATEMENT - Keith A. Myers
Assistant Director, US Army Materiel Systems Analysis Activity, APG, MD
- 2 Application of Modern Control Theory to the Design of a Helicopter Turret Control System
by N. Coleman and K. Lee
US Army Armament Research and Development Command
Dover, New Jersey 07801
N. K. Loh
School of Engineering
Oakland University
Rochester, Michigan 48063
D. H. Chyung
Division of Information Engineering
University of Iowa
Iowa City, Iowa 52242
- 3 Sub-Optimal State Estimation as Related to Predictive Fire Control System Design
by T. R. Perkins
US Army Materiel Systems Analysis Activity
Aberdeen Proving Ground, MD 21005
- 4 Non-Linear Least Chi-Square Algorithm an Improvement on Non-Linear Least Squares
by R. L. Moore, PhD
US Army Armament Research and Development Command
Dover, NJ 07801
- 5 Applications of Modern Control and Estimation Theory to the Guidance of Tactical Air-to-Air Missiles
by J. R. McClendon, 1Lt, USAF
P. L. Vergez, 1Lt, USAF
Air Force Armament Laboratory
United States Air Force
Eglin Air Force Base, Florida 32542
- 6 Delayed-Measurement Observers for Discrete-Time Linear Systems
by N. K. Loh
School of Engineering
Oakland University
Rochester, Michigan 48063
R. R. Beck
US Army Tank-Automotive Research and Development Command
Tank-Automotive Concepts Laboratory
Warren, Michigan 48090

- 7 On-Line Identification Methods
by Professor N. A. Kheir
 School of Science & Engineering
 The University of Alabama in Huntsville
 Huntsville, AL 35899
 D. W. Sutherlin
 US Army Missile Command
 Redstone Arsenal, AL 35898

SESSION II: Control Theory & Applications II

(Chairman - Toney Perkins - AMSAA)

- 8 Submarine System Identification (Confidential)
by Mr. W. E. Smith
 Mr. T. L. Moran
 David W. Taylor Ship R&D Center
 ATTN: Code 1576
 Bethesda, MD 20084
- 9 A Multiple Model Lead Prediction Algorithm for Maneuvering Target Engagement
by Pak T. Yip
 Control & Stabilization Team
 US Army Armament Research and Development Command
 Dover, New Jersey 07801
- 10 Multiple Model Adaptive Control
by Dr. R. D. Smith
 Mr. J. G. Dixon
 Weapon Synthesis Division
 Naval Weapons Center
 China Lake, CA 93555
- 11 A Design Methodology for Estimators and Prediction in Fire Control Systems
by Dr. James F. Leathrum
 Department of Electrical and Computer Engineering
 Clemson University
 Clemson, SC 29631
- 12 Optimal Control and Estimation for Strapdown Seeker Guidance of Tactical Missiles
by P. L. Vergez, 1LT, USAF
 J. R. McClendon, 1LT, USAF
 Air Force Armament Laboratory
 US Air Force
 Eglin Air Force Base, Florida 32542
- 13 Prediction of Aircraft Motion Based on Multisensor Integration
by E. B. Pate
 Max Mintz
 Department of Systems Engineering
 University of Pennsylvania
 Philadelphia, PA 19104
 Walter Dziwak
 Stanley A. Goodman
 US Army Armament Research and Development Command
 Dover, NJ 07801

SESSION III: Control Theory and Applications III/ (Chairman - Dr. Richard Moore - ARRADCOM)
Weapon System Simulation

- 14 An Adaptive Automatic Control System for Reduction of Helicopter Vibration
by C. E. Hammond
Applied Technology Laboratory
US Army Research and Technology Laboratories
Ft Eustis, VA 23604
- 15 On Control in Periodic Systems
by Leon Kotin
Center for Tactical Computer Systems
US Army Communications Research and Development Command
Fort Monmouth, NJ 07703
- 16 Mirror Track Antenna--An Application of Time-Optimal Control
by Kenneth J. Hintz
Surface Weapons Technology Branch, F14
Naval Surface Weapons Center
Dahlgren, VA 22448
- 17 Optimal Utilization of Gravity in a Homing Missile Problem
by Dr. William C. Kelly
Guidance and Control Directorate
US Army Missile Laboratory
US Army Missile Command
Redstone Arsenal, AL 35898
- 18 Evaluation of Gunner Station Configurations for Firing-on-the-Move
by Richard A. Lee
Tank-Automotive System Laboratory
US Army Tank-Automotive Research and Development Command
Warren, Michigan 48090
William D. West
US Army Armor and Engineer Board
Fort Knox, Kentucky 40121
Monica Glumm
US Army Human Engineering Laboratory
Aberdeen Proving Ground, MD 21005

SESSION IV: Weapon System Simulation (Chairman - Bill Kelly - MICOM)

- 19 (T62 HITPRO) An Engineering Simulation of a Soviet Tank (Confidential)
by Paul Cushman
General Electric Company
John Groff
US Army Materiel Systems Analysis Activity
Aberdeen Proving Ground, MD 21005
- 20 Dynamic Gun Tube Bending Analysis
by Richard A. Lee
1LT Dana S. Charles
Johnthan F. Kring
US Army Tank-Automotive Research and Development Command
Warren, Michigan 48090

- 21 FIRCON Helicopter Fire Control Simulation (Confidential)
 by Gary Drake
 US Army Materiel Systems Analysis Activity
 Aberdeen Proving Ground, MD 21005
- 22 Applications of the FIRCON Attack Helicopter Gun/Fire Control Model (Confidential)
 by Larry E. Cohen
 Air Warfare Division
 US Army Materiel Systems Analysis Activity
 Aberdeen Proving Ground, MD 21005
- 23 Analysis of Universal Turret Subsystem (UTS) in the AH-1S Modernized Cobra
 by T. Hutchings
 US Army Armament Research and Development Command
 Dover, NJ 07801

DISCUSSION AND SUMMARY

The second meeting of the Coordinating Group on Modern Control Theory brought into sharp focus both the wide range of applications of modern control theory to DOD weapon systems and a clear need for the services to investigate the full potential of optimal control and estimation theory in defending against highly maneuvering targets. Overall, there was general agreement that these meetings are constructive and have brought together into a single forum all of the participants actively engaged in modern control theory. The Chairman had raised the issue of inviting outside contractors into these proceedings. Views and opinions expressed by attendees appeared to indicate that this matter was more complex than appeared on the surface. The Chairman subsequently set this issue aside for further study.

It was announced that the 3rd meeting of the Coordinating Group on Modern Control Theory will be hosted by MICOM in mid-October 1981.

**This Page Intentionally
Left Blank**

DOCUMENTATION

These proceedings have been produced in two parts to assure rapid distribution of this document. Part I is unclassified, while Part II is Confidential.

ACKNOWLEDGEMENT

The Chairman would like to take this opportunity to thank Professor Nan K. Loh, Department of Electrical Engineering, Oakland University, Rochester, Michigan for his support in preparing the manuscript for several papers in this proceedings.

APPLICATION OF MODERN CONTROL THEORY TO THE
DESIGN OF A HELICOPTER TURRET CONTROL SYSTEM

N. Coleman and K. Lee
U.S. Army Armament Research and Development Command
DRDAR-SCF-CC
Dover, New Jersey 07801

N. K. Loh
School of Engineering
Oakland University
Rochester, Michigan 48063

D. H. Chyung
Division of Information Engineering
University of Iowa
Iowa City, Iowa 52242

ABSTRACT

The design and hardware implementation of optimal turret controllers for the XM-97 helicopter turret control system are considered. A modular approach of implementation consisting of various compatible plug-in electronic modules is employed. Extensive laboratory experiments in the form of non-firing and firing tests are carried out. The performance of the optimal turret is found to be much more satisfactory as compared with that of the original turret in both the non-firing and firing tests.

1. INTRODUCTION

The design of feedback controls using optimal regulator theory, observer theory and optional filtering theory has received a great deal of attention in the literature over the past two decades and continues today to be an area of active research. It is rather surprising, therefore, especially considering the maturity of the theoretical development to find relatively few applications of these modern design techniques to the actual design of feedback control systems. One of the principal aims of this paper is to bridge the gap between the theory and application and demonstrate the potential of this methodology to the design of precision weapon pointing systems.

Each of the designs presented in this paper, with the exception of the second order torque observer of Section 6, was implemented on a modular analog controller designed specifically to facilitate the hardware realization of state variable compensators. Physical constraints imposed by the analog electronics precluded implementation of many control designs, including the design presented in Section 6, which could perhaps substantially improve pointing accuracy. Discrete time versions of these higher performance control laws are currently being developed for implementation on an 8086 microprocessor-based digital pointing system which will be tested on the XM-97 turret during FY81. Some preliminary results along this line are presented in a separate paper of this proceedings.

The material presented in this paper is organized as follows: Section 2 gives a description of the XM-97 turret control system and the mathematical models used in developing control law designs. An optimal regulator design using a three-state turret model is discussed in Section 3 and a two-state design is developed in Section 4. Section 5 presents a two-state design with a first order Luenberger observer to estimate and suppress torque disturbances due to recoil and base motion. Although there was mismatch between the observer and the disturbance models, this design did provide some improvement over the previous designs. A second order Luenberger observer which is better matched to the actual input disturbance is discussed in Section 6. This design was not implemented, although simulation results are provided for performance comparison. Non-firing and firing test results are presented in Section 7 and 8 for the optimal two-state design. Performance results

of the remaining controller are similar for a given value of the cost functional weighting factor q_{11} , and will not be presented here.

2. SYSTEM DESCRIPTION AND PERFORMANCE OF EXISTING TURRET CONTROL SYSTEM

The XM-97 helicopter gun turret control system shown in Fig. 1 is essentially an inertial load driven by a pulse width modulated split series DC motor through a compliant gear box. The transfer functions of the system are as shown in Fig. 2. The system consists of two controllers: one controller positions the gun turret in azimuth and the other elevates and depresses the gun cradle and the gun. The two controllers are functionally similar and independent. As shown in Fig. 2, the only difference between the two controllers is the gear ratio N which is $N = 620$ for the azimuth channel and $N = 810$ for the elevation channel.

The gun turret control system employs angular position feedback and angular velocity feedback as shown in Fig. 2. With the state variables chosen as shown in Fig. 2, the turret dynamics is described by the following 8-dimensional vector differential equation (for both azimuth and elevation channels),

$$\dot{\underline{x}}(t) = A\underline{x}(t) + Bu(t), \quad \underline{x}(0) = \underline{x}_0, \quad (1)$$

where

$$\begin{aligned} \underline{x}(t) &= [x_1'(t) \ x_2'(t) \ x_3(t) \ x_4(t) \ x_5(t) \ x_6(t) \ x_7(t) \ x_8(t)]^T, \\ x_1'(t) &= \text{gun turret angular position relative to the hull (radians),} \\ x_2'(t) &= \text{motor angular velocity relative to the hull (radians/second),} \\ x_3(t) &= \text{motor torque (foot-pounds),} \\ x_4(t) &= \text{gun turret angular velocity relative to the hull (radians/second),} \\ x_5(t) &= \text{power amplifier output (volts),} \\ x_6(t) &= \text{low level electronics output (volts),} \\ x_7(t) &= \text{geared down shaft angular position relative to the hull (radians),} \\ x_8(t) &= \text{output of tachometer feedback loop (volts),} \\ x_r(t) &= \text{gunner command input (radians),} \\ u(t) &= \text{control input (volts)} = x_r(t) - x_1'(t), \end{aligned}$$

and A and B are, respectively, 8×8 and 8×1 constant matrices as given (see below). The actual and simulated step response in azimuth and elevation are given in Figs. 3(a), 3(b), 3(c) and 3(d).

The XM-97 turret model shown in Fig. 2 is further simplified as shown in Fig. 4. Since x_1' , x_2' and x_3 are accessible for on-line measurement, this model was used to develop an optimal three-state regulator design discussed in the next section.

$$A = \begin{bmatrix} 0 & 0 & 0 & 1 & 0 & 0 & 0 & 0 \\ 2/N \times 10^{10} & 0 & 0 & 4 \times 10^3 & 0 & 0 & -2/N \times 10^{10} & 0 \\ 0 & -9.6p_1 & -5 \times 10^2 & 0 & 5 \times 10^2 p_1 & 0 & 0 & 0 \\ -3.185 \times 10^5 & 0 & 0 & -3.185 \times 10^5 & 0 & 0 & 3.185 \times 10^5 & 0 \\ 0 & 0 & 0 & 0 & -5 \times 10^2 & 3.750 \times 10^3 & 0 & -3.750 \times 10^3 \\ -9.095 \times 10^4 & 0 & 0 & 0 & 0 & 0 & -1.70 \times 10^2 & 0 \\ 0 & 1/N & 0 & 0 & 0 & 0 & 0 & 0 \\ 2/N \times 10^{10} p_2 & 0 & 4 \times 10^3 p_2 & 0 & 0 & 0 & -2/N \times 10^{10} p_2 & -p_3 \end{bmatrix}, \quad B = \begin{bmatrix} 0 \\ 0 \\ 0 \\ 0 \\ 0 \\ 9.095 \times 10^4 \\ 0 \\ 0 \end{bmatrix}$$

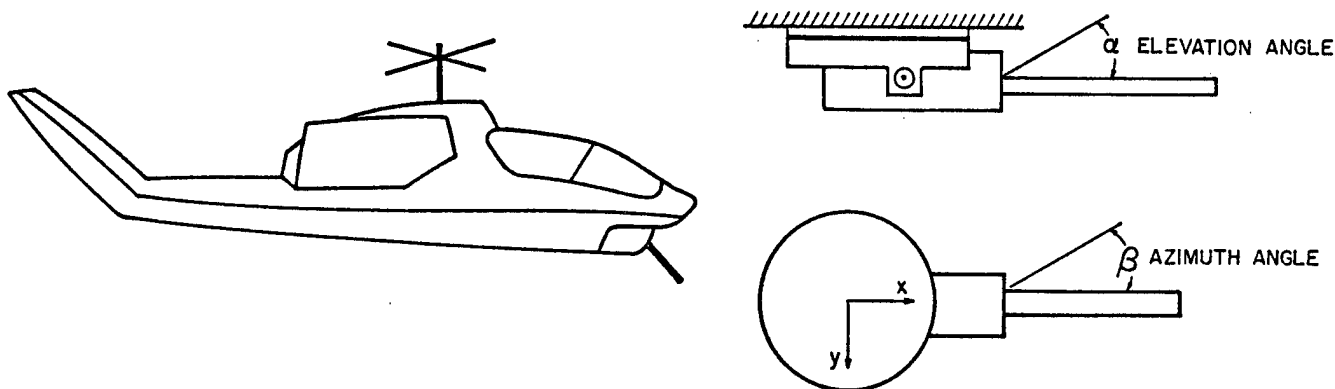
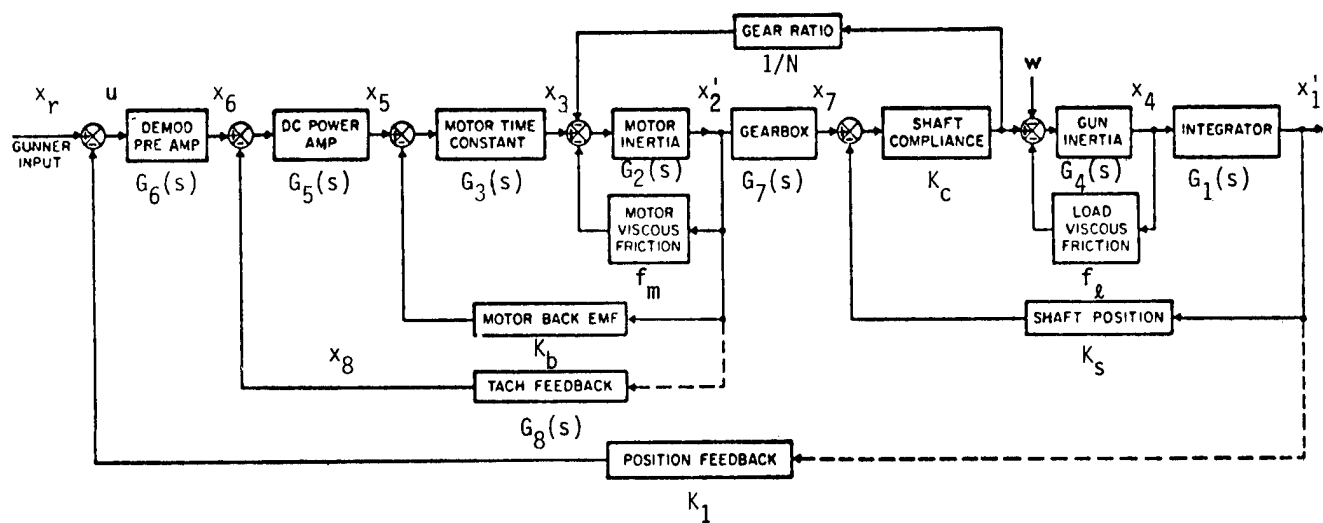


Fig. 1 XM-97 HELICOPTER TURRET



$$\begin{aligned}
 G_1(s) &= \frac{1}{s} & G_2(s) &= \frac{1}{0.00025s} & G_3(s) &= \frac{p_1}{1 + 0.002s} & G_4(s) &= \frac{1}{15.7s} \\
 G_5(s) &= \frac{7.5}{1 + 0.002s} & G_6(s) &= \frac{535}{1 + 0.005885s} & G_7(s) &= \frac{1}{Ns} & G_8(s) &= \frac{p_2 s}{s + p_3} \\
 K_p = K_s &= 1.0 & K_b &= 0.0192 & K_c &= 5000000.0 & f_m &= 0.0 & f_l &= 50.0 \\
 N &= 620 \text{ (AZIMUTH CHANNEL)} & N &= 810 \text{ (ELEVATION CHANNEL)} & p_1 &= 0.02 & p_2 &= .03 \text{ Az.} & p_3 &= 6.6 \text{ Az.} \\
 & & & & & & & .0375 \text{ El.} & & 6 \text{ El.}
 \end{aligned}$$

Fig. 2 EXISTING TURRET CONTROL SYSTEMS - AZIMUTH AND ELEVATION CHANNELS

DEMODULATED AZIMUTH ERROR - FILTER = 100HZ
TEST 012, 040CT79, MOD. TURRET CONTROLLER

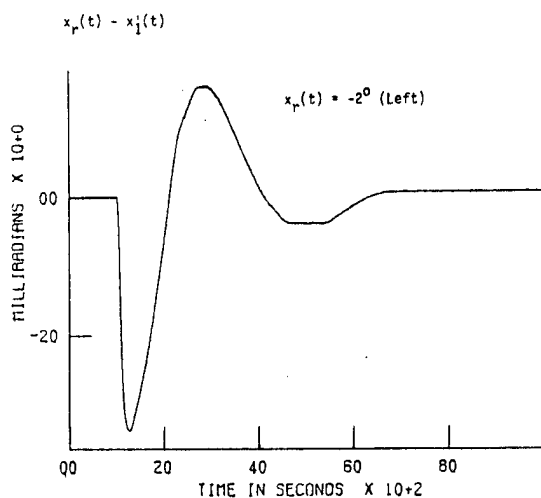


Fig.3(a) ACTUAL STEP RESPONSE
- AZIMUTH CHANNEL

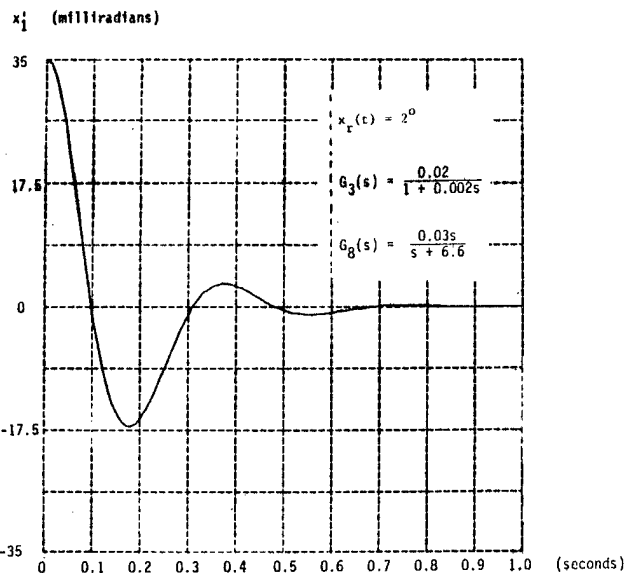


Fig.3(b) SIMULATED STEP RESPONSE
- AZIMUTH CHANNEL

TKK 9A DEMODULATED ELEVATION ERROR - FILTER=100HZ
TEST 131, 10MAR80, MTC / XM197

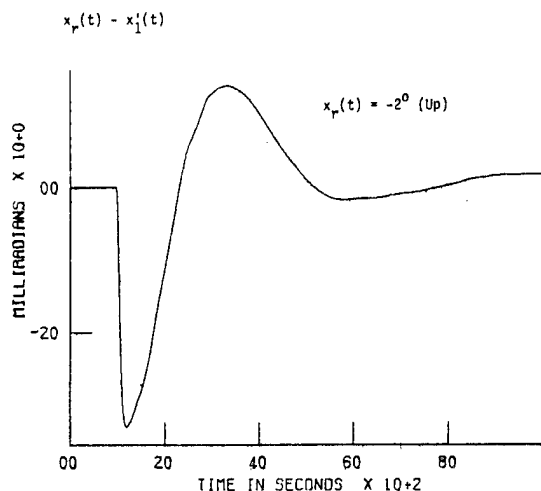


Fig.3(c) ACTUAL STEP RESPONSE
- ELEVATION CHANNEL

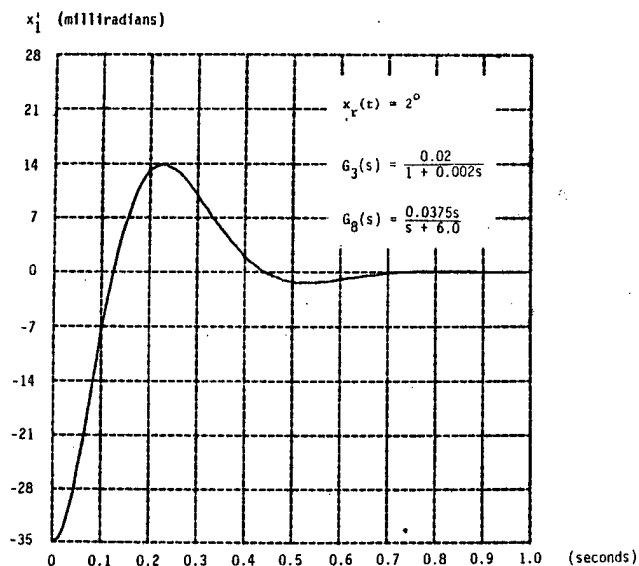


Fig.3(d) SIMULATION STEP RESPONSE
- ELEVATION CHANNEL

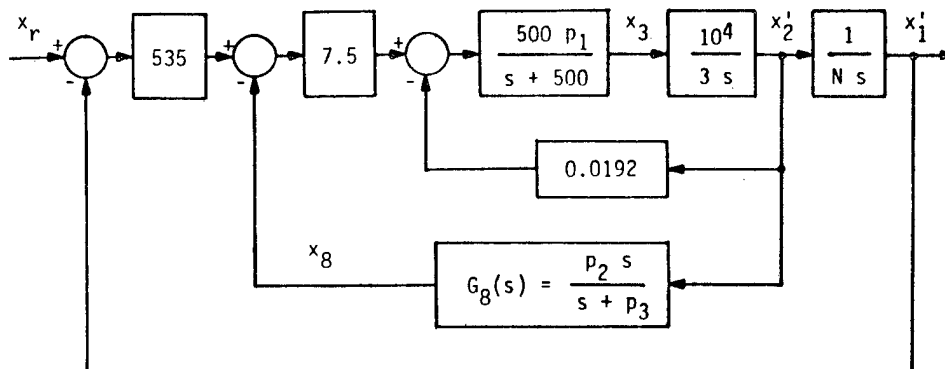


Fig.4 SIMPLIFIED MODEL USED FOR MODEL VERIFICATION

3. THREE-STATE OPTIMAL REGULATOR DESIGN

The open loop turret model required for the three-state optimal regulator design is readily derived from the simplified turret model shown in Fig. 4 by removing the tachometer feedback path containing the filter $G_0(s)$. A block diagram representation of this model is as shown in Fig. 5. It should be noted that sight rate feed-forward is automatically incorporated into x_2 state to ensure good tracking response as well as good stabilization response. The differential equation representation of this open-loop system is given by

$$\dot{\underline{x}}(t) = \underline{A}\underline{x}(t) + \underline{B}u(t) + \underline{F}v_r, \quad \underline{x}(0) = \underline{x}_0, \quad (2)$$

where

$$\underline{x}(t) = [x_1(t) \ x_2(t) \ x_3(t)]^T,$$

$$x_1(t) = x_r(t) - x_1'(t)$$

= error between the position command input $x_r(t)$ and the actual gun angular position $x_1'(t)$ (radians),

$$x_2(t) = Nv_r - x_2'(t)$$

= error between the velocity command v_r and the actual motor angular velocity $x_2'(t)$ (radians/second),

$$x_3(t) = \text{motor torque (foot-pounds) (converted to motor current for feedback),}$$

$$x_r(t) = x_r + v_r t$$

= step-plus-ramp position command input (radians),

$$u(t) = \text{control inputs (volts),}$$

and A , B and F are constant matrices given by

$$A = \begin{bmatrix} 0 & \frac{1}{N} & 0 \\ 0 & 0 & -\frac{1}{3} \times 10^4 \\ 0 & 9.6p_1 & -500 \end{bmatrix},$$

$$B = \begin{bmatrix} 0 \\ 0 \\ 2.00625 \times 10^6 p_1 \end{bmatrix}, \quad F = \begin{bmatrix} 0 \\ 0 \\ -9.6p_1 N \end{bmatrix}.$$

The prime control objective is to drive $\underline{x}(t)$ to the zero state and at the same time minimizing a quadratic performance measure. To achieve the objective, the control $u(t)$ is split into two parts,

$$u(t) = u_{fb}(t) + u_{ff}(t), \quad (3)$$

where $u_{fb}(t)$ is the feedback component responsible for driving $\underline{x}(t)$ to the zero state and $u_{ff}(t)$ is the feedforward component responsible for accommodating the velocity command v_r .

Substituting Eq. (3) into Eq. (2) yields

$$\dot{\underline{x}}(t) = \underline{A}\underline{x}(t) + \underline{B}u_{fb}(t) + \underline{B}u_{ff}(t) + \underline{F}v_r. \quad (4)$$

From Eq. (4), a suitable choice for the feedforward control $u_{ff}(t)$ is given by

$$u_{ff}(t) = \frac{9.6N}{2.00625 \times 10^6} v_r \triangleq k_r v_r. \quad (5)$$

Substituting Eq. (5) into Eq. (4) yields,

$$\dot{\underline{x}}(t) = \underline{A}\underline{x}(t) + \underline{B}u_{fb}(t). \quad (6)$$

Now consider the quadratic performance measure

$$J = \int_0^\infty [q_{11}x_1^2(t) + q_{22}x_2^2(t) + q_{33}x_3^2(t) + ru_{fb}^2(t)]dt \quad (7a)$$

$$= \int_0^\infty [\underline{x}^T(t)Q\underline{x}(t) + ru_{fb}^2(t)]dt, \quad (7b)$$

where $q_{11}>0$, $q_{22}>0$, $q_{33}>0$ and $r>0$ are weighting constants, and $Q = \text{diag}\{q_{11}, q_{22}, q_{33}\}$ with $\text{diag}\{q_{ii}\}$ denoting a diagonal matrix with diagonal elements q_{ii} . The first term in the integrand is chosen to discourage large angular position error $x_1(t) = x_r(t) - x_1'(t)$, the second term to discourage large angular velocity error $x_2(t) = Nv_r - x_2'(t)$, the third term to discourage large current associated with $x_3(t)$ and the last term to discourage large control input voltage $u_{fb}(t)$. The relative importance of the various terms may be adjusted by choosing suitable weighting constants q_{ii} . In general, large q_{ii} indicates the desire to keep $x_i(t)$ small. In our present case, we wish to make the actual gun angular position $x_1(t)$ to follow the commanded angular position as closely as possible. Hence the first term in the integrand will be weighted more heavily by choosing large value for q_{11} .

The optimal control $u_{opt}(t)$ which minimizes J is given by [1] - [2]

$$\begin{aligned} u_{fb}(t) &= u_{opt}(t) \\ &= -r^{-1}B^TK\underline{x}(t) \\ &= k_1x_1(t) + k_2x_2(t) - k_3x_3(t) \\ &= k_1[x_r(t) - x_1'(t)] + k_2[v_r - x_2'(t)] - k_3x_3(t), \end{aligned} \quad (8)$$

where k_1 , k_2 and k_3 are optimal gain constants, and K is the positive-definite solution of the algebraic Riccati equation

$$A^TK + KA + Q - KB^{-1}B^TK = 0. \quad (9)$$

It should be observed that $[A, B]$ and $[A, \sqrt{Q}]$ are completely controllable and completely observable, respectively, i.e.,

$$\begin{aligned} \text{rank } [B \mid AB \mid A^2B] &= 3, \\ \text{rank } [\sqrt{Q}^T \mid A^T\sqrt{Q}^T \mid A^{2T}\sqrt{Q}^T] &= 3, \end{aligned}$$

where $\text{rank } [\cdot]$ denotes the rank of $[\cdot]$ and \sqrt{Q} is the square root* of Q .

Hence Eq. (9) has a positive-definite solution K . From Eqs. (5) and (8), the complete control $u(t)$ is given by

$$u(t) = k_1[x_r(t) - x_1'(t)] + k_2[v_r - x_2'(t)] - k_3x_3(t) - k_rv_r. \quad (10)$$

Substituting Eq. (10) into Eq. (2) yields the optimal turret control system

$$\dot{\underline{x}}(t) = \hat{A}\underline{x}(t), \quad \underline{x}(0) = \underline{x}_0, \quad (11)$$

where

$$\hat{A} = \begin{bmatrix} 0 & \frac{1}{N} & 0 \\ 0 & 0 & -\frac{1}{3} \times 10^4 \\ 2.00625 \times 10^6 p_1 k_1 & 9.6 p_1 - 2.00625 \times 10^6 p_1 k_2 & -500 - 2.00625 \times 10^6 p_1 k_3 \end{bmatrix}.$$

The numerical values of the optimal gains k_1 , k_2 and k_3 for different values of q_{11} with $q_{22} = 0$ and $q_{33} = 0$ and the values of the feedforward gain k_r are given in Table 1. The corresponding eigenvalues of the optimal turret control systems, i.e., the eigenvalues of \hat{A} , are also given in Table 1. The output errors of the three-state regulator designed with $q_{11} = 5$ are as shown in Figs. 6 and 7 for the following step and step-plus ramp inputs, respectively,

$$\begin{aligned} x_r(t) &= 35 \text{ milliradians (mr)}, \\ x_r(t) &= 35 + 17.5t \text{ milliradians (mr)}. \end{aligned}$$

Note that after an initial transient, the turret tracks the input commands perfectly.

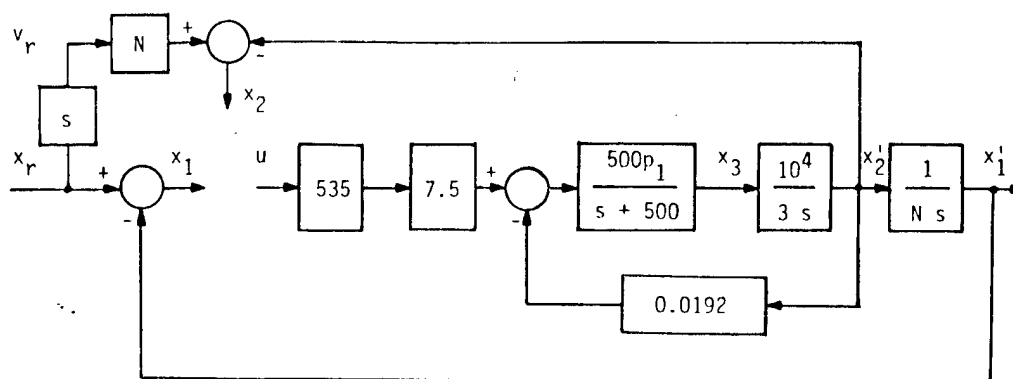


Fig.5 SIMPLIFIED OPEN-LOOP XM-97 HELICOPTER TURRET CONTROL SYSTEM

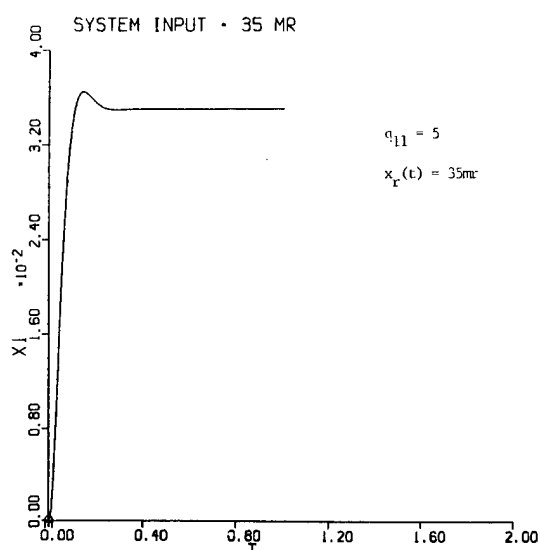


Fig.6 RESPONSE OF $x_1(t)$
-AZIMUTH CHANNEL

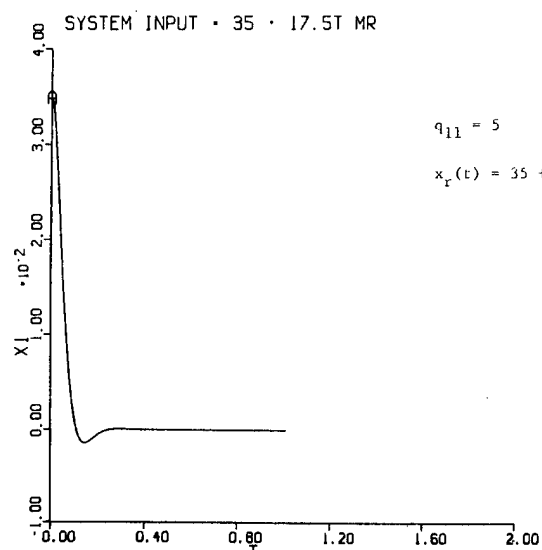


Fig.7 RESPONSE OF $x_1(t)$
-AZIMUTH CHANNEL

TABLE 1. OPTIMAL GAINS AND EIGENVALUES OF XM-97 HELICOPTER TURRET CONTROL SYSTEM

Channel		Azimuth Channel			Elevation Channel		
Choice of q_{11}		5	10	15	5	10	15
Optimal Gains	k_1	2.2361	3.1623	3.8730	2.2361	3.1623	3.8730
	k_2	1.6636×10^{-4}	2.0027×10^{-4}	2.2327×10^{-4}	1.4421×10^{-4}	1.7356×10^{-4}	1.9346×10^{-4}
	k_3	-1.0637×10^{-3}	1.2704×10^{-3}	1.4088×10^{-3}	9.2690×10^{-4}	1.1078×10^{-3}	1.2291×10^{-3}
	k_r	2.9667×10^{-3}	2.9667×10^{-3}	2.9667×10^{-3}	3.8759×10^{-3}	3.8759×10^{-3}	3.8759×10^{-3}
Eigenvalues of \hat{A}	λ_1	-21.980	-26.125	-28.900	-19.236	-22.865	-25.297
		$+j22.004$	$+j26.181$	$+j28.983$	$+j19.244$	$+j22.896$	$+j25.346$
	λ_2	-21.980	-26.125	-28.900	-19.236	-22.865	-25.297
		$-j22.004$	$-j26.181$	$-j28.983$	$-j19.244$	$-j22.896$	$-j25.346$
	λ_3	-498.72	-498.72	-498.73	-498.72	-498.72	-498.72

4. TWO-STATE OPTIMAL REGULATOR DESIGN

The three-state open-loop model in Fig. 5 can be further simplified by removing the high frequency pole at -500 and thus eliminating the motor torque state $x_3(t)$ as shown in Fig. 8. The equations of motion of the two-state-variable model are given by

$$\dot{\underline{x}}(t) = \underline{A}\underline{x}(t) + \underline{B}u(t) + \underline{F}v_r, \quad (12)$$

where $\underline{x}(t) = [x_1(t) \ x_2(t)]^T$, $x_1(t) \triangleq [x_r(t) - x_1'(t)]$, $x_2(t) \triangleq [Nv_r - x_2'(t)]$ are as defined in Eq. (2), and

$$\underline{A} = \begin{bmatrix} 0 & 1/N \\ 0 & -1.28 \end{bmatrix}, \quad \underline{B} = \begin{bmatrix} 0 \\ -2.675 \times 10^5 \end{bmatrix}, \quad \underline{F} = \begin{bmatrix} 0 \\ 1.28N \end{bmatrix}.$$

As before, the control is split into two parts given by

$$u(t) = u_{fb}(t) + u_{ff}(t). \quad (13)$$

Using Eqs. (12) and (13), the feedforward component $u_{ff}(t)$ is determined as

$$u_{ff}(t) = \frac{1.28N}{2.65 \times 10^5} v_r \triangleq k_r v_r. \quad (14)$$

Substituting Eqs. (13) and (14) into (12) yields

$$\dot{\underline{x}}(t) = \underline{A}\underline{x}(t) + \underline{B}u_{fb}(t). \quad (15)$$

Consider the performance measure

$$J = \int_0^\infty [q_{11}x_1^2(t) + ru^2(t)]dt, \quad (16)$$

where $q_{11} > 0$ and $r > 0$ are weighting constants.

The optimal control which minimizes J is given by

$$\begin{aligned} u_{fb}(t) &= u_{opt}(t) \\ &= -r^{-1} \underline{B}^T \underline{K} \underline{x}(t) \\ &= k_1 x_1(t) + k_2 x_2(t) \\ &= k_1 [x_r(t) - x_1'(t)] + k_2 [Nv_r - x_2'(t)], \end{aligned} \quad (17)$$

where k_1 and k_2 are optimal gains and \underline{K} is the positive definite solution of the algebraic Riccati equation

$$\underline{A}^T \underline{K} + \underline{K} \underline{A} + \underline{Q} - \underline{K} \underline{B} r^{-1} \underline{B}^T \underline{K} = 0 \quad (18)$$

with

$$\underline{Q} = \begin{bmatrix} q_{11} & 0 \\ 0 & 0 \end{bmatrix}.$$

Substituting Eq. (17) into Eq. (15) yields the optimal turret

$$\dot{\underline{x}}(t) = \hat{\underline{A}}\underline{x}(t), \quad \underline{x}(0) = \underline{x}_0, \quad (19)$$

where

$$\hat{\underline{A}} = \begin{bmatrix} 0 & 1/N \\ -2.675 \times 10^5 k_1 & -1.28 - 2.675 \times 10^5 k_2 \end{bmatrix}.$$

The numerical values of the optimal gains k_1 and k_2 for different values of q_{11} together with the value of the feedforward gain k_r and the corresponding eigenvalues of \hat{A} are given in Table 2. The output error responses of the two-state regulator similar to those of Figs. 6 and 7 have been obtained but will not be shown here.

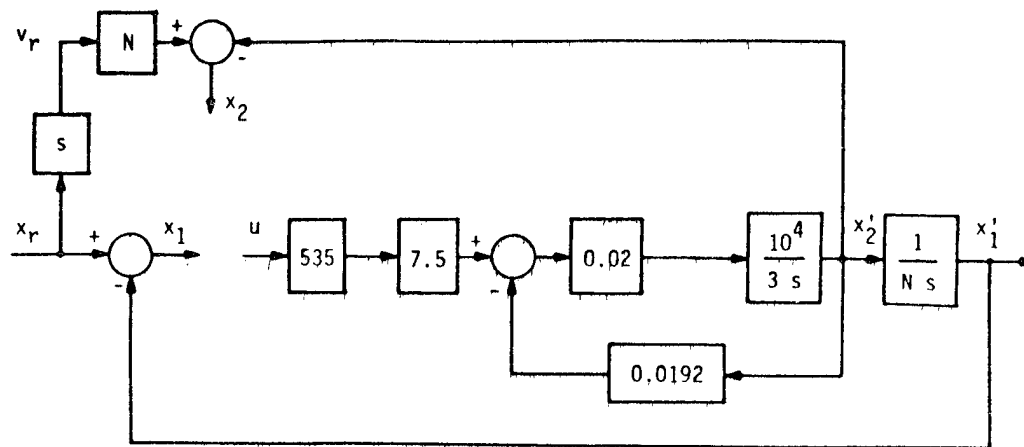


Fig.8 SIMPLIFIED OPEN-LOOP XM-97 HELICOPTER TURRET CONTROL SYSTEM
(TWO-STATE-VARIABLE SYSTEM)

TABLE 2. OPTIMAL GAINS AND EIGENVALUES OF XM-97 HELICOPTER TURRET CONTROL SYSTEM
(TWO-STATE-VARIABLE MODEL)

Channel	Azimuth Channel			Elevation Channel		
q_{11}	5	10	15	5	10	15
Optimal						
Gains k_1	2.2361	3.1623	3.8730	2.2361	3.1623	3.8730
k_2	1.5949×10^{-4}	1.9055×10^{-4}	2.1138×10^{-4}	1.3896×10^{-4}	1.6613×10^{-4}	1.8435×10^{-4}
k_r	2.9667×10^{-3}	2.9667×10^{-3}	2.9667×10^{-3}	3.8759×10^{-3}	3.8759×10^{-3}	3.8759×10^{-3}
Eigenvalues of \hat{A}	-21.972 $\pm j21.954$	-26.126 $\pm j26.111$	-28.912 $\pm j28.898$	-19.226 $\pm j19.205$	-22.860 $\pm j22.842$	-25.297 $\pm j25.281$

5. TWO-STATE OPTIMAL REGULATOR WITH DISTURBANCE ACCOMMODATION USING FIRST-ORDER TORQUE OBSERVER

One of the advantages of applying modern control theory to the design of feedback compensators is that external disturbances may be explicitly modeled and compensated in the control law design. This approach generally requires some type of observer or filter to estimate the disturbance input states and its success depends, to a large extent, on how well the model used in the observer design matches the actual disturbance inputs. The first-order torque observer discussed in this section is

based on a step input model of the disturbance and was implemented and tested on the XM-97 turret to obtain a better understanding and insight into the performance of turret control system and the observer. As the simulation results in Figs. 11, 12, and 13 show this design provides some improvement in low frequency disturbance suppression but provides little or no improvement against higher frequency disturbances. However, actual firing tests showed that the first-order torque observer did provide performance improvement in terms of projectile dispersion (see Fig. 22 in Section 8). The discussion in Section 6 will show in a fairly dramatic way that the torque observer does significantly improve pointing accuracy when the observer model more closely matches the actual disturbances.

The block diagram for the open-loop turret with disturbance input given in Fig. 9 and the corresponding equations of motion are given by

$$\dot{\underline{x}}(t) = A\underline{x}(t) + Bu(t) + Fv_r + Gw(t) \quad (20a)$$

$$y(t) = H\underline{x}(t), \quad (20b)$$

where $\underline{x}(t) = [x_1(t) \ x_2(t)]^T$, $x_1(t) \triangleq [x_r(t) - x_1^i(t)]$, $x_2(t) \triangleq [Nv_r - x_2^i(t)]$ are as defined in Eq. (2), $y(t) = [y_1(t) \ y_2(t)]^T$ is the observed vector, $w(t)$ is the disturbance torque, and A , B , F , G and H are given by

$$A = \begin{bmatrix} 1 & 1/N \\ 0 & -1.28 \end{bmatrix} \triangleq \begin{bmatrix} 0 & a_{12} \\ 0 & -a_{22} \end{bmatrix}, \quad B = \begin{bmatrix} 0 \\ -2.675 \times 10^5 \end{bmatrix} \triangleq \begin{bmatrix} 0 \\ -b \end{bmatrix}$$

$$F = \begin{bmatrix} 0 \\ 1.28N \end{bmatrix} \triangleq \begin{bmatrix} 0 \\ f \end{bmatrix}, \quad G = \begin{bmatrix} 0 \\ -10^4/3N \end{bmatrix} \triangleq \begin{bmatrix} 0 \\ -g \end{bmatrix}, \quad H = \begin{bmatrix} 1 & 0 \\ 0 & 1 \end{bmatrix}.$$

The control objective is to drive $\underline{x}(t)$ to the zero state in the presence of the disturbance torque $w(t)$, and in the same time minimizing a quadratic performance measure. To achieve the control objective, the control $u(t)$ is split into three parts as

$$u(t) = u_{fb}(t) + u_{ff}(t) + u_w(t), \quad (21)$$

where $u_{fb}(t)$ is the feedback component responsible for driving $\underline{x}(t)$ to the zero state, $u_{ff}(t)$ is the feedforward component responsible for accommodating the velocity command v_r , and $u_w(t)$ is the feedforward component responsible for accommodating the disturbance torque $w(t)$. It can easily be shown that $u_{ff}(t)$ and $u_w(t)$ are given by, respectively

$$u_{ff}(t) = \frac{1.28N}{2.675 \times 10^5} v_r \triangleq k_r v_r, \quad (22)$$

$$u_w(t) = -\frac{10^4}{3N \times 2.675 \times 10^5} w(t) \triangleq -k_w w(t). \quad (23)$$

Substituting Eqs. (21), (22), (23) into Eq. (20) yields

$$\dot{\underline{x}}(t) = A\underline{x}(t) + Bu_{fb}(t). \quad (24)$$

Consider the performance measure

$$J = \int_0^\infty [q_{11}x_1^2(t) + ru_{fb}^2(t)]dt, \quad (25)$$

where $q_{11} > 0$ and $r > 0$ are weighting constants.

The optimal control which minimizes J is given by Eq. (17), i.e.,

$$\begin{aligned}
u_{fb}(t) &= u_{opt}(t) \\
&= k_1 x_1(t) + k_2 x_2(t) \\
&= k_1 [x_r(t) - x_1'(t)] + k_2 [Nv_r - x_2'(t)] .
\end{aligned} \tag{26}$$

The numerical values of the optimal gains k_1 and k_2 for different values of q_{11} together with the values of feedforward gains k_r and k_w are given in Table 3. Note that k_1 , k_2 and k_r are the same as in Table 2 but are repeated in Table 3 for convenience and completeness.

TABLE 3 OPTIMAL GAINS FOR XM-97 HELICOPTER TURRET CONTROL SYSTEM

Azimuth Channel, N=620				Elevation Channel, N=810		
q_{11}	5	10	15	5	10	15
k_2	2.236	3.162	3.873	2.236	3.162	3.873
k_1	1.595×10^{-4}	1.906×10^{-4}	2.114×10^{-4}	1.390×10^{-4}	1.661×10^{-4}	1.843×10^{-4}
k_r	2.967×10^{-3}	2.767×10^{-3}	2.967×10^{-3}	3.876×10^{-3}	3.876×10^{-3}	3.876×10^{-3}
k_w	2.010×10^{-5}	2.010×10^{-5}	2.010×10^{-5}	1.538×10^{-5}	1.538×10^{-5}	1.538×10^{-5}

From Eqs. (21), (22), (23) and (26), the complete control $u(t)$ is given by

$$u(t) = k_1 x_1(t) + k_2 x_2(t) + k_r v_r(t) - k_w w(t) . \tag{27}$$

Since the disturbance $w(t)$ is not known, the control $u(t)$ can be implemented as

$$u(t) = k_1 x_1(t) + k_2 x_2(t) + k_r v_r - k_w \hat{w}(t) , \tag{28}$$

where $\hat{w}(t)$ is an estimate of $w(t)$.

The estimate $\hat{w}(t)$ of $w(t)$ considered in this section will be generated by a Luenberger observer [3] - [4]. For simplicity, the disturbance $w(t)$ will be approximated by a random step function described by

$$\dot{w}(t) = \sigma(t), \quad w(0) = w_0, \tag{29}$$

where $\sigma(t)$ is an unknown sequence of Dirac impulses included to take into account of the random jump in values of $w(t)$ [5] - [6].

Augmenting Eq. (29) to Eq. (20) yields

$$\begin{aligned}
\begin{bmatrix} \dot{x}(t) \\ \text{---} \\ \dot{w}(t) \end{bmatrix} &= \begin{bmatrix} A & G \\ \text{---} & \text{---} \\ 0 & 0 \end{bmatrix} \begin{bmatrix} x(t) \\ \text{---} \\ w(t) \end{bmatrix} + \begin{bmatrix} B \\ \text{---} \\ 0 \end{bmatrix} u(t) + \begin{bmatrix} F \\ \text{---} \\ 0 \end{bmatrix} v_r + \begin{bmatrix} 0 \\ \text{---} \\ 1 \end{bmatrix} \sigma(t) \\
&\stackrel{\Delta}{=} \tilde{A} \tilde{x}(t) + \tilde{B} u(t) + \tilde{F} v_r(t) + \tilde{G} \sigma(t) ,
\end{aligned} \tag{30a}$$

$$y(t) = [I_2 \mid 0] \begin{bmatrix} x(t) \\ \text{---} \\ w(t) \end{bmatrix} \stackrel{\Delta}{=} \tilde{H} \tilde{x}(t) , \tag{30b}$$

where the various vectors and matrices are as defined. Since the matrix pair $[\tilde{A}, \tilde{H}]$ is completely observable, i.e.,

$$\text{rank} \begin{bmatrix} \tilde{H}^T & \tilde{A}^T \tilde{H}^T & \tilde{A}^{2T} \tilde{H}^T \end{bmatrix}$$

$$= \text{rank} \begin{bmatrix} 1 & 0 & 0 & 0 \\ 0 & 1 & 1/N & -1.28 \\ 0 & 0 & 0 & -10^4/3N \end{bmatrix} \begin{bmatrix} \tilde{A}^{2T} & \tilde{H}^T \end{bmatrix} = 3 ,$$

the unknown disturbance $w(t)$ can be estimated by a reduced-order Luenberger observer.

A reduced-order Luenberger observer for generating $w(t)$ of $\hat{w}(t)$ is given by [7].

$$\hat{w}(t) = p(t) + Lx(t) , \quad (31a)$$

$$\dot{p}(t) = -LGp(t) - Lbu'(t) - (LA + LGL) x(t) , \quad (31b)$$

where

$$L = [\ell_{11} \ \ell_{12}] , \quad (31c)$$

$$u'(t) = k_1 x(t) + k_2 x_2(t) - k_w \hat{w}(t) . \quad (31d)$$

The elements ℓ_{11} and ℓ_{12} of the gain matrix L are to be chosen such that the observer is asymptotically stable. Note that only ℓ_{12} affects the stability of the observer. In component form, Eq. (31) may be expressed as

$$\hat{w}(t) = p(t) + \ell_{11}x_1(t) + \ell_{12}x_2(t) , \quad (32a)$$

$$\begin{aligned} \dot{p}(t) &= \ell_{12}gp(t) + \ell_{12}bu'(t) + \ell_{11}\ell_{12}gx_1(t) + \\ &\quad (\ell_{12}a_{22} - \ell_{11}a_{12} + \ell_{12}^2g)x_2(t) \\ &= \frac{10^4}{3N} \ell_{12}p(t) + 2.675 \times 10^5 \ell_{12}u'(t) + \frac{10^4}{3N} \ell_{11}\ell_{12}x_1(t) \\ &\quad + (-\ell_{11}/N + 1.28\ell_{12} + \frac{10^4}{3N} \ell_{12}^2)x_2(t) . \end{aligned} \quad (32b)$$

A block diagram for implementing Eq. (32) is as given in Fig. 10.

In the actual implementation of the reduced-order Luenberger observer, the following values will be chosen for the gain matrix L and for the weighting constant q_{11}

$$L = [0 \ -4] ,$$

$$q_{11} = 5 .$$

With the above choice of L and q_{11} , Eq. (32) reduces to, with $N = 620$,

$$\hat{w}(t) = p(t) + 4x_2(t) , \quad (33a)$$

$$\begin{aligned} \dot{p}(t) &= -21.5p(t) + 1.07 \times 10^6 [u_{fb}(t) + u_w(t)] + \\ &\quad 80.9x_2(t) . \end{aligned} \quad (33b)$$

The simulated responses of $x_1(t)$ for the azimuth channel and for different values of frequency of the disturbance $w(t)$ are as shown in Figs. 11, 12 and 13. We remark that the choice of $\ell_{11} = 0$ in the observer gain matrix simplifies implementation but with a resultant loss of information provided by the state variable $x_1(t)$. This results in some degradation during the observer transient but is relatively insignificant.

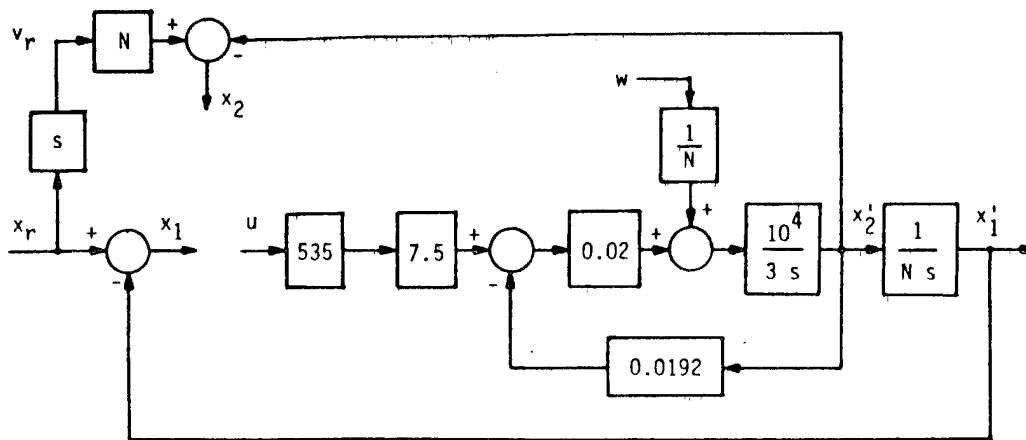


Fig.9 SIMPLIFIED OPEN-LOOP XM-97 HELICOPTER TURRET CONTROL SYSTEM WITH DISTURBANCE INPUT (TWO-STATE-VARIABLE MODEL)

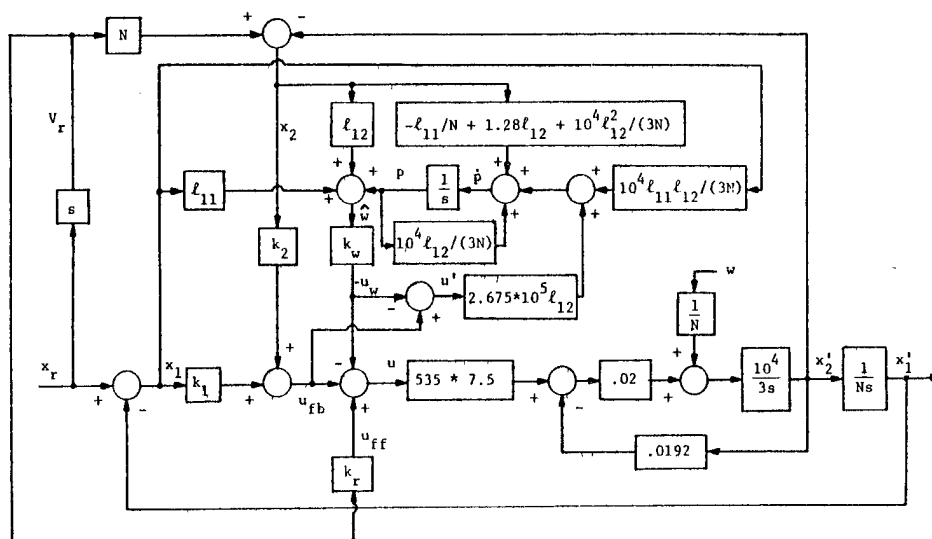


Fig.10 OPTIMAL XM-97 TURRET WITH FIRST-ORDER LUENBERGER OBSERVER

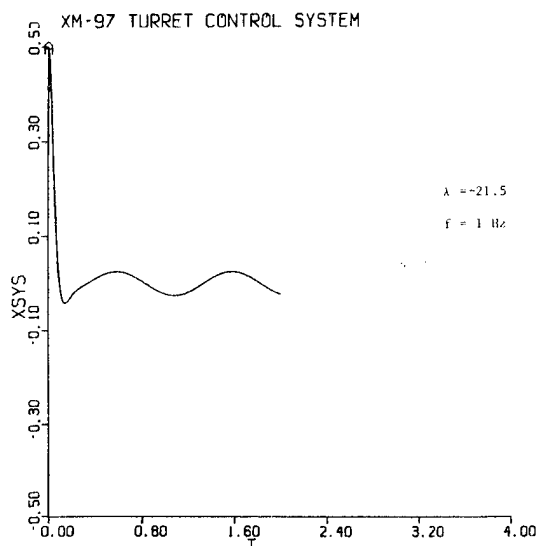


Fig.11 RESPONSE OF $x_1(t)$ -AZIMUTH CHANNEL

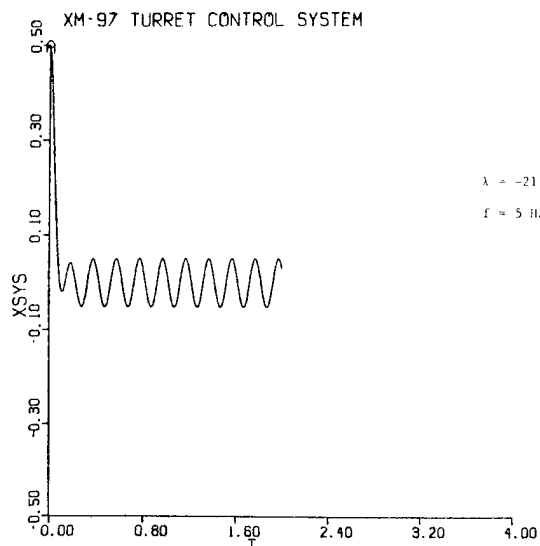


Fig.12 RESPONSE OF $x_1(t)$ -AZIMUTH CHANNEL

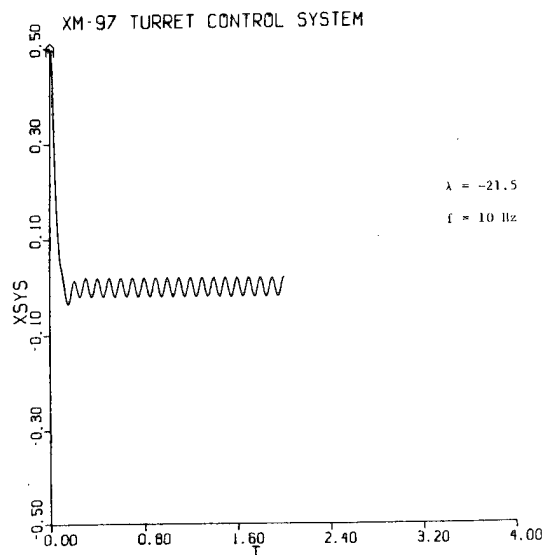


Fig.13 RESPONSE OF $x_1(t)$
- AZIMUTH CHANNEL

6. TWO-STATE OPTIMAL REGULATOR WITH DISTURBANCE ACCOMMODATION USING SECOND-ORDER TORQUE OBSERVER

In this section we discuss in more detail the important issue raised earlier that the ability to suppress or reject disturbances in a control system using observers is very much dependent on the quality of match between the observer model and the actual disturbance. We illustrate this point by designing an observer based on a sinusoidal model of frequency 1 Hz with observer poles placed at $-25 \pm j25$. The disturbance dynamics takes the form

$$\dot{\underline{w}}(t) \triangleq \begin{bmatrix} \dot{w}_1(t) \\ \dot{w}_2(t) \end{bmatrix} = \begin{bmatrix} 0 & 1 \\ (-2\pi f)^2 & 0 \end{bmatrix} \begin{bmatrix} w_1(t) \\ w_2(t) \end{bmatrix}, \quad (34)$$

$$\triangleq \underline{A}_w \underline{w}(t),$$

where $f = 1$ Hz.

The observer equations are given by

$$\hat{\underline{w}}(t) = \begin{bmatrix} \hat{w}_1(t) \\ \hat{w}_2(t) \end{bmatrix} = \begin{bmatrix} p_1(t) \\ p_2(t) \end{bmatrix} + \begin{bmatrix} \ell_{11} & \ell_{12} \\ \ell_{21} & \ell_{22} \end{bmatrix} \begin{bmatrix} x_1(t) \\ x_2(t) \end{bmatrix}, \quad (35a)$$

$$\begin{bmatrix} \dot{\hat{p}}_1(t) \\ \dot{\hat{p}}_2(t) \end{bmatrix} = \underline{M} \begin{bmatrix} p_1(t) \\ p_2(t) \end{bmatrix} - \underline{L} \underline{B} u'(t) + (\underline{M} \underline{L} - \underline{L} \underline{A}_w) \begin{bmatrix} x_1(t) \\ x_2(t) \end{bmatrix}, \quad (35b)$$

where $\underline{M} = \underline{A}_w - \underline{L} \underline{G}$. The \underline{G} matrix in Eq. (20a) is now given by

$$G = \begin{bmatrix} 0 & 0 \\ -g & 0 \end{bmatrix}$$

where $g = 10^4/3N$ and the observer gain matrix L is chosen such that the observer poles (eigenvalues of M) are located at $-25 \pm j25$. Since only ℓ_{12} and ℓ_{22} affect the placement of the observer poles, we simplify the discussion by setting $\ell_{11} = \ell_{21} = 0$, again with a resultant loss of information from the measure $x_1(t)$. With these simplifications, the observer equations for $\hat{w}(t)$ are

$$\begin{bmatrix} \hat{w}_1(t) \\ \hat{w}_2(t) \end{bmatrix} = \begin{bmatrix} p_1(t) \\ p_2(t) \end{bmatrix} + \begin{bmatrix} \ell_{12} \\ \ell_{22} \end{bmatrix} x_2(t) \quad , \quad (36a)$$

$$\begin{bmatrix} \dot{p}_1(t) \\ \dot{p}_2(t) \end{bmatrix} = \begin{bmatrix} \ell_{12}g & 1 \\ -4\pi^2\ell_{22}g & 0 \end{bmatrix} \begin{bmatrix} p_1(t) \\ p_2(t) \end{bmatrix} + \begin{bmatrix} 2.675 \times 10^5 \ell_{12} \\ 2.675 \times 10^5 \ell_{22} \end{bmatrix} u'(t) + \begin{bmatrix} 0 & \ell_{12}^2 \left(\frac{10^4}{3N} \right) + \ell_{22} + 1.28 \ell_{12} \\ 0 & -4\pi^2 \ell_{12} + \ell_{12} \ell_{22} \left(\frac{10^4}{3N} \right) + 1.28 \ell_{22} \end{bmatrix} \begin{bmatrix} x_1(t) \\ x_2(t) \end{bmatrix}. \quad (36b)$$

A block diagram representation of this system is shown in Fig. 14. The choice of $\ell_{12} = 9.3$ and $\ell_{22} = 225.16$ places the observer poles at $-25 \pm j25$ as required.

The performance of the two-state optimal controller under step position command with $q_{11} = 5$ and the second order torque observer given by Eq. (36) are as shown in Figs 15, 16 and 17 for sinusoidal disturbance inputs at 1, 5 and 10 Hz respectively. The 1 Hz disturbance is perfectly cancelled after an initial transient as would be expected since the observer model perfectly matches the disturbance input. The steady state pointing error increases slightly as the disturbance input frequency and consequently the model mismatch between the observer and the disturbance increases. In all cases, however, the performance is improved over the previous designs. Current efforts are being directed towards developing accurate models for torque input disturbances due to recoil and developing designs based on these models for implementation on a microcomputer-based controller to be tested in August 1981.

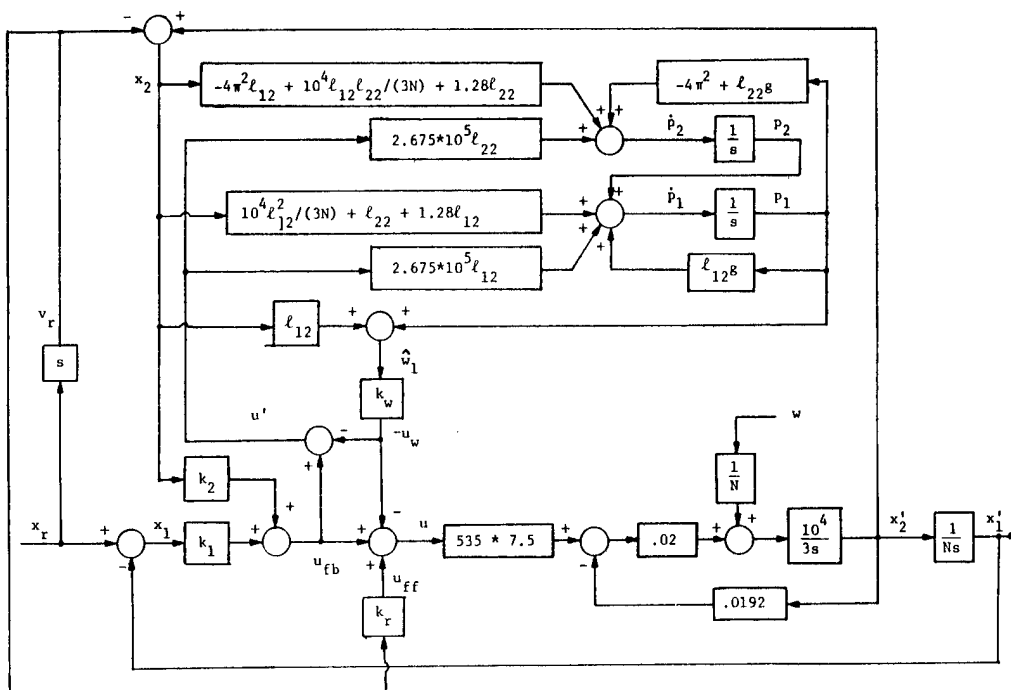


Fig.14 OPTIMAL XM-97 TURRET WITH SECOND-ORDER LUENBERGER OBSERVER

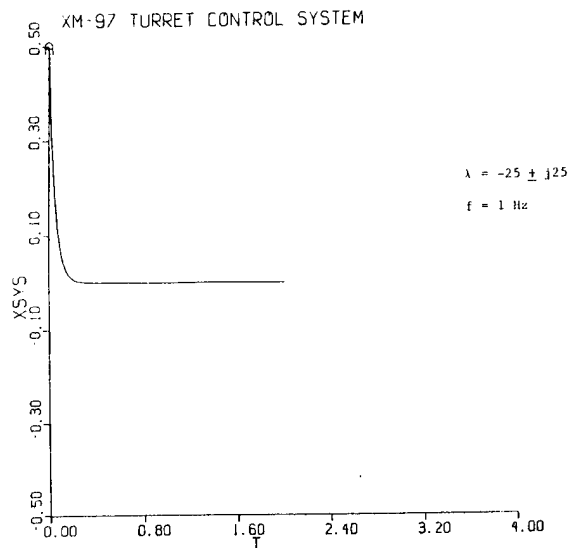


Fig.15 RESPONSE OF $x_1(t)$
- AZIMUTH CHANNEL

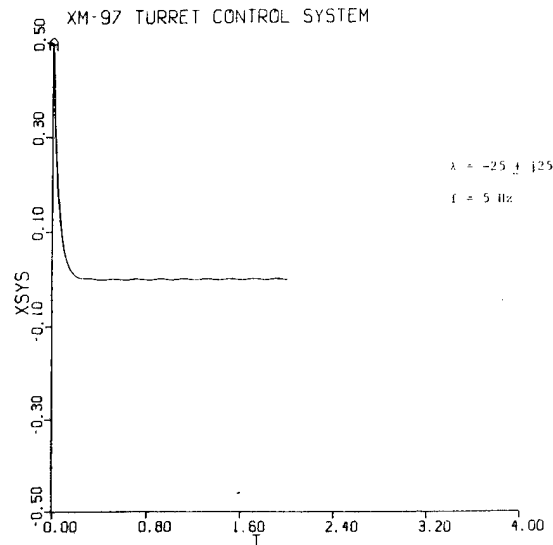


Fig.16 RESPONSE OF $x_1(t)$
- AZIMUTH CHANNEL

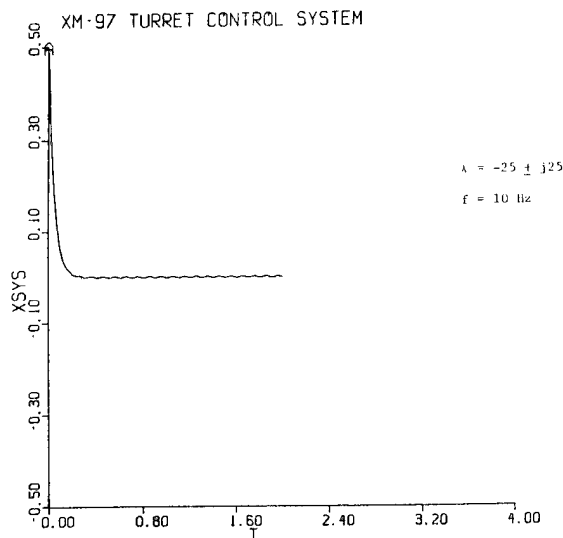


Fig. 17 RESPONSE OF $x_1(t)$
- AZIMUTH CHANNEL

7. NON-FIRING TEST RESULTS

The turret control designs discussed in previous sections were all implemented on a modular analog control device specially designed for test and evaluation purposes. In fact, the modular approach of implementation makes the device readily adaptable not only to a variety of controller designs but also to other armament systems as well. A detailed discussion of the control electronics used for implementation is beyond the scope of this paper. The interested reader is referred to the final report for more information on this subject.

Each control concept implemented on the XM-97 turret was subjected to two tests during the non-firing test phase. In the first test, a step reference command input was applied and the transient response of the turret was analyzed. In the second test, a constant tracking command input was applied and the resulting steady state error investigated. Figs. 18 and 19 show the responses of the original turret and the optimal turret to a 35 milliradians step input command. The performance improvements of the optimal controller over the original design are readily apparent in terms of settling time, overshoot, etc. Table 4 summarizes the step responses and tracking responses of the original turret and the optimal turret for cost functional weighting factor q_{11} of 5, 10 and 15. Since the performance of the optimal designs were similar for given cost functional weighting, only the optimal two-state results are shown.

TABLE 4 COMPARISON OF STEP AND TRACKING RESPONSES
OF THE ORIGINAL AND OPTIMAL XM-97 TURRET CONTROL SYSTEMS

		Azimuth Channel				Elevation			
		Settling Time (sec)		Max Tracking Error mr/sec		Settling Time (sec)		Max Tracking Error mr/sec	
System	Q	175 mr Step	35 mr Step	87 mr/sec	17.5 mr/sec	175 mr Step	35 mr Step	87 mr/sec	17.5 mr/sec
Original XM-97	NA	1.36	1.36	2.74	2.86	1.2	1.125	5.0	5.0
Optimal Design	5	.50	.375	.30	.80	.75	.50	.20	.80
	10	.50	.50	.20	.50	.625	.625	.2	.7
	15	.55	.55	.40	.50	.625	.625	.5	.5

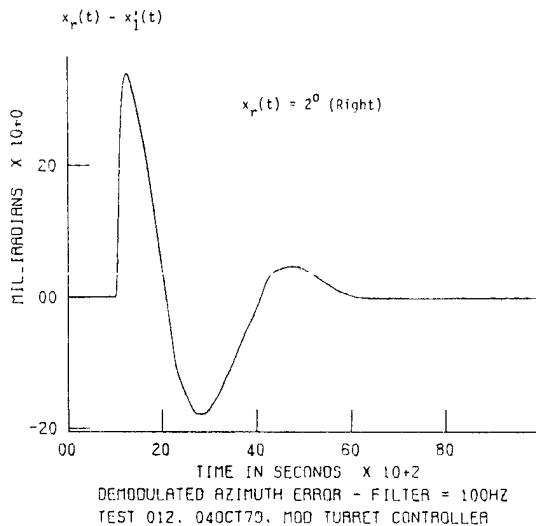


Fig.18 STEP RESPONSE OF ORIGINAL
TURRET - AZIMUTH CHANNEL

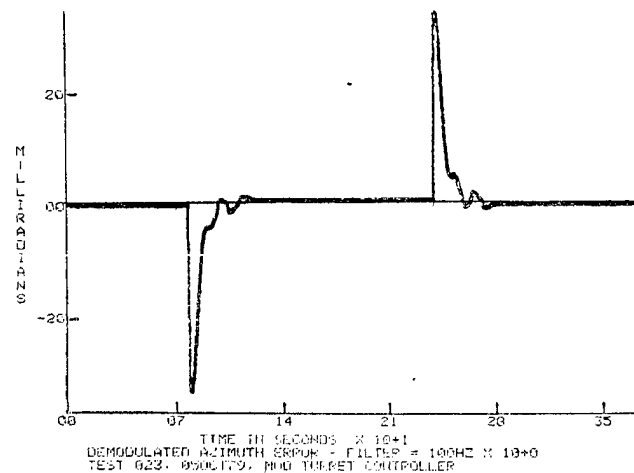


Fig.19 2-STATE OPTIMAL TURRET
- AZIMUTH CHANNEL

8. FIRING TEST RESULTS

Extensive firing tests were conducted to evaluate the performance of each control system design in the presence of recoil disturbances. The weapon used was the M-97 three barrel 20mm automatic cannon with the XM-97 turret mounted on an AH-1 Cobra helicopter air frame. The entire system was suspended from a six-degree of freedom simulator located in Rock Island Arsenal. Firing took place with a 1000 inch range using a paper target and with 20 pound bursts at 600 pounds per minute rate. Since linear motion of the air frame was not compensated, the first seven rounds in each test will be ignored in the performance evaluation in order to permit the hull motion to reach equilibrium under firing conditions.

A comparison fo projectile shot patterns for the original XM-97 turret and the optimal design with $q_{11} = 5$ and 10 is as shown in Figs. 20-23 respectively. The numbers indicate the order in which each projectile was fired. Since the automatic cannon has three barrels, it follows that every third round was fired from the same barrel.

As can be seen from Figs. 20-21, the original XM-97 turret gave wide dispersion pattern of impact points, and the projectiles from the three different barrels were all intermixed in random pattern. On the other hand, the impact point pattern of the optimal turret was quite different as can be seen from Figs. 22-23. Not only that the overall dispersion pattern was much tighter than the original but also projectiles from the same barrel were now closely grouped together forming three distinct groups of dispersion pattern according to the barrels from which the projectiles were fired. The relevant statistical data are summarized in Table 5.

TABLE 5 SHOT DISPERSION (mr)

Original XM-97		Optimal Design
Barrel #1	4.26	1.23
Barrel #2	3.58	.96
Barrel #3	2.22	.96
All Rounds	5.23	2.56

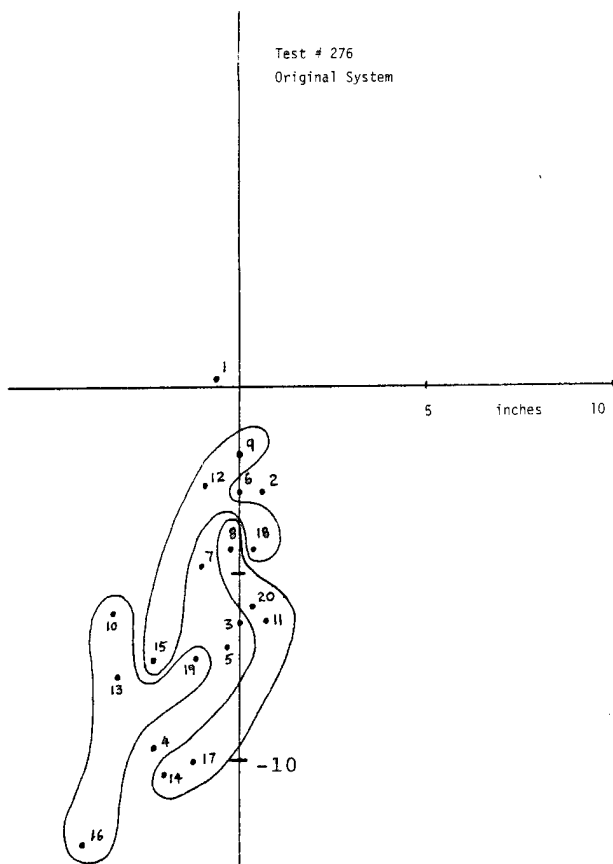


Fig. 20 DISPERSION PATTERN

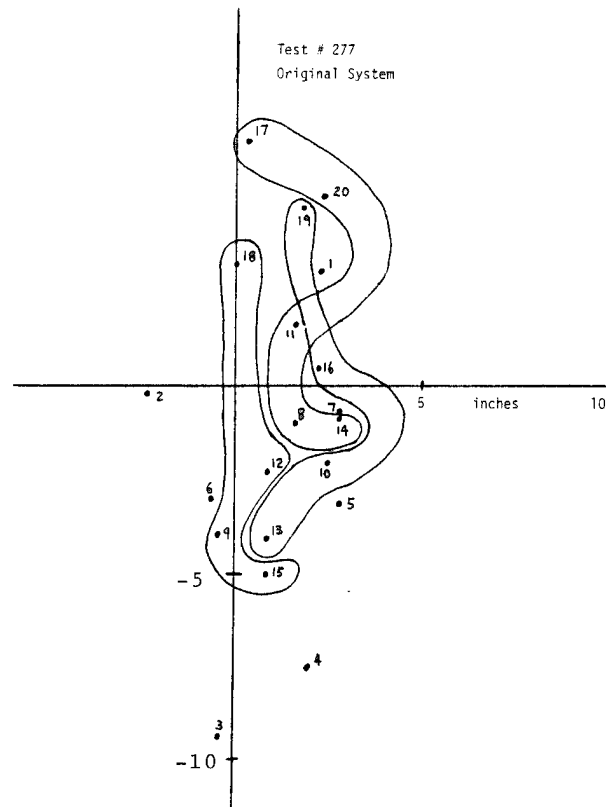


Fig. 21 DISPERSION PATTERN

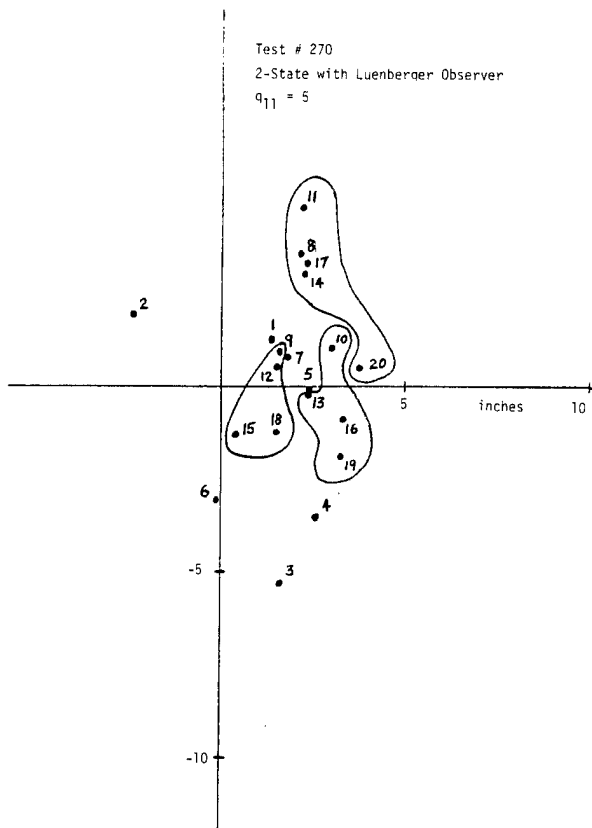


Fig.22 DISPERSION PATTERN

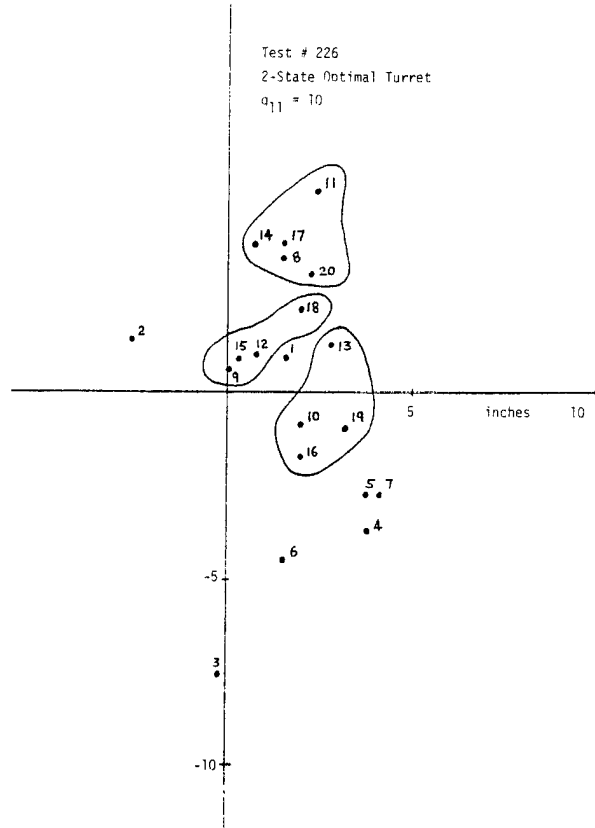


Fig.23 DISPERSION PATTERN

9. CONCLUSION AND DISCUSSIONS

The design of optimal controllers for the XM-97 helicopter turret control system has been investigated. Hardware implementation and fabrication of the optimal controllers using analog electronic components have been carried out. A modular approach of implementation consisting of various compatible plug-in modules has been employed. Extensive non-firing and firing tests have been conducted for both the original turret and the optimal turret. The non-firing tests are conducted using step and step-plus-ramp command inputs, while the firing tests are conducted with 20-round bursts at a firing rate of 600 rounds per minute. The performance of the optimal turret has been found to be much more satisfactory as compared with that of the original turret in both the non-firing and firing tests.

The studies carried out in this paper have shown that modern control theory and estimation theory are useful and practical design tools for the development of precision weapon pointing systems. Furthermore, in view of the fact that qualitative performance requirements, such as fast system responses, reduced system oscillations, improved hit probability, etc., can be transformed directly into quantitative design criteria, modern control system design techniques may often be more easy to apply than the classical design techniques in many practical situations. With the advances of high speed mini-computers and microprocessors, more weapon and industrial systems, both advanced and simple, are being designed using these intelligent digital electronic components. Modern control system design and synthesis techniques can best exploit and utilize the decision-making capability of a digital machine to achieve the kind of system performance which may otherwise be unattainable.

10. FUTURE WORK

An 8086 micro-computer-based digital weapon pointing system is currently under development and is scheduled for testing in August 1981. This system will incorporate observer designs based on more accurate models of the actual recoil and base motion disturbances.

Laboratory evaluation of digital control algorithms which compensate for barrel motion, friction and variations in plant parameters will be carried out during FY81 with follow on evaluations on XM-97 turret in FY82.

ACKNOWLEDGEMENT

The authors gratefully acknowledge the contributions of Mr. R. Radkiewicz, Mr. J. Strahl, and Mr. R. Peterson of the Ware Simulation Center, Rock Island Arsenal, Rock Island, Illinois, to the design and fabrication of the analog control electronics and the testing of the control system designs discussed in this paper.

REFERENCES

1. R. E. Kalman, "Contributions to the theory of optimal control," Bol. Soc. Mat. Mex., vol. 5, pp. 102-199, 1960.
2. H. Kwakernaak and R. Sivan, Linear Optimal Control Systems, New York: McGraw-Hill, 1966.
3. D. G. Luenberger, "Observing the state of a linear system," IEEE Trans. Mil. Electron., vol. MIL-8, pp. 74-80, April 1964.
4. D. G. Luenberger, "Observers for multivariable systems," IEEE Trans. Automat. Contr., vol. AC-11, pp. 190-197, April 1966.
5. C. D. Johnson, "Accommodation of external disturbances in linear regulator and servomechanism problems," IEEE Trans. Automat. Contr., vol. AC-16, pp. 635-644, December 1971.
6. C. D. Johnson, "Theory of disturbance-accommodating controller," in Control and Dynamic Systems; Advances in Theory and Applications, vol. 12, C. T. Leondes Ed. New York: Academic, 1976.
7. B. Gopinath, "On the control of linear multiple input-output systems," Bell Syst. Tech J., vol. 50, pp. 1063-1081, March 1971.

SUB-OPTIMAL STATE ESTIMATION AS RELATED TO PREDICTIVE FIRE CONTROL SYSTEM DESIGN

Toney R. Perkins
US Army Materiel Systems Analysis Activity
Aberdeen Proving Ground, MD 21005

ABSTRACT

The engagement of maneuvering land vehicles with gun systems place extreme performance requirements on the fire control system designs. The effectiveness of a gun fire control system depends on the capability to provide an accurate fire control solution, i.e., predict the future position of the target a projectile time-of-flight later. Non-linear prediction is shown to not only improve performance but to also increase available time for firing against maneuvering targets. Sub-optimal, multi-variable, adaptive estimation approaches are shown to improve the effectiveness of predictive fire control systems.

Sensitivity analyses are presented that relate system induced errors to tracking noise and prediction order. Relationships between system stability and performance for two basic types of fire control systems are presented.

INTRODUCTION

This paper discusses the fire control system problem, the nature of land vehicle mobility and agility and the ability of predictive fire control systems to effectively engage maneuvering vehicles. Existing performance specifications do not satisfactorily describe the level of maneuverability expected in a tactical situation. Rather, present specifications define performance requirements for fixed vehicle speed and heading movement which have resulted in the development of fire control system designs that are significantly degraded in a maneuvering target environment. The problem is addressed, in general, for the four cases of firing vehicle-target vehicle movements. The processes required in the fire control solution are identified and the sensitivity of system performance to the propagation of tracking errors is discussed. The stability and performance characteristics of two generic fire control system configurations are analyzed in some detail.

GUN FIRE CONTROL SYSTEM PROBLEM

The purpose of gun fire control systems is to have a projectile, that has been fired a time of flight previously, impact the target that was sighted a time of flight earlier. The critical motion parameters that degrade the performance of predictive fire control systems have been identified as cyclic oscillations exhibiting frequencies that are within the motion capabilities of tactical land vehicles.¹ Tracking error does not in itself cause the performance degradation. The inability of the fire control system to determine the motion derivatives of the line-of-sight (LOS) to the target and predict the future position of the target are the two main factors that cause fire control system degradation.

The error in the ability of a fire control system to cause the projectile to intercept the target a time of flight later is referred to as total gun pointing (TGP) error. TGP error is defined as the offset between the actual gun pointing direction at round exit and the location of the target centroid at round impact. The TGP error is the sum of the propagated system induced (SI) errors and target

induced (TI) errors (i.e., TGP error = SI errors + TI errors). The SI errors, considered in this study, are the tracking error (difference between the tracker LOS and true LOS to the target) at the time of firing and the estimation errors (difference between estimated LOS states and true LOS states). The SI errors propagated through a projectile time of flight result in a kinematic lead error. The TI error is caused by the target motion during the time of flight of the projectile. It is dependent on the order of the lead solution in the fire control system. For a first order lead system the TI error is the difference between the actual LOS movement during a projectile time of flight and the propagated LOS movement assuming perfect LOS rate at the time of fire. The first order predictor system TI error ignores the presence of actual target acceleration at time of firing and during projectile flight time. For a second order lead system the TI error is the difference between the actual LOS motion during a projectile time of flight and the propagated LOS movement assuming perfect LOS rate and acceleration at the time of firing. The second order predictor system TI error accounts for target acceleration at time of firing but ignores the target acceleration changes during projectile flight time. This distribution of errors is shown in Figure 1. The ballistic flight characteristics of the projectile are ignored.

The fire control solution occurs during a short time interval which is related to the time of flight of the projectile. The motion conditions of both the firer and the target are needed to understand and solve the fire control system problem. Four motion conditions exist: stationary firer-stationary target, stationary firer-moving target, moving firer-stationary target, and moving firer-moving target. The stationary firer-stationary target is the least dynamic situation and is the least complex case, and the moving firer-moving target is the most complex case. For each of the cases, the LOS between the firer and target is the key to which of the four fire control processes are being called upon in a demanding manner.

Fire Control System Processes

A fire control system may be broken down into four distinct processes. Each of these processes are present in all types of fire control systems. They are: tracking, estimation, prediction, and gun pointing. In specific designs these four processes are accomplished in different manners.

The tracking process is important in all four cases. For the moving firer cases, tracking becomes more critical because the base motion of the firer must be compensated and it may be affected in a secondary manner by target motion. Tracking is usually accomplished manually and is concerned with the alignment of the sight reticle with the target. The gunner is involved directly at this stage and accuracy of tracking will be a characterization of the ability of any given gunner to perform the task. Test data obtained from experimental investigations can be used to determine tracking error means, standard deviations, and correlation time constants useful for building models of the tracking errors.

The estimation process is the intermediate stage between the tracking process and the prediction process and its configuration is dependent upon the order of the prediction process. Estimation is the process of filtering the tracking data to provide the necessary target motion information required in the prediction process. The accuracy of the tracking data will influence the performance of the estimation process. The system error induced by the estimation process decreases with improvement in tracking accuracy.

Prediction of target future position to obtain intercept between projectile and target is dependent upon an estimate of the present motion of the target and the time of flight of the projectile. The output of the estimator is not a complete description of the present motion of the target, therefore, the predictor does not have the necessary information to calculate the target's future position exactly. If restrictions are placed on the allowable threat motions, then the predictor's ability to determine its future position is improved. Oversimplification of allowable threat motions has placed unrealistically simplified requirements on the operation of the estimation and prediction processes. Realistic threat motions are determined by the mobility capabilities of tactical vehicles. In the past, the majority of targets that have been studied have been nonaccelerating. The requirements of an estimator and a predictor for this type of motion are to combine the apparent

target velocity estimate and projectile time of flight for the lead solution. The required lead is constant and can be realized after some settling time. The existence of accelerating targets requires the system to develop constantly changing lead angles, hence, the need for non-linear prediction.

An important point to observe is that, for the stationary firer-moving target case, the prediction process is required to provide gun command orders that orient the gun to account for target motion during the projectile's time of flight, whereas in the moving firer-stationary target case this prediction process is not required because the LOS existing between the firer and target at instant of firing does not move during the projectile's time of flight. For the moving firer-moving target, the LOS also moves after projectile firing.

The gun pointing process is required to align and stabilize the gun along the predicted LOS to the target. The stabilization and response of the gun pointing loop are major concerns for fire control system performance against maneuvering targets. Stabilization of the gun pointing process could have an adverse effect on overall system performance. The moving firer cases will stress the gun pointing process most severely but it is possible that the gun pointing process will be equally stressed for the stationary firer-moving target case with non-linear prediction.

FIRE CONTROL SYSTEM CONFIGURATIONS

The three currently used fire control configurations are known as manual or iron sight, disturbed reticle and stabilized sight-director systems. A fourth method called closed loop refers to projectile spotting to adjust the fire control solution and is not considered in this discussion. The manual fire control system uses the brute force approach and concentrates on stabilizing the gun position exclusively. In this system the lead is introduced manually, therefore, there is no automation of the fire control estimation and prediction processes. The disturbed reticle system stabilizes the gun position and disturbs the position of the tracking reticle from the gun line position. In this scheme the tracking, estimation and prediction processes are inseparable and the fire control solution is automated. The rejection of firer vehicle base motion is difficult to accomplish in this type of system. The last system to be considered is the stabilized sight-director system. The tracking process is accomplished by a tracker which is isolated from the firer vehicle base movement. The resulting LOS orientation is referenced to inertial space, as contrasted to the gun line for disturbed reticle systems. The estimation process is the intermediate link between the tracking process and the prediction process. The prediction process uses the estimation process outputs combined with projectile time of flight to determine the gun pointing commands. The gun pointing process uses the estimated LOS to the target summed with the calculated lead to position the gun line.

How well a fire control system configuration performs is a function of target movement, firer movement and fire control system design. The analytical methodology required to study this problem should be constrained to real time solution mechanisms. Another way to say this is: post data analysis techniques using data obtained from field tests will not provide the insight that is required to obtain an understanding of the relative performance of different fire control systems. Probability of hit information is useful for an assessment of systems that have been fielded but is not applicable for tradeoff studies of the type required in this study. Analytical methodologies such as servo mechanism synthesis and modern filtering technology are required to study this problem.

MANEUVERING TARGET DESCRIPTION

A quantitative description of the threat is required to evaluate the performance of fire control systems operating against maneuvering targets. To develop this description, it is necessary to consider the mobility and agility characteristics of threat vehicles in a realistic combat environment. A thorough description of anticipated maneuvering seems to defy identification because threat maneuvers constitute a large set of possibilities even when constrained by tactical doctrine, driver policy, terrain and vehicle capabilities. Two approaches, analytical and empirical, are available for consideration in the attempt to identify the maneuver characteristics of land vehicles. An analytic approach would view each maneuver as being composed of elements from an idealized

group of movements. An empirical approach would view the maneuvers as having actually occurred during limited tests for different types of maneuvering vehicles. Neither of these approaches provide a complete maneuver description, but a combination of these two approaches offers some advantages and is the rationale adopted. The analytic approach will partially overcome the incompleteness of the empirical data base while the empirical data will offset the mathematical idealizations of the analytic methodology.

Empirical Approach

When using empirical data to demonstrate the performance of a gun fire control system, base-line performance can be determined with no concerns arising from idealization of the maneuvers. Since the number of maneuvers will be rather small, they neither provide sufficient information about the robustness of a fire control design methodology nor the pathology when the fire control system begins to degrade. When demonstrating the performance of a fire control system against experimental data, caution must be exercised to assure that the empirical data is properly inputted to the fire control system model. Matching of the data rates and noise levels often requires some preprocessing of experimental data to prepare it for use in simulation studies.

Analytic Approach

As a supplement to the empirical approach, the analytic approach is used to investigate sensitivity effects for a larger group of movements. Simulating new or pathological maneuvers require that the analytic capability superimpose maneuvers arising from random disturbances and intentional, voluntary vehicle driver commands.

The random disturbances may be represented in terms of time histories or power spectral densities. The time history approach is based on the development of a mathematical model of vehicle movement, influenced by terrain effects and arbitrary driving habits of individual drivers. It is assumed that for no random effects caused by terrain irregularities or driver input, the vehicle would follow a straight line constant speed path. Maneuvers are viewed as perturbations on this straight line constant speed path. Apparent acceleration, $a(t)$, which is correlated in time, accounts for the vehicle's deviation from a straight line path. Maneuver capability is expressed by three quantities: the variance, or magnitude of $a(t)$, the cyclic maneuver frequency and the time constant of the maneuver.

Intentional, voluntary vehicle driver commanded motion of land vehicles over terrain is a complicated subject in itself and will not be investigated in this study. It is recognized however, that an interaction between vehicle horsepower, weight, suspension, and locomotion concepts do combine with terrain over which it is moving to provide different levels of mobility with respect to a fixed reference frame. Therefore, different vehicle designs will have different mobility levels defined in terms of motion and derivatives of motion. Agility is closely related to mobility and yet it is a slightly different description of intentional vehicle motion. Where mobility describes the movement of a vehicle from one location to another location in a given period of time, agility describes the vehicle's ability to alter its mean path.

SENSITIVITY OF FIRE CONTROL PROCESSES

Degradation in gun pointing accuracy results from two major error sources-system and target induced errors. The target induced errors are caused by the motion of the target during the time-of-flight of the projectile. Since the target has the capability to maneuver within constraints of the terrain, vehicle characteristics and driver policy during a projectile's time-of-flight, there is no such thing as a correct (perfect) lead solution. The lead solution is based on the projected target position using the present target states and projectile time-of-flight. Therefore, the target induced error, in general, cannot be reduced to zero for a maneuvering target. However, it can easily be shown that proper selection of the prediction process is capable of reducing the gun pointing error due to target motion.

The system induced errors are made up of bias and random errors emanating from specific components and subsystems. The propagation of these errors degrade the performance of the fire control system. The system induced errors of major concern are those occurring in the tracking process. Sensitivity analyses have been performed to evaluate the degradation of gun pointing commands to tracking process errors. The analysis considers the fire control processes to be interfaced in tandem with no feedback of outputs to a previous process. The analysis is further limited to a segment of a maneuvering target path which was generated by a maneuvering target path simulation program. This analytically generated path provides an exact time history of the target states (position, velocity and acceleration).

The tracking process is modeled by summing random errors of known variance with the output of a perfect LOS sensor. The output of the tracking process is, by definition in LOS coordinates, however, cartesian coordinates are used by choice and not a limitation of the methodology in the estimation processes. For simplification the transformation from LOS to cartesian coordinates is accomplished prior to adding tracking noise.

A sub-optimal, adaptive Kalman filter (KF) is used for the estimation process in the generic fire control system under consideration. The noisy tracking process signal is processed by the KF to provide a "best" estimate of the target states (position, velocity and acceleration). The estimation errors are minimized by providing the filter with the correct variance of the observation noise. In practice, this perfect match of noise variance is not achievable but can be approached with detailed error analysis of the tracking process or with software methodology to estimate the noise. The latter is probably desirable and necessary because the variance of the tracking process error is not time invariant in a combat environment. The KF equations and theory are well known and are presented elsewhere.^{2,3} However, the adaptive feature of the designed KF, which requires online computation of the filter's gain, is outlined.⁴ The adaptive, time varying gain is obtained by changing the variance of the uncertainty of the embedded target dynamics, as a function of the estimated path geometry. The forcing function, μ , for the target dynamics is modeled as a random (Gaussian noise) rate of change of acceleration. The variance of μ is defined in the body coordinates of the target as constant, diagonal elements of the Q matrix. The Q matrix is rotated as the target maneuvers to provide a time varying Q matrix in the filter's coordinate system.

The sensitivity of the estimates to the tracking process noise is evaluated for a typical maneuvering target path. The ground track of the maneuver is shown in Figure 2. The maximum speed and lateral acceleration are 10 m/sec and 2 m/sec², respectively. Figure 3 shows the degradation in velocity estimates as the standard deviation of the tracking process noise on the assumed position observation is increased from 0.05 meter to 1.0 meter. The degradation in the estimates of lateral acceleration for the same noise levels is shown in Figure 4. A comparison of these two figures shows that the velocity estimates are not as sensitive to the propagation of tracking noise as the acceleration estimates. The prediction process provides the command for pointing the gun to the predicted target position. The estimated future position of the target depends on the order of the prediction process. Ideally, one would like to forecast the target position so that a projectile fired a time-of-flight earlier would arrive at a point in space simultaneously with the target. Unfortunately, only the present states, which are never known exactly, are available for use in computing future target position.

With knowledge of the true future position of the target available from the target motion simulator, the degradation in the gun pointing commands can be evaluated for different tracking errors. Target induced errors and the propagation of the tracking process noise are analyzed to evaluate their effect on gun pointing commands.

The target induced errors are functions of target maneuver characteristics, projectile time of flight and prediction order. For a given prediction order and with perfect knowledge of the present target state and time of flight, the resulting target induced errors are lower bound prediction errors. Effects of time of flight and order of prediction are shown in Figure 5 for a maneuvering target whose maximum speed and lateral acceleration is 10 m/sec and 3.5 m/sec². Prediction errors are improved for decreases in time-of-flight and higher order of prediction.

First order prediction is linear and requires only accurate estimates of velocity to approach the lower bounds of prediction error. Second order prediction requires not only accurate velocity but also acceleration estimates to minimize the prediction errors. Figure 6 shows the standard deviation of prediction error for the target maneuver shown in Figure 2 as a function of time-of-flight and variances of tracking process noise for first order prediction. These results indicate that the degradation in prediction error is minimized as the quality of tracking improves. However, the existence of the lower bound curve for second order prediction provides additional improvement, not realized by first order prediction. Assuming position observations (input to the KF) with a 1 σ noise of 1.0 meter, Figures 6 and 7 show that there is no large difference between first and second order prediction. However, second order prediction with a reduction in the tracking process error to 0.05 meter (25 microradians at a range of 2000 meters) provides a significant improvement in the lead solution. Unlike first order prediction, second order prediction is not only more sensitive to the tracking process noise but also to the observation state. Figure 7 shows that improvements are realized if the observations are rates rather than position. If tracking accuracies of 0.04 m/sec (20 microradian/sec at 2000 meters) are achieved, the prediction error is within about ten percent of the lower bound for second order prediction.

The lead errors discussed above are the differences between the predicted and actual target positions for given time-offlight. Targets are not point sources and a more meaningful criteria for evaluating the system is the percent time on target for a specified engagement time. Assuming a target size of 2.3 meters X 2.3 meters, independent of target orientation, the percent time on target for the same tracking accuracy in Figure 7 is depicted in Figure 8 for times of flight between 1.0 seconds and 2.5 seconds.

STABILITY ANALYSIS OF GENERIC FIRE CONTROL SYSTEMS

General Discussion

The three basic fire control configurations in existence: manual, disturbed reticle and stabilized sight-director have been identified in terms of how the fire control processes are mechanized. All existing operational systems utilize the human operator to null the difference between the observed target and the reticle position. The degree of participation of the human in each of the three types of fire control systems is considerably different. Concern about the stability of the closed loop man-machine system is an important consideration in determining performance and is one of the primary distinguishing features that characterizes the effectiveness of the three types of fire control systems. In the manual system, the tracking, estimation and prediction processes, are performed by the man and the machine serves only to orient the gun line in accordance with the information provided by man. The tracking is performed by the man in the disturbed reticle and stabilized sight-director systems, however, it is accomplished differently. The estimation and prediction processes are also mechanized differently in these two types of fire control systems. One of the important inherent advantages of a stabilized sight-director system compared to a disturbed reticle system is the decoupling of the tracking process from the estimation and prediction processes. The turret and gun position serve as the reference from which the reticle is disturbed in the disturbed reticle system. Involvement of the human gunner in the turret loop for the disturbed reticle system and his absence from the turret loop for the stabilized sight-director system is a distinguished feature of the systems. The tracking process is, therefore, more isolated from the estimation, prediction, and gun pointing processes in the stabilized sight-director system.

Disturbed Reticle Fire Control System

One fire control configuration in current use is the disturbed reticle concept. The following discussion is intended to describe in detail the functions of the disturbed reticle fire control system and identify the four processes, showing how each is related to the other. Figure 9 describes the signal flow and the four major processes are identified in terms of where in the system each is accomplished.

The input to the system is the LOS from the target to the reticle of the tracking system. The human operator moves the handle bar controller to align the reticle of the tracking system to be coincident with the target. The ability of any

human controller to accomplish this task defines the quality of the tracking process. Handle bar controller output, which is directly related to the LOS rate, is used to drive two interdependent subsystems. The first is the turret servo which is commanded to rotate at a rate directly proportional to the handle bar controller deflection. The second subsystem driven by the handle bar controller is a lead screw servo and reticle system. The displacement of the lead screw servo is directly proportional to the filtered handle bar controller deflection multiplied by the projectile time of flight. The lead screw displacement is used to position the reticle of the tracking system.

These are two distinct feedback signal paths in the disturbed reticle configuration and the human is a series subsystem in both paths. Another important observation is to note that the signal loop made by the turret servo-man-handle bar controller is a degenerative feedback loop because of the negative summing junction. The signal loop made by the filter-time of flight lead servoreticle servo-man handle bar controller is a regenerative feedback loop because of two negative summing junctions. During normal operation of the disturbed reticle system, the performance of these two feedback paths give rise to a dynamical system that exhibits some undesirable performance characteristics. Without further crossfeed compensation, the closed loop performance of the disturbed reticle system is at best marginally stable. To overcome this condition, compensation signal paths are added. The basic compensation is a tachometer generator signal from the lead screw servo which is combined with the turret servo error signal. This composite signal is fed to the turret servo and the reticle servo to compensate for the dynamical mismatch that occurs in the reticle and turret servos. However, there is no such thing as a perfect compensation and the undesirable performance characteristic alluded to earlier can never be completely nullified, not to mention the potentially precarious situation that might occur if any failure or gain change occurs in the compensation paths.

The important thing to observe about the root locations in Figures 10 and 11 is that there are numerator roots in the right half of the S plane. This arises from the basic disturbed reticle configuration and must be considered a fixed element phenomenon in this type of system. The poles or denominator roots describe the system operating point for a system gain of zero. The zeroes or numerator roots describe the system operating point for a system gain of infinity. The dotted trajectories connecting these two extremes are a pictorial description of the operating point loci for all intermediate gains. These systems exhibit conditional stability because of the presence of positive feedback in the equivalent transfer function between B and A. These are different closures than exist for a negative feedback that occurs when both the reticle and turret crossfeeds are present as shown in Figure 12. The existence of these simultaneous crossfeeds from the lead screw servo and turret servo error to the turret servo and reticle servo tend to offset the non-minimum phase root condition shown in Figures 10 and 11.

In summary, it is the location of the operating points that determine the system stability characteristics. The frequency content of the tracking error is directly related to the operating points, but equally important is the magnitude of the tracking error which is influenced by the location of the numerator roots of the closed loop transfer function. These effects are interrelated, but the fundamental underlying requirement is to achieve an adequate stability margin of the closed loop system. This stability consideration is important for fire control system performance and the designers must take these factors into account. The end result is system performance which may be acceptable or not acceptable.

It can be asked why so much concern about this situation because disturbed reticle systems have performed satisfactorily in the past. Perhaps this is so, but with the introduction of maneuvering targets, the performance of this type of system may be adversely affected. When the target LOS, θ_T , shown in Figure 9 moves at a constant rate, the human operator is required to move the handlebar controller a nominal fixed amount. The turret servo develops a fixed nominal rate and the lead servo assumes a fixed nominal position. It then becomes the task of the human to perturbate the handlebar controller about this normal position in order to minimize the tracking error. When the target LOS rate is not constant, which is the situation for maneuvering targets, the handlebar controller must be moved consistent with the changing target LOS rate. The nominal handlebar controller position is not the only difference in the system operation for maneuvering targets. The turret servo accelerates and decelerates and the lead screw servo is constantly being driven to a new

position. The new position of the reticle is a result of these two signals paths. The dynamic performance mismatches are guaranteed to be greater than for the non-maneuvering targets and the tracking performance will be degraded. This degradation occurs from the inability of the closed loop system to accurately null the constantly changing target LOS rate. The extent of this degradation may not be immediately obvious to the casual analyst, but the oscillatory nature of this degradation will be observed once a sufficiently close survey of the tracking error is made. It is imperative that the resulting stability margin of the closed man-machine system be large to insure acceptable performance against maneuvering targets.

Recent work has shown that tactical targets can execute maneuvers of such a nature that when projectile times of flight of 1.5-2.0 sec are considered, target induced motion after projectile firing will cause excessive miss distances when linear predictor fire control systems are assumed and moreover these miss distances can be significantly reduced when non-linear or higher order predictor fire control systems are employed.¹ These observations indicate lower boundary miss distances are possible for non-linear lead systems. When this situation is presented to the fire control designer, his inclination will be to consider the possibility of including non-linear prediction in the fire control system. In the disturbed reticle configuration shown in Figure 9, this may be a design impossibility because of the level of tracking performance obtainable from the operation of the disturbed reticle systems. To be more specific, the tracking error required for nonlinear prediction must be smaller than the tracking error for first order prediction. The trade-off between the propagated system induced errors for the non-linear estimation process must be offset by the target induced prediction error improvements realized by the higher order prediction. The key ingredient for this situation to exist in a fire control system is to have high quality tracking.

If the human tracker is replaced by an automatic tracker the performance limitations imposed by the loop structures in a disturbed reticle system may negate the potential improvement attainable from the improved tracking. It is the coupled nature of the tracking, estimation, prediction, and stabilization process occurring in the disturbed reticle configuration that restrict its growth to better fire control system performance, especially against maneuvering targets.

Stabilized Sight-Director Fire Control System

A stabilized sight-director fire control system, shown in Figure 13, is actually two distinct systems that are brought together to accomplish the tracking, estimation and prediction processes of a fire control system. Stabilization of the tracking system is independent from stabilization of the turret. The stabilized sight is decoupled from turret and hull motion by the reverse torquing of the outer gimbal of the tracker to account for disturbances of the tracker base which is mounted on the turret. This decoupling enhances the ability of the tracker to maintain coincidence between the sight reticle and the target LOS. The stabilized reticle position can utilize both position and rate feedback to augment the stability of the sight. The orientation of the sight reticle is, therefore, an independent process from the turret motion.

Position and rate of the LOS are fed to a filter or estimation process to determine the necessary information about the LOS to the target that will be needed to offset the turret servo from the stabilized tracker. Multi-variable, sub-optimal technology can be applied to further improve the quality of tracking that can be realized from the stabilized sight-tracker. Therefore, either linear or non-linear predictions are possibilities for the fire control solutions. If LOS accelerations are to be estimated, the appropriate modeling of target dynamics and tracker uncertainties will be required to insure that the degree of sub-optimality is not excessive. One very significant plus for coupling the estimation and tracking process in a favorable manner is the utilization of sight line rate aiding feedback to the tracker obtained from estimation of the target rates and acceleration. This concept relaxes the task of the human tracker or auto-tracker and will improve the minimization of tracking error.

Output of the target state estimator is used in two separate paths. The first path uses θ_T and $\dot{\theta}_T$ to drive the turret servo as a director to follow the tracker LOS. The second signal path combines target state estimates with projectile time of flight and offsets the gun from the tracker LOS by the

appropriate value to permit intercept of projectile and target a time of flight later.

Performance of the stabilized sightdirector system should not be compromised by maneuvering targets to the extent that the disturbed reticle system is compromised. The basic reason for this is that the tracking system is essentially decoupled from the lead prediction system. However, there are some inherent stabilization problems that can occur in this configuration and they are accentuated by the temptation to obtain high performance of the gun pointing process. The argument goes as follows: with increased tracker performance, the gun stabilization servo can be made to perform more rapidly, thereby increasing the overall capability of the system. However, with increased performance being required of the turret servo to follow the turret commands, the stability of the turret servo may be compromised because of the high gains in the director-follower loop. Experience with similar types of systems has shown that because of non-rigid gun tube and hull structures, the follower loop system must be phase stabilized and not gain stabilized, as is the case for less responsive systems such as disturbed reticle systems. This requires sophisticated compensation circuits to overcome system instabilities.

The stabilized sight is identified between the target input and the sight output in Figure 13. It drives the gun turret servos which are used to position the base of the stabilized sight. The signal flow diagram and root loci for the stabilized sight-director system are shown in Figure 14. This is the same basic root locus obtained in the disturbed reticle system when the crossfeeds were included. The dotted lines show the loci of the change in stability as the gain is increased. The addition of series compensation circuits in the tracker transfer function; such as $T_1 S+1$, which can easily be added in a

$$T_2 S+1$$

straight-forward manner will alter the shape of the loci to obtain an optimized operating point, which would be difficult in the disturbed reticle system. The fundamental purpose of the tracking process is to align θ_S with θ_T . Simultaneously any disturbances on the stabilized sight are compensated by orientation of the sight base thereby simplifying the tracking task.

CONCLUSIONS

The inherent ability of a stabilized sight-director fire control system to decouple the tracking estimation, prediction and gun pointing processes may be exploited to improve effectiveness when engaging maneuvering targets. Accurate tracking is necessary for non-linear prediction and multivariable, sub-optimal design technology is required to achieve the needed accuracy of the target state estimates for mechanizing non-linear prediction. Further studies are required to identify the specific details of the resulting system design. A complementary methodology employing stability and performance analyses will assist in this quest.

ACKNOWLEDGEMENT

The author thanks Mr. Warren Muehlberger for drawing the figures and Mrs. Jo Ann Marderness for typing the manuscript.

REFERENCES

1. Burke, Harold H., Fire Control System Performance Degradation When a Tank Gun Engages A Maneuvering Target, XVII US Army Operations Research Symposium, Ft. Lee, VA 6-9 Nov 78.
2. Leathrum, Dr. James F., An Approach to Fire Control System Computations and Simulations, US Army Materiel Systems Analysis Activity Technical Report No. 126, April 1975.
3. Gelb, Arthur, Applied Optimal Estimation, MIT Press, 1974.
4. Burke, Harold H., Toney R. Perkins, James F. Leathrum, State Estimation of Maneuvering Vehicles via Kalman Filtering, US Army Materiel Systems Analysis Activity Technical Report No. 186, October 1976.

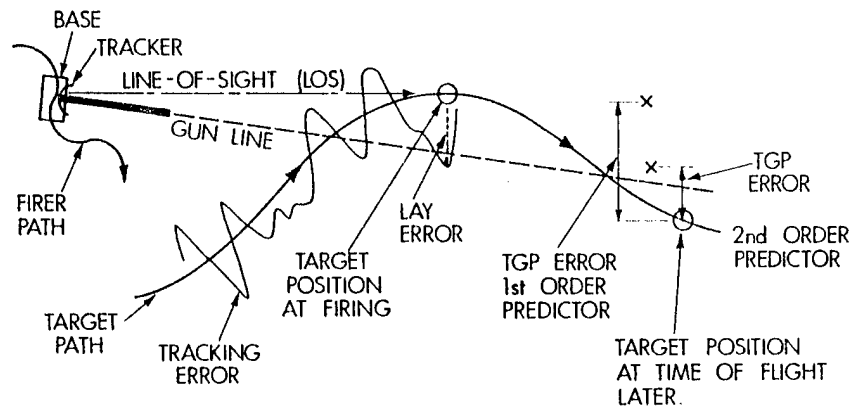


Figure 1. Fire Control System Error Sources.

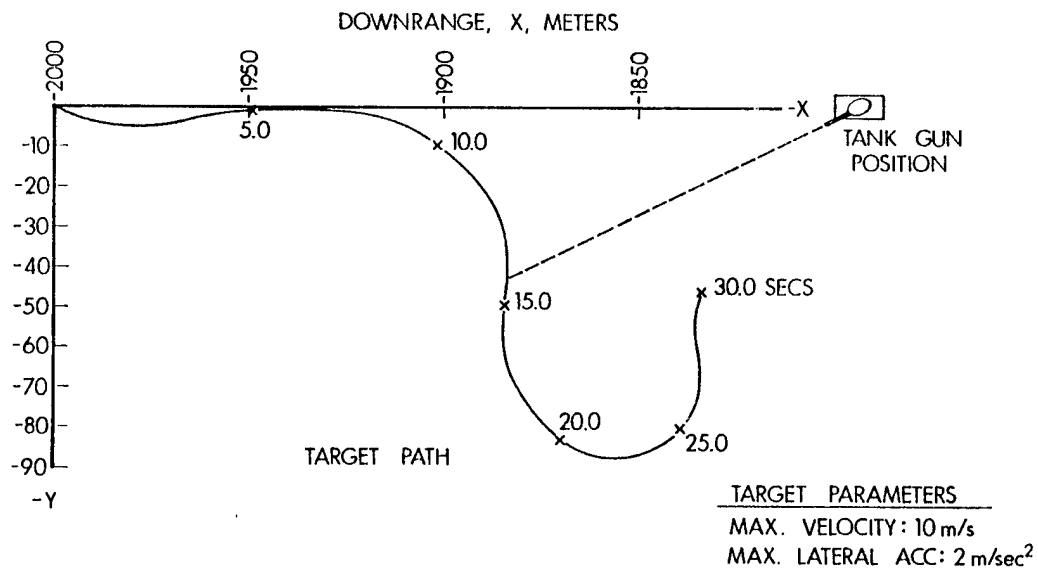


Figure 2. Typical Maneuvering Target Path.

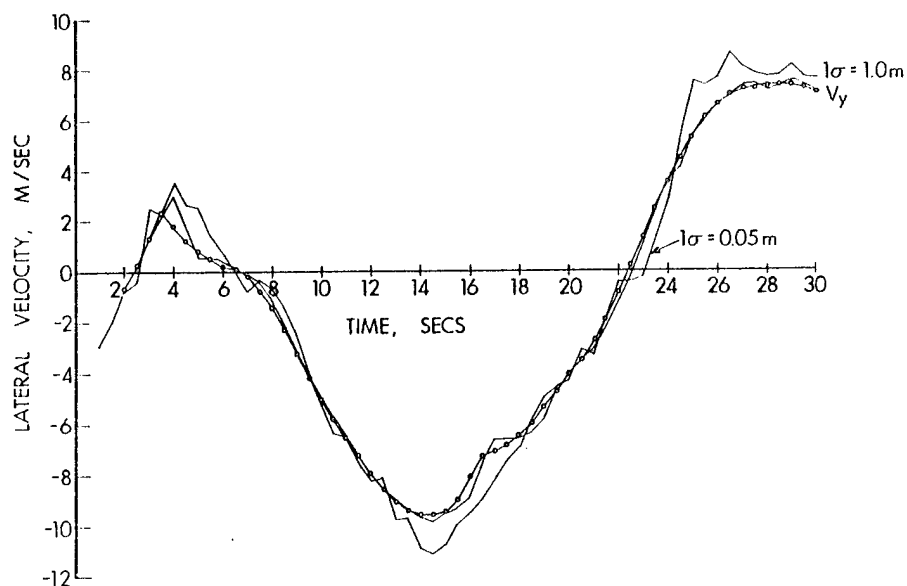


Figure 3. Sensitivity of Velocity Estimates to Observation Noise.

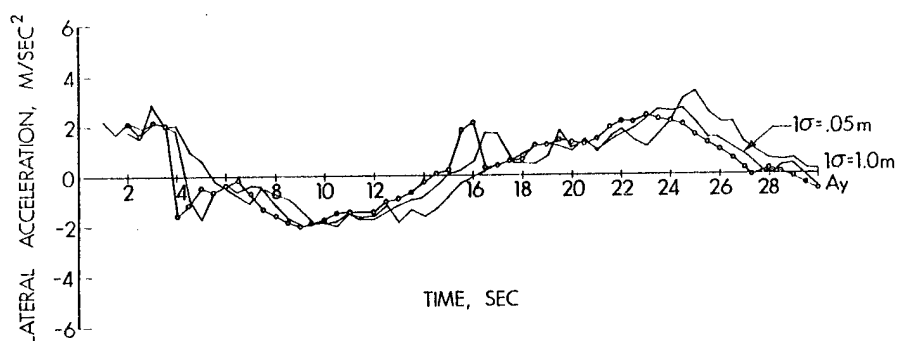


Figure 4. Sensitivity of Acceleration Estimates to Observation Noise.

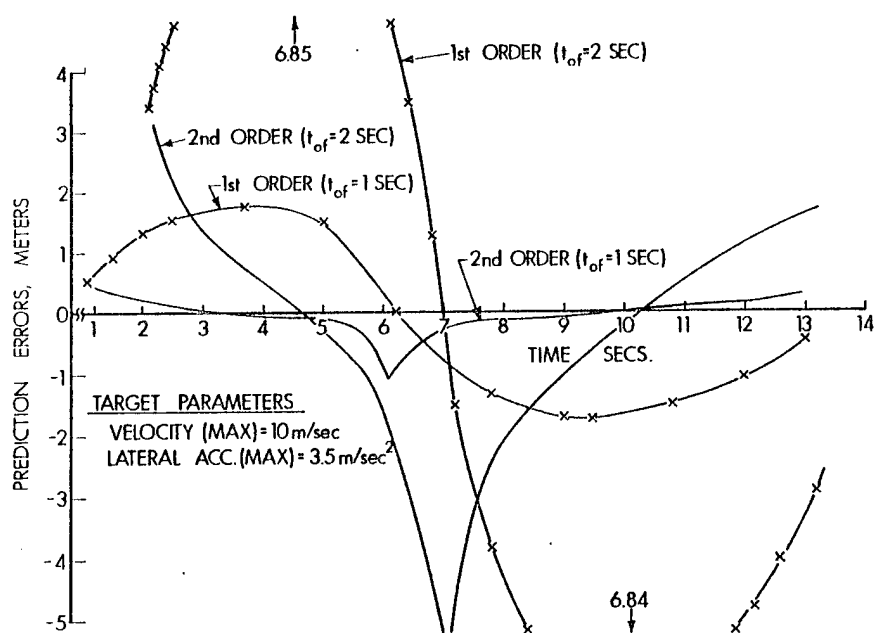


Figure 5. Effects of Time-of-Flight on Prediction.

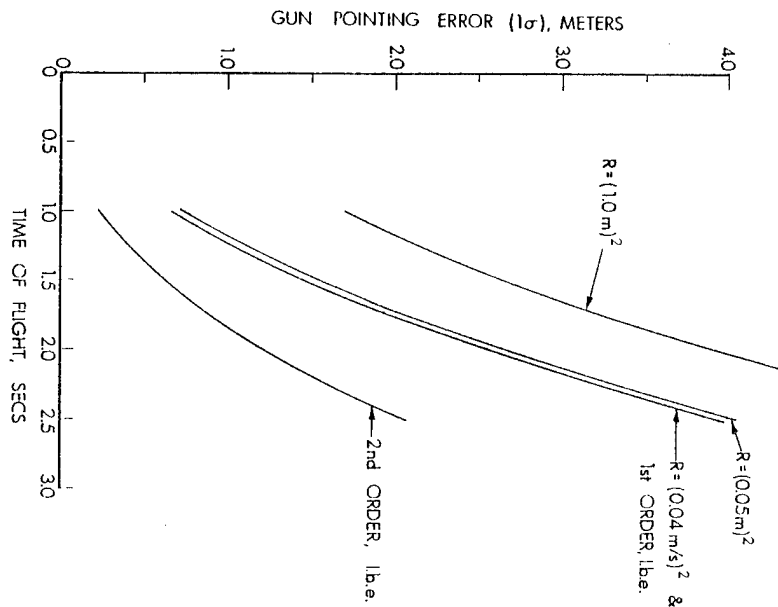


Figure 6. First Order Prediction Errors.

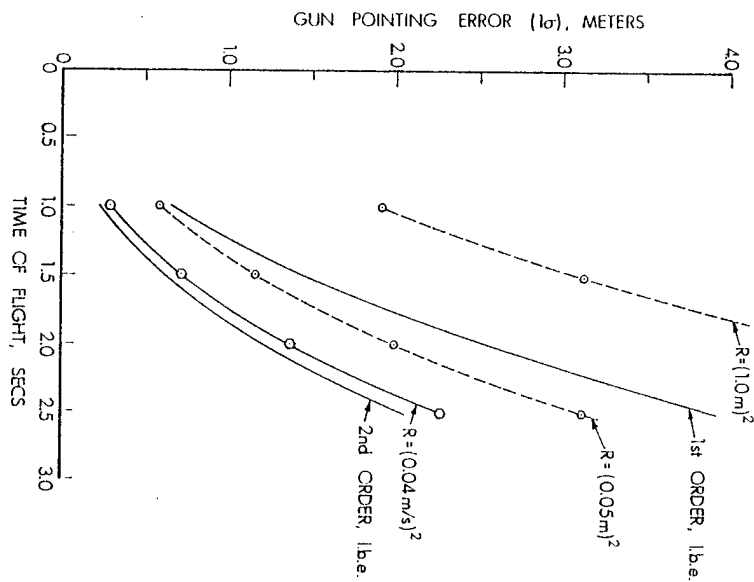


Figure 7. Second Order Prediction Errors.

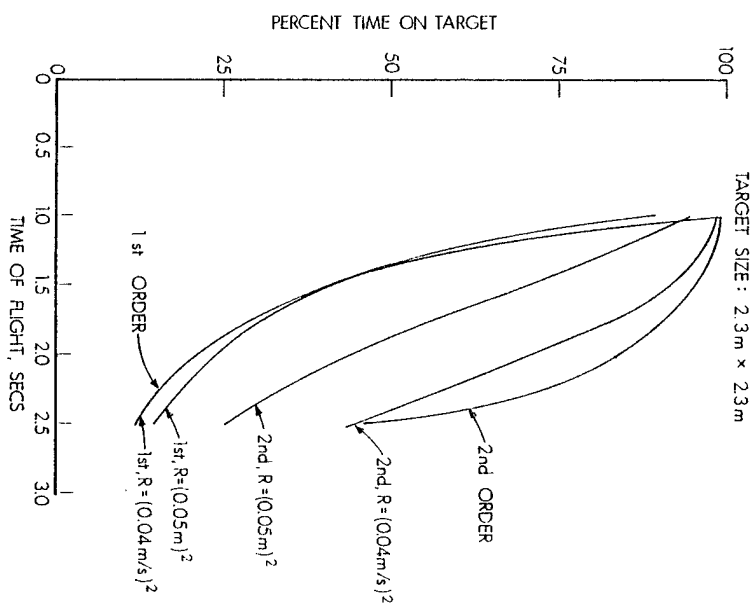


Figure 8. Time on Target.

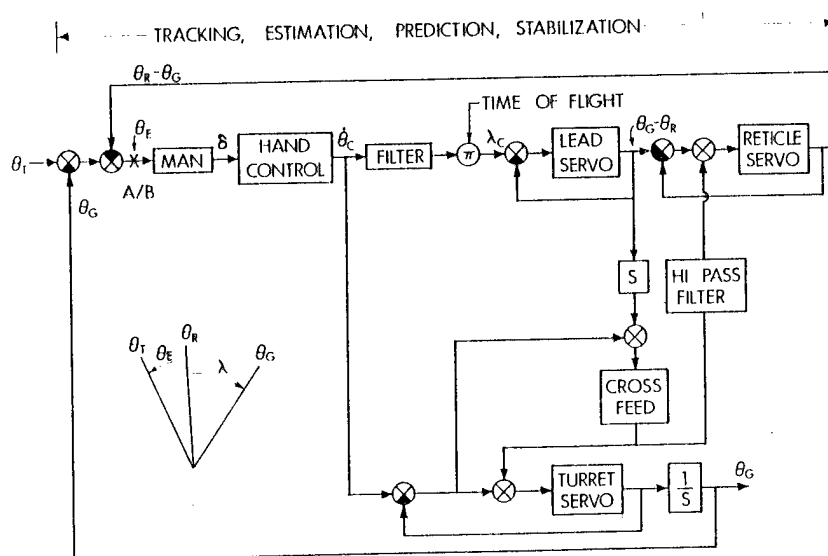


Figure 9. Disturbed Reticle Fire Control System.

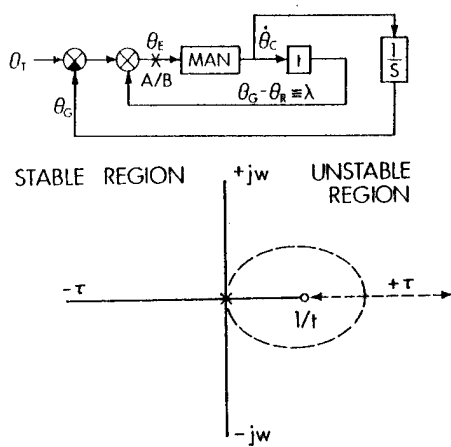


Figure 10. Disturbed Reticle Root Locus, Fixed Elements.

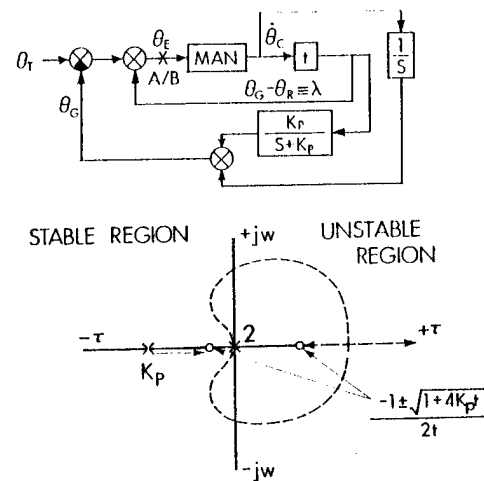


Figure 11. Disturbed Reticle Root Locus, Turret Servo Crossfeed.

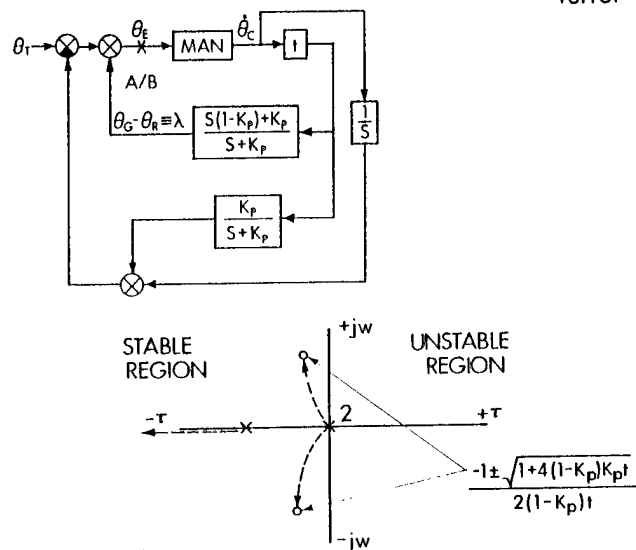


Figure 12. Disturbed Reticle Locus with Turret Servo and Reticle Crossfeeds.

NON-LINEAR LEAST CHI-SQUARE ALGORITHM
AN IMPROVEMENT ON NON-LINEAR LEAST SQUARES

Richard L. Moore, PhD
Armament Research and Development Command
Dover, N.J. 07801

INTRODUCTION

Because of the high cost of testing, many large weapon systems cannot be tested over the full range of possible battlefield parameters. As a result, the developer and the reviewing authorities have come to rely on system simulation to demonstrate the system capability over the range of untested parameters. These simulations also are useful to investigate the change in performance resulting from possible subsystem modifications. In some important programs, the Government relies on simulations of competing systems to indicate the relative performance of these systems in situations for which no tests have been made, although of course, simulations such as these have been validated as much as possible by system tests. In these instances the procurement decision rests heavily on the validity of the system simulations. Consequently the need arises for a generally accepted procedure which is without question fair to each contractor and which provides the maximum amount of objective judgment about the validity of the simulation. In any such procedure the Government must be able to rapidly evaluate simulations furnished from a variety of sources.

The procedure must be workable and economical -- that is it must apply a lot of leverage to the problem with regards to manpower, -- computer programmers and engineers -- the cost, -- computer running time and validation experiments -- and elapsed time. Implicit in this discussion is that planning for system simulation validation must be completed before the first system RFQ is issued.

RELATION TO OTHER METHODS

Many methods are used for system simulations: Monte Carlo, analog, hybrid, and digital simulation of differential equations. A variety of special and general purpose programs are available for the simulator's use. Among them are "SPERT", "ACSL," and HIT PRO." The problem for the user of these simulations comes when he needs to compare theory with experiment and asks the questions: How good is the theory? Is the agreement between theory and experiment good enough to validate the simulation? (As an example of these questions see Pastrick (1,2).) Another question to be considered is: Could it be that the experiment was defective in any way?

Many simulations have not been prepared in such a way so that they can be used to answer these questions. In the first place, the simulations are not designed to adjust parameters to fit data. In the second place, the system itself may be so complex that the computing time for complete system simulation is so long that adjusting the parameters to achieve a better fit between simulation and experiment is not feasible. Thus a new procedure is needed to combine theory and experiment.

The procedure suggested by this paper is the use of the least chi square computer program to simulate the major subsystems of a system simulation and validate it against test data.

CRITERIA FOR COMPARISON, AND ITERATION PROCEDURE

In fitting data to non-linear models of system performance such as systems of differential equations, the usual criteria is the iterative minimization of the sum of the squares of the residuals. Other criteria, such as generalized least squares have also been considered and demonstrated (3). In general, as Aitken (4) noted with respect to generalized least squares, the criteria to be used are a matter of choice. In other words, we are free to decide whether least squares is the best criteria for our purpose. A particular concern with the ordinary least squares procedure is whether the residuals are consistent with being drawn from a random sequence.

Many tests have been devised (5) for this purpose. One test of special interest in this paper is the Box-Pierce (6) test which is the sum of the squares of the autocorrelation coefficients divided by their variances. A typical term is r_j^2/V_j .

Given all these tests, no way had been devised to adjust the parameters to better satisfy the data until it was proposed that this criteria be combined with least squares to obtain a new criteria; least chi-square (Moore, 7, 8, 9). By finding the parameters which minimize chi-square, the probability is maximized that the residuals should come from a population with a given variance σ_e^2 , and from a random sequence. The variance be independently determined from theory or measurement as the measurement error.

Thus, a probability can be generated from the computed chi-square which permits the statistician and decision-maker to compare the "goodness of fit" of the simulation of several quite different systems. In this way a direct comparison of the validity of the simulations can be made.

The figure of merit, χ_T^2 (chi-square total) is the sum of $\sigma_e^{-2} d'd$ and $\sum_{j=1}^S r_j^2/V_j$ the Box-Pierce number.

DERIVATION

We will follow the procedure and most of the notation of Aitken (4) for generalized least squares:

Let the representation of the vector of data:

$$u = \{u(x_1), u(x_2), \dots, u(x_n)\}$$

by the theoretical vector, be:

$$y = \{y(x_1), y(x_2), \dots, y(x_n)\}$$

Let θ^* denote a column vector of $k + 1$ coefficients independent of x such that:

$$\theta^* = \{\theta_1^*, \theta_2^*, \theta_3^*, \dots, \theta_{k+1}^*\}$$

Define the matrix P^* as the matrix whose i th row is

$$\frac{\partial y_i^*}{\partial \theta_1}, \frac{\partial y_i^*}{\partial \theta_2}, \dots, \frac{\partial y_i^*}{\partial \theta_{k+1}}$$

(The asterisk symbol $*$ will be used to indicate an estimate or the indicated symbol where convenient. However, it will not be used on complex expressions involving χ_T^2 , $d'd$, and r_j^2 because of typographical difficulties).

In this expression V_j^{-1} is defined as follows:

$$V_1^{-1} = \begin{bmatrix} 0 & 1 & 0 & \dots & 0 \\ 0 & 0 & 1 & 0 & \dots & 0 \\ 0 & 0 & 0 & 1 & 0 & \dots & 0 \\ \dots & & & & & & \end{bmatrix}; V_2^{-1} = \begin{bmatrix} 0 & 0 & 1 & 0 & \dots & 0 \\ 0 & 0 & 0 & 1 & \dots & 0 \\ 0 & 0 & 0 & \dots & \dots & \dots \end{bmatrix} \quad V_j^{-1} = \begin{bmatrix} 0 & 0 & \dots & 0 & 1 & \dots & \dots \\ 0 & 0 & 0 & \dots & \dots & 0 & 1 & \dots & \dots \\ \dots & & & & & & & & \end{bmatrix}$$

In these, the subscript "j" indicates a unit value in each of the ith rows and (i + j)th column.

If V_j is the variance of r_j^2 , then $\chi_T^2 = \sigma_e^{-2} d'd + \sum_{j=1}^S r_j^2 / V_j$

and: $\kappa_j = d' V_j^{-1} d / (dd')$

(Note the difference between V_j^{-1} and V_j^{-1} .)

On differentiating (χ_T^2) with respect to (θ^*) and substituting

$$\{d^*\} = P^* [\delta\theta^*] - u^*.$$

as an estimate of the increment of the residuals needed to minimize χ_T^2 , the algorithm for $\delta\theta^*$ becomes:

$$[\delta\theta^*] = [P^{*'} \Gamma P^*]^{-1} P^{*'} \Gamma u^*.$$

where:

$$\Gamma = I + \sum_{i=1}^S \alpha_i r_i V_i^{-1} \quad \alpha_j = \frac{2 V_j^{-1}}{(d)'(d) / \sigma_e^2 - 2 \sum_{i=1}^S (r_i)^2 V_i^{-1}}$$

If Γ equals I, the expression for $\delta\theta^*$ reduces to $[P^{*'} P^*]^{-1} P^{*'} u^*$, which is the same as the algorithm for ordinary non-linear least squares used in such computer programs as provided by both IBM and CDC libraries as well as in SAAM-27.

By inspection, $P^{*'} \Gamma$ replaces $P^{*'}$ in the ordinary expression. To modify the ordinary expression, Γ is computed. $P^{*'}$ is postmultiplied by Γ , and the product placed in the computer memory where $P^{*'}$ is normally stored. χ_T^2 is substituted for $d'd$ wherever it occurs and no further change is needed in the iteration procedure.

SAACH COMPUTER PROGRAM

These expressions have been programmed into the Simulation and Analysis Modeling (SAAM-27) program of Berman et al. (10, 11) as indicated above, multiplying $P^{*'}$ by Γ , and letting the program proceed from that point. The usual iteration continues. The computer program resulting from this change has been designated as SAACH, and has been tested on the CDC 6600 at ARRADCOM, Dover, to determine the following questions:

1. How much change is there in the final parameter estimates?
2. What change, if any, is there in the number of iterations?
3. What change is there in the time per iteration?

Four problems of different origin and which use different mathematical models have been run on the SAACH program to answer the above questions. In the first example: Gun Chamber Pressure Waves, the mathematical model used is the superposition of two pressure waves generated by analytic models in the program, with the adjustment of up to eight parameters to obtain the best fit to observed data. In the second example, an aircraft control system simulation, the mathematical model is a set of four linear differential equations, simulating the Yaw Damper system on an aircraft. These equations were solved by a special procedure developed for SAAM-27 by Berman et al. (12), with up to four adjustable parameters. In the third example, a biomedical problem furnished as a test case by Miss Rita Straub of Brookhaven National Laboratory, the mathematical model was a set of seven coupled linear differential equations with five adjustable parameters; this was solved by the same method as used in the second case. In the fourth and final example: KEWB Kinetics, a simulation of the nuclear reactor transients of the Kinetic Experiment Water Boiler, the mathematical model was an extremely non-linear set of coupled differential equations as described by Hetrick and Gamble (13). These equations were integrated by the fourth order Runge-Kutte integration procedure of SAAM-27, with only one adjustable parameter. The results of the analysis which were discussed at the 1978 Design of Experiments Conference (9) and at the Army Science Conference are no longer valid because of corrections and changes made in the SAACH Computer Program. The nonlinear examples which follow have been run with the revised program.

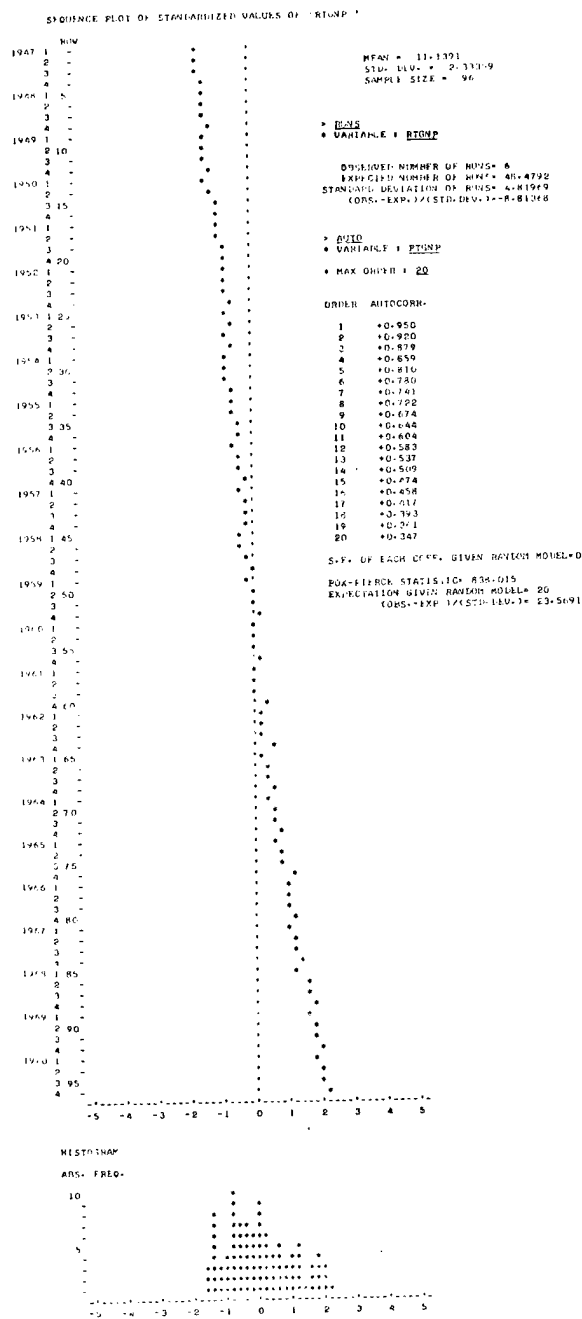


Figure 11-2. Square Root Transformation of GNP Data

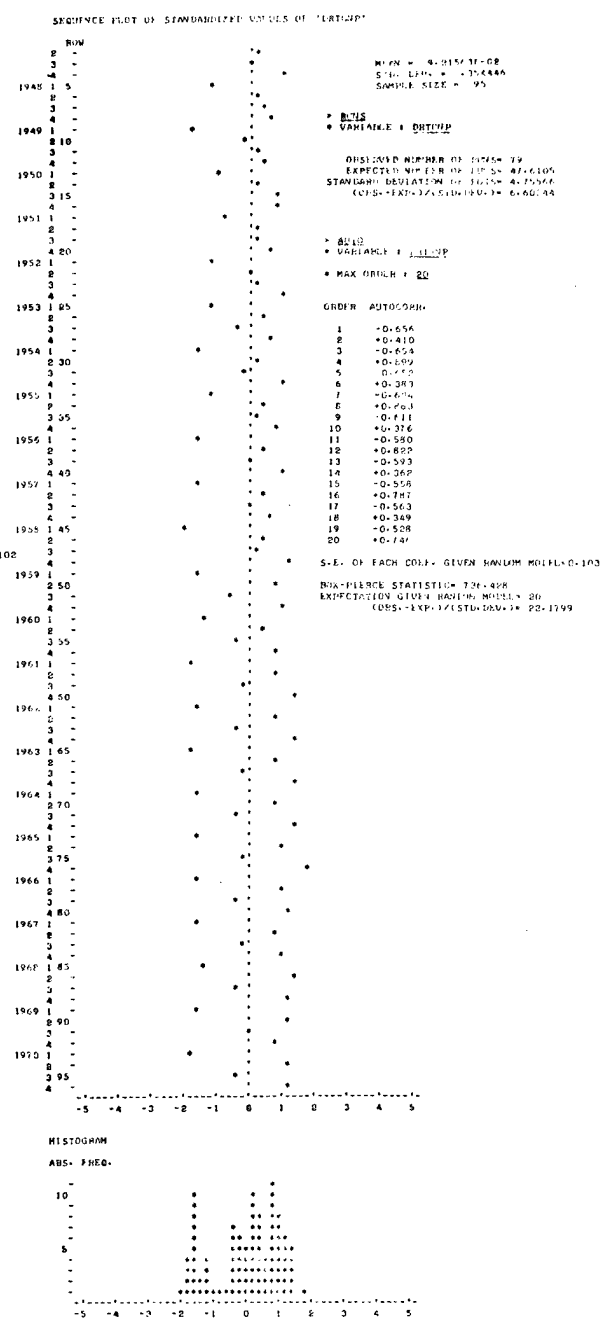


Figure 11-3. First Differences of GNP Data

Fig. 1 - Basic Data on GNP from Roberts' Analysis

Fig. 2 - First Differences from Roberts' Analysis

Order	1st Differences*	Fitted+		1st Differences	Fitted
1	-.686	.627	Box-Pierce) Statistic)		
2	+.410	.744		351.46	334.97
3	-.684	.544		8	8
4	+.899	.873	Ratio	43.9	41.9
5	-.652	.460			
6	+.383	.580	χ^2_T	363	354
7	-.624	.377	D.O.F.	104	104
8	+.863	.737			
9	-.611	.3057			
10	+.376	.4411			

Table 1 - Autocorrelation Coefficients for First Differences of GNP

σ_e	.1	.1	1.	
Mean	.0.	-.00045	.0021	
Order				Lagged
1	.284	.283	.284	-.041
2	.163	.163	.164	+.018
3	-.140	-.140	-.140	-.144
4	-.559	-.559	-.560	-.082
5	-.317	-.316	-.318	-.011
6	-.268	-.268	-.269	.038
7	-.048	-.048	-.049	-.052
8	.129	.129	.129	-.169
9	.184	.184	.184	-.001
10	.176	.176	.176	-.060
χ^2_1	1.31X10 ⁴	1.31X10 ⁴	1.31	
χ^2_2	58.09	58.05	58.21	
χ^2_T	1.32X10 ⁴	1.32X10 ⁴	59.53	

Table 2 - Analysis of Autocorrelations and
Chi-Square for Fourth/First Differences
of GNP.

CASE

UNITS	SYMBOL	301	301-5	301-10
kpsi	P_1	19.89	19.73	19.74
kpsi	P_2	5.245	4.633	4.445
sec	t_1	.0568	.0568	.0568
sec	t_2	.0555	.0557	.0557
sec	t_3	.0565	.0564	.0564
sec	σ_1	.00271	.00276	.00275
sec	σ_2	.00051	.00050	.000492
Hz	f	262.4	319.1	324.8
No. of Iterations		10	8	6
Computing Time (sec)		26.6	23.3	20.2

Table 3. Parameters Fitting Pressure Curve

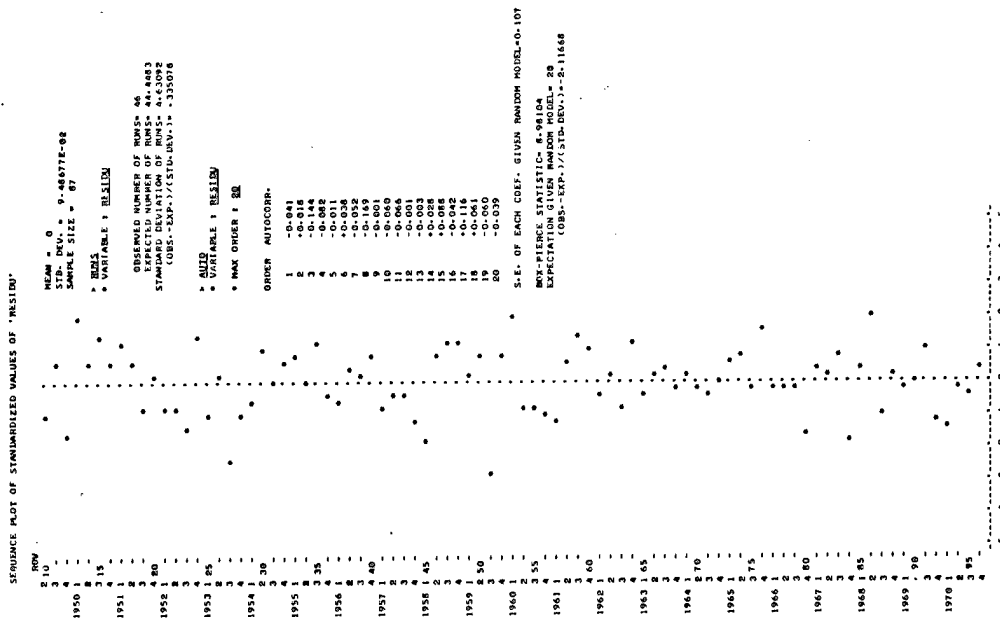


Fig 3 - Residuals after Completion of Roberts Analysis

GROSS NATIONAL PRODUCT

As an example of an analysis by the least chi-square method, I have repeated the analysis made by Roberts (17) in his book designed to introduce business students and other non-mathematicians to the Box-Jenkins methods of time series analysis. He has included a detailed analysis of the residuals, including an analysis of the "runs" and the Box-Pierce statistic. In Roberts' book, the emphasis is on predicting the future values in the series rather than system-parameter identification. The procedure is to introduce "differences" to accommodate the principal auto-correlations in the data, and then to use multivariate regression analysis on the residuals from this process using as predictors the lagged values of the residuals.

Figure 1 shows his initial analysis. The autocorrelation coefficients of rank 1 to 20 are large and he decides in accord with standard procedure to take the first 10 differences as shown in Figure 2. As shown in Table 1, the autocorrelations are still rather high, and the Box-Pierce statistic, or X_2^2 , is 351.46 for the first ten autocorrelations. I have used a linear least chi-square program to fit the data given in Figure 1 and find that the autocorrelations, and the residuals, are somewhat smaller, as shown in the column labeled "fitted".

Next, Roberts took the fourth differences to get a better fit to the data. The residuals are shown in Figure 3. As shown in Table 1, the autocorrelations for the case of a mean value of 0.0, which is the same as Roberts' case (I have recalculated the autocorrelation coefficients by my program, so as to have comparable data), have been greatly reduced. Using the linear least chi-square program on the same data, i.e., first and fourth differences, it iterated to find a mean of -.00045 for an "experimental standard deviation" of .1 to .0021 for 1.0, and to 0.0 for $\sqrt{2}$. As can be seen by the autocorrelation in Figure 2 and the value of X_2^2 , fit is slightly better for a mean of -.00045 than for the Roberts case of a mean of 0. The other values of σ_e tend to give slightly poorer values of X_2^2 .

The column called "lagged" is result of Roberts' calculations when the residuals are correlated with lagged values. I have not yet analyzed this case, because my linear program must be modified to do multiple linear regression. This is a simple change, and should be easy to do, and then the method can be used to extend the Box-Jenkins procedure.

GUN CHAMBER PRESSURE WAVES

Unusual pressure waves, suggestive of an acoustic wave superposed on the normal gun chamber pressure-time curve, have occurred in tests of the XM211 propellant charges at zone 3 for the M101 projectile in the 155mm gun (Knutelski (14)). The mathematical model used was:

$$P = P_1 \exp \left\{ - (t-t_1)^2 / 2\sigma_1^2 \right\} \\ + P_2 \exp \left\{ - (t-t_2)^2 / 2\sigma_2^2 \right\} \times \sin \left\{ 2\pi f (t-t_3) + \pi/2 \right\}$$

Three parallel cases were computed once the fit was good enough to permit iteration with different ranks of autocorrelation. Because of computing difficulties which arose when trying to converge on six or seven parameters, the iteration was initially restricted to four parameters: Once the fit was good and had converged using these four parameters, their final values were used as initial values for a six-parameter fit. Finally, all eight parameters were allowed to vary.

Two results of this series of analysis are plotted in Figures 4 and 5. The case numbers using these data are BGK-3.30356301-0, -5, -10 (-5 is not shown). The first (-0) used the usual non-linear least squares procedure; the others used 5 and 10 autocorrelations respectively. The parameters found in these cases are given in Table 1. In some cases, some of the parameters have substantially different values.

The "eyeball" fit from comparing the two plots (Figures 4 and 5) indicates a slightly better fit for the case of ten autocorrelations, as shown in Figure 5. A comparative plot of the residuals should probably be made to observe any difference, if any. There is a large difference in the total chi-square, as shown in Table 3. Case 301-10 has a much better fit on the basis of this number.

Case -5 appears to be anomalous because the total chi-square is larger than that for Case -0, contrary to theory. This result indicates that Case -5 has not really completed its needed number of iterations. When more are tried, they may reduce the chi-square total further. (Due to the need to complete this report for publication deadline, these results will not be presented.)

EXAMPLES

GROSS NATIONAL PRODUCT

As an example of an analysis by the least chi-square method I have repeated the analysis made by Roberts (17) in his book designed to introduce business students and other non-mathematicians to the Box-Jenkins methods of time series analysis. He has included a detailed analysis of the residuals including an analysis of the "runs" and the Box-Pierce statistic. In Roberts book the emphasis is on predicting the future values in the series rather than system-parameter identification. The procedure is to introduce "differences" to accomodate the principal autocorrelations in the data, and then to use multi variate regression analysis on the residuals from this process using as predictors the lagged values of the residuals.

Figure 1 shows his initial analysis. The autocorrelation coefficients of rank 1 to 20 are large and he decides in accord with standard procedure to take the first differences as shown in Figure 2. As shown in Table 1, the autocorrelations are still rather high, and the Box-Pierce statistic, or χ^2_a is 351.46 for the first ten autocorrelations. I have used a linear least chi-square program to fit the data given in Figure 1 and find that the autocorrelations, and the residuals are somewhat smaller as shown in the column labelled "fitted".

Next, Roberts, took the fourth differences to get a better fit to the data. The residuals are shown in Figure 3. As shown in Table 1., the autocorrelations for the case of a mean value of 0.0, which is the same as Roberts case - (I have recalculated the autocorrelation coefficients by my program, so as to have comparable data), have been greatly reduced. Using the linear least chi-square program on the same data, i.e. first and fourth differences, it iterated to find a mean of -.00045 for an "experimental standard deviation" of .1, to .0021 for 1.0, and to 0.0 for $\sqrt{10}$. As can be seen by the autocorrelation in Figure 2 and the value of χ^2_a , fit is slightly better for a mean of -.00045, than for the Roberts case of a mean of 0. The other values of σ^2_{ϵ} tend to give slightly poorer values of χ^2_a .

The column called "lagged" is result of Roberts calculations when the residuals are correlated with lagged values. I have not yet analysed this case because my linear program must be modified to do multiple linear regression. This is a simple change, and should be easy to do, and then the method can be used to extend the Box-Jenkins procedure.

GUN CHAMBER PRESSURE WAVES

Unusual pressure waves suggestive of an acoustic wave superposed on the normal gun chamber pressure-time curve, have occurred in tests of the XM211 propellant charges at zone 3 for the M101 projectile in the 155mm gun. (Knutelski, (14)). The mathematical model used was:

$$P = P_1 \exp\{-(t-t_1)^2/2\sigma_1^2\} + P_2 \exp\{-(t-t_2)^2/2\sigma_2^2\} \times \sin\{2\pi f(t-t_3) + \pi/2\}$$

Once the fit was good enough to permit iteration three parallel cases with different ranks of autocorrelation were computed. Because of computing difficulties which arose when trying to converge on six or seven parameters, the iteration was initially restricted to four parameters: Once the fit was good and had converged using these four parameters, their final values were used as initial values for a six-parameter fit. Finally, all eight parameters were allowed to vary.

Two results of this series of analysis are plotted in Figs 4, and 5. The case numbers are BGK-3.30356301-0, and 3.303301-10. The first has no autocorrelation coefficients; second 10, third (not shown) 5. The parameters for these cases are given in Table 3, (note that the last three digits only of the identifier are used here). Some parameters are quite different from case to case.

The apparent fit from the figures is best for the case of autocorrelations given in Fig. 5. The fit of this case was about the same as that for 5 autocorrelations which is not illustrated.

The reason for this conclusion lies in the fit to the second peak. The dip and peak fit better for Fig. 5 than in Fig. 4. As seen in Table 4 the higher order autocorrelations are less for Case 301-10 than for Case 301, thereby confirming the above eyeball test. The Box-Pierce number, χ^2_a , is much smaller for 301-10 than for 301, but the sum of the squares has only about 4% difference.

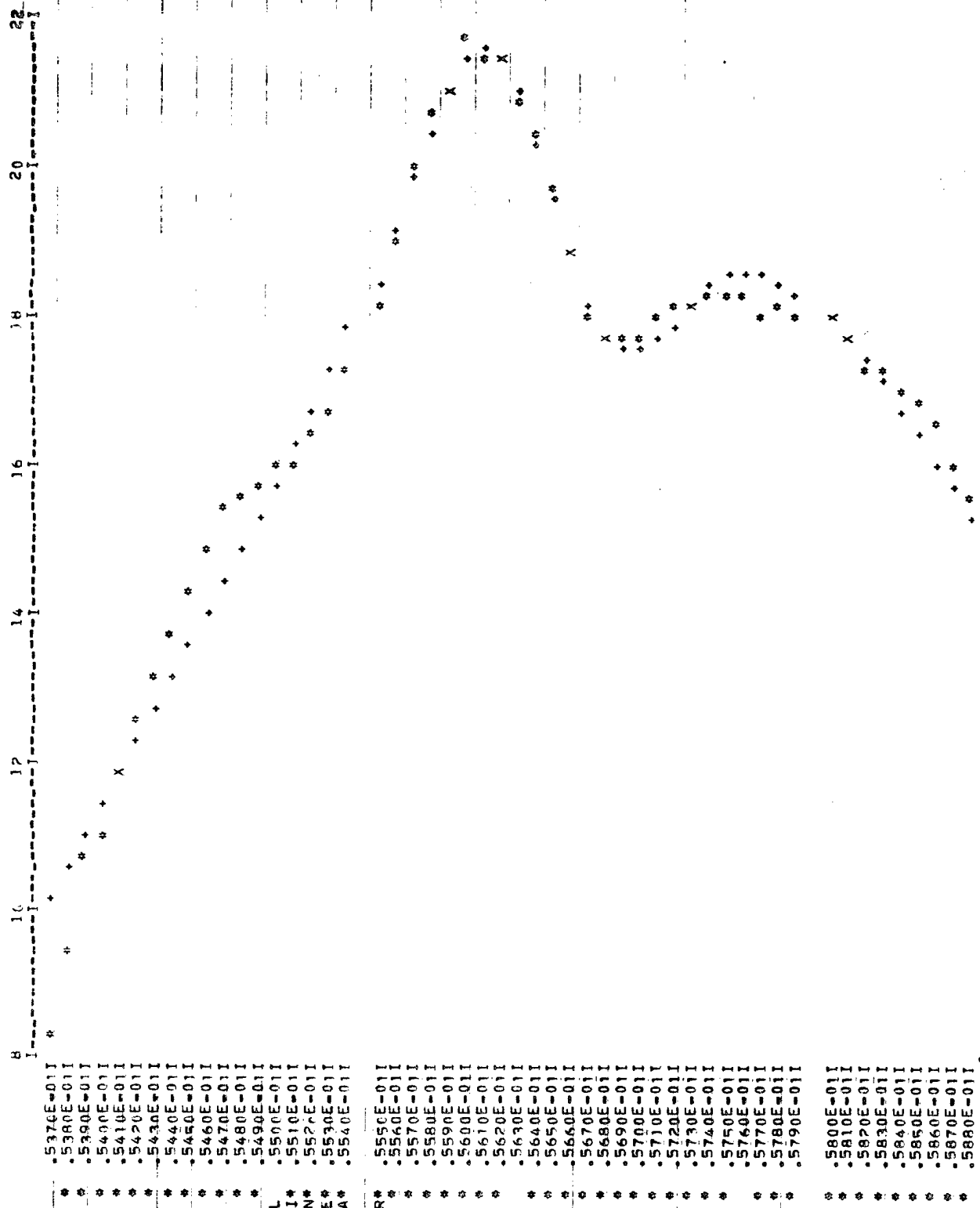


Fig. 4 - Plot of Experimental and Theoretical Points for Pressure Oscillation, Case 301-0 ("*" are experiment, "+" are Theoretical, "X" indicate both Coincide at that point).

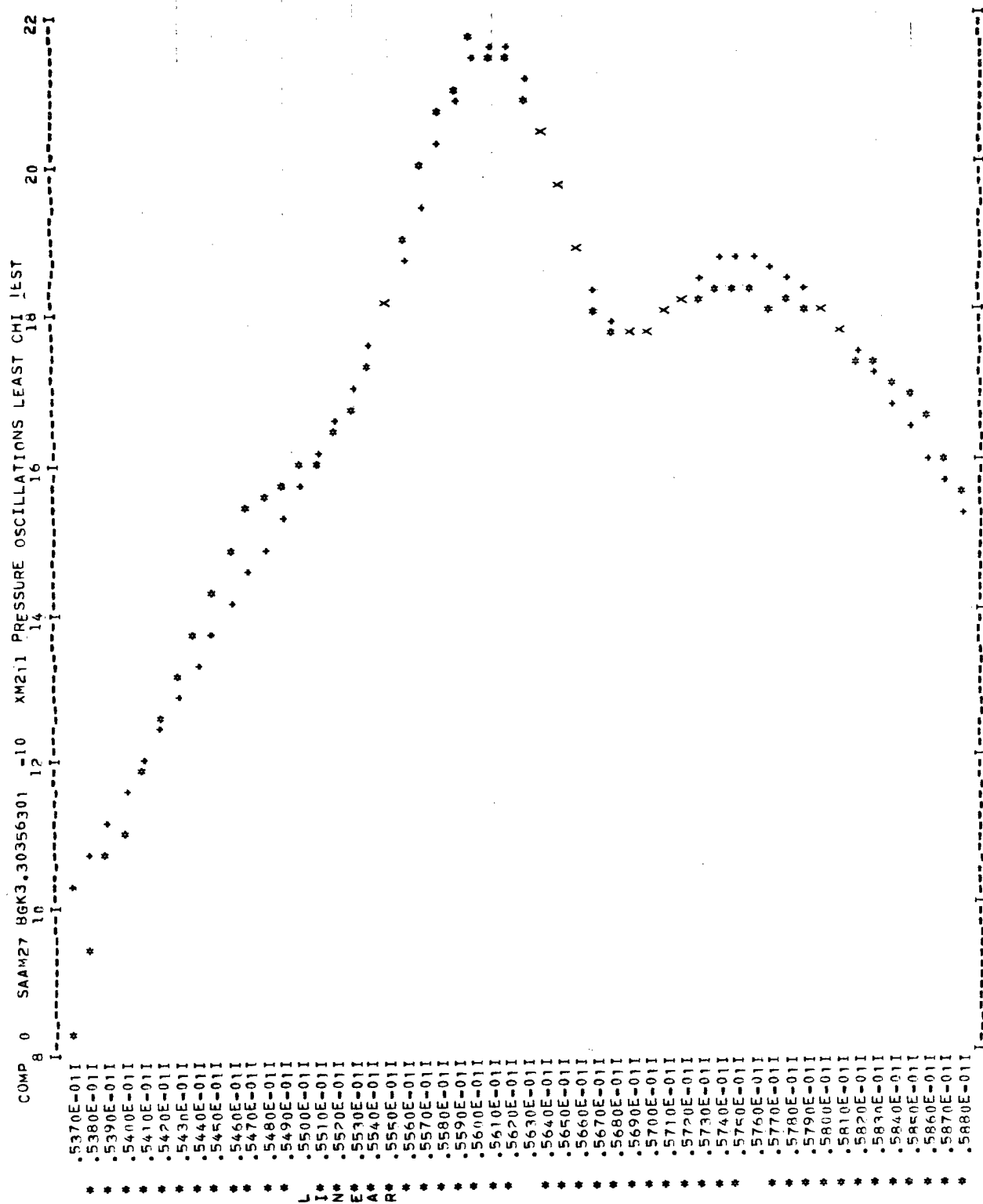


Fig. 5 - Plot of Pressure Oscillation for Case 301-10

CASE	301	301-5	301-10
ORDER			
1	.702	.692	.708
2	.445	.437	.464
3	.242	.250	.282
4	-.019	.011	.050
5	-.225	-.170	-.124
6	-.396	-.312	-.259
7	-.482	-.378	-.319
8	-.518	-.407	-.314
9	-.504	-.399	-.300
10	-.423	-.338	-.272
11	-.251	-.202	-.154
12	-.063	-.062	-.035
13	.092	.041	-.044
14	.243	.147	.121
15	.255	.128	.074
16	.247	.104	.021
17	.124	-.016	-.123
18	-.026	-.149	-.278
19	-.113	-.208	-.356
20	-.167	-.233	-.394
Sum Sqs	10.40	10.99	11.34
χ^2_1	104.12	109.97	113.5
σ_e	.3161	.3161	.3161
$\chi^2_2 (5)$	34.69	33.82	
χ^2_{tot}	138.81	143.79	
$\chi^2_2 (10)$	74.902		53.94
$\chi^2_{tot} (10)$	179.02		167.46

Table 4 - Autocorrelations and Chi-Square for Final
Model of XM211 Pressure Oscillations

Table 3 shows the "cost" of least chi-square in terms of the number of iterations and computing time. In this example, it is found that the number of iterations decreased and the total time decreased, although the time per iteration obviously increased from 2.7, to 2.9, to 3.4 sec, depending on the number of autocorrelations which had to be computed.

Table 4 shows the autocorrelations up to order 20 for the three cases. The values of X_1^2 , X_2^2 , and X_{tot}^2 for the number of autocorrelations used (0, 5, 10) are shown in the last rows of this table.

AIRCRAFT CONTROL SYSTEMS

A typical aircraft yaw damper design problem (15) was analyzed to illustrate the use of least chi-square. To optimize the design, four parameters may be adjusted to give the best fit to a desired response curve. These parameters are δ , κ_β , κ_ψ , and τ^{-1} . These correspond to the parameters $L(0,4)$, $L(4,1)$, $L(4,2)$, and $L(4,3)$. A vector of a random sequence of normally distributed errors from a population with variance of $(.033)^2$ was added to the data vector to simulate the effects of sampling error; this may be considered to represent an allowable error or tolerance in fitting the curve.

The value of σ_e^2 was set at $(.033)^2$; six autocorrelations were used for the problem, which was identified as CONRLM 4.011-6. Another run was used on the same data with the standard least squares algorithm. Figure 6 shows the fit obtained for the data and is typical of the results. Table 5 shows the number of iterations for each case. It took 4 iterations for the ordinary algorithm to converge, and only two for the least chi-square algorithm with six autocorrelation coefficients (CONRLM 4.011-6). The times to complete iteration were 8.2 and 8.1 sec. respectively. (Part of the increase in time for the least chi-square case was due to several attempts in both iterations to improve the fit by reducing the step size.) As shown in Table 5, the parameters $L(0,4)$, $L(4,2)$, and $L(4,3)$ appear to be different by significant amounts. (The autocorrelations for Case 4.011-6 appear well within the random range.) The normalized sum of squares of the residuals is less, as expected, for the ordinary least squares, case 4.012.

BROOKHAVEN EXAMPLE

A sample test case was received from Miss Rita Straub of Brookhaven National Laboratory. The exact nature of the problem was unspecified, but from the form of the differential equations it appears to be a kinetic problem in which the material in component one decays into components two to five, and component two may change into component one. Component seven is composed of components three, four, and five. Although some coupling parameters may actually be unknown, they were assumed known, because the present version of the program will not iterate either type of linear coupling parameter with the least chi-square algorithm. The data were available for the amount of components 1, 3, 4, and 6 as a function of time (where component 6 is the sum of components 1, 2, and 5).

Two basic cases were run on these data--a case with no autocorrelations and a case with five autocorrelations. For the case of five autocorrelations, three subcases were run with different values of the estimated experimental standard deviation. Case (a) used .1 for σ_e ; Case (b) 1., and Case (c) 3.162. As seen from Table 6, a wide variation was found for the values of the parameter $L(1,2)$ and $L(2,2)$, depending on the value taken for σ_e . Comparing Case -5(b) with Case -0, the Box Pierce number, X_2^2 (Table 6), is smaller for the former than the latter. The number of iterations and the time required (Table 8) is larger for the -5(b) than for -0. The case of -5(c) seems to be anomalous in some respects, since the value of X_2^2 is much larger than for the others. The fact that the number of iterations are smaller also indicates that further iterations should be attempted, possibly by placing lower limit on $L(2,1)$ and $L(2,2)$.

REACTOR KINETICS EXAMPLE

This example illustrates two things: First, the use of the least chi-square algorithm and second, an apparently good fit between data and a physically incorrect model. Hetrick and Gamble (13) proposed a non-linear feed-back term proportional to the energy in the reactivity of the KEWB reactor to describe the fit. Later experiments (16), where the void amount was inferred from measurements and where the thermal effects on reactivity were also carefully measured, showed that shutdown was due to thermal--not void--effects. In the simulation, the effect of the energy on void formation was simulated by the parameter $L(11,1)$. The functions correspond, in numerical order, to the functions used in the simulation: (1) Nuclear reactor power

COMP 3 SAA-27 CORREL 4.011 -6 TEST YAW DAMPER BY LEAST CHI
 .03000 .00000 .00000 .00000 .00000 .00000 .00000 .00000

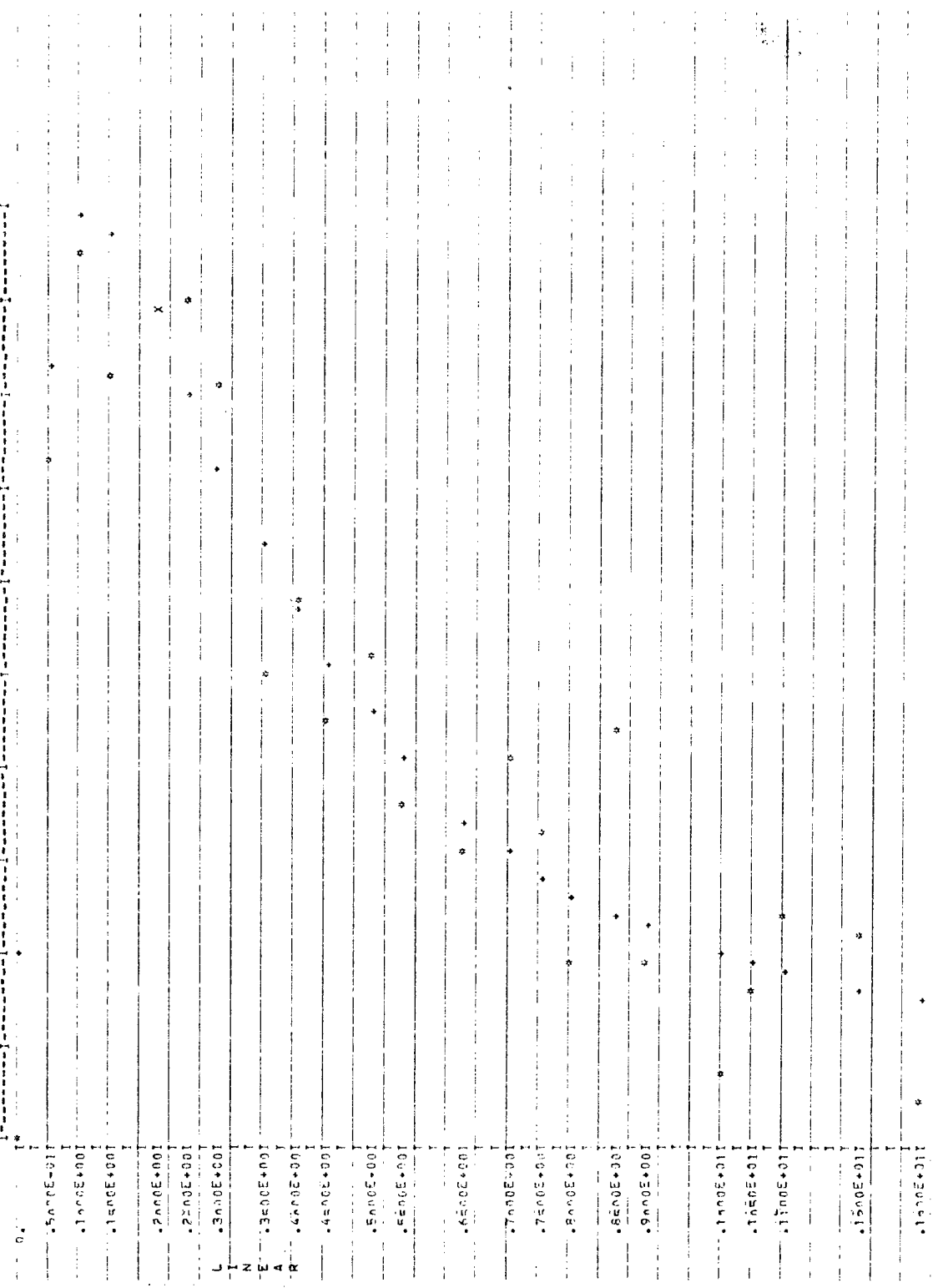


Fig. 6 - Plot of Simulated Points (*) and Computed Points for Yaw Damper Case 4011-6.

Case	4.012-0	4.011-6
No. of Iter.	4	2
Parameters		
L(0,4)	17.70	18.54
L(4,1)	53.11	52.91
L(4,2)	1.094	0.605
L(4,3)	6.204	10.25
Order		
1	-.116	-.113
2	-.247	-.248
3	.009	.014
4	.120	.076
5	-.151	-.149
6	.029	.036
Sum/Sqs	.03147	.03144
x_1^2	28.89	28.87
x_2^2	2.82	2.42
x_T^2	31.71	31.29

Table 5 - Results of Yaw Damper Calculations

ITEM/CASE	KJE 1.0021-0	(a)	KJE 1.0023-5 (b)	(c)
L(1,2)	.2155	.2295	.3337	9.787
L(2,1)	.4527	.4496	.4908	5.763
L(3,1)	.0431	.0434	.04495	.0500
L(4,1)	.0252	.0253	.0269	.0400
L(5,1)	.0743	.0869	.1255	.2388
Order				
1	.119	.087	.052	.145
2	.026	.022	.025	.236
3	.082	.086	.098	.004
4	-.287	-.216	-.229	-.269
5	.067	.054	.033	.012
σ_e	1	.1	1	3.162
x_1^2	31.22	3122.	31.72	10.30
x_2^2	2.65	1.26	1.31	3.016
x_{TOT}^2	33.87	3123.	33.03	13.316

Table 6 - Results of Brookhaven Example Calculations.

level, (2) Mean temperature, (3) Mean void volume, (4)-(9) Delayed neutron groups, (10) Not used, (11) Energy released to that time. The result of the iterations is shown in Figure 7, a logarithm plot of theoretical and experimental nuclear power. In Table 7, three different cases are shown:

Case 1.003-0 was ordinary least-squares. The values of the autocorrelations and chi-squares are shown for comparison with the other two cases. Case 1.005-3 used three autocorrelations with a small value of the experimental variance, thus resulting in a large value of X_1^2 . Both Case 1.007-6 and 1.003-0 use 1×10^7 for the experimental variance, thereby reducing the emphasis on the sum of the squares of the errors.

Cases 1.003-0 and 1.005-3 give almost exactly the same results. All cases took four iterations to converge. On comparing 1.003-0 with 1.007-6, a difference is found in the value of the adjustable parameter $L(11,1)$. The value of chi-square total is smaller for 1.007-6, and thus this result would be chosen over that of the other case.

The value of the chi-square or the Box-Pierce number is much smaller for Case 1.007-6, although X_1^2 is slightly larger for the same case, thus illustrating the trade-off between getting the minimum as in ordinary least squares and reducing the autocorrelations as in least chi-squares. The data for Case 1.003 show the values for $R(1)$ to $R(6)$ for comparison purposes. The data show that the sum of squares does not increase from one to the other appreciably, but X_2^2 , the Box-Pierce statistic, does change appreciably. Each of the calculations give a total chi-square which is too large to be consistent with the residuals being drawn from a random sample, and thus would have given support for the rejection of the Hetrick-Gamble model.

SIMULATION OF NON-LINEAR CONTROL SYSTEM

In order to show the basic power of the SAAM 27 program, I have included this example. The servo system of the azimuthal axis of a laser tracking system is shown in Figure 8. This one-of-a-kind system was demonstrated under contract to DARPA several years ago. Analysis of this system is offered to show the challenge that the system simulator faces in terms of the significant non-linearities encountered.

The non-linearities are indicated by the symbol NL. Figure 9 shows the various types of non-linearities. NL_1 is a step function or hysteresis loop. NL_2 is a "sticking" type of non-linearity, where for small inputs, no change occurs. NL_3 is linear through the origin, but limits at larger values of the input signals. NL_4 has a response which is linear through the origin, but has a smaller slope at higher amplitude input.

Figure 10 shows the conventional diagram of this servo system; we note four non-linearities on this diagram. This system has been represented as a system of ten differential equations as shown in Figure 11.

An early attempt was made to use SAAM 27 to simulate these non-linearities in the given system. The non-linearity NL_1 has been successfully included by Dr. G. Gobel in an unpublished study, when the driving function was linear. Including the other non-linearities made it difficult to integrate the equations so that they were approximated by straight lines. We note that in the structure of the equations, even this approximation results in a non-linear system of integrations.

The azimuthal position was found to change exponentially in response to a linear input.

I believe that it will prove possible to better simulate this control system, given further work on the problem. It may be necessary to modify the program itself, to do this. In any event, although it may not be possible to do all non-linearities, it is a significant achievement to have a program like SAAM 27 available for general use.

I reiterate that no programming was required to do this simulation; the program itself has the inherent capability to do the simulation given the proper choice of input functions.

CASE	KWB 1.003-0	KWB 1.005-3	KWB 1.0007-6
L(11,1)	5.318×10^{-4}	5.3161×10^{-4}	5.2822×10^{-4}
Order			
1	.805	.805	.810
2	.467	.468	.483
3	.107	.108	.137
4	-.231	--	-.185
5	-.369	--	-.312
6	-.284	--	-.221
x_1^2	121.38	1.2×10^9	122.04
x_2^2	37.68		34.88
x_T^2	159.06	1.20×10^9	156.93

Table 7 - Results of Kinetic Experiment Water Boiler Calculations

Case	No. of Adjustable Parameters	Rank of Auto-correlation	No. of Iterations	Time (sec)
Gun Chamber Pressure Curve	8	0	10	26.6
	8	5	8	23.3
	8	10	6	20.2
Yaw Damper	4	0	4	8.2
	4	6	2	8.1
Biomedical Test Case			σ_e	
	5	0	7	19.12
	5	5	.1	21.95
	5	5	1.	37.43
	5	5	3.162	39.201
Reactor Kinetics Experiment	1	0	4	84
	1	3	4	95
	1	6	4	95

Table 8 - Comparison of Computing Time and Number of Iterations.

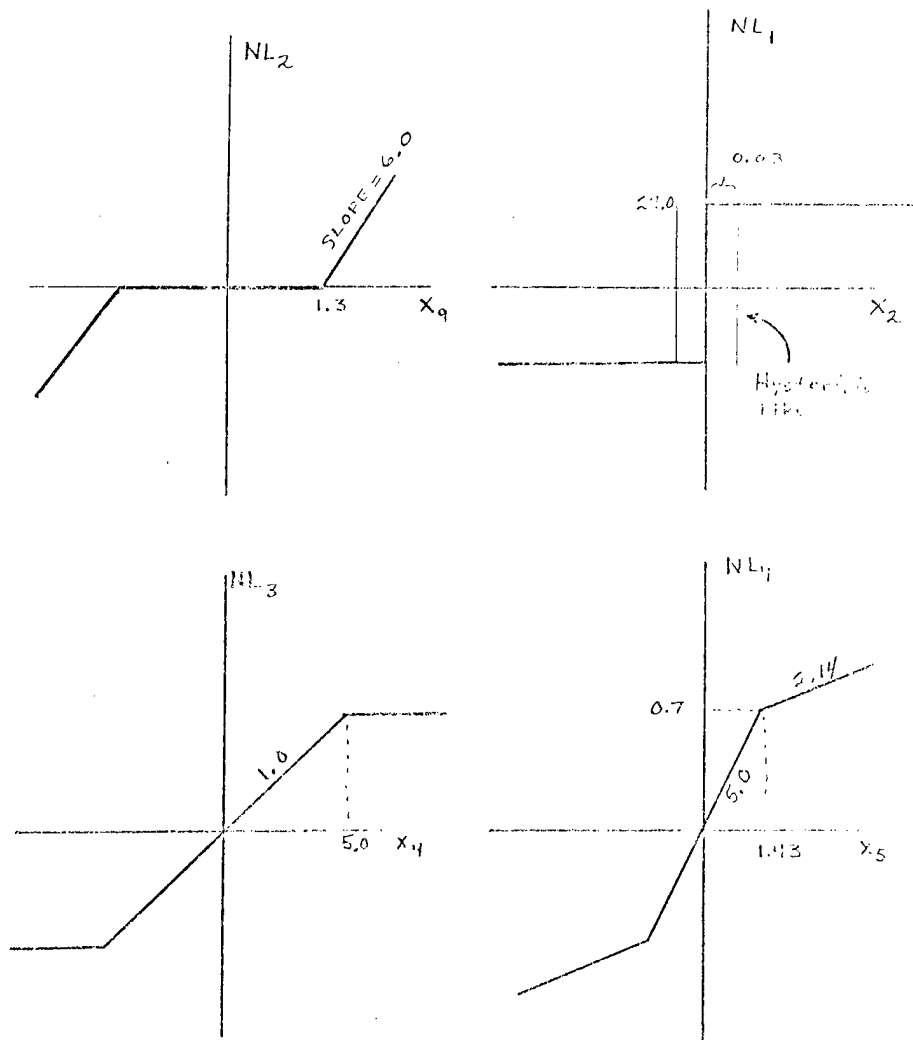


Fig. 9 - Diagram of Non-Linearities

$$\dot{X} = \begin{bmatrix} 0 & 1 & 0 & 0 & 0 & 0 & 0 & 0 \\ 0 & -\frac{1}{T}(D+NL_1) & K_T \frac{1}{T} & 0 & 0 & 0 & 0 & 0 \\ 0 & -\frac{K_1}{R_m T_e} & -\frac{1}{T_e} & -\frac{K_F NL_2}{R_m T_e} & \frac{K_F NL_4}{R_m T_e} & 0 & 0 & 0 \\ 0 & 0 & 0 & 0 & 1 & -\frac{b}{d} & -\frac{1}{a} & 0 \\ 0 & 0 & 0 & 0 & 0 & \frac{31.6}{d} & 0 & 0 \\ 0 & 0 & 0 & 0 & 0 & -1500 & 100 & 0 \\ 0 & 0 & 0 & 0 & 0 & 0 & \frac{10.90 NL_3}{130} & 0 \\ 0 & 0 & 0 & 0 & 0 & 0 & 0 & -\frac{52.5 NL_4}{13} \end{bmatrix} X$$

Fig 10 - Matrix of Differential Equations for Laser Tracker Servo System

COMPARISON OF COMPUTING TIME

Table 8 summarizes the comparison of the number of iterations to converge, and the computing time. The number of iterations was usually about the same. As seen in the last column the computing time is comparable, with a tendency for the computing time to be longer for least chi-square than for least squares. The relative difference is greater when the original total computing time is short. This just means that, as would be expected, it takes a larger fraction of the computing time to compute the matrix Γ and post-multiply into P^* for cases where the time of iteration is short.

CONCLUSIONS

Based on four different types of non-linear theoretical models for data analysis, our results indicate that:

- (1) Least chi-square is practicable for non-linear analysis.
- (2) Least chi-square gives a better fit, and may be a more reliable iteration procedure.
- (3) The computing time for least chi-square is longer for the models which use less computing time, but because the convergence of this iterative procedure is somewhat better, the number of iterations may be reduced, thus keeping the total computing time about the same. Those models with longer integrating time would be expected to benefit more from least chi-square.
- (4) In validation of simulations of future Army systems, the SAAM 27 computer program modified for least chi-square can be used at various states in the system development. First, as a tool to simulate subsystems and compare the projected performance with the designer's simulation. Second, as subsystems are built and tested, they can be run as "hardware in the loop" and the test data used in the least chi-square program to validate the computer simulation and provide system parameter identification. Because no programming is needed to run SAAM 27 on a variety of problems, both the programming time and the elapsed time is greatly reduced.

By planning ahead to use SAAM in the validation of the subsystem modeling and providing the needed subsystem tests, a Program Manager can reduce the time and effort needed to validate the contractor's system simulation and will be able to give an impartial, knowledgeable, and timely evaluation of each system.

ACKNOWLEDGEMENTS

Mr. J. Bay of ARRADCOM has capably performed the programming needed to modify SAAM 27. Discussions with Dr. Ray Boston of La Trobe University, Bundoora, Australia on details of the modification of SAAM 27 have been essential for its success.

REFERENCES

1. Pastrick, H. Proc., 23 Army Conference on Design of Experiments, ARO Report 1977.
2. Griner, Gary M., John Mango, and H. Pastrick, Validation of Simulation Models Using Statistical Techniques, Proc. of Summer Computer Simulation Conference, Newport Beach, Ca., July, 1978.
3. J.M. Chambers, Biometrika, 60, 1, (1973). A Celmins, A Manual for General Least Square Model Fitting, Ballistic Research Laboratory, TR-02167, June 79. Stewart, Warren E. and Jan P. Sorenson, Bayesian Estimation of Common Parameters from Irregular Multiple Response Data. Proc. 25th Army Conference on Design of Experiments, ARO Report, 1980.
4. Aitken, A. C, Proc. Roy. Soc. Edinb. A55, 42-47 (1934) and R.L. Plackett, Principles of Regression Analysis, Oxford, Clarendon Press, 1960.
5. Anscombe, F.J., and J.W. Tukey, Technometrics, 5, 141, 1963 and J.R. MacDonald, Rev. Mod. Phys. 41, 316, 1969.

6. Box, G.E.P. and D.A. Pierce, J. Amer. Stat. Assoc. 64, 1509, 1970.
7. Moore, R.L., Proc. 1975 Army Numerical Analysis Conference, ARO Report 75-3.
8. Moore, R.L., Proc. 23d Army Conference on Design of Experiments, ARO Report, 1977.
9. Moore, R.L. Proc. 25th Army Conference on Design of Experiments, ARO Report, 1980.
10. Berman M., E. Shahn, and M. F. Weiss, Biophys J. 2, 275, 1962.
11. Berman, Mones, and M.F. Weiss, USERS MANUAL FOR SAAM (Simulation, Analysis and Modeling) Version SAAM 27, April 15, 1977, Math Research Branch, National Institute of Arthritis and Metabolic Diseases, National Institutes of Health, Bethesda, MD.
12. Model 10 of reference 11.
13. Hetrick, D., and J. Gamble, Transient Reactivity during Power Excursions in a Water Boiler Reactor, Atomics International, Feb 9, 1958.
14. Knutelski, B.G., private communication.
15. Data from Dr. Y. Hiroshige of Douglas Aircraft Co.
16. Dunenfeld, M.S., R.K. Stett, Summary Review of the Kinetics Experiments on Water Boilers, Atomic International, SR 7087, Feb 1, 1963.
17. Roberts, Harry V., Conversational Statistics, The Scientific Press, Palo Alto, CA, 1974.

APPLICATIONS OF MODERN CONTROL AND ESTIMATION
THEORY TO THE GUIDANCE OF TACTICAL AIR-TO-AIR MISSILES

J. R. McCLENDON, 1Lt, USAF
P. L. Vergez, 1Lt, USAF
Air Force Armament Laboratory
United States Air Force
Eglin Air Force Base, Florida 32542

SUMMARY

This paper describes the basic research program instituted by the Air Force Armament Laboratory which is designed to yield effective, high performance guidance algorithms capable of meeting the demands of the modern air-to-air engagement. A simplistic guidance algorithm is derived from optimal control and estimation theory and is compared to proportional navigation. Results of the comparison are presented. Conclusions are drawn from the example and supporting research.

INTRODUCTION

The air-to-air missile-target intercept engagement is the most demanding of scenarios with respect to the terminal guidance law when compared with the surface-to-air, surface-to-surface, or air-to-surface scenarios. The extreme demands placed on the guidance law are due to the relatively short engagement times, complicated by rapidly changing kinematics. Because the engagement times are short, it is imperative for an air-to-air missile to rapidly acquire a target and efficiently use the resulting measurements to provide information inputs to the guidance law. Guidance algorithms currently employ proportional navigation guidance schemes which do not make the most efficient utilization of the information provided to them. It is therefore desirable to develop guidance algorithms which exploit the available information and provide improved guidance commands to the missile.

The Air Force Armament Laboratory began a basic research program in October 1977 to develop guidance algorithms which fully exploit the available information and improve overall missile performance in short range air-to-air missile-target intercept engagements. The initial program was structured into three phases. The first phase investigated the application of optimal control theory to guidance law development. The second phase utilized optimal estimation theory to derive algorithms which provide accurate estimates of observables necessary for guidance laws. The third phase is currently involved in investigating the interaction of modern control theory with estimation theory to better define the design methodology for the combined guidance/estimation problem.

To better understand the impetus for the research program, the next section of this paper reviews the classical approaches to guidance algorithm development. This is followed by a discussion of the modern control and estimation theories that have been and are currently being investigated. Then a development will be shown for a simplistic guidance algorithm derived via optimal control and estimation theory. The subsequent section will describe the evaluation process used to compare a classical guidance algorithm and the simplistic modern control algorithm described in the preceding section. Results of that evaluation will be presented. Finally, the conclusions thus far in the research program, and the recommendations for future study will be discussed.

CLASSICAL APPROACHES

The classical guidance laws to be described in this section are well over twenty five years old. The following general characteristics of these classical designs are found in most state-of-the-art tactical short range air-to-air missiles (4). The overall control of the missile is divided into two or more loops. The outer guidance loop controls translational degrees of freedom, while the inner autopilot loop controls missile altitude. In the inner loop, the roll, pitch and yaw channels are uncoupled and are typically controlled independently of each other. State estimators are not

generally used. Low pass filters are used to reject high frequency noise. Guidance commands are typically amplitude constrained to ensure autopilot stability. The following paragraphs will discuss the basic make-up, advantages, and disadvantages of pursuit navigation, proportional navigation, and pursuit plus proportional navigation respectively.

Velocity pursuit navigation is perhaps the oldest guidance technique that has been used in tactical air-to-air missiles. Pure pursuit guidance is implemented by requiring the missile velocity vector to always point at the target and therefore cause a seemingly unavoidable collision. This technique works well for non moving or slowly moving targets (such as surface targets), but its performance degrades significantly for the air-to-air mission. This is because the missile's velocity vector must turn to keep pointing at the moving target. As the distance to the target decreases, the turning rate of the missile increases and will eventually reach unachievable values before intercepting the target. This form of guidance law usually ends in a tail chase.

Proportional Navigation (pro-nav) ideally forces the missile to fly a straight line collision course with the target (see Figure 1). The straight line path implies that the missile velocity vector will lead the target line of sight (LOS). As can be seen in Figure 1, the LOS does not rotate in space when the missile is on a collision course.

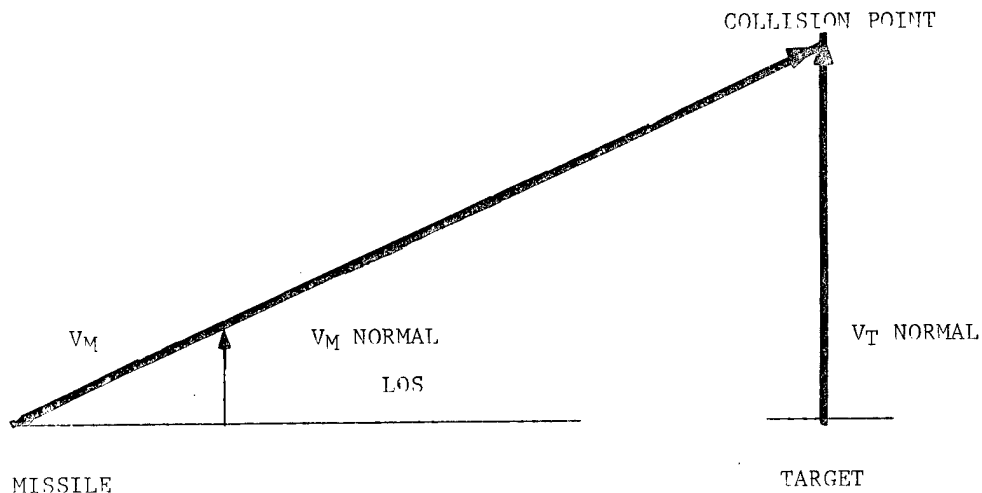


Figure 1. Proportional Navigation Trajectories

Therefore, in pro-nav, steering commands are implemented to drive the LOS rate to zero. Bryson & Ho (1) have shown that pro-nav is an optimal guidance law (with respect to minimizing miss distance) given the following assumptions:

- i) the target has constant velocity
- ii) the missile has unlimited and instantaneous response
- iii) the LOS angles remain small
- iv) the missile's velocity along the LOS vector is constant

The assumptions that both the missile and target have a constant velocity is an especially gross one in the short range air-to-air arena. The missile generally has uncontrolled accelerations in its axial direction, while the accelerations in the yaw and pitch planes are not instantaneous. Despite these serious assumptions, pro-nav is easy to implement and has been used for years in the guidance of tactical air-to-air missiles.

The incorporation of velocity pursuit and pro-nav into a composite guidance law has been attempted in the past. These attempts resulted in a "biased" pro-nav which for most applications, did not perform significantly better than pro-nav alone unless "tuned" for that specific application.

These three guidance laws represent some of the results of the classical approach to guidance law derivation. Pursuit navigation, though fairly insensitive to noise, demonstrates poor performance for a rapidly moving target. Proportional navigation's derivation is based upon several assumptions which pose rather serious limitations. Its performance is inaccurate against accelerating targets. Pro-nav is susceptible to high frequency noise and is therefore typically implemented with low pass filters. In addition, pro-nav fails to exploit all of the information available from the missile. Pursuit plus pro-nav is less susceptible to noise than pro-nav, for certain shots. However, for high off-boresight angle (OBA) shots, neither pro-nav nor pursuit plus pro-nav performs well.

It is therefore highly desirable to develop a guidance algorithm which:

- i) extracts important data from noise measurements
- ii) uses available information to derive guidance commands
- iii) increases launch opportunities while simultaneously decreasing miss distance.

These are the goals of the Air Force Armament Laboratory's basic research program in optimal control and estimation theory. The following sections will describe the research; present specific examples; evaluate the performance of an algorithm derived in the program; and give recommendations for future study.

ADVANCED GUIDANCE TECHNIQUES

In the past two decades modern control and estimation theory has been discounted as a viable approach for guidance algorithm derivation because of the problems associated with implementing such algorithms in real-time while on-board a tactical missile. Inherent in guidance algorithms derived from modern control and estimation theory is the fact that they are computationally expensive. Often iterative numerical techniques must be used to solve the optimal control problem because it cannot be solved in closed form. Only the most simplistic or simplified optimal control problems may be solved in closed form. For these reasons, guidance algorithms continued to be derived via a classical approach in the past.

However, recent advances in microprocessor capability have made modern control and estimation theory much more attractive for use as a basis for missile guidance law development. In addition to hardware advances, new numerical techniques for solving complex equations have been developed. The Air Force Armament Laboratory observed this trend and initiated its optimal control and estimation theory (as applied to tactical missiles) basic research program in October 1977.

When the program began, several problem areas that needed to be addressed were outlined. Primary among those problem areas was the difficulty in specifying a valid performance index (P.I.) which effectively translates the performance drivers into mathematical terms. In addition, the mathematical model of the system, the equality/inequality constraints placed on the system, and the estimation problem had to be thoroughly investigated as well. The feedback states for an optimal control law are functions of the quality of the estimates used. Only under linear, quadratic, gaussian (LQG) assumptions does the control/estimation problem become uncoupled. Because the basic research program is not limited to LQG assumptions, the relationships between the control and estimation problems must be investigated.

During the first eighteen months of the program, the problem was formulated using standard textbook optimal control and estimation theories. These results provided a theoretical baseline for the research endeavor. The initial phase provided these significant determinations (5):

1. Through optimal control and estimation theory it is possible to develop guidance laws which outperform pro-nav given a missile capable of high maneuverability.
2. It is critical to have a well-designed autopilot that provides rapid and stable response to realize the full potential of an optimal control guidance law
3. Overall performance with an Extended Kalman Filter (3) is as good as that obtained with more complicated filtering techniques when miss distance is considered as the evaluation parameter.

Several optimal control and estimation theories have been investigated in the research program.

1. Linear Quadratic Theory
2. Linear Quadratic Gaussian Theory
3. Singular Perturbation Theory
4. Reachable Set Theory
5. Differential Game Theory
6. Adaptive Control Theory
7. Dual Control
8. Extended Kalman Filters
9. Second Order Filters
10. Adaptive Filters
11. Splines
12. Polynomial Approximations

In past studies the guidance and estimation problems have been treated as separate entities. Some current studies are being conducted using a combined approach, as well as a dual control approach where the guidance law performance index contains state estimate enhancement terms as well as other important parameters which are to be maximized (or minimized). The ultimate goal of this research is to integrate the best performing guidance and estimation algorithms into an efficient guidance package which can be utilized in state-of-the-art tactical air-to-air missile concepts.

The current basic research program is also initiating new efforts to study:

1. Strapdown seeker guidance
2. End game guidance
3. Beyond Visual Range guidance

These programs should provide useful inputs to the overall tactical missile guidance problem. The research has shown the potential for dramatic improvements in tactical missile performance through the use of guidance algorithms derived from optimal control and estimation theory. The following sections will present a guidance algorithm development from the in-house research program and present results of a comparison between this guidance algorithm and pro-nav implemented with a low-pass filter.

IV ADVANCED GUIDANCE ALGORITHM

This research program has resulted in numerous guidance algorithms derived from various optimal control and estimation theories, all of which cannot be presented here. Therefore, to dramatize the significance of this research, the most simplistic algorithm will be presented and then compared to pro-nav. This guidance law was derived (6) using Linear Quadratic Gaussian Theory. The derivation of the guidance law is given below.

Consider the engagement scenario depicted in Figure 2. Let M be the missile, T be the target, and

\overline{r}_M \overline{v}_M \overline{a}_M - Missile's position, velocity, and acceleration vectors relative to some fixed inertial reference frame.

\overline{r}_T \overline{v}_T \overline{a}_T - Target's position velocity, and acceleration vectors relative to the same inertial reference frame

Define the state vector as follows:

- x_1 = the target/missile relative position in the x direction
($x_1 = r_{Tx} - r_{Mx}$)
- x_2 = the target/missile relative position in the y direction
($x_2 = r_{Ty} - r_{My}$)
- x_3 = the target/missile relative position in the z direction
($x_3 = r_{Tz} - r_{Mz}$)
- x_4 = the target/missile relative velocity in the x direction
($x_4 = \dot{x}_1 = v_{Tx} - v_{Mx}$)
- x_5 = the target/missile relative velocity in the y direction
($x_5 = \dot{x}_2 = v_{Ty} - v_{My}$)
- x_6 = the target/missile relative velocity in the z direction
($x_6 = \dot{x}_3 = v_{Tz} - v_{Mz}$)
- x_4 = the target/missile relative acceleration in the x direction
($\dot{x}_4 = a_{Tx} - a_{Mx}$)
- x_5 = the target/missile relative acceleration in the y direction
($\dot{x}_5 = a_{Ty} - a_{My}$)
- x_6 = the target/missile relative acceleration in the z direction
($\dot{x}_6 = a_{Tz} - a_{Mz}$)

Thus we have a linear model describing the engagement.

$$\begin{aligned}
 \dot{x}_1 &= x_4 \\
 \dot{x}_2 &= x_5 \\
 \dot{x}_3 &= x_6 \\
 \dot{x}_4 &= a_{Tx} - a_{Mx} \\
 \dot{x}_5 &= a_{Ty} - a_{My} \\
 \dot{x}_6 &= a_{Tz} - a_{Mz}
 \end{aligned} \tag{1}$$

In the derivation of this guidance law, several simplifying assumptions will be made.

ASSUMPTION 1

Let $a_{Tx} = a_{Ty} = a_{Tz} = 0$. This means that the target has constant velocity in both magnitude and direction.

If the control vector, \underline{u} , is defined to be the missile acceleration and it is assumed that target acceleration is zero then Equation (1) can be written in state space form such that

$$\dot{\underline{x}} = \underline{A}\underline{x} + \underline{B}\underline{u} \tag{2}$$

Where

$$\underline{A} = \begin{bmatrix} 0 & \vdots & \mathbf{I} \\ \dots & \dots & \dots \\ 0 & \vdots & 0 \end{bmatrix}, \quad \underline{B} = \begin{bmatrix} 0 \\ \dots \\ \mathbf{I} \end{bmatrix}$$

Where \mathbf{I} is an Identity Matrix with dimension 3×3 .

And

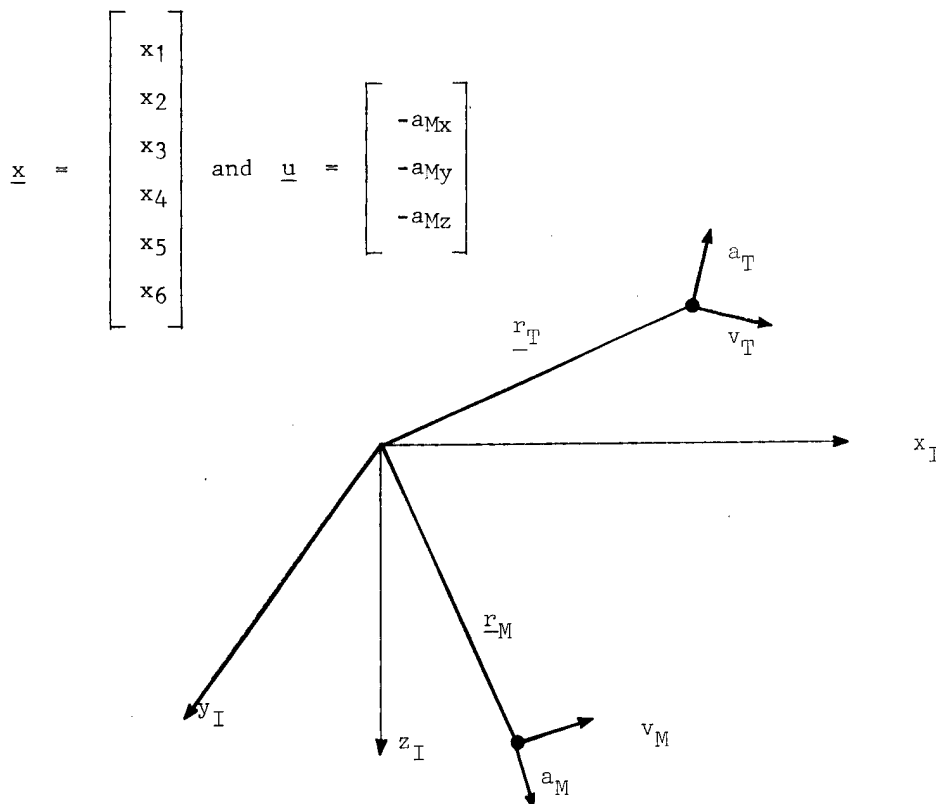


Figure 2. Missile and Target Kinematic States Relative to Inertial Reference Frame

ASSUMPTION 2

In defining the control vector \underline{u} as the missile acceleration, it is implied that the missile has perfect and instantaneous control over all three inertial acceleration components. In the real world tactical missile with conventional propulsion, the axial component of acceleration is uncontrollable. In addition, the lateral and normal accelerations are neither instantaneous nor unlimited.

OPTIMAL CONTROL FORMULATION

The cost functional to be minimized is

$$J = \underline{x}^T(t_f) S_f \underline{x}(t_f) + \frac{1}{2} \int_{t_0}^{t_f} \underline{u}^T R \underline{u} \, dt \quad (3)$$

where $S_f = \begin{bmatrix} I & \cdot & 0 \\ \cdot & \cdot & \cdot \\ 0 & \cdot & 0 \\ \cdot & \cdot & \cdot \end{bmatrix}$ and $R = \begin{bmatrix} b & 0 & 0 \\ 0 & b & 0 \\ 0 & 0 & b \end{bmatrix}$, b = weighting on each control

Given the cost functional, Equation (3), and the state equation, Equation (2), the optimal control solution can be determined analytically. The solution is straight forward but tedious.

Given J and state equation (Eq 2) the Hamiltonian is constructed.

$$H = 1/2 \underline{u}^T R \underline{u} + \underline{p}^T A \underline{x} + \underline{p}^T B \underline{u} \quad (4)$$

Where \underline{p} is the co-state vector with dimension 6×1 .

The necessary conditions for optimality are

$$\dot{\underline{p}} = - \frac{\partial H}{\partial \underline{x}} = -A^T \underline{p} \quad (5)$$

$$0 = \frac{\partial H}{\partial \underline{u}} = R \underline{u} + B^T \underline{p} \quad (6)$$

Equation (6) can be written

$$\underline{u} = -R^{-1} B^T \underline{p} \quad (7)$$

Substituting Equation (7) into Equation (2) yields

$$\dot{\underline{x}} = A \underline{x} - B R^{-1} B^T \underline{p} \quad (8)$$

From Equations (8) and (5) we get

$$\begin{bmatrix} \dot{\underline{x}} \\ \dot{\underline{p}} \end{bmatrix} = \begin{bmatrix} A & \vdots & -B R^{-1} B^T \\ \vdots & \ddots & \vdots \\ 0 & \vdots & -A^T \end{bmatrix} \begin{bmatrix} \underline{x} \\ \underline{p} \end{bmatrix} \quad (9)$$

The solution to Equation (9) has the form

$$\begin{bmatrix} \underline{x}(t_f) \\ \underline{p}(t_f) \end{bmatrix} = \begin{bmatrix} F(t_f, t) \end{bmatrix} \begin{bmatrix} \underline{x}(t) \\ \underline{p}(t) \end{bmatrix} \quad (10)$$

From the boundary equations we get

$$\underline{p}(t_f) = S_f \underline{x}(t_f) \quad (11)$$

Using Equations (10) and (11), $\underline{p}(t)$ can be determined analytically and applied directly to Equation (7) to find the optimal control. For this example the control solution is

$$\underline{u}(t) = \frac{-3 T_{go}}{3b + T_{go}^3} \begin{bmatrix} I & \vdots & T_{go} I \end{bmatrix} \underline{x}(t) \quad (12)$$

where $T_{go} = (t_f - t)$

The theory that was used to obtain the solution assumed that t_f , final time, was specified; therefore, to insure optimality t_f must be known a priori or accurately estimated during flight.

ESTIMATION ALGORITHM

The estimation algorithm to be used in this example is the extended Kalman Filter. The measurements are noisy line-of-sight angles and missile body accelerations. The equations used for this implementation will not be shown here, however they are documented in Chapter VI of (7).

ESTIMATING TIME-TO-GO

The derivation of Equation (12), the guidance law, required that the final time be fixed. This means that final time or time-to-go ($t_f - t_{\text{current}}$) must be continuously estimated throughout the entire engagement. Our research has shown that the estimate of time-to-go (T_{go}) is a key ingredient of the overall accuracy of the guidance algorithm.

Traditionally, the most common T_{go} estimate is given by

$$T_{go} = -R/\dot{R} \quad (13)$$

where R = range-to-go
 \dot{R} = range rate

However, this method of estimating T_{go} assumes that the velocity along the line-of-sight is constant. This is a gross assumption for the air-to-air missile-target intercept problem.

The research program has investigated many different T_{go} estimation algorithms via both contractual and in-house studies. The best performing T_{go} algorithm, from a performance versus complexity of implementation standpoint, is an algorithm derived in-house (6). Several assumptions are made in the algorithm's development:

- 1) Assume the missile's axial component of acceleration dominates the missile's contribution to the line-of-sight acceleration.
- 2) Assume that good estimates of S_R and V_R are available from the Kalman Filter.
- 3) Assume A_{m_x} is measurable.

With these simplifying assumptions, the derivation is straight forward. Rewriting Equation 12 in its component form yields

$$A_{m_x} = 3 (S_{R_x}/T_{go}^2 + V_{R_x}/T_{go}) \quad (14a)$$

$$A_{m_y} = 3 (S_{R_y}/T_{go}^2 + V_{R_y}/T_{go}) \quad (14b)$$

$$A_{m_z} = 3 (S_{R_z}/T_{go}^2 + V_{R_z}/T_{go}) \quad (14c)$$

Recall the assumption that stated missile acceleration is instantaneous and perfectly controllable. For conventional propulsion, the axial component of acceleration is uncontrollable, and therefore in the past, Equation (14a) was ignored. This algorithm uses Equation (14a) to solve for T_{go} .

Solving equation (14a), noting that $V_{R_x} < 0$ for a missile closing on the target, yields

$$T_{go} = \frac{2 S_{V_x}}{-V_{R_x} \pm \sqrt{V_{R_x}^2 + 4/3 S_{R_x} A_{m_x}}} \quad (15)$$

The advantages of this time-to-go algorithm is that it explicitly accounts for the effect of missile acceleration in estimating time-to-go; thus it provides a better estimate of time-to-go resulting in more optimal lateral and normal acceleration commands.

Using the LQG guidance law (Equation 12) the extended Kalman filter, and the T_{go} algorithm, a performance evaluation was made. The description of the evaluation and the results follow.

EVALUATION

The evaluation tool used for this comparison is a detailed six-degree-of-freedom (6-DOF) digital simulation. The simulation contains the detailed math model of a generic bank-to-turn short range missile. Major subsystems such as seeker, autopilot, propulsion system, and sensors are modelled as well. The simulation also incorporates realistic noise models. Additionally, the simulation contains a three-degree-of-freedom model of a "smart" target which incorporates a nine-g out-of-plane evasive maneuver algorithm.

The guidance algorithm developed in the previous section is compared against pro-nav which is implemented with well designed low-pass filters for smoothing the seeker measurements and a navigation gain optimized to minimize miss distance.

The evaluation consists of a large number of Monte Carlo runs for a large number of engagement conditions. Effective launch opportunity envelopes are generated by defining the geometrical region in space from which the missile can be launched and obtain a mean miss distance of less than ten feet. Additional constraints are placed on the results in that the standard deviation of the mean miss distance after ten Monte Carlo runs has to be less than the mean miss, or additional Monte Carlo runs are performed.

The initial launch conditions are co-altitude (10,000 feet) and co-speed (.9 Mach). The target performs its evasive maneuver when range becomes less than or equal to 6,000 feet. Both algorithms use passive seeker measurement information.

The effective launch opportunity envelopes (6) are shown in Figures 3 and 4. Figure 3 depicts the case for 0° off boresight launch. The off boresight angle is defined as the angle between the initial LOS vector and the initial missile velocity vector. Figure 4 shows the 40° off boresight case. A 0° off boresight, 0° aspect angle case is a tail-on shot. Conversely, a 0° off-boresight, 180° aspect angle case is a head-on shot.

These figures demonstrate the dramatic performance improvement in terms of miss distance and launch opportunity that can be achieved through the use of guidance algorithms derived from optimal control theory over the performance offered by pro-nav which is currently being used in most existing air-to-air short range tactical missiles.

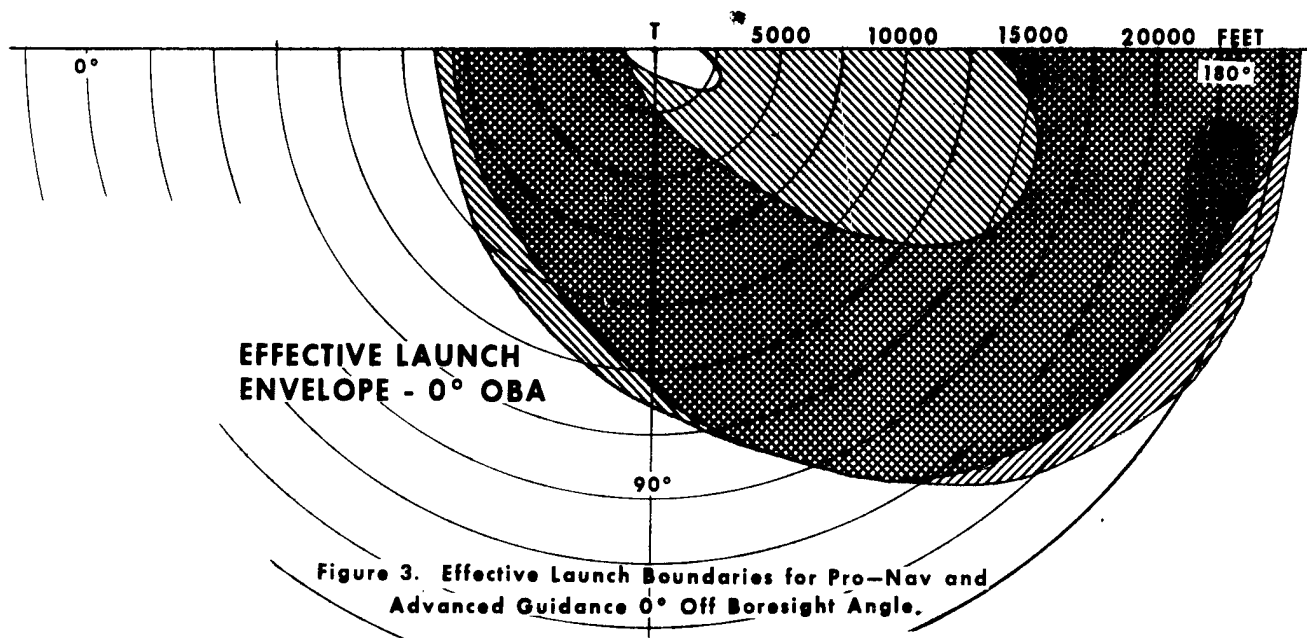
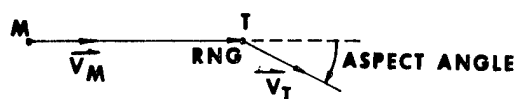
CONCLUSIONS AND RECOMMENDATIONS

The basic research program was designed to demonstrate the viability of optimal control and estimation theory as a basis for guidance algorithm development for tactical air-to-air missiles. The results have shown that optimal control theory is a powerful alternative. It should be realized that the results shown here for the most simplistic guidance algorithm derived in this program. Other more complex guidance laws have the potential for improving the results to a greater extent than demonstrated here.

Thus far, the basic research program has been concerned explicitly with the short range tactical missile engagement. New programs are scheduled to investigate guidance for beyond visual range missiles, for missiles which employ strapdown seekers, and for application in the end game (last few seconds of time-to-go) of the terminal engagement where the information available to the guidance algorithm is severely restricted. The application of optimal control and estimation theory to these areas needs to be fully explored. Additional work needs to be performed in thoroughly defining the on-board computer requirements for the realization of the algorithms.

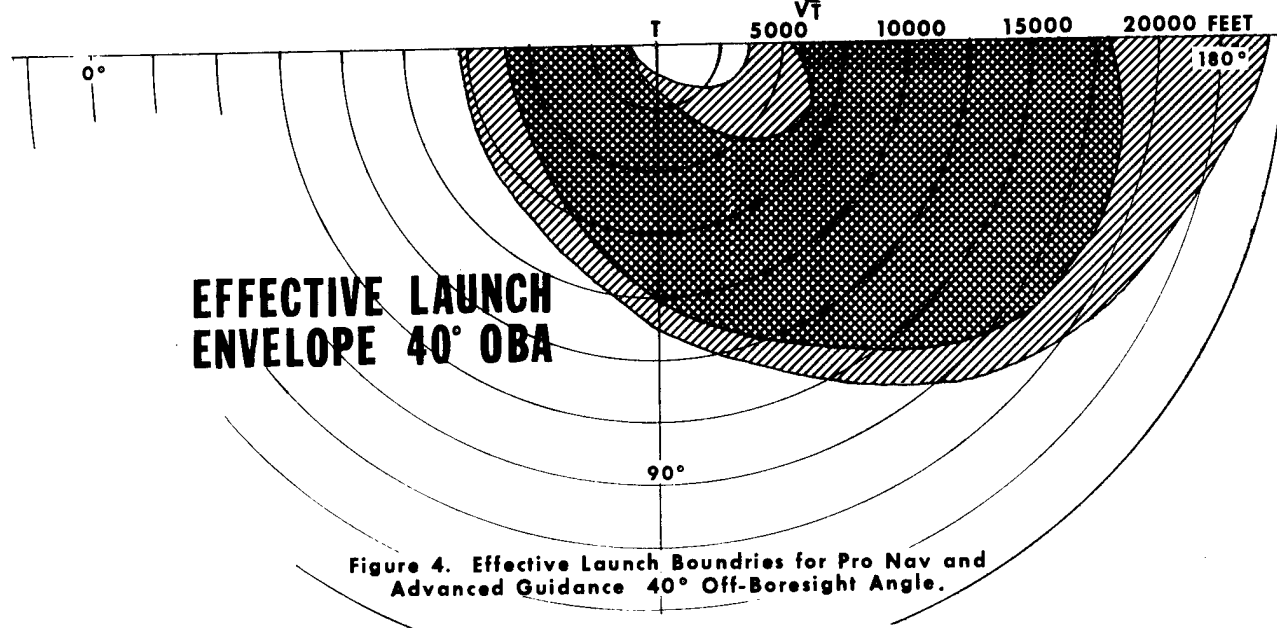
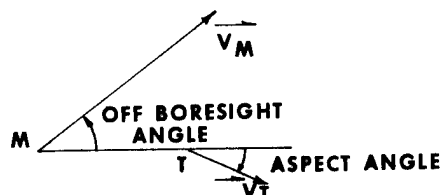
In conclusion, as the example demonstrates, optimal control and estimation theory provides a viable alternative to classical guidance design techniques. The hardware implementation barriers for guidance algorithms derived from optimal control and estimation theory no longer exist. These guidance laws offer the potential for increased missile performance at little or no cost increase for the next generation of missiles.

LEGEND
 PRO NAV
 ADV GUID
 OVERLAP



LEGEND

PRO NAV
 ADV GUID
 OVERLAP



REFERENCES

- (1) Bryson, Jr., A.E. & Ho, Y.C., Applied Optimal Control, Hemisphere Publishing Co., 1975.
- (2) Riggs, T.L. "Linear Optimal Guidance for Short Range Air-to-Air Missiles," Proceedings of NAECON 1979, Vol II., pages 757-764, May 1979.
- (3) Speyer, J.L. & Hull, D.G., "Comparison of Several Extended Kalman Filter Formulations for Homing Missile Guidance," AIAA Guidance and Control Meeting, August 11-13, 1980.
- (4) Gonzalez, J. "New Methods In the Terminal Guidance and Control of Tactical Missiles," Guidance and Control for Tactical Guided Weapons with Emphasis on Simulation and Testing. AGARD, May 1979.
- (5) Riggs, T.L. "An Overview-Optimal Control and Estimation For Tactical Missiles Research Program," Proceedings of NAECON 1979, Vol II., pages 752-756, May 1979.
- (6) Riggs, T.L. "Optimal Control and Estimation for Terminal Guidance of Tactical Missiles," to be published, AGARD, May 1980.
- (7) Sammons, J.M., et al, "Development and Comparison of Optimal Filters", AFATL-TR-79-87, October 1979.

**This Page Intentionally
Left Blank**

DELAYED-MEASUREMENT OBSERVERS FOR DISCRETE-TIME LINEAR SYSTEMS

N. K. Loh
School of Engineering
Oakland University
Rochester, Michigan 48063

R. R. Beck
U.S. Army Tank-Automotive
Research and Development Command
Tank-Automotive Concepts Laboratory
Warren, Michigan 48090

ABSTRACT

This paper considers the development of a discrete-time delayed-measurement observer for a discrete-time-invariant linear system. The delayed-measurement observer developed has several unique features: it utilizes discrete time delayed measurements as part of its inputs and it is an $(n-q)$ th order observer for an n th order linear system with m linearly independent outputs, where $q \geq m$. The dimension of a delayed-measurement observer is therefore lower than that of the well known $(n-m)$ -minimal-order Luenberger observer. Furthermore, a delayed-measurement observer becomes a minimal order Luenberger observer when $q = m$, and becomes a pseudo-observer with no dynamics when $q = n$. The results obtained in the paper may readily be extended to discrete-time time-varying linear systems.

INTRODUCTION

The design and implementation of a linear optimal control system using state space techniques often requires the availability of all state variables associated with the system [1]-[4]. However, in practice, not all state variables in a system are accessible for direct measurement nor is it economical to measure all state variables directly. Furthermore, the measurement data may be contaminated by measurement errors. The design problem caused by the unknown and/or inaccessible state variables may be solved by replacing the unknown and/or inaccessible state variables by their estimated values. For linear systems, there are two well known filters which may be used to generate estimates of the unknown and/or inaccessible state variables, namely, the Kalman-Bucy filter [5] and the Luenberger observer [6]-[7]. The Kalman-Bucy filter uses noise contaminated measurements to reconstruct estimates of the unknown and/or inaccessible state variables. The order of the filter is the same as the order of the associated system. On the other hand, when the measurements are perfect, i.e., contain no measurement errors, and there are no random disturbances acting on the system, a Luenberger observer may be used to generate the desired estimates of the unknown and/or inaccessible state variables. The order of a Luenberger observer is generally less than that of the associated system [6]-[9]; specifically, the $n-m$ unknown and/or inaccessible state variables of an n th order linear system with m linearly independent outputs may be constructed by a minimal-order observer of order $n-m$ (see in particular, [9]).

Since the pioneering work of Luenberger [6]-[7], observer theory has been studied extensively in the literature [10]-[21], where in [14]-[21], observer theory has been extended to stochastic systems. Observer theory has also played an important role in the design of disturbance accommodating control systems [22]-[27], where various minimal-order observers have been developed to provide estimates of various unknown system disturbances which either have a specific waveform structure or can be approximated by a specific waveform structure.

In this paper, a new reduced-order observer for discrete-time linear systems will be developed. The essential idea is to utilize the past or time-delayed measurements to extract more information about the unknown and/or inaccessible state variables. We will call the observer developed a delayed-measurement observer to reflect the fact that time-delayed measurements are utilized in the observer equations. The delayed-measurement observer is an $(n-q)$ th order observer with $(n-q) \leq (n-m)$, for

an n th order system with m linearly independent outputs. The dimension of a delayed-measurement observer is therefore lower than that of the corresponding $(n-m)$ -minimal-order Luenberger observer. Furthermore, $n-q$ may be varied and may be reduced by using more time-delayed measurements. When enough delayed measurements are used, $n-q$ is reduced to zero and the delayed-measurement observer becomes a "pseudo-observer" or an observer with no dynamics which reconstructs the present values of the unknown and/or inaccessible state variables instantaneously. In view of its reduced dimension, a delayed-measurement observer is particularly useful for microprocessor implementation. State estimation using a pseudo-observer has been considered in [28]-[30]. A microprocessor-based delayed-measurement observer has been designed and constructed in [27] to provide estimates necessary for the implementation of an actual optimal control system.

DELAYED-MEASUREMENT OBSERVER

Consider a discrete-time linear system described by

$$x(k+1) = Ax(k) + Bu(k), \quad x(0) = x_0 \quad (1)$$

with measurements given by

$$y(k) = Cx(k) \quad (2)$$

where $x(k) \in \mathbb{R}^n$, $u(k) \in \mathbb{R}^r$, $y(k) \in \mathbb{R}^m$ are, respectively, the state input and output vectors; A , B and C are, respectively, $n \times n$, $n \times r$ and $m \times n$ constant matrices. We assume that $\text{rank } [C] = m$, A is invertible¹, and that the system is completely controllable and completely observable.

From (1) and (2), we obtain, by using d time-delayed measurements with $d \leq k$ and $d \leq (n-1)$,

$$\begin{bmatrix} y(k) \\ y(k-1) \\ \vdots \\ y(k-d) \end{bmatrix} = \begin{bmatrix} C \\ CA^{-1} \\ \vdots \\ CA^{-d} \end{bmatrix} x(k) - \begin{bmatrix} 0_{m \times r} & \cdots & 0_{m \times r} \\ CA^{-1}B & \cdots & 0_{m \times r} \\ \vdots & \vdots & \vdots \\ CA^{-d}B & \cdots & CA^{-1}B \end{bmatrix} \begin{bmatrix} u(k-1) \\ u(k-2) \\ \vdots \\ u(k-d) \end{bmatrix} \quad (3)$$

Defining

$$y_d^T(k) \triangleq [y^T(k-1) : y^T(k-2) : \cdots : y^T(k-d)], \quad (4)$$

$$u_d^T(k) \triangleq [u^T(k-1) : u^T(k-2) : \cdots : u^T(k-d)], \quad (5)$$

$$H_d^T \triangleq [C^T : (A^{-1})^T C^T : \cdots : (A^{-d})^T C^T], \quad (6)$$

$$B_d \triangleq \begin{bmatrix} 0_{m \times r} & \cdots & 0_{m \times r} \\ CA^{-1}B & \cdots & 0_{m \times r} \\ \vdots & \vdots & \vdots \\ CA^{-d}B & \cdots & CA^{-1}B \end{bmatrix}, \quad (7)$$

we obtain, from (3)-(7),

$$\begin{bmatrix} y(k) \\ \vdots \\ y_d^T(k) \end{bmatrix} = H_d x(k) - B_d u_d(k), \quad (8)$$

where $y_d^T(k)$ is an md -dimensional time-delayed measurement vector, $u_d(k)$ is an rd -dimensional time-delayed input vector; H_d and B_d are, respectively, $m(d+1) \times n$ and $m(d+1) \times rd$ matrices.

¹The matrix A is invertible if (1) is the discretized version of a continuous-time system, since in that case, A is a nonsingular transition matrix.

Equation (8) yields the time-delayed measurement equation

$$\begin{bmatrix} y(k) \\ \vdots \\ y_d(k) \end{bmatrix} \triangleq \begin{bmatrix} y(k) \\ \vdots \\ y_d^*(k) \end{bmatrix} + B_d u_d(k) \quad (9a)$$

$$= H_d x(k), \quad (9b)$$

where $y_d(k)$ as defined is known for all $k \geq d$, since the right-side of (9a) is known for all $k \geq d$. We note that the time-delayed measurement equation (9) is similar to (2) in form and that $\text{rank}[H_d] = q$, where $m \leq q \leq n$. Furthermore, if $\text{rank}[H_d] = n$, then H_d becomes a constructibility matrix [31] and is equivalent to the observability matrix associated with $[A, C]$ when A is nonsingular [31]-[32].

Given the time-delayed measurement equation (9), we wish to obtain an estimate $\hat{x}(k)$ of $x(k)$ generated by a discrete-time linear system of the form

$$z(k+1) = Fz(k) + G \begin{bmatrix} y(k) \\ \vdots \\ y_d(k) \end{bmatrix} + Mu(k), \quad (10a)$$

$$z(0) = T\alpha, \quad (10b)$$

$$\hat{x}(k) = Pz(k) + [V+PK] \begin{bmatrix} y(k) \\ \vdots \\ y_d(k) \end{bmatrix}, \quad (11)$$

where $z(k) \in \mathbb{R}^{n-q}$, $\alpha \in \mathbb{R}^n$ is an arbitrary vector, F, G, K, M, P, T and V are, respectively, $(n-q) \times (n-q)$, $(n-q) \times m(d+1)$, $(n-q) \times m(d+1)$, $(n-q) \times r$, $n \times (n-q)$, $(n-q) \times n$, and $n \times m(d+1)$ suitable constant matrices. We assume that

$$\text{rank}[P] = n-q, \quad (12a)$$

$$\text{rank}[T] = n-q. \quad (12b)$$

Definition: The discrete-time linear system described by (10) is called a delayed-measurement observer for the system described by (1) and (9) if and only if there exist, respectively, $(n-q) \times m(d+1)$, $n \times (n-q)$, $(n-q) \times n$ and $n \times m(d+1)$ constant matrices K, P, T and V such that, for arbitrary α and $u(k)$,

$$\lim_{k \rightarrow \infty} [\hat{x}(k) - x(k)] = 0. \quad (13)$$

The dimension $n-q$ of such an observer, if it exists, is smaller than the dimension $n-m$ of a corresponding reduced-order Luenberger observer [6]-[9]. For systems with large $n-m$, the ability to develop an observer with a dimension lower than $n-m$ may be of practical importance. There are various ways which may be used to determine the constant matrices P, T and V . We will use the following matrix decomposition theorem [33] (see also [22]-[24]).

Theorem 1 (Matrix Decomposition Theorem)

Let $X_i, i=1, 2, \dots, k$, be $n \times n_i$ real matrices of $\text{rank}[X_i] = r_i$. If $\sum_{i=1}^k r_i = n$, then the following conditions are equivalent:

$$(a) \quad X_i^T X_j = 0_{n_i \times n_j} \text{ for all } i \neq j,$$

$$(b) \quad \sum_{i=1}^k X_i (X_i^T X_i)^{\#} X_i^T = I_n,$$

where $[\cdot]^{\#}$ denotes a generalized inverse of $[\cdot]$.

To proceed, consider the algebraic equation

$$H_d P = 0_{m(d+1) \times (n-q)}. \quad (14)$$

Since (14) is consistent², a solution for P of full rank always exists, is generally

²The matrix equation $AX = Y$ is consistent if $\text{rank}[A] = \text{rank}[A:Y]$.

non-unique and can easily be determined. Also since $\text{rank}[H_d] + \text{rank}[P] = n$, then by the matrix decomposition theorem, we obtain,

$$PT + VH_d = I_n, \quad (15)$$

where we have chosen T and V as

$$T = (P^T P)^{-1} P^T, \quad (16)$$

$$V = H_d^T (H_d H_d^T)^{\#}. \quad (17)$$

Define

$$e_x(k) \triangleq \hat{x}(k) - x(k), \quad (18)$$

$$e_z(k) \triangleq z(k) - Tx(k) + K \begin{bmatrix} y(k) \\ \vdots \\ y_d(k) \end{bmatrix}, \quad (19)$$

where $e_x(k)$ and $e_z(k)$ are error vectors.

We obtain, from (9b), (11), (15), (18) and (19),

$$e_x(k) = Pe_z(k). \quad (20)$$

We note that if $e_z(k) \rightarrow 0$ as $k \rightarrow \infty$, then $e_x(k) \rightarrow 0$ so that $\hat{x}(k) \rightarrow x(k)$. Also we obtain, from (1), (9b), (10a) and (19),

$$\begin{aligned} e_z(k+1) &= Fe_z(k) + [M - (T-KH_d)B]u(k) \\ &\quad + [F(T-KH_d) - (T-KH_d)A + GH_d]x(k). \end{aligned} \quad (21)$$

If the second and third terms in (21) vanish for arbitrary $u(k)$ and $x(k)$, then

$$e_z(k+1) = Fe_z(k). \quad (22)$$

We have the following theorem.

Theorem 2: The discrete-time linear system described by (10) is a delayed-measurement observer for (1) and (9) if and only if the following conditions hold:

(a) F is asymptotically stable, i.e., all the eigenvalues of F lie within the unit circle in the complex plane,

$$(b) \quad (T-KH_d)A - F(T-KH_d) = GH_d, \quad (23)$$

$$(c) \quad M = (T-KH_d)B. \quad (24)$$

A proof of the theorem may be obtained in a similar fashion as in [34].

Using (15) and (23), we obtain,

$$[F - (T-KH_d)AP : G - FK - (T-KH_d)AV] \begin{bmatrix} T \\ \vdots \\ H_d \end{bmatrix} = 0_{(n-q) \times n}. \quad (25)$$

Given T and H_d , (25) is consistent and a solution always exists.³ A sufficient condition which satisfies (25) and therefore (23) is that

$$F = (T-KH_d)AP \triangleq F_o - KH_o, \quad (26)$$

$$G = FK + (T-KH_d)AV, \quad (27)$$

where $F_o \triangleq TAP$ and $H_o \triangleq H_d AP$. Equation (26) shows that there exists an observer gain matrix K such that all the eigenvalues of F can be placed within the unit

³We also note that $\text{rank}[T^T : H_d^T] = n$.

circle in the complex plane (subject to the restriction that complex eigenvalues occur in complex conjugate pair) if and only if $[F_0, H_0]$ is a completely observable pair [3], [35], while $[F_0, H_0]$ is completely observable if $[A, C]$ is completely observable. A suitable scheme for constructing K is as follows. Set

$$K = F_0 \bar{L} H_0^T (R + H_0 \bar{L} H_0^T)^{-1}, \quad (28)$$

where \bar{L} is the $(n-q) \times (n-q)$ symmetric positive-definite solution of

$$\bar{L} = F_0 \bar{L} F_0^T - F_0 \bar{L} H_0^T (R + H_0 \bar{L} H_0^T)^{-1} H_0 \bar{L} F_0^T + Q, \quad (29)$$

where Q and R are, respectively, $(n-q) \times (n-q)$ and $m(d+1) \times m(d+1)$ arbitrary symmetric positive-definite matrices. Equation of the form of (29) has been studied extensively in the literature [36]-[40]. With K given by (28), it can be shown that (22) and therefore the homogenous part of (10a) is asymptotically stable (see Appendix I).

DESIGN OF CANONICAL DELAYED-MEASUREMENT OBSERVER

The $(n-q)$ th order delayed-measurement observer described by (10) is in a general form and may be simplified for ease of analysis and implementation. In a simplified convenient form, much insight into the role played by the delayed-measurement observer may be gained.

Consider (1) and (9). Since $\text{rank}[H_d] = q$, there are $m(d+1)-q$ redundant output variables in the md -vector $y_d(k)$. Interchanging rows and columns of H_d , if necessary, and also possibly introducing a coordinate transformation for $x(k)$ (see Appendix II), and (1) and (9) may be expressed in the following forms

$$\begin{bmatrix} x_1(k+1) \\ \hline x_2(k+1) \end{bmatrix} = \begin{bmatrix} A_{11} & A_{12} \\ \hline A_{21} & A_{22} \end{bmatrix} \begin{bmatrix} x_1(k) \\ \hline x_2(k) \end{bmatrix} + \begin{bmatrix} B_{11} \\ \hline B_{21} \end{bmatrix} u(k), \quad (30)$$

$$\begin{bmatrix} y(k) \\ \hline y_{1d}(k) \\ \hline y_{2d}(k) \end{bmatrix} = \begin{bmatrix} I_q & 0_{qx(n-q)} \\ \hline H_{21} & 0_{sx(n-q)} \end{bmatrix} \begin{bmatrix} x_m(k) \\ \hline x_{q-m}(k) \\ \hline x_{n-q}(k) \end{bmatrix} \\ = H_d \begin{bmatrix} x_1(k) \\ \hline x_2(k) \end{bmatrix}, \quad (31)$$

where $x_m(k) \in \mathbb{R}^m$, $x_{q-m}(k) \in \mathbb{R}^{q-m}$, $x_1^T(k) = [x_m^T(k); x_{q-m}^T(k)]$, $x_2(k) \triangleq x_{n-q}(k) \in \mathbb{R}^{n-q}$,

$y_{1d}(k) \in \mathbb{R}^{q-m}$, $y_{2d}(k) \in \mathbb{R}^s$ with $s \triangleq [m(d+1)-q]$, and the various partitioned matrices have compatible dimensions. We note that the elements of $y_{2d}(k)$ are the redundant output variables and may be discarded if so desired.

Utilizing (14) and (31), we pick

$$P = \begin{bmatrix} 0_{qx(n-q)} \\ \hline I_{n-q} \end{bmatrix}, \quad (32)$$

and from (16) and (17), T and V are computed as

$$T = [0_{(n-q) \times q} | I_{n-q}], \quad (33)$$

$$V = \left[\begin{array}{c|c} (I_q + H_{21}^T H_{21})^{-1} & (I_q + H_{21}^T H_{21})^{-1} H_{21}^T \\ \hline 0_{(n-q) \times q} & 0_{(n-q) \times s} \end{array} \right] \quad (34a)$$

$$\triangleq \left[\begin{array}{c|c} V_{11} & V_{12} \\ \hline 0_{(n-q) \times q} & 0_{(n-q) \times s} \end{array} \right], \quad (34b)$$

where the generalized inverse $(H_d H_d^T)^{\#}$ is computed as [33], [41]

$$(H_d H_d^T)^{\#} = \begin{bmatrix} I_q \\ H_{21} \end{bmatrix} (I_q + H_{21}^T H_{21})^{-2} [I_q \mid H_{21}^T]. \quad (35)$$

A canonical minimal-order delayed-measurement observer can now be obtained by substituting (26), (27), (32), (33) and (34) into (10) and (11). The results are summarized in the following lemma.

Lemma 1: A canonical delayed-measurement observer for the system described by (30) and (31) is given by

$$\begin{aligned} z(k+1) = & (A_{22} - K_{11} A_{12})z(k) + (B_{21} - K_{11} B_{11})u(k) \\ & + [(A_{22} - K_{11} A_{12})K_{11} + (A_{21} - K_{11} A_{11})V_{11}] \begin{bmatrix} y(k) \\ \vdots \\ y_{1d}(k) \end{bmatrix} \\ & + (A_{21} - K_{11} A_{11})V_{12}y_{2d}(k), \end{aligned} \quad (36)$$

with the estimate $\hat{x}(k)$ given by

$$\hat{x}_1(k) = V_{11} \begin{bmatrix} y(k) \\ \vdots \\ y_{1d}(k) \end{bmatrix} + V_{12}y_{2d}(k), \quad (37)$$

$$\hat{x}_2(k) = z(k) + K_{11} \begin{bmatrix} y(k) \\ \vdots \\ y_{1d}(k) \end{bmatrix}, \quad (38)$$

where the gain matrix K has been chosen as $K = [K_{11} \mid 0_{(n-q) \times s}]$ with K_{11} an $(n-q) \times q$ matrix. The gain matrix K_{11} should be chosen such that $(A_{22} - K_{11} A_{12})$ in (36) is asymptotically stable. Such a K_{11} exists if and only if $[A_{22}, A_{12}]$ is completely observable [3], [35] and $[A_{22}, A_{12}]$ is completely observable if and only if $[A, H_d]$ is completely observable [42]. A suitable K_{11} may be computed in a similar fashion as in (28) and (29) by setting

$$K_{11} = A_{22} \bar{A}_{12}^T [R + A_{12} \bar{A}_{12}^T]^{-1}, \quad (39)$$

with \bar{A}_{12} the $(n-q) \times (n-q)$ symmetric positive-definite solution of

$$\bar{A}_{12} = A_{22} \bar{A}_{22}^T - A_{22} \bar{A}_{12}^T (R + A_{12} \bar{A}_{12}^T)^{-1} A_{12} \bar{A}_{22}^T + Q, \quad (40)$$

where Q and R are, respectively, $(n-q) \times (n-q)$ and $q \times q$ arbitrary symmetric positive-definite matrices.

Some interesting observations may be made from (36), (37) and (38), and are given in the following remarks.

Remark 1: If no time-delayed measurements are used, then $q = m$, and H_d becomes $H_d = C = [I_m \mid 0_{m \times (n-m)}]$. Furthermore, $y_{1d}(k)$ and $y_{2d}(k)$ vanish. Equations (36), (37) and (38) then reduce to the well known minimal-order Luenberger observer developed in [9].

Remark 2: The estimate $\hat{x}_1(k)$ given by (37) is actually a least-square estimate of $x_1(k)$. To see that, consider (31) which may be written as

$$\begin{bmatrix} I_q \\ \hline H_{21} \end{bmatrix} x_1(k) = \begin{bmatrix} y(k) \\ \hline y_{1d}(k) \\ \hline y_{2d}(k) \end{bmatrix} \quad (41)$$

Equation (41) immediately yields the least-square of $x_1(k)$ given by (37). The least-square estimate $\hat{x}_1(k)$ given by (37) is obviously useful when the measurements $\{y(k), k=0,1,\dots\}$ contain small measurement errors. If all the measurements are error-free, then $y_{2d}(k)$ is redundant and may be discarded by setting $H_{21} = 0$ resulting $V_{12} = 0$ in (36) and (37).

Remark 3: If $\text{rank}[H_d] = q = n$, then $z(k)$ and $\hat{x}_2(k)$ vanish and $\hat{x}_1(k)$ becomes the whole of $\hat{x}(k)$. In this case, we obtain from (37) or (31),

$$\hat{x}(k) = (H_d^T H_d)^{-1} H_d^T \begin{bmatrix} y(k) \\ \hline y_{1d}(k) \\ \hline y_{2d}(k) \end{bmatrix}, \quad (42)$$

where $H_d^T = [I_n | H_{21}^T]$.

APPLICATION

The delayed-measurement observer developed in this paper will be applied to the estimation problem associated with the design of a turret control system of a surface combat vehicle system. The two channels, elevation channel and azimuth channel, of the turret control system are functionally independent and the controller for each channel may be designed independently. Only the elevation channel will be considered here and a block diagram of the open-loop control system is as shown in Fig. 1. The numerical values of the constants are given in Table 1.

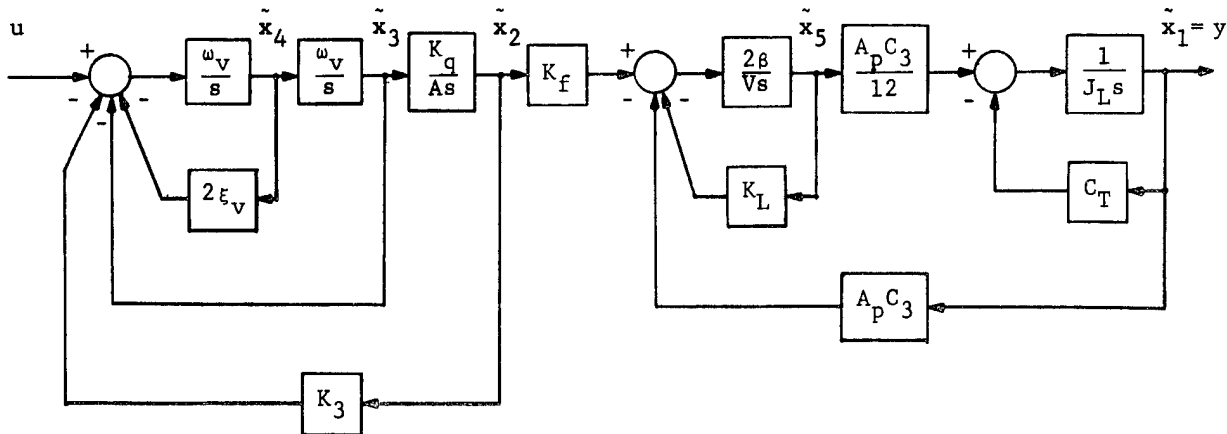


Fig. 1 Elevation Channel of Turret Control System

TABLE 1: CONTROL SYSTEM CONSTANTS

Symbol	Value	Unit	Description of Constant
A_p	1.902	in^2	Actuator Piston Area
C_3	2.14	ft	Actuator Moment Arm
C_T	420	---	Damping Coefficient
$2\beta/V$	1.01×10^4	$\text{lb}/\text{in}^2/\text{in}^3$	Oil Compliance Coefficient
J_L	120	lb-ft-sec^2	Load Inertia
K_L	0.0	$\text{in}^2/\text{sec}/\text{lb}/\text{in}^2$	Leakage Constant
K_3	66.45	ma/in	Servo Valve Feedback Gain
K_q	0.5	$\text{in}^3/\text{sec}/\text{ma}$	Servo Valve Gain
K_f	270.1	$\text{in}^3/\text{sec}/\text{in}$	Hydraulic Flow Gain
A	0.25	in^2	Spool Input Area
ω_V	313	rad/sec	Undamped Natural Frequency
ξ_V	0.8	---	Damping Ratio

Using the values of the constants listed in Table 1, the state-space equation for the turret control system is easily obtained as

$$\dot{\tilde{x}}(t) = \begin{bmatrix} -3.5 & 0 & 0 & 0 & 2.83 \times 10^{-3} \\ 0 & 0 & 2.0 & 0 & 0 \\ 0 & 0 & 0 & 313 & 0 \\ 0 & -2.08 \times 10^4 & -313 & -501 & 0 \\ -4.11 \times 10^4 & 2.73 \times 10^6 & 0 & 0 & 0 \end{bmatrix} \tilde{x}(t) + \begin{bmatrix} 0 \\ 0 \\ 0 \\ 313 \\ 0 \end{bmatrix} u(t) , \quad (43a)$$

$$y(t) = \tilde{x}_1(t) = [1 \ 0 \ 0 \ 0 \ 0] \tilde{x}(t) , \quad (43b)$$

where $\tilde{x}(t) = [\tilde{x}_1(t) \ \tilde{x}_2(t) \ \tilde{x}_3(t) \ \tilde{x}_4(t) \ \tilde{x}_5(t)]^T$.

Using a sampling interval of 0.01 second, (43) is discretized as,

$$\tilde{x}(k+1) = \begin{bmatrix} 0.96 & 0.34 & 1.86 \times 10^{-3} & 7.3 \times 10^{-4} & 2.77 \times 10^{-5} \\ 0 & 0.41 & 7.10 \times 10^{-3} & 4.69 \times 10^{-3} & 0 \\ 0 & -48.7 & -0.326 & -6.18 \times 10^{-2} & 0 \\ 0 & 4.1 & -0.249 & -0.227 & 0 \\ -4.03 \times 10^2 & 2.18 \times 10^4 & 1.65 \times 10^2 & 77.8 & 0.994 \end{bmatrix} \tilde{x}(k)$$

$$\begin{aligned}
& + \begin{bmatrix} 5.48 \times 10^{-4} \\ 8.93 \times 10^{-3} \\ 0.734 \\ -6.18 \times 10^{-2} \\ 8.15 \times 10^{-2} \end{bmatrix} u(k) \\
& = \tilde{A}\tilde{x}(k) + \tilde{B}u(k) \quad , \quad (44a)
\end{aligned}$$

$$\begin{aligned}
y(k) &= [1 \ 0 \ 0 \ 0 \ 0] \tilde{x}(k) \\
&= \tilde{C}\tilde{x}(k) \quad , \quad (44b)
\end{aligned}$$

where it can readily be checked that $[\tilde{A}, \tilde{C}]$ is completely observable.

Since only $\tilde{x}_1(k)$ is measured, a fourth-order Luenberger observer would be needed to generate the estimates of the four inaccessible state variables $\tilde{x}_2(k)$, $\tilde{x}_3(k)$, $\tilde{x}_4(k)$ and $\tilde{x}_5(k)$. However, if three delayed measurements are used, it can be shown that only $\tilde{x}_5(k)$ needs to be estimated by a first-order delayed-measurement observer.

Using three delayed measurements, (9) or (31) becomes

$$\begin{aligned}
\begin{bmatrix} y(k) \\ y_{1d}(k) \\ y_{2d}(k) \\ y_{3d}(k) \end{bmatrix} &= \begin{bmatrix} 1 & 0 & 0 & 0 & 0 \\ 1.03 & 0.59 & -1.72 \times 10^{-4} & 5.69 \times 10^{-3} & -2.87 \times 10^{-5} \\ 1.048 & 19.49 & 0.159 & 0.318 & -5.81 \times 10^{-5} \\ 1.055 & 545.6 & 4.855 & 8.52 & -8.79 \times 10^{-5} \end{bmatrix} \tilde{x}(k) \\
&= \tilde{H}_d \tilde{x}(k) \quad , \quad (45)
\end{aligned}$$

where

$$\begin{aligned}
y_{1d}(k) &= y(k-1) - 3.0 \times 10^{-3} u(k-1), \\
y_{2d}(k) &= y(k-2) - 0.267 u(k-1) - 3.0 \times 10^{-3} u(k-2), \\
y_{3d}(k) &= y(k-3) - 7.9 u(k-1) - 0.267 u(k-2) - 3.0 \times 10^{-3} u(k-3).
\end{aligned} \quad (46)$$

In (45), \tilde{H}_d is not yet in the canonical form of (31). However, from (II-9) of Appendix II, we obtain

$$\tilde{T} = \left[\begin{array}{ccccc|c} 1 & 0 & 0 & 0 & 0 & 0 \\ 1.03 & 0.59 & -1.72 \times 10^{-4} & 5.69 \times 10^{-3} & -2.87 \times 10^{-5} & \\ 1.048 & 19.49 & 0.159 & 0.318 & -5.81 \times 10^{-5} & \\ 1.055 & 545.6 & 4.855 & 8.52 & -8.79 \times 10^{-5} & \\ \hline 0 & 0 & 0 & 0 & 1 & \end{array} \right] \quad , \quad (47)$$

and from (II-10) of Appendix II, we obtain

$$\tilde{T}^{-1} = \left[\begin{array}{cccc|c} 1 & 0 & 0 & 0 & 0 \\ -2.43 & 2.79 & -0.44 & 1.45 \times 10^{-2} & 5.6 \times 10^{-5} \\ 141.2 & -108.9 & -28.95 & 1.15 & -4.71 \times 10^{-3} \\ 7.52 & -117. & 44.68 & -1.47 & -8.91 \times 10^{-4} \\ \hline 0 & 0 & 0 & 0 & 1 \end{array} \right], \quad (48)$$

so that

$$\mathbf{x}(k) = \tilde{\mathbf{T}}\tilde{\mathbf{x}}(k), \quad (49)$$

$$\mathbf{H}_d = \tilde{\mathbf{H}}_d \tilde{\mathbf{T}}^{-1} = \left[\begin{array}{cccc|c} 1 & 0 & 0 & 0 & 0 \\ 0 & 1 & 0 & 0 & 0 \\ 0 & 0 & 1 & 0 & 0 \\ 0 & 0 & 0 & 1 & 0 \end{array} \right], \quad (50)$$

and $\mathbf{A} = \tilde{\mathbf{T}}\tilde{\mathbf{A}}\tilde{\mathbf{T}}^{-1}$ and $\mathbf{B} = \tilde{\mathbf{T}}\tilde{\mathbf{B}}$.

Since $\text{rank} [\mathbf{H}_d] = 4$, the delayed-measurement observer described by (36) becomes a one-dimensional observer. Let the eigenvalue of \mathbf{F} be chosen as 0.1. Then we obtain

$$\mathbf{F} = 0.1,$$

$$\mathbf{K}_{11} = [3.376 \times 10^4 \quad -8.16 \times 10^{-4} \quad -3.881 \times 10^{-3} \quad -0.232].$$

From (36), (37) and (38), we obtain, after performing the inverse transformation,

$$\begin{aligned} z(k+1) &= 0.1 z(k) + 64.86 u(k) \\ &+ [-3.58 \times 10^4 \quad 1.11 \times 10^4 \quad -5.07 \times 10^3 \quad 1.88 \times 10^2] \begin{bmatrix} y(k) \\ y_{1d}(k) \\ y_{2d}(k) \\ y_{3d}(k) \end{bmatrix}, \end{aligned} \quad (51)$$

$$\hat{\mathbf{x}}_5(k) = z(k) + [3.376 \times 10^4 \quad -8.16 \times 10^{-4} \quad -3.881 \times 10^{-3} \quad -0.232] \begin{bmatrix} y(k) \\ y_{1d}(k) \\ y_{2d}(k) \\ y_{3d}(k) \end{bmatrix}, \quad (52)$$

$$\begin{bmatrix} \hat{\mathbf{x}}_2(k) \\ \hat{\mathbf{x}}_3(k) \\ \hat{\mathbf{x}}_4(k) \end{bmatrix} = \begin{bmatrix} -2.43 & 2.79 & -0.44 & 1.45 \times 10^{-2} \\ 141.2 & -108.9 & -28.95 & 1.15 \\ 7.52 & -117. & 44.68 & -1.47 \end{bmatrix} \begin{bmatrix} y(k) \\ y_{1d}(k) \\ y_{2d}(k) \\ y_{3d}(k) \end{bmatrix} + \begin{bmatrix} 5.6 \times 10^{-5} \\ -4.71 \times 10^{-3} \\ -8.91 \times 10^{-4} \end{bmatrix} \hat{\mathbf{x}}_5(k). \quad (53)$$

Simulation results of the open-loop turret control system (elevation channel) using a step input $u(k) = 1, k = 0, 1, \dots$, are as shown in Figs. 2 - 6. All estimates $\hat{x}_2(k), \hat{x}_3(k), \hat{x}_4(k)$ and $\hat{x}_5(k)$ took about 0.05 second to converge to their true values. Faster responses can, of course, be obtained by choosing suitable values for F , for example $F = 0.0$. It may be remarked that microprocessor-based implementation of the delayed-measurement observer developed in this paper are currently underway and excellent results have been obtained.

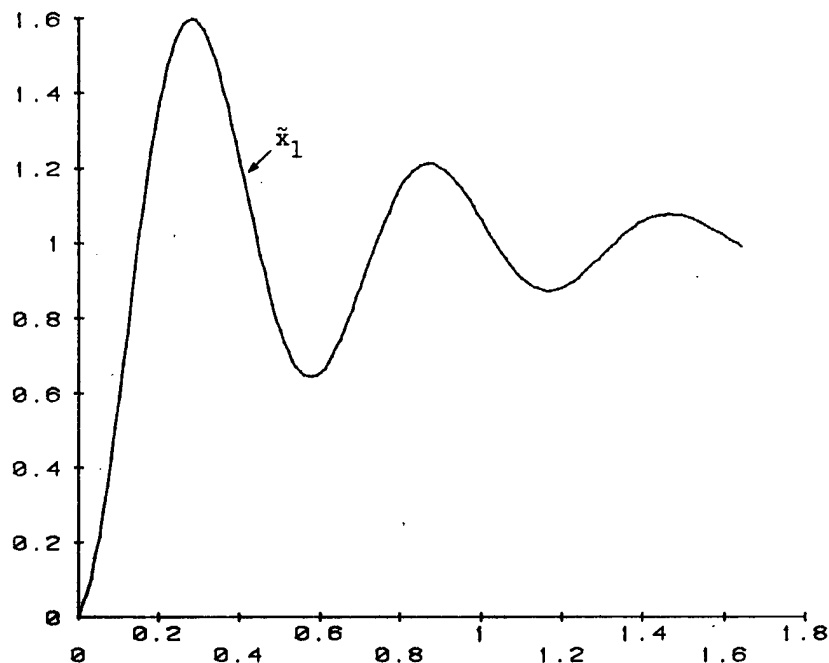


Fig. 2 OPEN-LOOP TURRET RESPONSE

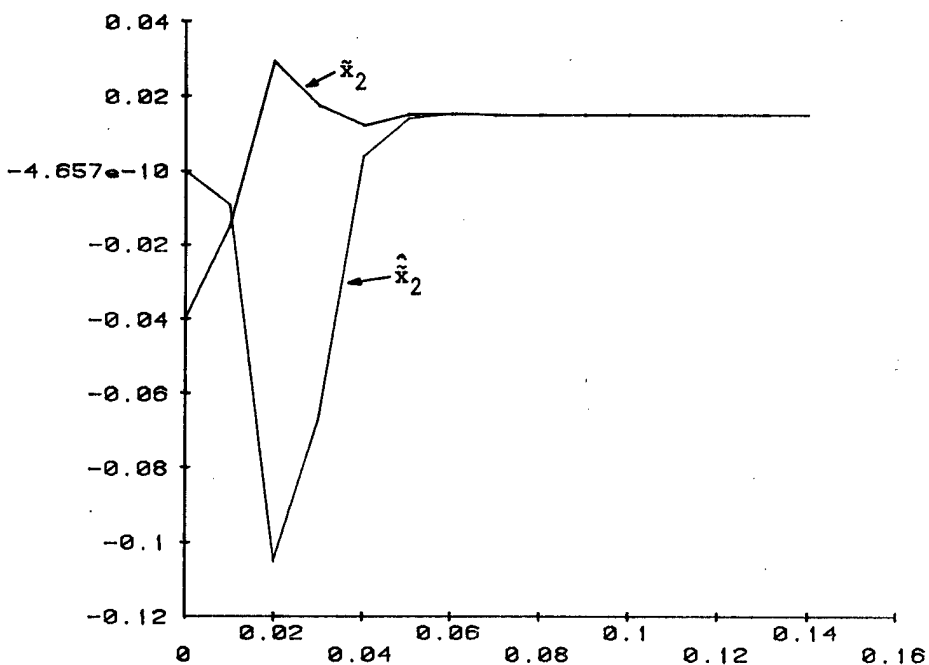


Fig. 3 OPEN-LOOP TURRET RESPONSE

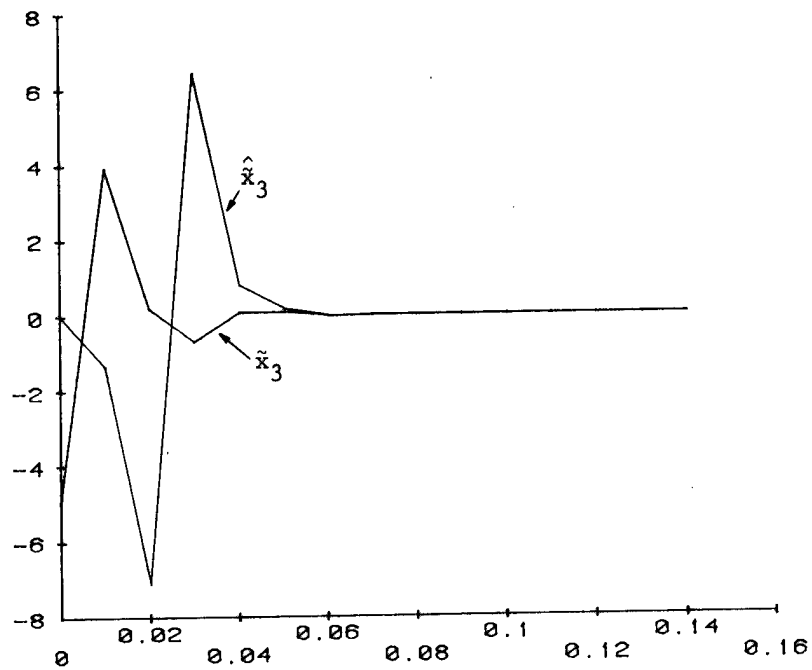


Fig. 4 OPEN-LOOP TURRET RESPONSE

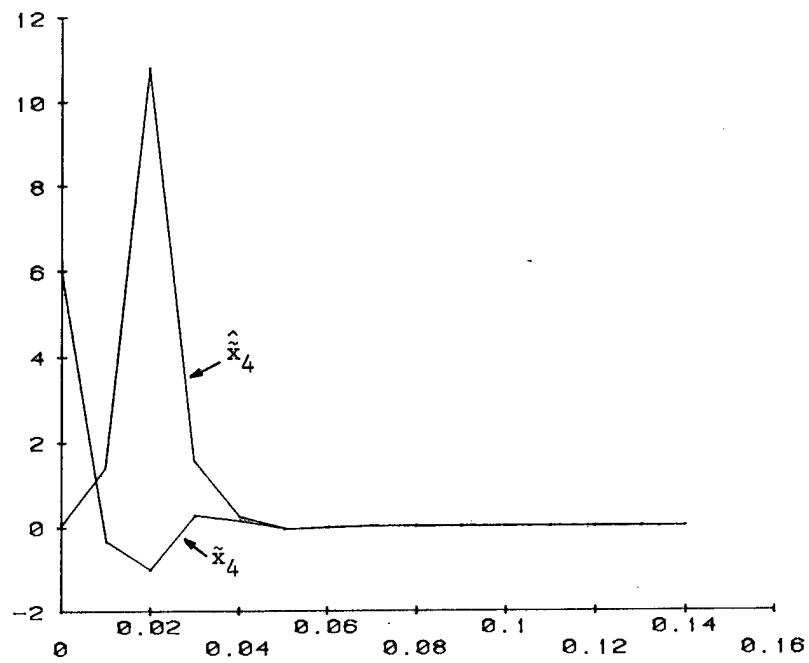


Fig. 5 OPEN-LOOP TURRET RESPONSE

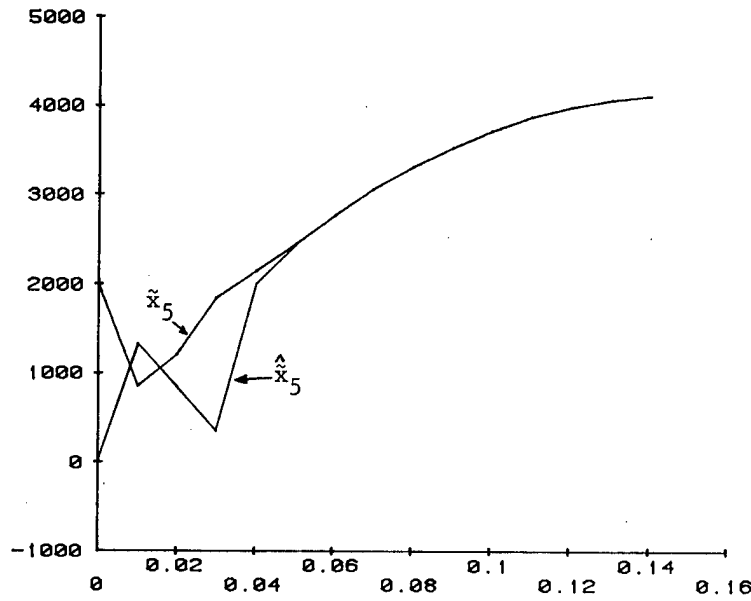


Fig. 6 OPEN-LOOP TURRET RESPONSE

APPENDIX I

We wish to show that (22) is asymptotically stable. Substituting (28) into (22) yields

$$e_z(k+1) = F_o[\bar{\Gamma} - \bar{\Gamma}H_o^T(R + H_o\bar{\Gamma}H_o^T)^{-1}H_o\bar{\Gamma}]\bar{\Gamma}^{-1}e_z(k), \quad (I-1)$$

and substituting the matrix inversion lemma

$$X - XH^T(R + HXH^T)^{-1}HX = (X^{-1} + H^TR^{-1}H)^{-1} \triangleq Y^{-1} \quad (I-2)$$

into (I-1) yields

$$e_z(k+1) = F_oY^{-1}\bar{\Gamma}^{-1}e_z(k). \quad (I-3)$$

Furthermore, using (I-2) in (29) yields

$$\bar{\Gamma}^{-1} = (F_oY^{-1}F_o^T + Q)^{-1}. \quad (I-4)$$

Consider the Lyapunov function

$$V(e_z) = e_z^T(k)\bar{\Gamma}^{-1}e_z(k). \quad (I-5)$$

From (I-2), (I-3), (I-4) and (I-5), we obtain the change $\Delta V(e_z)$ along the trajectories of (I-3),

$$\begin{aligned} \Delta V(e_z) &= e_z^T(k+1)\bar{\Gamma}^{-1}e_z(k+1) - e_z^T(k)\bar{\Gamma}^{-1}e_z(k) \\ &\leq e_z^T(k+1)\bar{\Gamma}^{-1}e_z(k+1) - e_z^T(k)\bar{\Gamma}^{-1}e_z(k) + \\ &\quad e_z^T(k)H_o^T(R + H_oH_o^T)^{-1}H_o e_z(k) \\ &= -e_z^T(k)\bar{\Gamma}^{-1}[Y^{-1} - Y^{-1}F_o^T(F_oY^{-1}F_o^T + Q)^{-1}F_oY^{-1}]\bar{\Gamma}^{-1}e_z(k), \end{aligned} \quad (I-6)$$

which becomes, upon using (I-2) again,

$$\Delta V(e_z) \leq -e_z^T(k)\bar{\Gamma}^{-1}(Y + F_o^TQ^{-1}F_o)^{-1}\bar{\Gamma}^{-1}e_z(k). \quad (I-7)$$

Hence $\Delta V(e_z) < 0$ for all $e_z(k) \neq 0$ so that (22) is asymptotically stable.

APPENDIX II

Consider an $m \times n$ matrix \tilde{W} of rank q given by

$$\tilde{W} = \left[\begin{array}{c|c} A & B \\ \hline C & D \end{array} \right] \quad (\text{II-1})$$

where A , B , C and D are, respectively, $q \times q$, $q \times (n-q)$, $(m-q) \times q$, $(m-q) \times (n-q)$ matrices. Without loss of generality, \tilde{W} is arranged such that A is nonsingular. The columns of $[B^T; D^T]$ may be expressed as linear combinations of the columns of $[A^T; C^T]$, i.e.,

$$\left[\begin{array}{c} A \\ \hline C \end{array} \right] X = \left[\begin{array}{c} B \\ \hline D \end{array} \right], \quad (\text{II-2})$$

where X is an $q \times (n-q)$ matrix. From (II-2), we obtain

$$X = A^{-1}B, \quad (\text{II-3})$$

$$D = CX = CA^{-1}B. \quad (\text{II-4})$$

Using the nonsingular transformation,

$$\tilde{T}^{-1} = \left[\begin{array}{c|c} A^{-1} & -A^{-1}B \\ \hline 0_{(n-q) \times q} & I_{n-q} \end{array} \right], \quad (\text{II-5})$$

we obtain

$$W = \tilde{W}\tilde{T}^{-1} = \left[\begin{array}{c|c} I_q & 0_{q \times (n-q)} \\ \hline CA^{-1} & 0_{(n-q) \times (n-q)} \end{array} \right] \quad (\text{II-6})$$

Now consider (1) and (9). Suppose these equations are originally given in terms of a state vector $\tilde{x}(k)$ not in the forms of (30) and (31), i.e.,

$$\tilde{x}(k+1) = \tilde{A}\tilde{x}(k) + \tilde{B}u(k) \quad (\text{II-7})$$

$$\begin{aligned} \left[\begin{array}{c} y(k) \\ \hline y_{1d}(k) \\ \hline y_{2d}(k) \end{array} \right] &= \tilde{H}_d \tilde{x}(k) = \left[\begin{array}{cc|c} C_{11A} & C_{11B} & C_{12} \\ H_{11A} & H_{11B} & H_{12} \\ \hline H_{21A} & H_{21B} & H_{22} \end{array} \right] \tilde{x}(k) \\ &\triangleq \left[\begin{array}{c|c} W_{11} & W_{12} \\ \hline W_{21} & W_{22} \end{array} \right] \tilde{x}(k), \end{aligned} \quad (\text{II-8})$$

where \tilde{H}_d has been arranged such that the $q \times q$ matrix W_{11} is nonsingular, and where by (II-4), $W_{22} = W_{21}W_{11}^{-1}W_{12} \triangleq H_{22}$.

The nonsingular transformation

$$\tilde{T} = \left[\begin{array}{c|c} W_{11} & W_{12} \\ \hline 0_{(n-q) \times q} & I_{n-q} \end{array} \right] \quad (\text{II-9})$$

with inverse

$$\tilde{T}^{-1} = \left[\begin{array}{c|c} W_{11}^{-1} & -W_{11}^{-1}W_{12} \\ \hline 0_{(n-q) \times q} & I_{n-q} \end{array} \right] \quad (\text{II-10})$$

yields (30) and (31) with $x(k) = \tilde{T}\tilde{x}(k)$, $A = \tilde{T}\tilde{A}\tilde{T}^{-1}$, $B = \tilde{T}\tilde{B}$, $H_d = \tilde{H}_d\tilde{T}^{-1}$ and $H_{21} = W_{21}W_{11}^{-1}$.

REFERENCES

- [1] R. E. Kalman, "Contributions to the theory of optimal control," Bol. Soc. Mat. Mex., vol. 5, pp. 102-199, 1960.
- [2] M. Athans and P. L. Falb, Optimal Control, New York: McGraw-Hill, 1966.
- [3] H. Kwakernaak and R. Sivan, Linear Optimal Control Systems, New York: Wiley-Interscience, 1972.
- [4] A. P. Sage and C. C. White, III, Optimum Systems Control, Second Edition, Englewood Cliffs, New Jersey: Prentice-Hall, 1977.
- [5] R. E. Kalman and R. S. Bucy, "New results in linear filtering and prediction theory," Trans. ASME, J. Basic Eng., ser. D, pp. 95-108, Mar. 1961.
- [6] D. G. Luenberger, "Observing the state of a linear system," IEEE Trans. Mil. Electron., vol. MIL-8, pp. 74-80, Apr. 1964.
- [7] D. G. Luenberger, "Observers for multivariable systems," IEEE Trans. Automat. Contr., vol. AC-11, pp. 190-197, Apr. 1966.
- [8] D. G. Luenberger, "An introduction to observers," IEEE Trans. Automat. Contr., vol. AC-16, pp. 596-602, Dec. 1971.
- [9] B. Gopinath, "On the control of linear multiple input-output systems," Bell Syst. Tech. J., vol. 50, pp. 1063-1081, Mar. 1971.
- [10] W. A. Wolovich, "On state estimation of observable systems," in 1968 Joint Automatic Control Conf., Preprints, pp. 210-220.
- [11] J. J. Bongiorno, Jr. and D. C. Youla, "On observers in multivariable control systems," Int. J. Contr., vol. 8, pp. 221-243, Sept. 1968.
- [12] Y. O. Yuksel and J. J. Bongiorno, Jr., "Observers for linear multivariable systems with applications," IEEE Trans. Automat. Contr., vol. AC-16, pp. 603-613, Dec. 1971.
- [13] M. Aoki and J. R. Huddle, "Estimation of the state vector of a linear stochastic system with a constrained estimator," IEEE Trans. Automat. Contr., vol. AC-12, pp. 432-433, Aug. 1967.
- [14] K. G. Brammer, "Lower order optimal linear filtering of nonstationary random sequences," IEEE Trans. Automat. Contr., vol. AC-13, pp. 198-199, Apr. 1968.
- [15] E. Tse and M. Athans, "Optimal minimal-order observer-estimators for discrete linear time-varying systems," IEEE Trans. Automat. Contr., vol. AC-15, pp. 416-426, Aug. 1970.
- [16] E. Tse and M. Athans, "Observer theory for continuous-time linear systems," J. Inform. Contr., vol. 22, pp. 405-434, 1973.
- [17] C. T. Leondes and L. M. Novak, "Optimal minimal-order observers for discrete-time systems - a unified theory," Automatica, vol. 8, pp. 379-387, 1972.
- [18] S. C. Iglehart and C. T. Leondes, "A design procedure for intermediate-order observer-estimators for linear discrete-time dynamical systems," Int. J. Contr., vol. 16, pp. 401-415, Mar. 1972.
- [19] J. O'Reilly and M. M. Newmann, "Minimum-order observer-estimators for continuous-time linear systems," Int. J. Contr., vol. 22, pp. 573-590, Apr. 1975.
- [20] L. M. Novak, "Discrete-time optimal stochastic observers," in Control and Dynamic Systems; Advances in Theory and Applications, vol. 12, C. T. Leondes Ed. New York: Academic, 1976.
- [21] F. W. Fairman, "Hybrid estimators for discrete-time stochastic systems," IEEE Trans. Syst. Man, Cybern., vol. SMC-8, pp. 849-854, Dec. 1978.
- [22] C. D. Johnson, "Accommodation of External disturbances in linear regulator and servomechanism problems," IEEE Trans. Automat. Contr., vol. AC-16, pp. 635-644, Dec. 1971.

- [23] C. D. Johnson, "Accommodation of disturbances in optimal control problems" Int. J. Contr., vol. 15, pp. 209-231, Feb. 1972.
- [24] C. D. Johnson, "Theory of disturbance-accommodating controller," in Control and Dynamic Systems; Advances in Theory and Applications, vol. 12, C. T. Leondes Ed. New York: Academic, 1976.
- [25] N. K. Loh and K. C. Cheok, "Design and implementation of optimal controllers for XM-97 helicopter turret control system," Technical Report TR-80-11-160, School of Engineering, Oakland University, Rochester, Michigan, Nov. 1980.
- [26] Special Issue on Disturbance-Accommodating Control Theory, J. Interdis. Model. & Simul., vol. 3, N. K. Loh and C. D. Johnson Co-Ed., Jan. 1980.
- [27] K. C. Cheok, N. K. Loh and R. R. Beck, "A microprocessor-based state estimator and optimal controller," Proc. of the 23rd Midwest Symposium on Circuits and Systems, University of Toledo, Toledo, Ohio, pp. 318-324, Aug. 1980.
- [28] N. K. Loh and D. H. Chyung, "State reconstruction from delayed observations," Proc. of the Fifth Annual Pittsburgh Conference on Modeling and Simulation, vol. 5, pp. 961-963, Apr. 1974.
- [29] D. H. Chyung and N. K. Loh, "State reconstruction from delayed partial measurements in discrete linear systems," Proc. of the Sixth Annual Pittsburgh Conference on Modeling and Simulation, vol. 6, pp. 159-161, Apr. 1975.
- [30] D. H. Chyung, "On a method for reconstructing inaccessible state variables using time delays," Division of Information Engineering, University of Iowa, Iowa City, Iowa, 1979.
- [31] J. L. Casti, Dynamical Systems and Their Applications: Linear Theory. New York: Academic Press, 1977.
- [32] T. Kailath, Linear Systems. Englewood Cliffs, New Jersey: Prentice Hall, 1980.
- [33] C. R. Rao and S. K. Mitra, Generalized Inverse of Matrices and Its Applications. New York: John Wiley, 1971.
- [34] T. E. Fortmann and D. Williamson, "Design of low-order observers for linear feedback control laws," IEEE Trans. Automat. Contr., vol. AC-17, pp. 301-308, June 1972.
- [35] W. M. Wonham, "On pole assignment in multi-input controllable linear systems," IEEE Trans. Automat. Contr., vol. AC-12, pp. 660-665, Dec. 1967.
- [36] K. L. Hitz and B. D. O. Anderson, "Iterative method of computing the limiting solution of the matrix Riccati differential equation," Proc. IEEE, vol. 119, pp. 1402-1406, Sept. 1972.
- [37] W. H. Kwon and A. E. Pearson, "A note on the algebraic matrix Riccati equation," IEEE Trans. Automat. Contr., vol. AC-22, pp. 143-144, Feb. 1977.
- [38] R. V. Patel and M. Toda, "On norm bounds for algebraic Riccati and Lyapunov equations," IEEE Trans. Automat. Contr., vol. AC-23, pp. 87-88, Feb. 1978.
- [39] K. Yasuda and K. Hirai, "Upper and lower bounds on the solution of the algebraic Riccati equation," IEEE Trans. Automat. Contr., vol. AC-24, pp. 483-487, June 1979.
- [40] B. D. O. Anderson and J. B. Moore, Optimal Filtering. Englewood Cliffs, New Jersey: Prentice-Hall, 1979.
- [41] G. Strang, Linear Algebra and Its Applications. New York: Academic Press, 1976.
- [42] D. L. Russell, Mathematics of Finite-Dimensional Control Systems. New York: Marcel Dekker, 1979.

ON-LINE IDENTIFICATION METHODS

Naim A. Kheir
School of Science & Engineering
The University of Alabama in Huntsville
Huntsville, AL 35899

and

Donald W. Sutherlin
U. S. Army Missile Command
Redstone Arsenal, AL 35898

ABSTRACT

A recent survey of the on-line identification techniques of process dynamics is presented and developments related to numerical behavior of algorithms addressed.

INTRODUCTION

Many techniques for identification of process dynamics have been reported during the last years as indicated by many of the references given in [1]. Basically identification, according to the definition given by Zadeh, is: "The determination, on the basis of input and output, of a system within a class of systems (models), to which the system under test is equivalent." From the definition of the term identification, there follows a classification of the different methods of identification:

- class of models: parametric versus non-parametric models,
- class of input signals: impulse, step, sinusoidal, white noise, colored noise, pseudo-random binary sequences,
- class for the equivalence of model and system: usually defined in terms of a criterion or a loss function,
- computational aspects: one-shot versus iterative (sequential) approaches,
- off-line methods
- on-line (real time) methods.

It is almost unique for identification problems occurring in automatic control to: (i) perform experiments on the system to obtain lacking knowledge, and/or (ii) design a control strategy as the purpose of the identification.

In general, some important major considerations for system identification are as follows:

- it is difficult to give a general answer to the question of what identification method should be used in a specific case; choice is intimately related to purpose of identification.
- the choice depends on so many factors, many of which are unknown when the method has to be chosen.
- it is often not possible to compare models obtained using different methods in a relevant way.
- for parametric models (with determined structure and order) it is not usually an easy task to choose model order.
- the a priori knowledge of the process strongly influences the results; for example, the more that is known about the properties of the disturbance of a process the more will be known about the accuracy of the model.
- properties of available data (experiment length, signal to noise ratio, sampling size ...).
- it is often necessary to carry out experiments during "normal operation"; thus introduced perturbations must be small.

The literature has reported a wide range of engineering and non-engineering applications where identification techniques have been quite useful, a sample may be found in References [2] - [7]. The problem of identification and the area of parameter

estimation have been the subject of many textbooks [8] - [18]. References [1] and [17] - [22] are selected survey papers on the subject.

Among the widely used identification techniques are the following:

- (1) least-squares regression
- (2) tally principle
- (3) generalized least-squares
- (4) instrumental variable method
- (5) Baye's method
- (6) Correlation technique
- (7) First and Second-order Stochastic Approximation
- (8) Kalman-Filtering algorithm
- (9) Square-Root algorithm
- (10) Box-Jenkins approach
- (11) the maximum likelihood method.

The non-parametric methods include the cross-correlation function approach, spectral analysis and covariance functions.

Before we present a detailed discussion on the on-line identification techniques, we will briefly outline the methods useful for off-line identification. The earliest methods of system identification are based on frequency, step and impulse responses. These techniques assume off-line identification and are applicable only to linear stationary processes where input/output relationships for one set of inputs hold for all inputs. The derivation of the complex gain of the system for an input of frequency ω is easily obtained by numerical Fourier transform using $G(j\omega) = \frac{X(j\omega)}{Y(j\omega)} =$

output $(j\omega)$ /input $(j\omega)$. This approach is, however, a lengthy one even if Fast Fourier transforms are used. Bode magnitude and phase plots are quite helpful in this regard. When using step response identification however, the initial rise-time (zero in an ideal step situation) should be much shorter than the period of the highest frequency of interest in the identification. Again Fourier transform could be used in this off-line identification using step responses. When impulse-response identification is used, the delta function is usually approximated by pulses of finite width.

ON-LINE TECHNIQUES

One useful on-line method is based on the employment of correlation-function techniques to transform the identification problem into impulse-response problem without actual need to apply impulse functions. This is achieved when white noise is applied as an input to the process (white noise is defined as an uncorrelated random input with an infinite flat frequency spectrum and zero mean). If noise is used with a sufficiently low amplitude, it might be super-imposed on the normal-operation input to the system without any effect on its performance. Defining the input auto-correlation function:

$$\phi_{yy}(\theta) = \lim_{T \rightarrow \infty} \frac{1}{2T} \int_{-T}^T y(t) y(t - \theta) dt$$

and the cross-correlation function $\phi_{xy}(\theta)$ as:

$$\phi_{xy}(\theta) = \lim_{T \rightarrow \infty} \frac{1}{2T} \int_{-T}^T x(t) y(t - \theta) dt$$

It can be shown that the system's response $g(t)$ to an impulse input at $t = \theta$ is easily obtained from:

$$\begin{aligned} \phi_{xy}(\theta) &= \int_0^{\theta} g(\tau) \delta(\theta - \tau) d\tau \\ &= g(\theta) \end{aligned}$$

where the autocorrelation integral of a white noise input, due to its uncorrelated randomness properties, is a delta function. It is interesting to note how the frequency response is related to correlation functions. Since a white noise input $y(t)$, satisfies

$$\phi_{yy}(\theta) \approx \delta(\theta)$$

we get

$$\phi_{yy}(j\omega) \approx 1$$

thus

$$G(j\omega) = \phi_{xy}(j\omega).$$

From a computational point of view, rather than deriving $\phi_{xy}(j\omega)$, $\phi_{yy}(j\omega)$ and then find $G(j\omega)$ it is much faster to find the Fourier Transform $X(j\omega)$ of $x(t)$ and $Y(j\omega)$ of $y(t)$. In this procedure, no computation will be required for $\phi_{xy}(\theta)$ and $\phi_{yy}(\theta)$ and:

$$\begin{aligned} \phi_{xy}(j\omega) &= X(j\omega) Y^*(j\omega) \quad \text{where } Y^* \text{ is conjugate of } Y \\ \text{and } \phi_{yy}(j\omega) &= Y(j\omega) Y^*(j\omega). \end{aligned}$$

It is worth noting that even when $\phi_{xy}(\theta)$ and $\phi_{yy}(\theta)$ are required, their calculation could be performed by first computing the Fast Fourier transform $\phi_{xy}(j\omega)$ and $\phi_{yy}(j\omega)$ and subsequently perform an inverse FFT to them.

On-line multi-variable identification is also possible through least-squares regression procedures. Curve-fitting, as an example, illustrates the idea behind this technique where it is usually desired to find a functional form of some specified order that best fits a given set of data (measurements). The criterion for goodness of fit is to minimize the sum of squares of differences between real world data and the estimated functional form or curve. One characteristic of regression techniques, in general, is that they require the accumulation of nonsteady state input/output data over at least $m + 1$ sampling intervals (where m is the number of parameters to be identified) before regression can be performed.

If \underline{V} is a vector of measurement noise and \underline{Z} is a set of measurements, then the unknown quantities \underline{X} are related to \underline{Z} and \underline{V} as follows:

$$\underline{Z} = \underline{H}\underline{X} + \underline{V}.$$

The question is then to find an estimate $\hat{\underline{X}}$ that minimizes the sum of the squares of the elements of the vector difference: $\underline{Z} - \underline{H}\hat{\underline{X}}$. It can be shown that the least-squares estimate is:

$$\hat{\underline{X}} = (\underline{H}^T \underline{H})^{-1} \underline{H}^T \underline{Z}$$

where $()^T$ and $()^{-1}$ indicate transpose and inverse respectively. It is obvious that this procedure requires matrix inversion. This inversion could be avoided if one uses a sequential formulation of this regression technique. Moreover, sequential least-squares are not only applicable to linear and nonlinear stationary systems but they also require little computer storage and are fast to implement. There are two further drawbacks to the classical method of least-squares; first there can be no missing data pairs in the sampled input/output data sequence (which could be a very restrictive feature), and secondly the effects of new observations can be accounted for only by rerunning the whole estimation using the expanded set of data. An on-line identification of parameters using recursive generalized least-squares procedure has been reported in Ref. (23). In this recursive situation, there will be no need to store past measurements for the purpose of computing present estimates.

The maximum likelihood identification method has been widely used in the field of process parameter identification. The original method is found to be inconvenient for an on-line situation. A recursive on-line maximum likelihood identification algorithm has been suggested by Gertler and Banyasz [25]. This modified version is similar to the recursive generalized least-squares method of Hastings-James and Sage [23].

Recalling the model of the measurement process:

$$\underline{Z} = \underline{H} \underline{X} + \underline{V}$$

One may seek to minimize the weighted sum of squares of deviations:

$$\underline{J} = (\underline{Z} - \underline{H} \hat{\underline{X}})^T \underline{R}^{-1} (\underline{Z} - \underline{H} \hat{\underline{X}})$$

where \underline{R}^{-1} is a symmetric, positive definite weighting matrix, the weighted-least-squares estimate is obtained as:

$$\hat{\underline{X}} = (\underline{H}^T \underline{R}^{-1} \underline{H})^{-1} \underline{H}^T \underline{R}^{-1} \underline{Z}$$

The maximum likelihood technique suggests $\hat{\underline{X}}$ as that value which maximizes the probability of measurements \underline{Z} which actually occurred taking into account known statistical properties of noise \underline{V} . Note that in this discussion no statistical model is assumed for the variable \underline{X} . For the case of \underline{V} being of Gaussian joint distribution such that:

$$E(\underline{V} \underline{V}^T) = \underline{R} \text{ (with } E \text{ denoting expectation)}$$

the above expression for $\hat{\underline{X}}$ becomes a minimum variance linear estimate of \underline{X} since it maximizes the likelihood function of $p(\hat{\underline{V}}) = p(\underline{Z} - \underline{H} \hat{\underline{X}})$. It is interesting to note that for Gaussian \underline{V} , when \underline{V} is independent, with $\underline{R} = \sigma^2 \underline{I}$, the least-squares regression estimate is a maximum likelihood estimate. A discussion on the maximum likelihood estimation of the coefficients of multiple output linear system and noise correlations from noisy measurements of input and output is presented in [26].

Less widely used on-line identification methods are the quasilinearization approach and the invariant imbedding identification. The quasilinearization technique [27] is concerned with the transformation of nonlinear multi-point boundary value problem into a linear nonstationary problem. Here, the type of nonlinearity must be given at least in terms of an approximation. Quasilinearization procedure converges to the true parameters only if the initial guess of the parameter value is within the convergence bounds; thus it requires a certain prior knowledge of the parameter range of values. It is interesting to note that the quasilinearization approach is based upon a "fixed" number of measurements rather than on a growing number of measurements. The invariant imbedding identification [28] is usually employed for nonlinear systems; it also requires prior knowledge of the forms of nonlinear functions whose parameters are to be identified. Some a priori knowledge of the range of parameter values is required. Inadequate choices of initial values may cause divergence or slow convergence of the identification. In spite of the generality of this method, it is of limited use for on-line identification due to its computation complexity.

Let us direct our attention to two widely used on-line identification approaches, the Kalman-Filter and the Autoregressive Moving Average (ARMA) models. As was stated earlier, a recursive filter is one in which there is no need to store past measurements for the purpose of computing estimates. In order to appreciate the value of a recursive filter, let us compare the following two expressions for $\hat{\underline{X}}_{k+1}$, the value of $\hat{\underline{X}}$ at t_{k+1} , if

$$\underline{Z}_i = \underline{X} + \underline{V}_i \quad (i = 1, 2, \dots, k)$$

where \underline{Z}_i is noise-corrupted measurement, and

\underline{V}_i is the measurement noise (could be assumed white noise)

$$(i) \quad \hat{\underline{X}}_{k+1} = \frac{1}{k+1} \sum_{i=1}^{k+1} \underline{Z}_i$$

$$(ii) \quad \hat{\underline{X}}_{k+1} = \hat{\underline{X}}_k + \frac{1}{k+1} (\underline{Z}_{k+1} - \hat{\underline{X}}_k)$$

In the latter expression, the need to store past measurements is eliminated and this is where the value of a recursive linear estimate lies. Note that $(\underline{Z}_{k+1} - \hat{\underline{X}}_k)$ is usually termed the measurement "residual." The discrete formulation of a linear system state at discrete points in time, t_k , usually takes the form:

$$\underline{X}_k = \Phi_{k-1} \underline{X}_{k-1} + \underline{W}_{k-1}$$

where \underline{W}_k is a zero mean white sequence of covariance

$$Q_k = E[\underline{W}_k \underline{W}_k^T] .$$

As before, we express the measurements \underline{Z}_k at time t_k as a linear combination of the system state variables corrupted with white noise:

$$\underline{Z}_k = H_k \underline{X}_k + \underline{V}_k .$$

\underline{V}_k here represents random noise quantities with zero mean and covariance $R_k = E[\underline{V}_k \underline{V}_k^T]$. Denoting $\hat{\underline{X}}_k(-)$ as the a priori estimate of the system state at time t_k , we define $\hat{\underline{X}}_k(+)$ as the updated estimate based on the use of \underline{Z}_k . Thus, a linear recursive form for the update estimate becomes:

$$\hat{\underline{X}}_k(+) = \hat{K}_k \hat{\underline{X}}_k(-) + K_k \underline{Z}_k$$

where \hat{K}_k and K_k are time-varying weighting matrices.

In the discrete-Kalman filter [12], [17], [18], [29], [30], we define $\tilde{\underline{X}}_k(-)$ and $\tilde{\underline{X}}_k(+)$ to be the estimation error such that:

$$\begin{aligned} \hat{\underline{X}}_k(+) &= \underline{X}_k + \tilde{\underline{X}}_k(+) \\ \hat{\underline{X}}_k(-) &= \underline{X}_k + \tilde{\underline{X}}_k(-) . \end{aligned}$$

Using these equations in the update form, we get:

$$\tilde{\underline{X}}_k(+) = [\hat{K}_k + K_k H_k - I] \underline{X}_k + \hat{K}_k \tilde{\underline{X}}_k(-) + K_k \underline{V}_k .$$

Since $E[\underline{V}_k] = \underline{0}$ and if $E[\tilde{\underline{X}}_k(-)] = \underline{0}$ and $E[\tilde{\underline{X}}_k(+)] = \underline{0}$ the term in brackets i.e., $[\hat{K}_k + K_k H_k - I]$ must equal zero as well resulting this form of the estimation error:

$$\tilde{\underline{X}}_k(+) = (I - K_k H_k) \tilde{\underline{X}}_k(-) + K_k \underline{V}_k .$$

Defining the error covariance matrix as:

$$P_k(+) = E[\tilde{\underline{X}}_k(+) \tilde{\underline{X}}_k(+)^T]$$

and using the above results we obtain:

$$P_k(+) = (I - K_k H_k) P_k(-) (I - K_k H_k)^T + K_k R_k K_k^T .$$

In arriving at this result we assumed that the measurement errors were uncorrelated and thus:

$$E[\tilde{\underline{X}}_k(-) \underline{V}_k^T] = E[\underline{V}_k \tilde{\underline{X}}_k^T(-)] = 0 .$$

The optimum choice of K_k is based on minimizing a weighted scalar sum of the diagonal elements of the error covariance matrix $P_k(+)$, i.e.

$$J_k = E[\tilde{\underline{X}}_k(+)^T S \tilde{\underline{X}}_k(+)]$$

where S is any positive semidefinite matrix. Letting $S = I$ the Kalman gain matrix becomes:

$$K_k = P_k(-) H_k^T [H_k P_k(-) H_k^T + R_k]^{-1}$$

The optimized updated estimation error covariance matrix $P_k(+) = [I - K_k H_k] P_k(-)$, and the error covariance extrapolation matrix thus becomes:

$$P_k(-) = \Phi_{k-1} P_{k-1}(+) \Phi_{k-1}^T + Q_{k-1}$$

Kailath [31] has defined the sequence:

$$\underline{v}_1 = \underline{z}_1 - H \hat{\underline{x}}_1$$

as the "innovation sequence" and had shown that for an optimal filter this sequence is a Gaussian white noise sequence. Mehra [29] used the innovation sequence to check the optimality of a Kalman filter. Moreover, he used it to estimate the process noise covariance matrix Q and the measurement noise covariance matrix, R . Mehra, in Reference [30], has used the innovation property to handle an important problem and that is of the determination of the order of a system. Martin and Stubberud [17] have devoted in their recent study a comprehensive review of the innovations property and its applications to identifications; they discussed some relative advantages of computational and computer implementation simplicity. It is worth mentioning that extending the applicability of the Kalman filter to nonlinear cases has been successful, and CADET [18] has been developed as an analytical technique for analyzing nonlinear stochastic systems. The equations for the continuous-discrete Extended Kalman Filter are on page 188 of Reference [18]. See Reference [3] for an application of Extended Kalman Filter to postflight data analysis.

One of the major reported problems with the minimum-variance recursive Kalman filter estimator is what has been termed the "divergence problem" in some applications. Divergence is said to occur when the error covariance calculated by the estimator becomes inconsistent with the actual error covariance. Nahi and Schaffer [32] have based their divergence prevention scheme on constant checking the consistency of the calculated and the actual error covariances. They designed a test for inconsistency and an adaptive decision-directed procedure for adjusting the calculated covariance. Their approach is accomplished by testing whether or not the observation at each stage is likely to have come from a distribution with the calculated covariance.

Bierman [12] discusses several types of divergence phenomena that may exist with Kalman's solution to the linear parameter estimation problem:

- (i) divergence due to the use of incorrect statistics and unmodeled parameters,
- (ii) divergence due to the presence of nonlinearities, and
- (iii) divergence due to the effects of computer roundoff.

Bierman has recommended a square root information filter (SRIF) which compares favorably with conventional algorithm mechanization in terms of algorithms complexity, storage and computer run times. The improved numerical behavior of the SRIF is due in the large part to a reduction of the numerical ranges of the variables, and thus producing results comparable with a Kalman filter that uses twice its numerical precision.

Saridis and Stein (33) have presented a generalized algorithm for on-line identification of stochastic linear discrete-time system using noisy input and output measurements. Their stochastic approximation approach converges for arbitrary but known numerator dynamics and for noisy measurement conditions, provided that the noise variances are specified. The mean square convergence of the stochastic approximation algorithm to the correct result is guaranteed under conditions that are, for many physical systems, easily satisfied. In Reference (17), the authors, in order to reduce the required convergence time, use an adaptive version of the stochastic approximation method due to Sakrison [34].

A fundamental property of random signals with Gaussian is that when processed through a linear dynamic system, the resulting output is also Gaussian. Thus, any Gaussian time sequence may be considered to be the output of some linear system whose input is an independent Gaussian time sequence. The Kalman filter is in this regards the optimal linear predictor for predicting a Gaussian process. Let the following transfer function $G(s)$ represent a general linear model for a stationary time sequence:

$$\begin{aligned} G(s) &= \frac{x(s)}{u(s)} \\ &= \frac{D_m s^m + D_{m-1} s^{m-1} + \dots + D_1 s + D_0}{A_n s^n + A_{n-1} s^{n-1} + \dots + A_1 s + A_0} \end{aligned}$$

where s is the Laplace transform variable. Defining Z^{-1} as the backward shift operator ($Z^{-n} x_k = x_{k-n}$), the above equation will assume the discrete form:

$$G(Z) = \frac{\beta_0 + \beta_1 Z^{-1} + \dots + \beta_m Z^{-m}}{\alpha_0 + \alpha_1 Z^{-1} + \dots + \alpha_n Z^{-n}} = \frac{x(Z)}{u(Z)}$$

Using B in place of Z^{-1} , we write:

$$G(B) = K \frac{1 + b_1 B + \dots + b_m B^m}{1 + a_1 B + \dots + a_n B^n}$$

where $\alpha_0/\beta_0 = K$; $\beta_1/\beta_0 = b_1$; $\alpha_1/\alpha_0 = a_1$.

x denotes the message and u is a Gaussian random input signal with zero mean.

The discrete transfer function above could be rewritten as:

$$\begin{aligned} x_k + a_1 x_{k-1} + \dots + a_n x_{k-n} &= u_k + b_1 u_{k-1} + \dots + b_m u_{k-m} \\ \text{or} \quad x_k &= \sum_{i=1}^n \phi_i x_{k-i} + \sum_{j=0}^m \theta_j u_{k-j} \end{aligned}$$

where $k = 0, 1, 2, \dots$; $t = kT$.

and $E[u_j] = 0$ for all j .

This equation represents a mixed autoregressive-moving-average (ARMA) model of x_k . The ϕ 's denote the autoregressive coefficients related to the history of the message itself while the θ 's are termed the moving average coefficients related to the history of the random input signal. Rewriting the ARMA equation we get:

$$\begin{aligned} \phi(B) x_k &= \theta(B) u_k \\ \text{or} \quad \theta^{-1}(B) \phi(B) x_k &= u_k. \end{aligned}$$

This is a convergent infinite pure autoregressive (AR) process. We may likewise write the ARMA model as:

$$x_k = \phi^{-1}(B) \theta(B) u_k$$

which is a convergent infinite moving-average (MA) process. The convergence features of the infinite models facilitate them to be expressed in terms of finite orders. It should be noted here that identification should aim at the minimum adequate order. In References 6 and 7, this writer has developed an ARMA model to adequately fit a noise time series. Graupe [35] has outlined a procedure for sequentially estimating the parameters and orders of mixed ARMA models. The procedure is based on first identifying a purely AR signal model. The uniqueness of the maximum likelihood estimates of the parameters of an ARMA model has been discussed by Astrom [36].

According to the Box-Jenkins time-series techniques, once the parameters of the mixed ARMA model are available, it yields forecasts (predictions) that are comparable to those obtained from a Kalman Filter whose parameters are known. The difference between the two approaches lies in the fact that forecasting via ARMA models requires the reconstruction of the inputs from, say, the least-squared prediction errors, whereas, the equivalent Kalman Filter avoids this reconstruction through sequentially updating gains associated with the last error term. It should be noted that it is possible to transform an ARMA model into a state-space formulation to yield and to update a Kalman filter model for subsequent prediction without reconstruction of inputs (with the Kalman filter, however, the parameters and orders must be known). A discussion on developing an AR model based on the maximum likelihood has been developed; see, for example, Reference [37].

ACKNOWLEDGMENT

This work was supported by the U. S. Army Research Office for the U. S. Army Missile R & D Command, Redstone Arsenal. This research was performed during the Summer of 1978 under the Laboratory Research Cooperative Program (LRCP).

REFERENCES

1. K. J. Astrom and P. Eykhoff, "System Identification - A Survey," *Automatica* 7, pp. 123-162, 1971.
2. S. R. Brubacher and G. T. Wilson, "Interpolating Time Series with Application to the Estimation of Holiday Effects on Electricity Demand," *Appl. Statistic* 25, pp. 107, 1976.
3. J. Mendel, "Postflight Data Analysis by Means of Adaptive, Extended Kalman Filtering," *IEEE Trans. Vol. AC-19*, pp. 467, October 1974.
4. F. D. Galiane, et al, "Identification of Stochastic Electric Load Models from Physical Data," *IEEE Trans. Vol. AC-19*, pp. 887, December 1974.
5. F. M. Fisher, "The Identification Problem in Econometrics," McGraw-Hill, N.Y., 1966.
6. N. A. Kheir and L. Greene, "On Validating Missile Simulation: Field Data Analysis and Time-Series Model," U. S. Army Missile R & D Command, Tech. Report No. T 78-40, March 1978.
7. N. A. Kheir and D. Sutherlin, "Missile Simulation in Presence of Noise and Multi-Source Environment," *Proc. of the Summer Computer Simulation Conference, California*, pp. 435-438, July 1978.
8. A. P. Sage and J. L. Melsa, System Identification, Academic Press, 1972.
9. R. C. K. Lee, Optimal Estimation; Identification and Control, MIT Press, 1964.
10. P. Eykhoff, System Parameter and State Estimation, J. Wiley, 1974.
11. D. Graupe, Identification of Systems, R. E. Krieger Publishing Co., 1976.
12. G. Bierman, Factorization Methods for Discrete Sequential Estimation, Academic Press, *Math in Science and Engineering Series*, Vol. 128, 1977.
13. C. E. P. Box and C. M. Jenkins, Time Series Analysis, Forecasting and Control, Holden Day, 1970.
14. A. H. Jazwinski, Stochastic Processes and Filtering Theory, Academic Press, 1970.
15. C. E. P. Box, et al, Models for Forecasting Seasonal and Non-seasonal Time Series, *Advanced Seminar on Spectral Analysis of Time Series* (edited by B. Harris), pp. 271-311, J. Wiley, 1967.
16. R. L. Kashyap, et al, Stochastic Approximation, in Adaptive, Learning and Pattern Recognition Systems, (edited by J. Mendel and K. S. Fu), Academic Press, 1970.
17. W. C. Martin and A. R. Stubberud, "The Innovations Process with Applications to Identifications," in *Control and Dynamic Systems*, (edited by C. T. Leondes), Vol. 12, Academic Press, pp. 193-258, 1976.
18. A. Gelb, et al, Applied Optimal Estimation, The MIT Press, 1974.
19. P. Eykhoff, "Process Parameter and State Estimation," *Automatica* 4, 205-233, 1968.

20. A. V. Balakrishman and V. Peterka, "Identification in Automatic Control Systems, Automatica 5, 817-829, 1969.
21. M. Cuenod and A. Sage, "Comparison of Some Methods for Process Identification," Automatica 4, 235-269, 1968.
22. Eykhoff, Van Der Grinten, Kwakernaak, and Veltman, "System Modeling and Identification," Proc. Third IFAC Congress, London, 1966.
23. R. Hastings-James, et al, "Recursive Generalized Least Squares Procedure for On-line Identification of Process Parameters," Proc. of IEEE Control & Sciences Vol. 116, p. 2057-2062, 1969.
24. K. J. Astrom and T. Bohlin, "Numerical Identification of Linear Dynamic Systems from Normal Operating Records," presented at the IFAC Symp. Theory of Self-Adaptive Cont. Syst., Teddington, England, 1965.

Also in P. H. Hammond Ed., Theory of Self-Adaptive Control Systems, New York, Plenum, 1966.
25. J. Gertler and C. Banyasz, "A Recursive (on-line) Maximum Likelihood Identification Method," IEEE Trans. Vol. AC-19, No. 6, pp. 816, Dec. 1974.
26. R. L. Kashyap, "Maximum Likelihood Identification of Stochastic Linear Systems," IEEE Trans., Vol. AC-15, No. 1, pp. 25-34, February 1970.
27. A. P. Sage and B. R. Eisenberg, "Experiments in Nonlinear and Nonstationary System Identification via Quasilinearization and Differential Approximation," Proc. Joint Aut. Control Conf., pp. 522-530, 1965.
28. A. P. Sage and G. W. Masters, "On Line Estimation of States and Parameters of Discrete Non-linear Dynamic Systems," Proc. National Electronics Conf., Vol. 22, pp. 677-682, 1966.
29. R. K. Mehra, "On the Identification of Variances and Adaptive Kalman Filtering," IEEE Trans. Vol., AC-15, No. 2, pp. 175, April 1970.
30. R. K. Mehra, "On Line Identification of Linear Dynamic Systems with Applications to Kalman Filtering," IEEE Trans., Vol. AC-16, No. 1, p. 12, February 1971.
31. T. Kailath, "An Innovation Approach to Least Squares Estimation," Part I, IEEE Trans., Vol. AC-13, pp. 646-655, December 1968.
32. N. E. Nahi and B. M. Schaffer, "Decision-Directed Adaptive Recursive Estimators: Divergence Prevention," IEEE Trans., Vol. AC-17, No. 1, pp. 61, February 1972.
33. G. N. Saridis and G. Stein, "Stochastic Approximation Algorithms for Linear Discrete-Time System Identification," IEEE Trans., Vol. AC-13, No. 5, pp. 515, Oct. 1968.
34. D. L. Sakrison, Adv. Comm. Syst., Vol. 2, 1966.
35. D. Graupe, et al, "Identification of ARMA Parameters of Time-Series," IEEE Trans., pp. 104, February 1975.
36. K. J. Astrom and T. Soderstrom, "Uniqueness of the Maximum Likelihood Estimates of the Parameters of an ARMA Model," IEEE Trans., Vol. AC-19, No. 6, pp. 769, December 1974.
37. F. C. Schweppe, "Uncertain Dynamic Systems," Prentice-Hall, 1973, pp. 444-445.

Next page is blank.

A MULTIPLE MODEL LEAD PREDICTION ALGORITHM FOR MANEUVERING TARGET ENGAGEMENT

Pak T. Yip
Control & Stabilization Team
FC&SCWSL, US ARRADCOM
Dover, New Jersey 07801

ABSTRACT

The effective engagement of maneuvering or non-cooperative targets is a problem which has been of interest in tank fire control for several years. The approach to this problem taken in this paper involves a multiple model adaptive filter structure to process target range and bearing measurements required for target state estimation and gun lead angle computation. This paper discusses the status of technical efforts directed toward the real time microcomputer implementation of this fire control concept.

INTRODUCTION

Effective engagement of maneuvering or non-cooperative targets has been an area of interest in tank fire control for several years. Solutions to this problem include, among others, upgrading the tracker, the sensor, and the stabilization as well as consideration of advanced lead prediction algorithms. With the rapid advancement of microcomputer technology, it has now become feasible to consider the real time implementation of these advanced fire control algorithms and thereby enhance the overall performance of the fire control system.

Roughly, we have four major tasks to consider: system modeling, system configuration, digital simulation, and real time simulation. System modeling includes system data analysis, model formulation, and parameter identification. System configuration includes choice of basic algorithm, arrangement of models, and selection of adaptive policy. Digital simulation requires choice of data segment, choice of nominal conditions, generation of noise for input data, Monte Carlo simulations, and the evaluation of system performance. But, numerical stability, accuracy of computation, memory size of microprocessor, and computational speed are additional considerations in real time implementation. This paper discusses each of these areas as it relates to tank fire control engagement of maneuvering targets.

SYSTEM MODELING

The energy spectra of target maneuver data provides qualitative information useful in determining target model structure and initial parameter values while maximum likelihood identification has proved to be a valuable tool for optimizing the selection of the model parameters.

The Antitank Missile Test (ATMT) Phase II data base¹ was used to identify the target acceleration models since it represents the best available experimental test data reflecting the maneuver characteristics of vehicles such as M60A1 tank, Scout vehicle and Twister vehicle, covering a broad spectrum of speed up to 30 miles per hour and acceleration up to 0.5 g. Since our interest was in modeling the target acceleration, the position data was sampled at a frequency of 2 cps and twice differentiated to obtain the acceleration estimates which was then resolved into along-track and cross-track components. The power spectral density of this data was computed by the maximum entropy methods² which assumes the data is generated by an autoregressive process. The power spectral density $S(f)$ is given by

$$S(f) = \frac{2 \sigma^2}{\left| 1 - \sum_{i=1}^M \alpha_i \exp(-j2\pi f i) \right|^2}$$

where σ_g is the standard deviation of a Gaussian noise process; α_i is the i -th coefficient of the autoregressive process; M is the number of coefficients, and the coefficients α 's are estimated recursively. The number of coefficients of autoregression is determined by minimizing the Akaike's final prediction error³.

The number of the autoregressive coefficients is usually larger than three which is not desirable for Kalman Filtering. However, the power density spectrum affords enough information for estimating essential poles and zeros of a simple rational polynomial model structure. The simplified model has the following form:

$$A(s) = \frac{S + \delta}{S^2 + \beta_1 S + \beta_2} q(s)$$

where $q(s)$ is the Gaussian noise process; $A(s)$ is the system acceleration; δ , β_1 and β_2 are parameters to be identified for the chosen vehicle paths and each of the along-track and cross-track formulations.

Since the target range and azimuth are processed as measurements and the target accelerations are defined in the target coordinates, while the mathematics is done in a cartesian system, the required transformation of coordinates introduces nonlinearity into the estimation problem. Hence, the acceleration model was embedded in an Extended Kalman Filter algorithm. The model parameter vector is chosen to maximize the likelihood function⁴, or equivalently minimize the negative log likelihood function $M(\underline{Z}^k; \underline{\alpha})$, where \underline{Z}^k was the entire sequence of k samples of the measurement vector \underline{Z} . The Gauss-Newton method was used in the minimization procedure:

$$\underline{\alpha}_{j+1} = \underline{\alpha}_j - \rho D^{-1} \frac{\partial M(\underline{Z}^k; \underline{\alpha}_j)}{\partial \underline{\alpha}_j}$$

where $\rho = 1$ for this method, and D , the expected Hessian

$$D = E \left\{ \frac{\partial^2 M(\underline{Z}; \underline{\alpha}_j)}{\partial \underline{\alpha}_j^2} \right\}$$

The test for convergency was given by

$$(\underline{\alpha}_{j+1} - \underline{\alpha}_j)^T D (\underline{\alpha}_{j+1} - \underline{\alpha}_j) < 10^3$$

SYSTEM CONFIGURATION

There exists a maximum level of maneuver that the ground vehicles under study can attain. This maximum level provides a non-trivial range of dynamic motion that can be quantized to a finite number of maneuver levels. In this study, five different parameter values were selected and the corresponding Extended Kalman Filters structured to simultaneously process tracking input data in parallel and output target state estimates. One of the filters in the design was a simple 4-state filter based on a constant velocity target model. The remaining four filters were identified with various maneuver levels.

Several interesting options are available to provide some adaptive capability to the algorithm including adapting the plant noise model or adapting the prediction model. The approach taken in this investigation is to select the filter with the maximum computed likelihood function. More precisely, target range and azimuth angle are processed by the parallel filters and the filter having the largest likelihood function is automatically chosen to provide the best estimate for lead prediction and gun orders. The prediction model is the common second order function of projectile time of flight.

DIGITAL SIMULATION

A Monte Carlo simulation of 100 runs was set up to process a large number of 10 second segments representing various maneuver levels of the M60A1 tank, Twister and Scout vehicles. These segments of data were different from those used for the parameter identification tasks discussed earlier. For the introduction of measurement noise, two Gaussian random number generators were used with different seeds to start each run.

For evaluating the system performance, the perpendicular miss distance of the predicted line of sight from the real target position was defined as the prediction error. The firing time points were fixed for each segment under process. The performance indicator

ph at each firing time point was defined as the ratio of the number of times that the prediction error is less than 1.15 meters to the total number of runs. Basically, they are hit probabilities considering the prediction errors alone.

For an engagement range of approximately 2000 meters, 45° cross range (across the range vector), / sigma range measurement error of 2 meters, / sigma azimuth tracking error of 0.3 mils, a projectile speed of 1500 meters per second and 7 firing points per segment, the hit probability results are summarized in the following table:

Target Type	Number of Segments	Mean ph	
		Constant Velocity Model	Adaptive Model
M60A1	13	.41	.49
SCOUT	10	.27	.38
TWISTER	8	.20	.26

For an engagement range of approximately 1500 meters, 60° cross range, / sigma range measurement error of 3 meters, / sigma azimuth tracking error of 0.3 mils, a projectile speed of 1158 meters per second and four firing points per segment, the hit probability results are summarized in the following table:

Target Type	Number of Segments	Mean ph	
		Constant Velocity Model	Adaptive Model
M60A1	6	.51	.56
TWISTER	6	.31	.37

The results from the Monte Carlo simulations indicated that the performance of the multiple model adaptive filter design was generally comparable to a filter which was tuned to the target dynamics of that particular tracking interval. In particular, the results showed that the adaptive prediction consistently performed better than the constant velocity prediction with an improvement in prediction ranging from 10 to 40 percent. The system sensitivity results from looking at a maneuvering target segment of data indicated that the system performance for the azimuth channel was heavily dependent on the angular measurement noise and the projectile time of flight in terms of range, and was not very sensitive to the range measurement noise and the range sampling rate. The results also indicated that higher probability of hit could be obtained in the cross range geometry than in the down range (coming down along the range vector) geometry.

MICROCOMPUTER IMPLEMENTATION & EVALUATION (REAL TIME)

A number of important issues arise in addressing the problem of real time microcomputer implementation and algorithm evaluation. Particularly critical are problems of numerical stability and accuracy imposed by the finite word length constraint of current microcomputers. Also, important are considerations of memory size and computational speed and hardware flexibility to perform parallel and floating point operations.

A filter algorithm which seems to be particularly well suited to real time microcomputer implementation is Bierman's UD algorithm⁵ for the propagation of the state error covariance. The algorithm has the desirable feature of computational accuracy and stability and its required memory size and number of multiplications are comparable to those of the conventional extended Kalman filter algorithm. The original filter algorithms and software were therefore modified to incorporate the UD covariance algorithm.

The Intel 86/12A single board computer was selected for the real time implementation and evaluation of the configured system. Each board has 32K of random access memory (RAM) and 16K of electronic programmable read only memory. It can be easily extended to 64K of RAM. The dual port RAM in the main computer board is accessible by other single board computers through the multibus lines, providing a common area for information transfer among the computers. The 8087 coprocessor is designed to work with the 86/12A computer. It has the desirable capability of 64 bit floating point operation which will save the programmer a large amount of time in scaling the variables and documenting the scaling procedure. Its 27 micro-second computation time for 64 bit multiplication is considered very fast.

The final configuration of the fire control system to be simulated is shown in Figure 1.

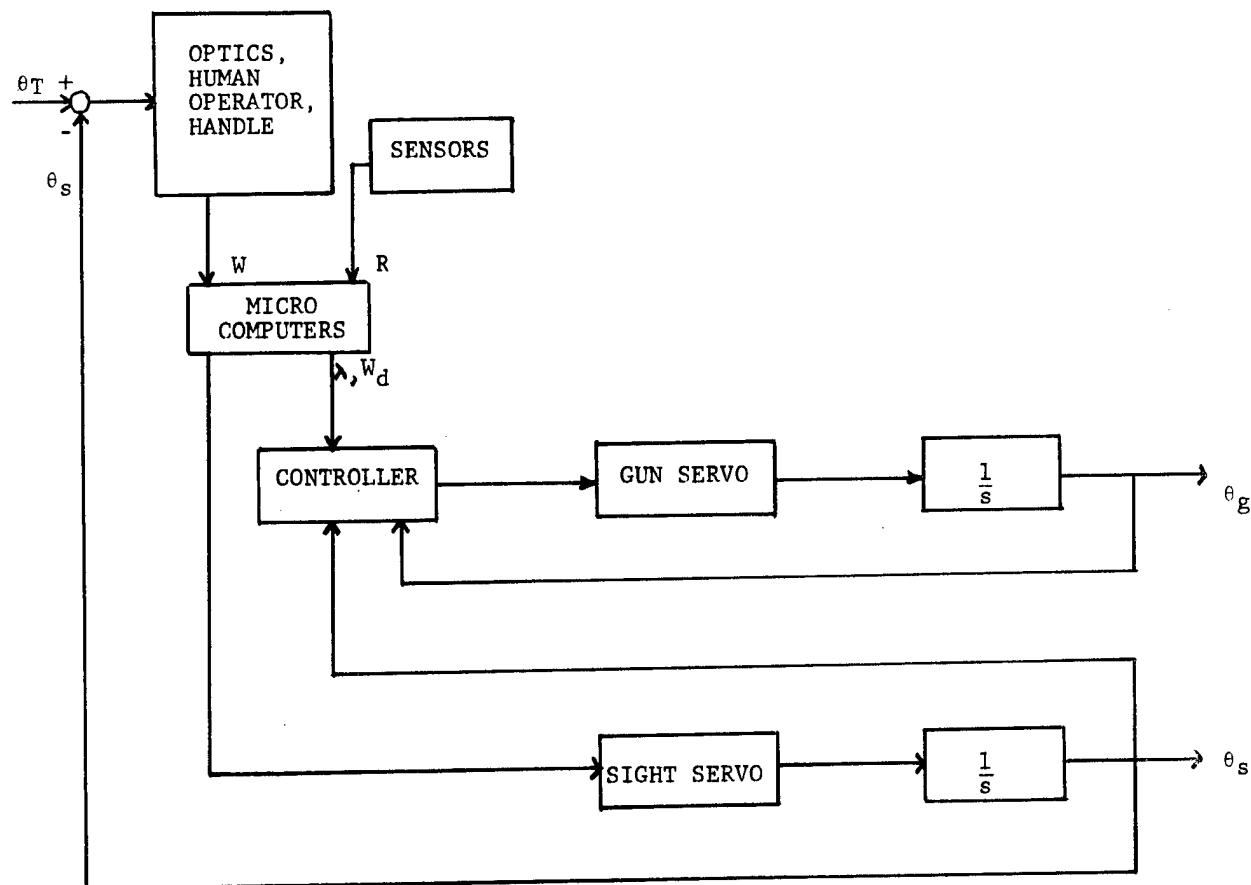


Figure 1

The difference between the target angle and the sight angle provides the actuating signal for the auto-tracker or the human operator (with handle) which outputs the angular rate signal. The angular rate signal together with the range measurements are fed to the multimodel processor which computes the estimated target states for the sight servo commands and the lead angle and the desired gun angular rate for the gun servo commands. This is a stabilized sight gun director type of configuration.

CONCLUSION

In the tank fire control problem with emphasis on maneuvering vehicle engagement, four major tasks were dealt with contiguously. System modeling and system configuration were carried out first. The ATMT data base was chosen to run through a maximum entropy spectral analysis. Models were formulated and their parameters were then identified by the maximum likelihood method. The models were embedded in the Extended Kalman Filters which were processed in parallel to provide adaptive estimates for gun lead prediction. A Monte Carlo simulation provided us the system sensitivity and the system performance in terms of the probability of hit. The real time simulation is an intermediate step between the digital simulation and the real system experiment.

Real time microcomputer implementation requires careful consideration of both software and hardware issues. The Bierman's UD algorithm with better numerical characteristics replaced the conventional Kalman propagation of state error covariance. The Intel 86/12A single board computers were selected for their flexibility, capability of floating point operation, and high speed of 64 bit multiplication.

Moreover, the human operator is a very nonlinear complex system which calls for a real person to be included in the control loop. In all, the experience of this real time exercise may enable us to appreciate the real world problem and provide us a realistic perspective of the entire tank fire control business.

REFERENCES

1. "Antitank Missile Test, Experiment FC019", Phase II, Project Analysis, ACN 22273, USADEC, Fort Ord, CA, 30 June 1975.
2. Tad J. Uloych, Thomas N. Bishop, "Maximum Entropy Spectral Analysis & Autoregressive Decomposition", *Reviews of Geophysics & Space Physics*, Vol. 13, No. 1, February 1975, pp 183-200.
3. H. Akaike, "Statistical Predictor Identification", *Ann. Inst. Statist. Math.*, 22, 203-217, 1970.
4. N. K. Gupta, R. K. Mehra, "Computational Aspects of Maximum Likelihood Estimation & Reduction in Sensitivity Function Calculations", *IEEE Trans on AC*, December 1974, pp 774-783.
5. G. J. Bierman, "Factorization Methods for Discrete Sequential Estimation", Academic Press, New York, 1977.

MULTIPLE MODEL ADAPTIVE CONTROL

Robert D. Smith
James G. Dixon
Weapon Synthesis Division
Naval Weapons Center
China Lake, California 93555

INTRODUCTION

Multiple Model Adaptive Control (MMAC) is a conceptually simple approach to the problem of controlling nonlinear dynamic systems. The technique utilizes several state estimators running in parallel. Each state estimator is designed to match a linearized model of the nonlinear system. State variable feedback for control purposes is implemented using the output of the "best" state estimator. The resulting system is highly nonlinear, and the success of this approach is highly dependent on the algorithm used to select the proper state estimator.

Adequate MMAC design techniques currently do not exist and a common sense trial and error approach must be employed. Despite this apparent limitation, several problems studied at the Naval Weapons Center using MMAC have shown encouraging results. In this paper the classic problem of stabilizing a radar guided missile in the presence of severe nonlinear radome boresight errors is used to illustrate the potential of MMAC.

MULTIPLE MODEL ADAPTIVE CONTROL STRUCTURE

A block diagram of the MMAC structure is shown in Figure 1.

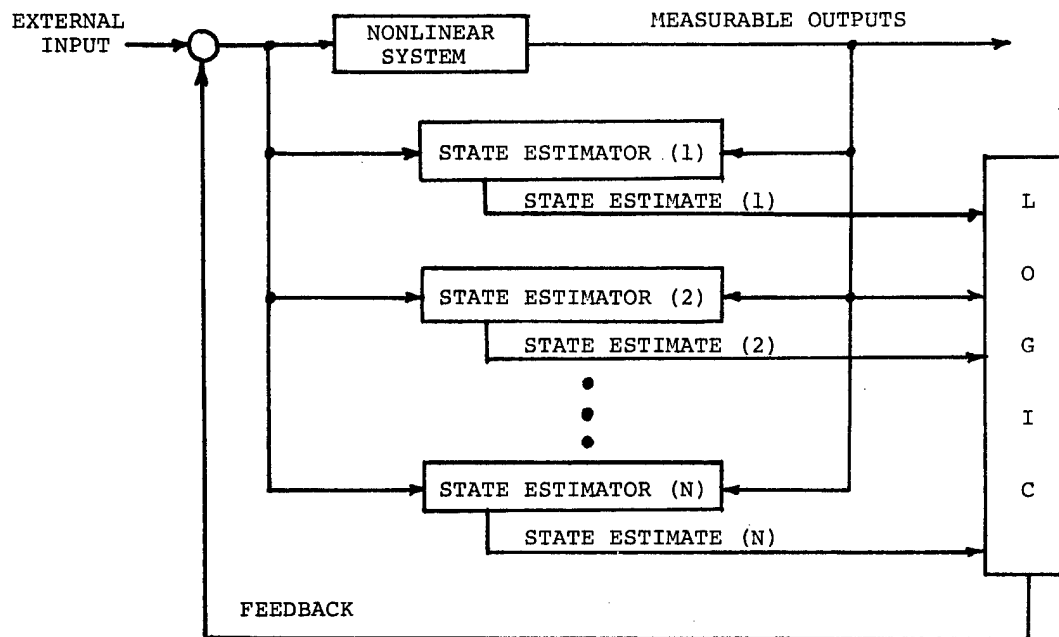


FIGURE 1. MMAC Structure.

The structure consists of the nonlinear system to be controlled and several state estimators running in parallel driven by the inputs and measurable outputs of the nonlinear system. Each of the state estimators is based on a linearized model of the nonlinear system about some operating point. It is the function of the logic element to determine which of the state estimators is providing the "best" estimate of the nonlinear system's states. The estimated states in conjunction with the appropriate gain matrix are used as feedback to modify the dynamics of the nonlinear system.

The concept of MMAC is not unique to this paper. A brief history of the concept and an extensive investigation of the MMAC technique for flight control of an F-8 aircraft are provided in a report by Athans et al.¹ However, the deterministic design (i.e., Luenberger observers vice Kalman filters) and the logic element in the MMAC structure reported in this paper differ from that of Reference 1. In particular, the logic element used in this report defines one state estimator (Luenberger observers) as "best" when the differences between its estimated outputs and the measured outputs of the nonlinear system are minimal. In addition, the states of the remaining state estimators are initialized to the states of the "best" state estimator for that update period. Thus, the state variable feedback is derived from one state estimator and not a linear combination of state estimator outputs as described in Reference 1.

A summary of the major elements of the MMAC structure described in this paper is provided below.

NONLINEAR SYSTEM

The restrictions on the nonlinearities and dynamics which limit the utility of the MMAC technique are not well understood at this time.

STATE ESTIMATORS

Luenberger observers as defined in References 2, 3, and 4 are utilized. The state estimators are based on linearized models of the nonlinear system. No a priori guidelines exist which define the number of state estimators required.

LOGIC

The logic function performs two operations on a periodic basis. First, the "best" state estimator is chosen, based on the minimum of the sum of the absolute values of the differences between the estimated outputs and the measured outputs. Second, the states of the remaining state estimators are initialized to the states of the "best" state estimator. Although not well defined, the update rate of the logic function must be consistent with the bandwidth of the desired closed loop system.

FEEDBACK

The feedback consists of state variable feedback utilizing the estimated states of the "best" state estimator. The feedback gain matrix is precalculated based on the linearized system model associated with each state estimator, and the desired closed loop characteristics of the nonlinear system being controlled.

EXAMPLE

The classic problem of stabilizing a radar guided missile in the presence of severe nonlinear radome boresight errors is used to illustrate the potential of the MMAC technique. The radome data used in this model is typical of existing radomes. The missile is modelled as a simple second order system whose acceleration normal to the velocity vector is proportional to the line of sight rate between the missile and the target.

RADOME BORESIGHT ERROR MODEL

Figure 2 defines the geometry used in this model.

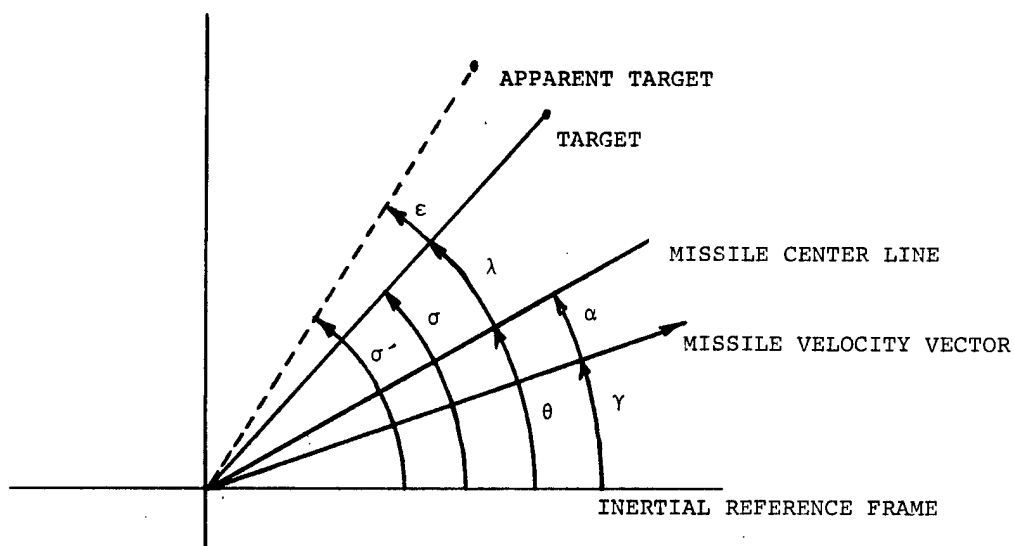


FIGURE 2. Geometry.

The various angles are defined below.

γ = missile velocity vector angle

θ = missile center line angle

σ = line of sight angle to the target from the inertial reference frame

σ' = apparent line of sight angle caused by radome errors

ϵ = angular error caused by the radome

λ = look angle

α = angle of attack.

Thus,

$$\sigma' = \sigma + \epsilon(\lambda),$$

where $\epsilon(\lambda)$ indicates that the angular error introduced by the radome is a nonlinear function of the look angle. For the purposes of this example it is convenient to obtain the time rate of change of the previous equation.

Differentiating with respect to time yields

$$\dot{\sigma}' = \dot{\sigma} + K_R(\lambda)\dot{\lambda},$$

where $\dot{\sigma}' = \frac{d}{dt} \sigma'$

$$\dot{\sigma} = \frac{d}{dt} \sigma,$$

$$\dot{\lambda} = \frac{d}{dt} \lambda,$$

and $K_R(\lambda) = \frac{d\epsilon(\lambda)}{d\lambda}.$

$K_R(\lambda)$ is the nonlinear radome boresight error slope. The data used for this example is shown in Figure 3.

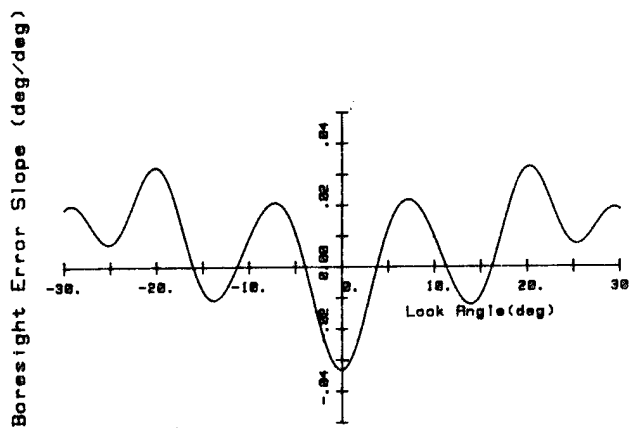


FIGURE 3. Radome Boresight Error Slope.

MISSILE MODEL

The missile is modelled as a simple second order system whose acceleration normal to the velocity vector is proportional to the line of sight rate between the missile and the target. Figure 4 is a block diagram of the missile model.

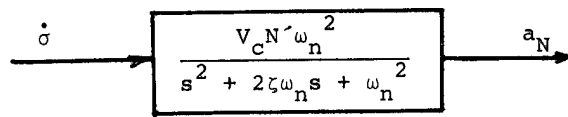


FIGURE 4. Missile Model Block Diagram.

The parameters of this model are defined as follows.

a_N = missile acceleration normal to its velocity vector

V_c = closing velocity between the missile and the target

N' = effective navigation ratio

ω_n = natural frequency of the missile

ζ = damping ratio of the missile.

In the presence of radome errors, the missile is driven by $\dot{\sigma}'$ where

$$\dot{\sigma}' = \dot{\sigma} + K_R(\lambda)\dot{\lambda}$$

as derived in the previous section. For very large missile to target ranges $\dot{\sigma}$ is very small and can be neglected. Thus

$$\dot{\sigma}' = K_R(\lambda)\dot{\lambda},$$

which represents a nonlinear feedback loop around the missile. This so called parasitic feedback loop is the source of the stability problem caused by radome boresight errors. To complete the block diagram it is necessary to derive the relationship between the rate of change of the look angle ($\dot{\lambda}$) and the missile's normal acceleration (a_N). From Figure 2,

$$\lambda = \sigma - \theta,$$

$$\text{and } \dot{\lambda} = \dot{\sigma} - \dot{\theta}.$$

Since $\dot{\sigma}$ is assumed to be zero,

$$\dot{\lambda} = -\dot{\theta}.$$

In addition

$$\dot{\theta} = \dot{\gamma} + \dot{\alpha}.$$

The quantity $\dot{\gamma}$ is directly related to a_N since

$$a_N = V_M \dot{\gamma},$$

where V_M is the missile's velocity. The angle of attack (α) is related to a_N through the relationship

$$a_N = C\alpha,$$

where C is the missile's airframe gain which relates angle of attack to normal acceleration for a given missile velocity and altitude. Combining the above relationships and using Laplace notation yields

$$\dot{\theta} = \frac{1}{V_M} \left(\frac{V_M}{C} s + 1 \right) a_N$$

Using the relationship $\dot{\lambda} = -\dot{\theta}$, the block diagram for the missile with the nonlinear parasitic feedback loop can be completed and is shown in Figure 5.

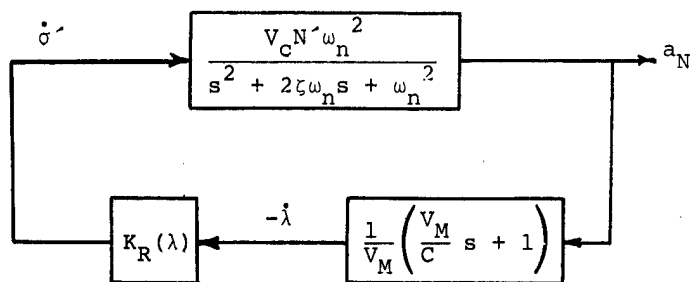


FIGURE 5. Missile with Parasitic Feedback Loop.

Figure 5 is the nonlinear system of interest and the one used to demonstrate the potential of the MMAC technique.

MMAC CONFIGURATION

Sixteen second order state estimators were used for this example. Each estimator was based on a linear model of the missile obtained from Figure 5 by fixing the value of $K_R(\lambda)$. Values of $K_R(\lambda)$ from -0.035 to +0.040 in increments of 0.005 were used. The dynamics of the state estimators were patterned after the linearized missile models, and the feedback gains were chosen to yield error dynamics with a natural frequency of 10 Hz and a damping ratio (ζ) of 0.9. (see Reference 4). The logic function was performed every 0.01 seconds, and the measurable output was assumed to be the missile's normal acceleration (a_N).

The open loop characteristics of the missile model are defined below.

$$\omega_n = 2\pi \text{ (rad/sec)} \quad (1.0 \text{ Hz})$$

$$\zeta = 0.1 \text{ (1/sec)}$$

$$N' = 4.0$$

$$V_C = 7000 \text{ (ft/sec)}$$

$$V_M = 3000 \text{ (ft/sec)}$$

$$C = 675 \text{ (ft/sec}^2\text{/rad)}$$

The state variable feedback gains used by the MMAC were calculated to give the closed loop missile a natural frequency of 2 Hz (4π rad/sec) and a damping ratio of 0.7.

RESULTS

Figure 6 is a plot of the missile's desired (dashed line) initial condition response and its uncompensated (solid line), as defined by Figure 4, response. Extending the time of this response would show a limit cycle behavior for the uncompensated system. Figure 7 compares the MMAC (solid line) and desired (dashed) responses. The success of the MMAC is evident. Although the initial condition errors were zero for this case, Figure 8 illustrates the MMAC response (solid line) for a mismatch in the estimated normal acceleration (a_N). For this case the estimated normal acceleration was assumed to be 4 g's. The importance of initializing the states of the state estimators at each update cycle is illustrated in Figure 9. For this case no state initializing was utilized. This response differs markedly from the original MMAC configuration of Figure 7. Saving the best for last, the most impressive feature of the MMAC technique is illustrated by the response shown in Figure 10. For this case the same MMAC used in the previous examples was employed, but the sign of the radome boresight error model was reversed. Again, the MMAC yielded an excellent response (solid line) relative to the desired response (dashed line).

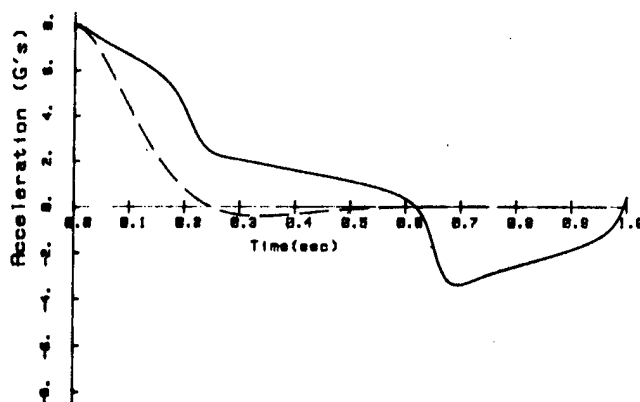


FIGURE 6. Uncompensated Missile Response (solid line) and Desired Response (dashed line).

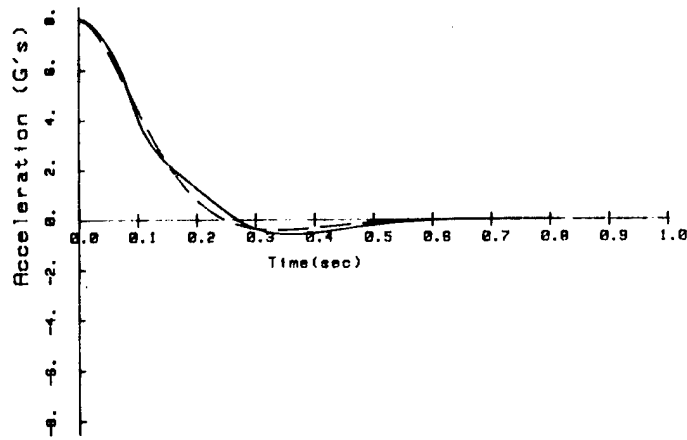


FIGURE 7. MMAC Response (solid line) and Desired Response (dashed line).

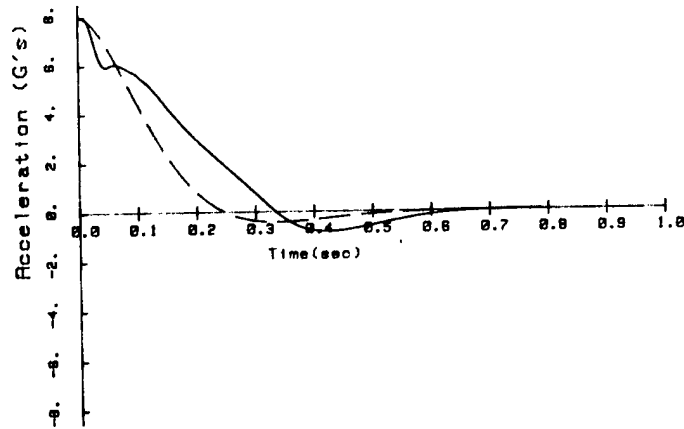


FIGURE 8. MMAC Response with Initial Condition Error (solid line) and Desired Response (dashed line).

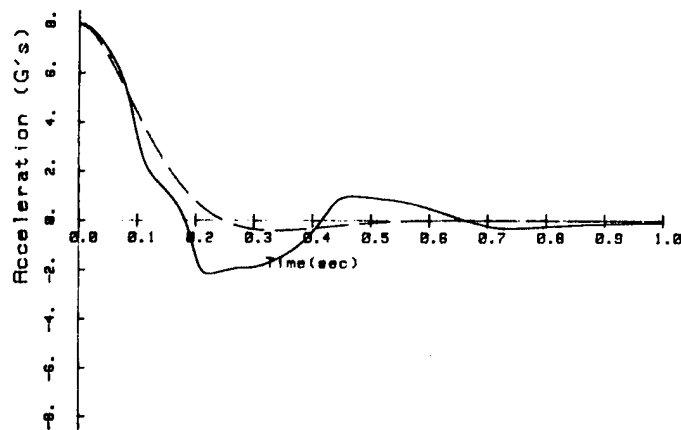


FIGURE 9. MMAC Response with No State Initializing (solid line) and Desired Response (dashed line).

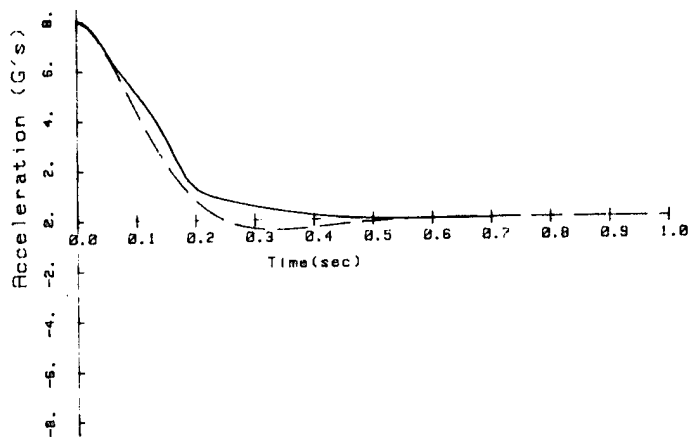


FIGURE 10. MMAC Response with Radome Boresight Error Model Sign Reversed (solid line) and Desired Response (dashed line).

CONCLUSIONS

The potential of the MMAC technique has been demonstrated via a simple example. The technique is conceptually simple and seems to enjoy a reasonable degree of insensitivity to the exact form of nonlinearity involved. That is, the bounds of the nonlinearity are more important than the exact shape of the nonlinearity. However, design guidelines do not currently exist which relate the characteristics of the nonlinear system to the number of state estimators required and the update rate of the logic function. Finally, the burden of implementing the computations imposed by the parallel structure of the MMAC technique will diminish as technology continues to reduce the size and increase the speed of computers.

REFERENCES

1. M. Athans, Y. Baram, D. Castanon, K. P. Dunn, C. S. Green, W. H. Lee, N. R. Sandell, Jr., and A. S. Willsky, "Investigation of the Multiple Model Adaptive Control (MMAC) Method for Flight Control Systems," NASA Contractor Report 3089, May 1979.
2. D. G. Luenberger, "Observing the State of a Linear System," IEEE Trans. on Military Electronics, Vol. MIL-8, pp. 74-80, April 1964.
3. D. G. Luenberger, "Observers for Multivariable Systems," IEEE Trans. on Automatic Control, pp. 190-197, April 1966.
4. Thomas E. Fortmann and Konrad L. Hitz, An Introduction to Linear Control Systems, Marcel Dekker, Inc., New York, 1977.

Next page is blank.

A DESIGN METHODOLOGY FOR ESTIMATORS AND PREDICTORS IN FIRE CONTROL SYSTEMS

Dr. James F. Leathrum
Department of Electrical and Computer Engineering
Clemson University
Clemson, SC 29631

ABSTRACT

In the interest of establishing a systems approach to the design of fire control systems, the design of estimators and predictors is formalized into a direct procedure. The usual, trial-and-error approach to fixing the parameters of estimators is circumvented. The performance requirements of the fire control system are used at the outset as inputs to the computation of filter parameters. Component specifications are an important outcome of this design process. In particular, tracking accuracy requirements emerge as results of the design process. Tradeoffs between first and second order predictors are quantified and used to select the best predictor.

The state-of-the-art in the design of Kalman filters for fire control systems leaves the designer with several parameters to be used to overcome the effects of modeling errors. These parameters are the model and observer noise variances, and they are usually fixed by searching for satisfactory operating conditions. The methodology developed here uses miss distance and target bandwidth characteristics to fix the noise variances. The miss distance is a system performance requirement, and the bandwidths are obtainable from the analysis of broad classes of targets. The result is a direct design methodology which is free of searching.

THE ROLE OF ESTIMATORS IN FIRE CONTROL SYSTEMS

One of the fundamental processes which arises in gun fire control is the process of estimating the state of the target. This estimation process is readily discernible in even the least sophisticated systems. As the system design is augmented to include capabilities against maneuvering targets, the burden upon the estimation process becomes progressively greater both in terms of accuracy and number of states to be estimated. For instance, for straight-line, constant velocity targets, there is no need to estimate acceleration. On the other hand, the utility of a velocity estimate will depend directly upon the accuracy of the estimate. An inaccurate lead may be worse than no lead at all. The same argument holds for the higher derivatives of motion.

At any point in the evolution of fire control technology there is probably a practical limit to the dimensionality and accuracy of the estimation process. Considerations of processor speed, observer accuracy, and target identification (modeling) would be expected to determine the number and accuracy of the state variable estimates. If the estimator technology is critical in the sense that no other technology would inhibit the system implementation, the design strategy is one of achieving the most sophisticated system which can be supported by the estimator. In the current state-of-the-art, the estimator and observer (sight or tracking) technologies seem to share critical roles. The solution of the tracking part of the design problem will require much of

*This work was performed while serving as a consultant to the US Army Materiel Systems Analysis Activity, Aberdeen Proving Ground, Maryland 21005

the same technological resources as the estimator (i.e., processor speed and models). In addition, most of the additional cost of a highly sophisticated system will probably fall in the sight or tracking mechanism.

Acknowledging this set of interacting technologies, the purpose of this paper is to formalize some of the issues in terms of simple models of observers, estimators and predictors. The performance of predictors working in tandem with optimal estimators will be used to specify the parameters of the estimators and observers. Tradeoffs between observer technology and overall (predictor) performance will become apparent. The propagation of errors through typical predictors will be used to assess the trade-offs between Nth and N+1th order predictors.

A by-product of this work is the formulation of a direct design methodology for Kalman filters in fire control systems. The unknown noise statistics will be assessed in terms of the power spectra of generic targets and allowable performance limits of the predictor.

CONVENTIONAL DESIGN METHODOLOGY

The conventional approach to the design of estimators and predictors for fire control systems is best illustrated by the following development of models and parameters. One would start by formulating target and observer models of the form.

(a) Target Model

$$X_{k+1} = \Phi_k X_k + B_k U_k$$

(b) Observer Model

$$Y_k = H_k X_k + V_k$$

These models immediately involve a linearization approximation. The target model captures the well defined motion in the state transition matrix, Φ_k , and leaves the less defined part of the motion to a noise term, $B_k U_k$. The observer is usually a statement that not all the state components are visible, and that the observations are corrupted by an error, V_k . (The index, k , is a discrete time index). If one can further approximate U_k and V_k by white gaussian, zero mean processes, an estimator of X_k can be formulated as:

$$\tilde{X}_{k+1} = \Phi_k \hat{X}_k \quad (\text{Predicted State})$$

$$\hat{X}_k = \tilde{X}_k + K_k (Y_k - H_k \tilde{X}_k) \quad (\text{Corrected State})$$

which is the Kalman Filter wherein

$$K_k = \tilde{P}_k H_k^T (R_k + H_k \tilde{P}_k H_k^T)^{-1} \quad (\text{Filter Gain})$$

$$\tilde{P}_{k+1} = \Phi_k \hat{P}_k \Phi_k^T + B_k Q_k B_k^T \quad (\text{Predicted Variance})$$

$$\hat{P}_k = \tilde{P}_k - K_k H_k \tilde{P}_k \quad (\text{Corrected Variance})$$

$$R_k = E(U_k U_k^T) \quad (\text{Observer Noise Variance})$$

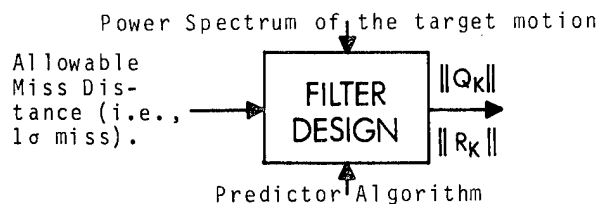
$$Q_k = E(V_k V_k^T) \quad (\text{Model Noise Variance})$$

In the most sophisticated fire control systems, the target noise is represented in a target oriented coordinate system. Thus, the given Q_k will rotate as the target moves which in turn leads to a nonsteady K_k . The Kalman gains tend to change throughout the estimation process. In addition, R_k may be range dependent which leads to further variability in K_k .

In designing such a filter, the implementor is left with choices of the magnitude of Q_k and R_k (i.e., $\|Q_k\|$ and $\|R_k\|$). A conventional design process would require assessing $\|R_k\|$ from the accuracy of the instrumentation used by the observer. Since $\|Q_k\|$ represents unmodeled behavior, it is usually adjusted to achieve some other objective, such as white innovation, or minimum ensemble miss distances. Whatever the objective, the last phase is unguided by the theory and thus usually requires extensive simulation to determine $\|Q_k\|$.

A DIRECT DESIGN METHODOLOGY

A methodology which could utilize maximum allowable miss distances to assess the design parameters directly would have some obvious advantages over the conventional process. Such a methodology is proposed here with the design features shown, i.e.,



THE DIRECT DESIGN OF ESTIMATORS

The principles of the design will be illustrated by restricting the discussion to a single dimension and further restricting the models to

Φ : Upper Triangular

Q_k : Scalar constant, q

R_k : Scalar constant, r

These restrictions do not limit variability of the gains in the final design, but only allow one to focus attention to the magnitudes of the parameters in each direction. The design process requires solution of the steady state filter equations which become

$$\tilde{P} = \Phi \tilde{P} \Phi' + B q B' - \Phi P H' (r + H \tilde{P} H')^{-1} H \tilde{P} \Phi'$$

The solution for \tilde{P} in terms of r and q requires iteration. However, a closed form solution for \tilde{P}/q and r/q in terms of bandwidth of the target motion is possible. For instance, for a third order model, it requires the observation from the analogous continuous models that

$$\hat{P}_{33}/q = (1/\omega_v) \cdot \Delta t$$

where ω_v is the bandwidth for velocity, and $\Delta t = t_{k+1} - t_k$ is the time

increment between observations. This in turn, fixes \tilde{P}_{33}/q by passing \hat{P}_{33}/q through the predicted variance equation, i.e.,

$$\tilde{P}_{33}/q = (\Phi_{33})^2 \hat{P}_{33}/q + B^2_3$$

From this starting point, all the other variance ratios can be found. The required bandwidths can be assessed from the power spectrum observed in field tests of generic targets. The ratios (\tilde{P}/q and r/q) completely specify the one dimensional, steady design, but they do not produce the magnitudes, $\|Q\|$ and $\|R\|$, needed in a multidimensional design. The required magnitudes are obtained from the variance of miss distance

$$\frac{\sigma_{\text{miss}}}{\sqrt{q}} = (T_N \hat{P}/q T_N')^{1/2}$$

In an optimal design, the \hat{P} is interpreted as the variance of the estimator error. \tilde{P}/q is obtained from \hat{P}/q by passing the latter through the corrected variance equation. The T_N vector is the coefficient vector for an Nth order predictor. Thus, the above equation represents the variance propagation through an Nth order predictor. Since \tilde{P}/q is available (from \hat{P}/q), one can directly determine $\sigma_{\text{miss}}/\sqrt{q}$. A specification of σ_{miss} will lead to q thence to r (from r/q).

The logical outcome of this process is specification of q and r in terms of the filter bandwidth, the miss distance, and the predictor coefficients. Once r is found, the question is raised as to whether an observer with an accuracy of r is achievable. Thus, this design process may provide direct motivation for enhancing the observer technology.

PATHOLOGICAL DESIGNS

The design methodology outlined in the previous section must be approached with an appreciation that the results may not always be reasonable and achievable. The resulting $\|R\|$ and $\|Q\|$ may be thought of as intensities of noise on the observer and the target respectively. The $\|R\|$ may be so small that it will not be achievable using the evolving technology of sight mechanisms. Conversely, the $\|Q\|$ may be so large that targets cannot possibly achieve such a intensity of maneuver (i.e., rate of change of acceleration). Both situations represent pathological cases. In the best of situations, the $\|Q\|$ may be brought in bounds by reducing the variance of miss distance without seriously deflating $\|R\|$, thus not forcing new observer technology. Alternately, if the $\|Q\|$ is within bounds, the miss distance requirements may be relaxed to bring $\|R\|$ within current technological constraints.

In the worse case, both $\|R\|$ and $\|Q\|$ may be beyond reasonable bounds. Changing the miss distance requirements would not alleviate this pathology. The only recourse at this point is to reassess the frequency response of the filter. As the bandwidth filter is reduced, the ratio, $\|Q\|/\|R\|$, is reduced. Thus, in order to achieve reasonable noise intensities, it may be necessary to filter out some of the higher frequency components of the target motion. Such a redesign is in the direction of model mismatching and thus toward progressively less optimal estimation. A deterioration in actual miss distance (as opposed to propagated variances) is inevitable.

SOME TYPICAL FILTER DESIGNS

In order to illustrate the design methodology and in order to support a trade-off study, several typical filters were considered. These filters are parameterized

by the equation for the acceleration variance, \hat{p}_{33}/q , i.e.,

$$\hat{p}_{33}/q = (1/\omega_v) \cdot \Delta t$$

The variance ratios, \hat{p}/q , are computed from the steady state filter equation given in The Direct Design Methodology section along with

$$\Phi = \begin{bmatrix} 1 & \Delta t & \Delta t^2/2 \\ & 1 & \Delta t \\ & & 1 \end{bmatrix}; B = \begin{bmatrix} \Delta t^3/6 \\ \Delta t^2/2 \\ \Delta t \end{bmatrix}$$

$$H = [1 \ 0 \ 0];$$

$$\Delta t = 0.1 \text{ sec};$$

and

$$\tilde{p}_{33}/q = \hat{p}_{33}/q + \Delta t^2$$

Propagating these variances through a second order predictor with a 1.5 sec time-of-flight (TOF) leads to variances at impact as typified in Figures 1 and 2. The utility of the designs can be visualized by noting that for a particular time-of-flight, the bandwidth and impact error define the q and r of the filter. As a hypothetical case, consider the targets with frequency bandwidth at $\omega_v = 0.25$ hz. In order to insure a 68 percent minimum hit probability against a target width of 2.3 meters which behaves according to the imbedded model, the RMS impact error would be limited to 1.15 meters (i.e., σ_{miss}). These targets could be hit with such a probability with a second order predictor and 1.5 sec time-of-flight if they exhibit an RMS jink of no more than 2.676 m/sec^3 (i.e., \sqrt{q}). The observer must be able to "see" the target with an RMS error of no more than 1.06 meters (i.e., \sqrt{r}). The restriction to behavior according to the imbedded

model will limit the total impact error to that propagated through the predictor from the estimation process. If the target is exhibiting higher order behavior, then the performance would be degraded.

FIRST AND SECOND ORDER PREDICTOR TRADE-OFFS

The preceding discussion of typical designs was predicated upon the proposal that the target was properly modeled by a third order difference equation (i.e., position, velocity, and acceleration as state variables) with white noise at the jink level and that the predictor was second order. This section considers the case where the target is third order, but a first order predictor is used. Such an arrangement leads to a trade-off between model mismatch errors and propagated errors. A general development of the prediction errors for N to N + 1th order mismatches appears in Appendix A.

In a first order predictor, the acceleration effects would not be utilized. The resulting prediction error is

$$\epsilon_p = [1 \ t_f \ 0] [\hat{X} - X] \\ - [0 \ 0 \ t_f^2/2] \cdot X$$

where the first term is the propagated error from the 1st order predictor. The second term is the effect of the unused state variable. The variance of the prediction error is

$$E(\epsilon_p^2) = [1 \ t_f \ 0] \hat{P} [1 \ t_f \ 0]' \\ + [0 \ 0 \ t_f^2/2] E(XX') [0 \ 0 \ t_f^2/2]' \\ - 2[1 \ t_f \ 0] E[(\hat{X}-X)X'] [0 \ 0 \ t_f^2/2]'$$

where the last two terms represent additional errors which do not arise by propagation of estimation errors through the predictor.

Suppose a filter had been designed to achieve certain miss distance constraints using a 2nd order predictor. It is now possible to assess the relative performance of a first order predictor using the same estimates (i.e., optimal estimators for a third order system). The point of interest is the equality of the first and second order predicted error variances, i.e.,

$$E(\epsilon_p^2)_{1st} = E(\epsilon_p^2)_{2nd}$$

where

$$E(\epsilon_p^2)_{2nd} = [1 \ t_f \ t_f^2/2] \hat{P} [1 \ t_f \ t_f^2/2]' \\ = \sigma_{miss}^2$$

Equating the two variances defines a linear relation of the form

$$E(XX')_{3,3} = E(acc^2) = a \sigma_{miss}^2$$

That is, the variance of acceleration is linear in the variance of miss distance at the condition of indifference between the predictors. A trade-off function is obtained as shown in Figure 3. In fact, a family of trade-off is obtained, one for each value of the pair (ω_y , time of flight).

With one additional datum, the variance of accelerations, the designer can effectively choose between first and second order predictors. Alternately, the fire control system may be programmed to compute a moving average of the acceleration squared and use these results to switch predictors.

THE DESIGN PROCEDURE

The purpose of this section is to review and summarize the design procedure developed in the preceding sections. The design process will be discussed in terms of the major steps which lead to fixing the filter parameters.

STEP 1: ASSESS THE BANDWIDTH OF THE TARGET MOTION

In this step the designer may refer to power spectral density data for targets of the broad generic type of interest. The filter will be designed to pass velocity motion up to ω_y in frequency.

STEP 2: ASSESS THE MAXIMUM RMS MISS DISTANCE AND TIME OF FLIGHT

Here, the size of the target and nominal hit probabilities are used to assess the maximum RMS miss distance (σ_{miss}). Nominal ranges will determine the time of flight.

STEP 3: DESIGN THE FILTER TO ACHIEVE σ_p FOR THE PROPAGATED ERROR THROUGH A SECOND ORDER PREDICTOR

This step utilizes the results from Figures 1 and 2 to obtain r and q of the filter. The achievability of observers of accuracy on the order of \sqrt{r} may force the procedure back to Step 1 at this point.

STEP 4: USE THE FILTER FROM STEP 4 TO ASSESS THE MEAN SQUARED ACCELERATION

This step is an off-line data analysis of the acceleration levels for typical targets.

STEP 5: DETERMINE THE ORDER OF THE PREDICTOR

In this step, the choice between first and second order predictors is made. A line of indifference such as Figure 3 provides the boundary between the two predictors.

This design process is completely free of iteration. The design evolves from an assessment of target power spectra to sight accuracy, \sqrt{r} , and predictor order (Step 5). The designs are based upon an idealized target model, and, thus, still require experimental verification.

APPENDIX A

ANALYSIS OF PREDICTION ERRORS

The purpose of this section is to outline the derivation of prediction errors in fire control systems. It will be presumed that predictors are designed as linear combinations of estimated states, i.e.,

$$X_p(t + t_f) = T_m \hat{X}(t)$$

where T_m is usually of the form

$$T_m = [1 \ t_f \ t_f^2/2 \dots t_f^m/m!]$$

and the states are successive derivatives of position. The predicted position, X_p , is to be compared to the true position of the target which is modeled as

$$X(t + t_f) = X_d(t + t_f) + X_{TI}(t + t_f)$$

where $X_d(t + t_f)$ is the deterministic position which can be determined by the state at t . $X_{TI}(t + t_f)$ is the target induced (TI) position and represents behavior which could not be known from the state at t . The deterministic part of the true position is modeled as

$$X_d(t + t_f) = T_N X(t)$$

which is an N th order Taylor series approximation.

The target induced motion may be modeled as

$$(X_{TI})_{k+1} = \Phi_k (X_{TI})_k + B U_k$$

which is the same form as the target model employed in the filter. It represents random walk in acceleration. It is convenient to assume that $(X_{TI})_0$ is identically zero and that U_k is white noise.

The prediction error will be the difference between the predicted position and the true position

$$\begin{aligned} \epsilon_{PE} &= X_p(t + t_f) - X(t + t_f) \\ &= T_m \hat{X}(t) - T_N X(t) - X_{TI}(t + t_f) \end{aligned}$$

Utilizing the independence of X_{TI} , and the \hat{X} and X variables, the variance of prediction error is

$$\begin{aligned} \sigma_{PE}^2 &= E(T_m \hat{X}(t) - T_N X(t))^2 + E(X_{TI} X_{TI}') \\ &= \sigma_p^2 + \sigma_{TI}^2 \end{aligned}$$

where σ_p^2 is the "propagated variance."

The predictors of greatest interest are the under-designed ones where $m \leq N$. For the case where $m = N$,

$$\sigma_p^2 = T_N \hat{P} T_N'$$

Likewise, for $m + 1 = N$

$$\begin{aligned} \sigma_p^2 &= T_m \hat{P} T_m' - 2 T_m Z T_N'^* \\ &\quad + T_N^* E(X X') T_N'^* \end{aligned}$$

where

$$Z \equiv E[(\hat{X} - X) X']$$

$$T_N^* = [0 \ 0 \ 0 \dots \ t_f^N / N!]$$

The additional terms in the above raise the question of under what conditions do the m th and $m + 1$ th predictors produce the same variance, i.e.,

$$(\sigma_p^2)_m + \sigma_{TI}^2 = (\sigma_p^2)_{m+1} + \sigma_{TI}^2$$

The target induced effects cancel out, leaving a relationship between the variance of the unused states in the m th order predictor (i.e., $E(X X')$) and the filter design. This relationship is the indifference function between the m th and $m+1$ th predictors.

The cross covariance term, Z , is obtainable from the steady state equation

$$Z = (I - KH) (\Phi Z \Phi' - BB')$$

where $K = \tilde{P}/q \ H' \ (r/q + H \tilde{P}/q \ H')^{-1}$

The only column of Z which is of interest is the one corresponding to the $m+1$ element of X . Utilizing the fact that $\Phi(i, m+1) = 0$ for all $i \leq m$ and $(m+1, m+1) = 1$ leads to

$$\text{Col}_{m+1}(Z) = (I - KH)(\Phi \text{Col}_{m+1}(Z) - B_{m+1} \cdot B)$$

which is linear in the $m + 1$ th column of Z .

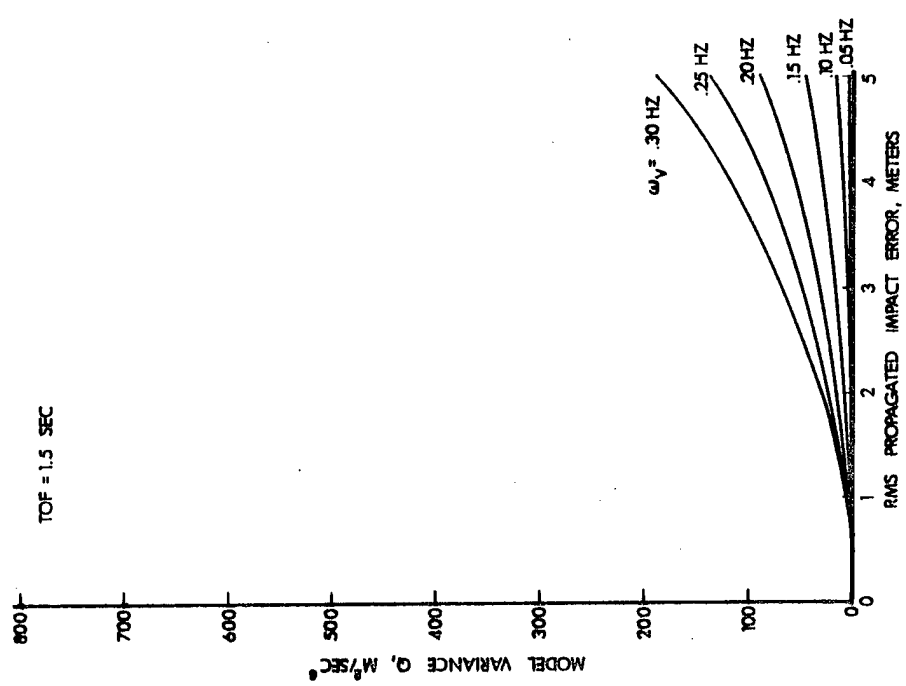


Figure 1. Model Variance vs RMS Propagated Impact Error (2nd Order Predictor).

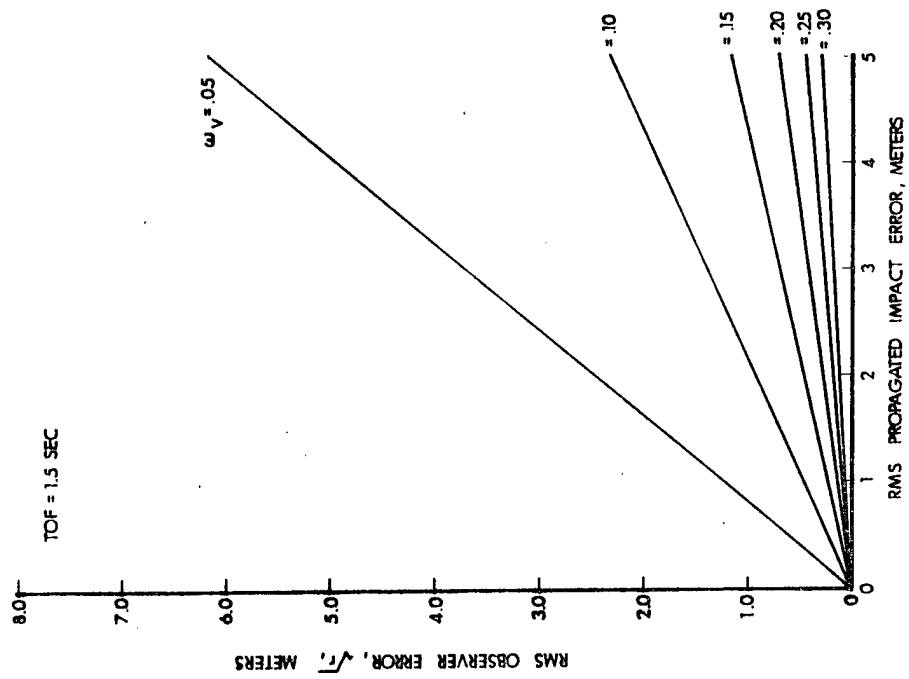


Figure 2. Observer Error vs RMS Propagated Impact Error (2nd Order Predictor).

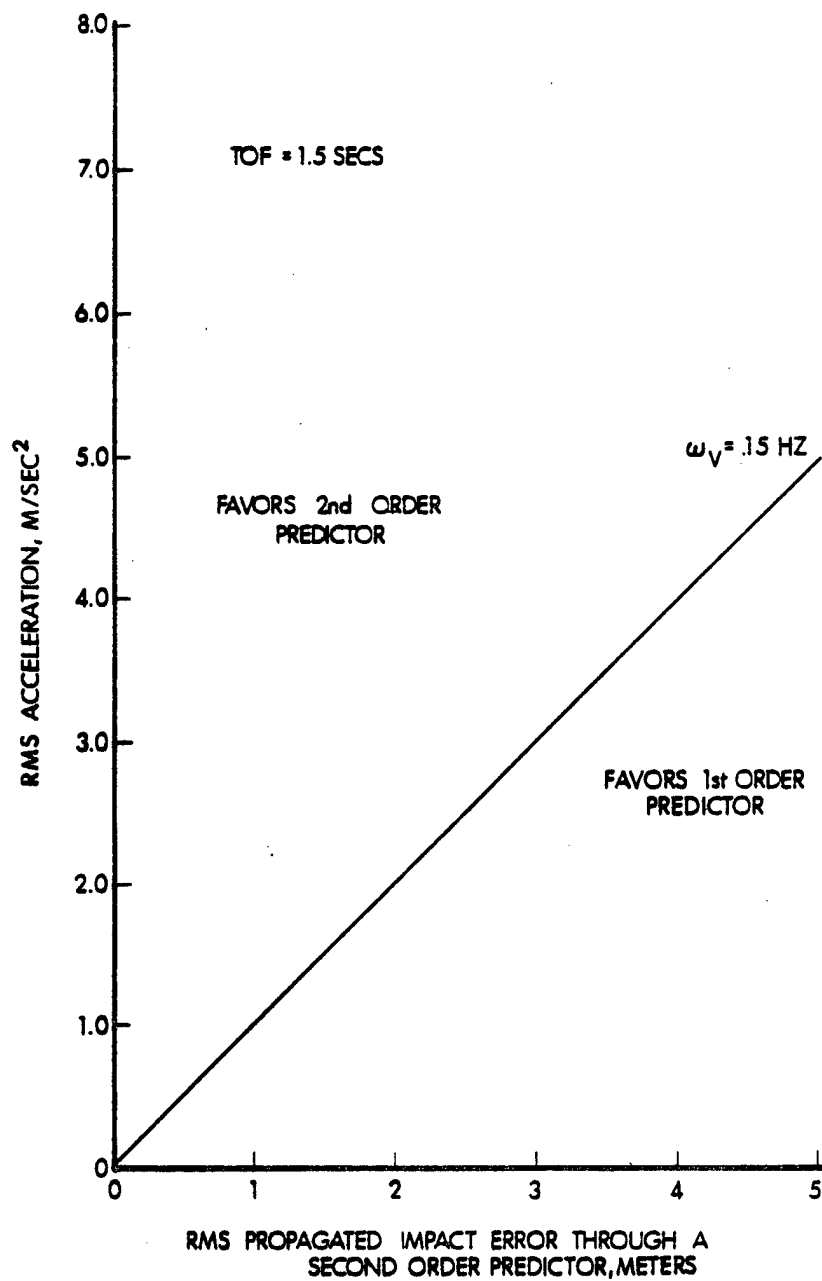


Figure 3. A Typical Line of Indifference Between First and Second Order Predictors.

Next page is blank.

OPTIMAL CONTROL AND ESTIMATION FOR STRAPDOWN
SEEKER GUIDANCE OF TACTICAL MISSILES

P. L. Vergez, 1Lt, USAF
J. R. McClendon, 1Lt, USAF
Air Force Armament Laboratory
United States Air Force
Eglin Air Force Base, Florida 32542

SUMMARY

Inertially stabilized gimballed platforms have been used with seekers in the past for tactical missile applications because of limited seeker fields-of-view. Gimballed platforms increase the total field-of-view of the missile, i.e., if a seeker has a field-of-view of $+3^\circ$, the gimballed platform increases the missile's field-of-view to approximately $\pm 60^\circ$. Future guided missiles will be required to operate in much higher dynamic engagements which demand the use of expensive gimbals for conventional seekers. Recent advances in seeker technology have increased the fields-of-view significantly, such that future missiles could have the seeker fixed to its body (eliminating the gimbals) with fields-of-view in excess of $+90^\circ$. These body-fixed (strapdown) seekers introduce large measurement errors caused by their optics and electronics. Conventional guidance and filtering techniques do not work well with strapdown seeker measurements. Recent dither adaptive approaches to generate inertial measurements from the body fixed measurements in order to use conventional guidance have failed to work in high g engagements. However, recent Air Force Armament Laboratory in-house studies indicate that guidance and estimation algorithms derived from optimal control theory can function well with strapdown seeker measurements in high g engagements, resulting in greatly improved missile performance.

INTRODUCTION

Most contemporary tactical guided weapons utilize proportional navigation as the terminal guidance law and an inertially stabilized gimballed seeker to provide guidance information. The proportional guidance law is most often used because it can be easily implemented. It has been shown that proportional navigation is most effective under restrictive engagement conditions, i.e., small off-boresight angle launches, intercepting low-maneuverability targets; however, when employed in engagements that deviate from these conditions, proportional navigation's performance is degraded. Inertially stabilized gimballed seekers, which track the target, have been used in the past because of field-of-view limitations, physical implementation requirements to maintain seeker lock-on, and the practical consideration that this method provides the most direct means of obtaining the required inertial line-of-sight rates necessary for proportional navigation.

The air-to-air engagement (fighter versus fighter) is analytically and operationally the most demanding and complex scenario in the guided weapons arena from the point of view of the kinematics of the engagement. Further, trends in operational requirements indicate that future air-to-air missiles will require a high probability of kill under total sphere launch engagement conditions and a launch and leave capability when employed against a wide variety of highly maneuverable, intelligent targets. These requirements, when applied to conventional guided weapons, demand the use of expensive gimbals which can function under high dynamic conditions; however, this does not guarantee good missile performance. Recent advancements in seeker technology have resulted in seeker designs with much larger fields-of-view and seeker tracking characteristics which do not require the seeker centerline to point in the general vicinity of the target. Examples of such seekers include optical and radar correlators, holographic lens used with laser detectors, and phased array antennas.

The potential advantages of such seekers are numerous and result basically from the fact that the seeker can now be rigidly fixed to the weapon body. These body-fixed seekers (also referred to as strapdown seekers) have the potential of eliminating the tracking rate limits and structural limitations of inertially stabilized gimballed

seekers while simultaneously reducing the mechanical complexity of implementation and calibration. The elimination of mechanical moving parts would in turn eliminate frictional cross-coupling between pitch and yaw tracking channels and accuracy degradation due to missile acceleration, and would create the potential for an increase in reliability of electronic components over mechanical ones. Finally, there are potentially significant cost savings associated with eliminating the gimbals.

Despite all these advantages, there are potential hazards associated with integrating strapdown seekers into the overall guidance system. These strapdown seekers introduce large measurement errors caused by their optics and electronics. Conventional guidance techniques do not work well with strapdown seeker measurements for two reasons: first, the measurement errors introduced by strapdown seekers are much more severe than measurement errors from a gimballed seeker, making conventional filtering techniques inadequate for filtering the noise from the measurements; second, conventional guidance requires inertial referenced measurements but strapdown seekers only provide body-fixed measurements.

Recent Air Force Armament Laboratory contract efforts investigated either adaptive approaches to synthetically generate inertial line-of-sight rate, such that proportional navigation could be used. These approaches worked well against low-g maneuvering targets; however, they proved to be ineffective against high-g maneuvering targets. In terms of future operational requirements, this approach is unacceptable. In order to satisfy these requirements, future air-to-air missiles will require advanced guidance algorithms. Additionally, in order to implement these advanced guidance algorithms, more information about the missile and target dynamic states will have to be accurately measured or estimated on board the missile. The very nature of this problem lends itself to the use of modern control theory to derive the advanced guidance laws and modern estimation theory to develop techniques for processing the available information and estimating the unmeasured information.

The second section of this paper presents a background on strapdown seeker guidance technology performed by the Air Force Armament Laboratory. The third section discusses the basic differences between gimballed seeker systems and strapdown seeker systems. The next section presents the guidance law and estimation algorithms derived for this study. This section is followed by the evaluation and results. Finally, the conclusions of this study and recommendations for future study are discussed.

BACKGROUND

For the past four years the Air Force Armament Laboratory has been investigating strapdown seeker guidance technology for tactical missiles. Contract No. F08635-77-C-0144 investigated the feasibility of implementing strapdown seekers on air-to-surface tactical weapons. Algorithms were developed to synthetically generate inertial line-of-sight rate from the measurements generated by a strapdown seeker such that proportional navigation could be used. The algorithms designed and evaluated throughout the study were developed with the concept of digital implementation in mind. This was the first study in which a digital implementation of the strapdown seeker and sensor signal processing was considered and attempted via high-speed, low cost microprocessors. The results indicated that an air-to-surface guided weapon incorporating a strapdown seeker had a performance comparable to the same weapon incorporating a gimballed seeker.

3.1 Contract No. F08635-77-C0137 investigated the feasibility of implementing strapdown seekers on air-to-air tactical weapons and also designed and evaluated an autopilot for the air-to-surface weapon used in the first contract. The results of the feasibility study indicated that this approach worked well for a skid-to-turn missile against a low-g maneuvering target (<4 g's); however, the performance was poor against high-g maneuvering targets (9 g's). This approach also performed poorly for a bank-to-turn missile against a target maneuvering outside the missile's pitch plane because the missile would then have to roll. The high roll rate characteristics of a bank-to-turn missile created extreme problems for this approach.

3.2 In January 1980, the Air Force Armament Laboratory's basic research program in optimal control theory applications to tactical weapons began an in-house effort to determine the feasibility of applying optimal control theory to the strapdown seeker guidance problem. A bank-to-turn missile model was used along with realistic strapdown seeker error sources identified in Contract No. F08635-79-C-0137. Guidance and estimation algorithms were developed to improve the missile's performance in short range, high-g engagements. Performance was greatly improved over that shown in previous contractual studies. The performance was still not as good as that obtained

from the same missile model with a gimballed seeker. The latter result was not totally unexpected, since this is a beginning effort. The results from this basic research study thus far have shown, that advanced guidance laws and estimation algorithms can be developed and applied to air-to-air missiles utilizing strapdown seekers. Future efforts in this area should demonstrate this approach's full potential.

BASIC CONCEPTS

There are major differences between gimballed seekers and strapdown seekers. A gimballed system has a seeker that is mounted on a two gimbal platform. The seeker in a gimballed system has a small field-of-view (FOV) (perhaps as little as ± 3 degrees). The gimballed platform permits the seeker to cover a much larger field-of-view. The gimballed seeker provides measurements of inertial line-of-sight (LOS) angle and LOS rate for a passive seeker, and range and range-rate for an active seeker. The strapdown system has a seeker that is rigidly mounted to the missile's body, doing away with a gimballed platform. The strapdown seeker provides measurements of range, range-rate, and error angles, (the angle between the missile's X-axis, the X-axis pointing out of the nose of the missile, and the line-of-sight vector). In a gimballed system the measurements are virtually independent of missile body motion; however, in a strapdown system the measurements contain the body motion. The major error sources of a gimballed system are gyro drift, gimbal friction, gimbal cross-couplings, and acceleration sensitivity. In a strapdown system the major error sources are the seeker measurements themselves, with the major contributors being scale factor error, radome errors, glint noise, and inherent angle alignment errors.

For the purposes of this paper the error sources used are scale factor error and thermal noise. The approach is to develop an Extended Kalman Filter that explicitly accounts for these error sources and to estimate the state information required by an advanced guidance law. This approach along with some digital simulation results are presented in this paper.

4.1 The Air Force Armament Laboratory's basic research program has been investigating many control and estimation theories. The guidance law selected for this study has been found to be good in terms of performance versus complexity with the performance assessed by maximizing inner and outer launch boundaries for a specified maximum miss distance, and complexity measured in terms of digital implementation in state-of-the-art weapon systems. The guidance law selected is derived from Linear Quadratic Gaussian Theory. The only assumption made in the derivation of the guidance law is that the missile has instantaneous response and complete control over its acceleration. The guidance law is expressed in the following equations:

$$A_{MX} = 3 (S_{RX}/tgo^2 + V_{RX}/tgo + K_T A_{TX}) \quad (1a)$$

$$A_{MY} = 3 (S_{RY}/tgo^2 + V_{RY}/tgo + K_T A_{TY}) \quad (1b)$$

$$A_{MZ} = 3 (S_{RZ}/tgo^2 + V_{RZ}/tgo + K_T A_{TZ}) \quad (1c)$$

The quantities appearing in the guidance law equations are described below.

- S_{RX}, S_{RY}, S_{RZ} - Three components of relative position vector S_R referenced to the missile body (Ft)
- V_{RX}, V_{RY}, V_{RZ} - Three components of relative velocity vector V_R referenced to the missile body (Ft/sec)
- A_{TX}, A_{TY}, A_{TZ} - Three components of target acceleration vector A_T referenced to the missile body (Ft/sec²)
- A_{MX}, A_{MY}, A_{MZ} - Three components of missile acceleration command vector A_M referenced to the missile body (Ft/sec²)
- K_T - Target acceleration gain
- $K_T = (e^{-\lambda tgo} - \lambda tgo + 1) / \lambda^2 tgo^2 \quad (2)$
- λ - Target acceleration response time coefficient.
- tgo - Time-to-go (sec) (reference 1)

$$t_{go} = \frac{2 S_{RX}}{-V_{RX} + \sqrt{V_{RX}^2 + 4 S_{RX} A_{XX} / 3}} \quad (3)$$

A_{XX} - Difference between missile acceleration command and K_T X target acceleration in the axial direction (ft/sec²)

$$A_{XX} = A_{MX} - K_T' A_{TX} \quad (4)$$

K_T' - K_T evaluated at the previous time interval

$$K_T' = K_T \Big|_{(t-\Delta t)} \quad (5)$$

The time-to-go algorithm has the advantage of explicitly accounting for the missile's axial acceleration, which has been ignored in the past; thus resulting in more optimal lateral and normal acceleration commands.

Since the measured information is in the missile's body fixed coordinate system and the acceleration commands needed for the autopilot are also in the missile's body fixed coordinate system it would be desirable to design a filter/guidance package that operates in the same coordinate system. This is illustrated in Figure 1, where p , q , and r are the three missile's body and angular rates (roll, pitch, and yaw rate), σ_{rB} and σ_{qB} are the azimuth and elevation angles referenced to the missile body, A_{MB} is the missile's achieved acceleration vector referenced to the missile body, and all the other variables are the same as defined above.

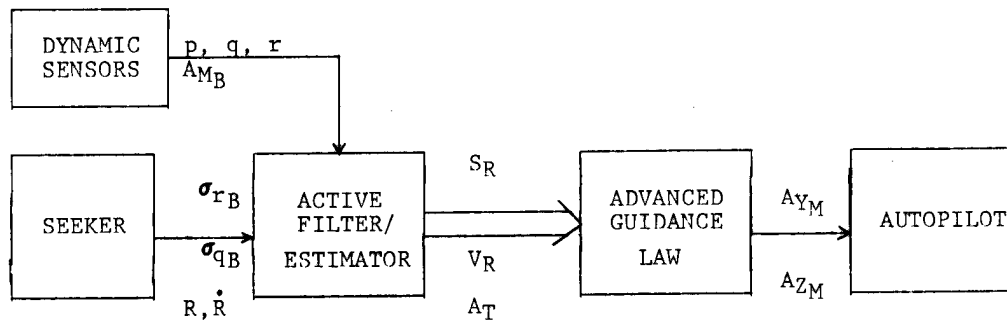


Figure 1. Guidance and Estimation Missile Body Mechanization

The active filter/estimator selected for this study is an Extended Kalman Filter (EKF). This type of filter was selected because the measurements could be modelled using nonlinear equations. The filter is needed to process the noise from a strapdown seeker and to estimate the information needed by the guidance law referenced to the missile's body-fixed coordinate system. The time invariant standard EKF will only work in an inertial fixed coordinate system and will only process Gaussian white noise (thermal noise); therefore, the filter must be modified to estimate information referenced to the body-fixed coordinate system and to process noises other than Gaussian white noise. A flow diagram of the modified EKF designed for the study is illustrated in Figure 2, with the modifications noted with an asterisk *. \hat{X} and \hat{P} are the estimates of the filter's state and error covariances, respectively. The remaining steps in the diagram are accomplished in the same manner as a time invariant standard EKF. This paper is limited to the investigation of the filter modifications, with the standard steps left for the reader to investigate (References 2 and 5).

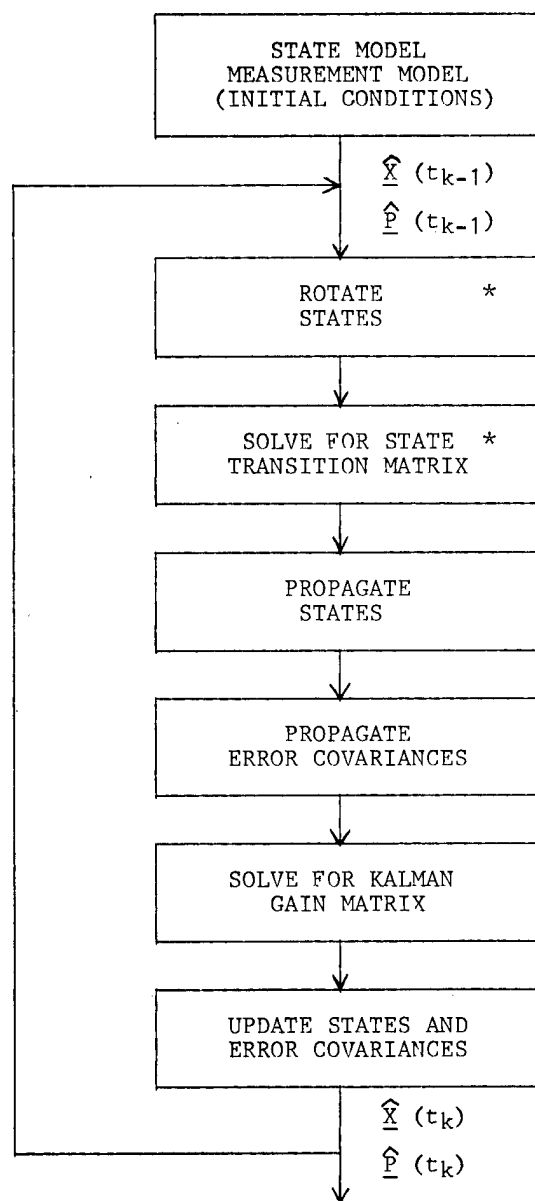


Figure 2. Modified EKF Flow Diagram

To mechanize the EKF with its state model and measurement model referenced in the missile's body fixed coordinate system and to process both thermal noise and scale factor error requires special modifications. An eleven state EKF was used where the states are composed of the three components of relative position (S_R), relative velocity (V_R), target acceleration (A_T) and the longitudinal and lateral components of scale factor error (E_S).

$$S_R = [S_{RX} \quad S_{RY} \quad S_{RZ}] \quad (6a)$$

$$V_R = [V_{RX} \quad V_{RY} \quad V_{RZ}] \quad (6b)$$

$$A_T = [A_{TX} \quad A_{TY} \quad A_{TZ}] \quad (6c)$$

$$E_S = [E_{SY} \quad E_{SZ}] \quad (6d)$$

The differential equations are written as (reference 2).

$$\dot{S}_R = V_R \quad (7a)$$

$$\dot{V}_R = A_T - A_M + W_M \quad (7b)$$

$$\dot{A}_T = -\lambda A_T + W_T \quad (7c)$$

$$\dot{E}_S = 0 + W_S \quad (7d)$$

where W_M , W_T , and W_S are the process noises for missile acceleration, target acceleration, and scale factor error, respectively.

S_R , V_R , and A_T are the necessary variables used for the guidance law and E_S is used in the EKF to explicitly account for scale factor error. Since the scale factor error is a constant multiplicative error on the measurements, equation (7d) is a valid approximation.

The nonlinear measurement equations are written as

$$\sigma_{q_B} = V + (1+E_{S_Z}) \left[\tan^{-1} \left(\frac{-S_{R_Z}}{\sqrt{S_{R_X}^2 + S_{R_Y}^2}} \right) \right] \quad (8a)$$

$$\sigma_{r_B} = V + (1+E_{S_Y}) \left[\tan^{-1} \left(\frac{S_{R_Y}}{S_{R_X}} \right) \right] \quad (8b)$$

where σ_{r_B} and σ_{q_B} are the azimuth and elevation angles, respectively, and V is the process noise for σ_{r_B} and σ_{q_B} . The other two measurement states are range and range-rate (R and \dot{R}).

This modification now accounts for both thermal noise and scale factor error in the EKF, however, there is still the problem of referencing the state model in the missile's body fixed coordinate system. This problem occurs because the standard EKF for a time-invariant system is designed to translate its states for a given Δt , but does not account for the missile's rotations. The missile's rotations are implicitly accounted for in the measurements. If the measurements are referenced to the missile's body, all knowledge of the missile's rotation is divested from the EKF. For the EKF to work, the missile's rotation must be modelled explicitly in the filter design.

To rotate the filter's states (\underline{X}) it is necessary to have a good measure of the angular displacement of the missile over a given Δt . The filter's states and the time interval Δt are written as

$$\underline{X} = \begin{bmatrix} S_R & V_R & A_T & E_S \end{bmatrix}^T \quad (9)$$

$$\Delta t = t_k - t_{k-1} \quad (10)$$

The angular rates (p , q , & r) are known for any given point in time and can be used to obtain the angles necessary to rotate the filter's states. If the assumption is made that the angular accelerations are constant over Δt , the angular displacement (ϕ , θ , & ψ) can be derived in the following manner:

$$\phi(\Delta t) = \frac{\Delta t (p(t_k) + p(t_{k-1}))}{2} \quad (11a)$$

$$\theta(\Delta t) = \frac{\Delta t (q(t_k) + q(t_{k-1}))}{2} \quad (11b)$$

$$\psi(\Delta t) = \frac{\Delta t (r(t_k) + r(t_{k-1}))}{2} \quad (11c)$$

To rotate the filter states from time t_{k-1} to time t_k , the following operation is needed.

$$\hat{\underline{X}}'_{t_k} = T'(\phi, \theta, \psi) \hat{\underline{X}}(t_{k-1}) \quad (12)$$

Where $\hat{\underline{X}}'_{t_k}$ are the states which are to be propagated and T' is a roll, pitch, yaw ordered rotational matrix represented by:

$$T' = \begin{bmatrix} T_1 & T_2 & T_3 & \vdots & & \vdots & & \vdots & \\ T_4 & T_5 & T_6 & 0 & & \vdots & 0 & & \vdots & 0 \\ T_7 & T_8 & T_9 & \vdots & & \vdots & & \vdots & & \\ \hdashline & & & \vdots & T_1 & T_2 & T_3 & & \vdots & \\ & 0 & & \vdots & T_4 & T_5 & T_6 & 0 & & \vdots & 0 \\ & & & \vdots & T_7 & T_8 & T_9 & \vdots & & \vdots & \\ \hdashline & & & \vdots & & & & \vdots & & \vdots & \\ & 0 & & \vdots & 0 & & \vdots & I & & \vdots & 0 \\ & & & \vdots & & & \vdots & & & \vdots & \\ \hdashline & & & \vdots & & & \vdots & & & \vdots & \\ & 0 & & \vdots & 0 & & \vdots & 0 & & \vdots & I \\ & & & \vdots & & & \vdots & & & \vdots & \end{bmatrix} \quad (13)$$

11x11

where

$$T_1 = \cos \theta \cos \psi + \sin \theta \sin \psi \sin \phi \quad (14a)$$

$$T_2 = \sin \psi \cos \phi \quad (14b)$$

$$T_3 = -\sin \theta \cos \psi + \cos \theta \sin \psi \sin \phi \quad (14c)$$

$$T_4 = -\cos \theta \sin \psi + \sin \theta \cos \psi \sin \phi \quad (14d)$$

$$T_5 = \cos \psi \cos \phi \quad (14e)$$

$$T_6 = \sin \theta \sin \psi + \cos \theta \cos \psi \sin \phi \quad (14f)$$

$$T_7 = \sin \theta \cos \phi \quad (14g)$$

$$T_8 = -\sin \phi \quad (14h)$$

$$T_9 = \cos \theta \cos \phi \quad (14i)$$

Note that T' does not rotate the target acceleration states nor the scale factor errors. This is because the target acceleration is simply modeled as a process and does not realistically represent the target's acceleration. Scale factor error is a constant and does not require rotation. This poses a special problem for propagating the states and error covariance matrix since the relative position and velocity are in

a different coordinate system than the target acceleration. This can be handled through the state transition matrix by including the rotation in its derivation. Given the state model

$$\dot{\underline{X}}(t) = F \underline{X}(t) + b \underline{U}(t) \quad (15)$$

and making the substitution from equation (12), the state model becomes:

$$\dot{\underline{X}}'(t) = T' F (T')^{-1} \underline{X}'(t) + T' b \underline{U}(t) \quad (16)$$

where F is the state matrix and $b \underline{U}(t)$ is the state forcing function.

The state transition matrix, $\Phi'(t_k, t_{k-1})$ is:

$$\Phi'(t_k, t_{k-1}) = \mathcal{L}^{-1} \left\{ (sI - T' F (T')^{-1})^{-1} \right\} \Big|_{(t=\Delta t)} \quad (17)$$

$$= \begin{bmatrix} I & \vdots & \Delta t I & \vdots & T' F_1 I & \vdots & 0 \\ \dots & \dots & \dots & \dots & \dots & \dots & \dots \\ 0 & \vdots & I & \vdots & T' F_2 I & \vdots & 0 \\ \dots & \dots & \dots & \dots & \dots & \dots & \dots \\ 0 & \vdots & 0 & \vdots & e^{-\lambda \Delta t} I & \vdots & 0 \\ \dots & \dots & \dots & \dots & \dots & \dots & \dots \\ 0 & \vdots & 0 & \vdots & 0 & \vdots & I \end{bmatrix}_{11 \times 11} \quad (18)$$

where

$$F_1 = \frac{e^{-\lambda \Delta t} + \Delta t \lambda - 1}{\lambda^2} \quad (19a)$$

$$F_2 = \frac{1 - e^{-\lambda \Delta t}}{\lambda} \quad (19b)$$

Because T' changes each time the filter is called, the state transition matrix will have to be updated every Δt .

The propagation and update equations for the filter states and error covariances and the solution for the Kalman gain matrix are the same as that outlined in reference (2).

The filter is now estimating relative position (S_R) and velocity (V_R) with respect to the missile's body-fixed coordinate frame and target acceleration (A_T) in a non-rotating coordinate frame. To use equation (1) in body-fixed coordinates, A_T will have to be rotated into the missile's body-fixed coordinate frame in the following fashion:

$$A_T' = T'^{-1} A_T \quad (20)$$

where

$$T'' = \begin{bmatrix} T_1 & T_2 & T_3 \\ T_4 & T_5 & T_6 \\ T_7 & T_8 & T_9 \end{bmatrix} \quad (21)$$

with $T_1, T_2, T_3, T_4, T_5, T_6, T_7, T_8, T_9$ defined in equation (14).

The target acceleration is rotated in the guidance law because it is now considered as actual target acceleration instead of a Markov Process.

The guidance law now looks like:

$$A_{MX} = 3 (S_{RX}/tgo^2 + V_{RX}/tgo + K_T A' T_X) \quad (22a)$$

$$A_{MY} = 3 (S_{RY}/tgo^2 + V_{RY}/tgo + K_T A' T_Y) \quad (22b)$$

$$A_{MZ} = 3 (S_{RZ}/tgo^2 + V_{RZ}/tgo + K_T A' T_Z) \quad (22b)$$

with K_T defined in equation (2).

Now the guidance law is in the missile's body-fixed coordinate frame which feeds directly into the autopilot without any transformation.

EVALUATION

To evaluate the guidance and estimation algorithms developed for this study a detailed six-degree-of-freedom (6-DOF) simulation of a generic bank-to-turn short range air-to-air missile was used. The target used in the simulation incorporated a "smart" target algorithm incorporating a nine-g out-of-plane evasive maneuver. The simulation contains detailed nonlinear math models of the major missile subsystems including the seeker, autopilot, and propulsion systems; realistic noise models of the on-board sensors and seeker models; detailed aerodynamic models of missile airframe characteristics; and the models that describe the missile's equations of motion. This missile/target combination was selected because it represents desired performance capabilities for the future guided weapons.

It is difficult to establish a baseline for comparison because no previous approaches using strapdown seekers have provided successful performance results when using the same missile/target models. To evaluate the algorithms, a plot of miss distance versus launch range was generated for the case of 0° off-boresight (the off-boresight angle defines the angle between the initial line-of-sight vector and the initial missile velocity vector, therefore 0° off-boresight means the missile was launched directly at the target) and 90° aspect angle (the angle between the initial line-of-sight vector and the targets velocity vector at launch). The missile and target were co-altitude (10000 feet) at launch and were co-speed at launch (.9 Mach). The target performed its evasive out-of-plane maneuver when the range became less than 6000 feet. This case was selected because in previous studies it represented one of the most challenging shots for the inertially referenced guidance and estimation algorithms to handle. Figure 3 shows the results of this evaluation. The solid line represents the results if all the information required by the guidance law was available without any noise corruptions (this represents the deterministic results). The dashed line represents the results using the guidance and estimation algorithms and realistic noise models. Because the noise models represent random processes, numerous Monte Carlo analyses had to be performed. A mean miss distance of ten feet or less was considered a hit, and anything greater than ten feet was considered a miss.

As can easily be seen from Figure 3, the advanced guidance and estimation algorithms perform very well for launch ranges up to 13000 feet.

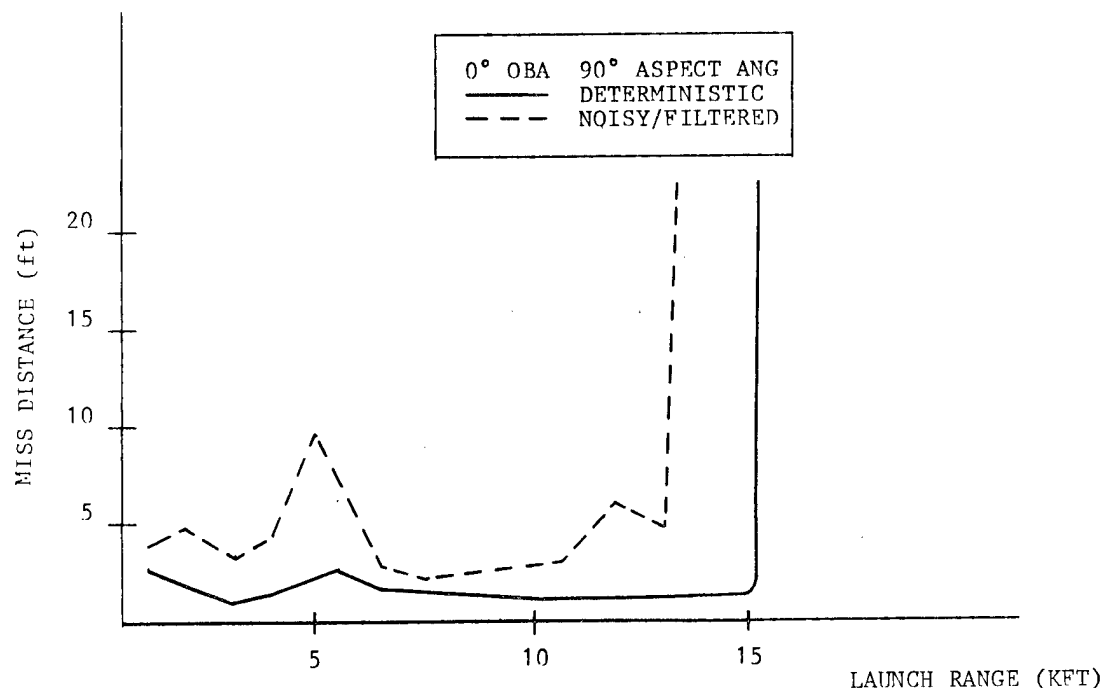


Figure 3. Performance Evaluation

CONCLUSIONS AND RECOMMENDATIONS

The results of this effort have demonstrated the feasibility of using optimal control and estimation theory for deriving advanced tactical missile strapdown seeker guidance concepts to yield high performance guidance algorithms. This was accomplished strictly through software modifications without changing the characteristics of the other missile's subsystems.

The fact that the algorithms did not perform well in the longer range launches can be attributed to two things; first, the large noise levels from a strapdown seeker, and second, the fact that the guidance law was derived to improve the missile's short range capabilities.

To pursue the full potential of this high pay-off technology, a more detailed program geared toward the derivation of guidance and estimation algorithms using theories (such as dual control theory) that are more applicable to the strapdown seeker guidance problem should be considered. The consideration of all typical noise sources from a strapdown seeker should also be included in this program.

The advantages of strapdown seekers over those with two-axis gimbals should make them attractive for future applications. These advantages include increased reliability with the elimination of moving parts and the elimination of errors due to gimbal friction and missile accelerations. Strapdown systems could potentially be lower in weight and cost. This would be particularly true in the long term as the cost of electronic components decreases with respect to mechanical components.

REFERENCES

1. Riggs, T.L., "Optimal Control and Estimation for Terminal Guidance of Tactical Missiles", Proceedings of AGARD 1980, pages 48-1-48-11, May 1980.
2. Sammons, J.M. *et al*, "Development and Comparison of Optimal Filters", AFATL-TR-79-87, October 1979.
3. Emmert, R.I. Ehrich, R.D., "Strapdown Seeker Guidance for Air-to-Surface Tactical Weapons", AFATL-TR-78-60, May 1978.
4. Ehrich, R.D., Vergez, P.L., "Strapdown Seeker Technology for the Terminal Guidance of Tactical Weapons", Proceedings of AGARD 1980, pages 31-1-31-15, May 1980.
5. Gelb, A., *et al*, "Applied Optimal Estimation," The Analytic Sciences Corporation, 1974.

PREDICTION OF AIRCRAFT MOTION
BASED ON MULTISENSOR INTEGRATION

Emory B. Pate and Max Mintz
Dept. of Systems Engineering
University of Pennsylvania
Philadelphia, PA 19104

&

Walter Dziwak and Stanley A. Goodman
US Army Armament Research
and Development Command
Dover, NJ 07801

SUMMARY

This is a preliminary report of current research on the development of enhanced mathematical models to characterize and predict the motion of an attack aircraft engaged in air-to-ground weapon delivery maneuvers. The salient feature of this study is the application of an integrated modeling technique which combines game theory, markov chains, and multivariable time series models. The goals of this study are twofold: (i) the delineation of mathematical models which lead to an increased understanding of the effective attributes of evasive maneuvering by attack aircraft, and (ii) the development of improved filtering and prediction algorithms for the related AAA fire control problem.

The present study is an outgrowth of an earlier study (1) which characterized, identified, and validated robust mathematical models for the motion of an attack aircraft during its weapon delivery pass against a defended target. These new maneuver models provided the basis for enhanced filtering and prediction algorithms was based on a synthesis of univariate time series methods and game theoretic analysis. This synthesis lead to (i) the development and validation of a practical design procedure for high performance target state estimators in the presence of moderate to large parameter uncertainty, and (ii) a technique for designing a class of "worst case" maneuver processes to blunt the effectiveness of AAA systems.

A central aspect of the research reported in (1) was the use of authentic flight test data, which consisted of eleven sample flight profiles an aircraft might perform while attacking a defended ground target. The actual data was gathered during flight tests with an A7-E aircraft at the NWTC, China Lake, California. These attack profiles, which also constitute the flight test data base for this present study, are described in detail in Chapter II of reference (1). This kinematic data base describes the aircraft motion in a cartesian coordinate system, where the origin of this coordinate system is the aircraft's intended target, as well as the assumed location of the AAA weapon system. The kinematic data describing the eleven flight profiles in the XYZ coordinate system includes consistent position, velocity, acceleration, and acceleration-dot data in each coordinate with a time increment of 0.1 sec. The primary models developed in (1) characterize the aircraft motion in terms of "decoupled" autoregressive (AR) models for the individual acceleration-dot time series in X, Y, and Z. We summarize the salient results of this earlier study with the following remarks: (1) Although the eleven flight paths appear significantly different to the "naked eye," the thirty-three acceleration-dot time series in the data base -- eleven flight paths times three directions -- are shown to be accurately modeled by a single robust fifth-order autoregressive model. The eleven flight paths in this data base include three dive toss maneuvers, five dive maneuvers, and three pop-up maneuvers. The acceleration-dot processes were incorporated in the model development since the acceleration, velocity, and position time series

are all significantly nonstationary. (ii) Substantial improvements in overall prediction capability are achievable by using robust, high-order filter-predictor algorithms based on a fifth-order AR model of acceleration-dot instead of the "usual" (benchmark) third-order algorithms based on a first-order AR model of acceleration. (iii) Typical improvements in average hit probability achieved by the new models developed in (1) versus the standard benchmark model based on a first-order AR model of acceleration, ranged from 25 to 35 percent. The specific enhancement in average hit probability associated with these new filter-predictor algorithms depends on the specific flight path, and the noise levels in the unfiltered observations. The unfiltered observations were modeled by target range, azimuth, elevation, and the respective rates.

THE NEW MODELS

The new models being developed and tested in this present study are based on an integration of finite markov chain models for aircraft normal acceleration with autoregressive integrated moving average (ARIMA) models for aircraft tangential acceleration and bank angle. The consideration of dynamic stochastic models for target motion based on target aspect (bank angle) as well as aerodynamic variables (normal and tangential acceleration) was motivated by an earlier investigation reported in (2). These preliminary results indicated that enhanced prediction capability might be achievable based on prediction algorithms defined in terms of target aspect, airspeed, and normal acceleration, particularly over extended prediction intervals (e.g., 3 - 5 sec.). We remark that other investigators working in the air-to-air fire control environment have recently considered state estimation algorithms based on target aspect and normal acceleration. However, these collateral works, which are reported in (3) & (4), do not make use of any flight test data.

The factors which suggest modeling target motion in terms of bank angle, normal acceleration, and tangential acceleration are: (i) A desire to describe target motion in terms of decision variables under the control of the pilot. (ii) The recognition, based on theoretical considerations as well as empirical studies, that the stochastic dynamic behavior of the individual X, Y, & Z acceleration-dot time series for a given flight profile are strongly coupled in a noncausal fashion. (iii) The recognition that alternative models for target motion based on aspect and aerodynamic variables could allow the exploitation of partially redundant dynamic data in the context of seeking enhanced prediction capability through multisensor integration.

PRELIMINARY RESULTS

(1) The first phase of the present study focused on the identification and estimation of univariate time series models for target bank angle (BA), normal acceleration (NA), and tangential acceleration (TA). These results indicate that the eleven BA, NA, & TA time series can be adequately modeled by three separate ARIMA models. (ii) A single input single output (SISO) transfer function analysis indicates that while there are weak causal relations between BA and NA, and between NA and TA, it is adequate to treat the individual BA, NA, & TA time series for a given flight path as independent series. (iii) The NA time series for each flight path exhibits significant piecewise linear behavior. This suggests that the rate of change of normal acceleration can be modeled as a finite state markov chain. Preliminary analysis suggests that this markovian model is quite competitive with the previously described ARIMA model for NA as judged by the relative prediction capability of each model. (iv) Preliminary versions of these new models provide overall prediction capability which is comparable to that provided by the models described in (1). However, since these results were obtained in a noiseless environment and since the supporting game theoretic sensitivity analysis remains to be completed, we view the present results as a good indication of future prospects.

REFERENCES

1. Huling, S. F. and M. Mintz, Enhanced Filtering & Prediction for AAA Fire Control: An Application of Game Theory and Time Series Analysis, Final Report on Contract No. DAAK10-78-C-0186, Submitted to US Army ARRADCOM, May 1980.

2. Huling, S. F. and M. Mintz, Robust Autoregressive Predictors for Aircraft Maneuvers: A Comparative Study, Final Report on Contract No. DAAA25-76-C-0435, Submitted to US Army Frankford Arsenal, October 1978.
3. Kendricks, J. D., Estimation of Aircraft Target Motion Using Pattern Recognition, Ph. D. Dissertation, Air Force Institute of Technology, 1978.
4. McNary, C. A., et al, Motion Estimation Using Target Aspect (META) Feasibility Study, Interim Report on Contract No. F33615-77-C-1227, Submitted to US Air Force Avionics Laboratory, October 1979, AFAL-TR-79-1077.

Next page is blank.

AN ADAPTIVE AUTOMATIC CONTROL SYSTEM
FOR REDUCTION OF HELICOPTER VIBRATION

C. E. HAMMOND
Applied Technology Laboratory
U.S. Army Research and Technology Laboratories
(AVRADCOM)
Ft. Eustis, VA 23604

ABSTRACT

The paper presents results of a wind tunnel test program using a dynamically-scaled helicopter rotor model to evaluate the use of higher harmonic blade pitch control as a means for reducing helicopter vibration levels. The test program involved the use of an adaptive automatic control system which employed Kalman filter estimation of parameters and optimal control theory. Test data are presented to show that significant reductions in the rotor vibratory vertical force and vibratory pitching moment were obtained over the range of advance ratios tested. Simultaneous reduction of the vibratory rolling moment was not achieved at all advance ratios, and the reasons behind this result remain an open issue. The wind tunnel results indicate that the higher harmonic inputs resulted in an increase in the edgewise bending moments, torsional moments, and control loads. The increased loads experienced during the test were, however, well within the design loads. The results of the test program thus indicate that active higher harmonic blade pitch control offers a viable means of achieving reduced helicopter vibration levels.

SYMBOLS

C_1, C_2	caution terms
E	expected value of a stochastic quantity
J	magnitude of optimal control penalty function
T	transfer matrix relating higher harmonic inputs to vibratory responses
T_0	nominal value of transfer matrix
W_Z	matrix of response weights
W_0	matrix of control weights
Z	column of vibratory responses
Z_0	column of baseline vibratory responses (without higher harmonic control)
Z_{00}	nominal values of baseline vibratory responses
δT	perturbation transfer matrix
δZ_0	perturbation baseline response vector
$\delta \theta$	perturbation higher harmonic input vector
θ	higher harmonic input vector
$\bar{\theta}$	nominal higher harmonic input vector

SUPERSCRIPTS

T	transpose of a matrix
\wedge	estimated value from Kalman filter
$*$	optimum higher harmonic inputs

INTRODUCTION

The U. S. Army Research and Technology Laboratories (AVRADCOM) have a wide ranging research program aimed at investigating means for achieving reduced vibration levels in helicopters. One of the concepts being explored is higher harmonic rotor blade pitch control.

Higher harmonic control (HHC) is a means whereby reduced vibration levels in the airframe are sought through tailoring of the vibratory aerodynamic loads on the blades. In this concept the vibratory forces and moments which cause airframe vibration are altered, at their source, before they reach the airframe. This is in contrast to the more conventional passive means of vibration control such as vibration absorbers^{1,2} and vibration isolators³ which deal with the vibratory loads after they have been generated.

The current program has involved the development of algorithms for determining the higher harmonic control inputs and the wind tunnel testing of the higher harmonic control concept using aeroelastically-scaled articulated rotor models. A flight test program is planned to further evaluate the wind-tunnel-developed HHC system. This paper will present results from recent tunnel testing which involved the application of a closed loop "automatic" control system.

HIGHER HARMONIC CONTROL CONCEPT

Higher harmonic control is achieved by superimposing non-rotating swashplate motions at the blade-passage frequency (4P for a 4 bladed rotor) upon the basic collective and cyclic flight control inputs. (Note: Harmonics of the rotor rotational frequency will subsequently be denoted as 1P, 2P, 3P, etc.) The frequency of the inputs is picked at the blade passage frequency because this is the frequency of the loads which are to be suppressed. The amplitude and phase of the higher harmonic inputs are chosen so as to achieve minimization of the responses being controlled.

This approach to control vibratory loads has been the subject of a number of recent wind tunnel investigations.^{4,5,6} These investigations, which were each conducted on significantly different types of rotor systems, all showed that higher harmonic control was successful in reducing the vibratory loads transmitted by the rotor to the airframe. These tests further indicated that the amplitude of higher harmonic blade pitch inputs required to achieve the desired reductions was small--on the order of one degree for the conventional helicopter flight envelope.

The primary parameters which determine the success of the higher harmonic inputs in reducing the vibratory loads are the amplitudes and phases of the various inputs. In the references 4, 5, and 6, these inputs were determined through trial and error testing. This trial and error approach is satisfactory if one is using a single input to control a single response. However, when three controls are used to control one or more responses, then the number of possible combinations of inputs becomes too numerous for the trial and error approach to be successful. Furthermore, if the higher harmonic control technique is to be applied to production helicopters then some systematic means must be available to determine, automatically, the required inputs. The means for automatically determining the higher harmonic inputs constitutes a closed loop active control system.

ACTIVE CONTROL SYSTEM

A schematic of the active control system employed in obtaining the results reported herein is shown in figure 1. In this case a four-bladed rotor wind tunnel model (to be discussed later) was used and the 4P higher harmonic inputs were used to control the 4P vibratory responses in vertical force, pitching moment, and rolling moment. In figure 1, the vibratory responses from the model (containing all the harmonics) are input to an electronic control unit (ECU). The ECU actually performs two separate functions, the first of which is to extract from the total vibratory response signals the amplitude and phase of the 4P contribution, since it is this contribution which is to be minimized. The ECU contains an analog implementation of a demodulation scheme which provides the sine and cosine components (from which the amplitude and phase may be determined) of the 4P responses in real time.

The sine and cosine components of the 4P responses are passed from the ECU to a digital computer which contains the software for the control algorithms. The nature of the control algorithms will be discussed in a subsequent section. The control software makes use of the measured responses to previous 4P higher harmonic inputs to determine the "optimum" higher harmonic inputs. The sine and cosine components of these "optimum" inputs are output from the computer as d.c. voltages which are passed to the ECU. The ECU then performs its second function which is to convert the d.c. voltages from the computer to 4P oscillatory analog signals having the correct amplitude and phase to drive the control system servos. The model then responds to these inputs and the control loop begins again.

The 1P and 64P signals shown on figure 1 are timing signals used by the ECU in extracting the 4P components of the responses.

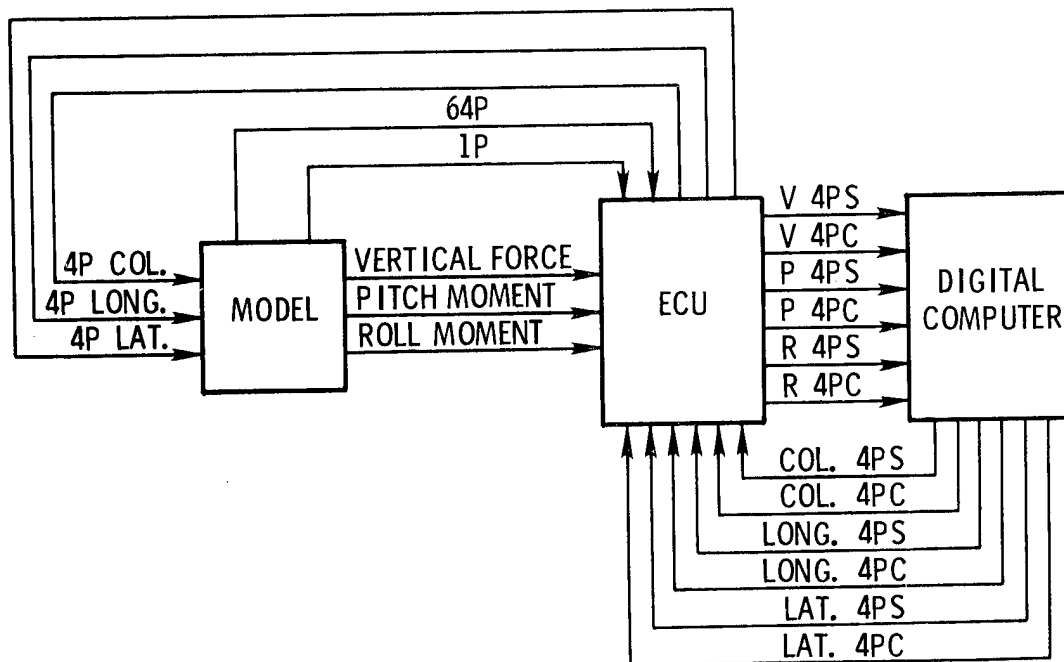


Fig. 1 Block diagram of closed loop higher harmonic control system.

CONTROL ALGORITHMS

The control algorithms employed in the program make use of digital optimal control theory.⁷ In implementing the theory, it is assumed that the 4P system response may be described by the following equations.

$$\{Z\} = \{Z_0\} + [T] \{\theta\} \quad (1)$$

Note that these equations constitute a static linear representation. The equations state that the system 4P response is made up of a baseline response plus a response which is related to the 4P inputs by a transfer matrix. Thus, if the number of responses is the same as the number of inputs and if the baseline responses and transfer matrix are known, then a set of 4P inputs could be found which would null the 4P responses.

The first portion of the control strategy is thus to determine the baseline response and the transfer matrix. Since it is undesirable to turn the control system off to measure the baseline response, and since information about the system is available from past HHC inputs and the resulting responses, an identification algorithm is used to determine Z_0 and T . The identification algorithm used is the Kalman filter.⁸

This algorithm may be thought of as a generalized form of a least-squares algorithm which accounts for the fact that the measured responses may be contaminated by noise and the transfer matrix may be changing with time.

Once the baseline responses and the transfer matrix are known, optimal control theory can be used to determine the "optimum" inputs. Several "controllers" were developed for the active control system and these controllers were extensively tested using computer simulation prior to the wind tunnel testing. Four of these controllers will be discussed briefly to illustrate their salient features.

The first controller is one which will minimize the performance index.

$$J = Z^T W_Z Z + \theta^T W_\theta \theta \quad (2)$$

If it is assumed that the transfer matrix is known without error, then the inputs which minimize the above performance index are given by

$$\theta^* = -[\hat{T}^T W_Z \hat{T} + W_\theta]^{-1} [\hat{T}^T W_Z \hat{Z}_0] \quad (3)$$

Note from equation (3) that if the response weighting matrix, W_Z , is the identity matrix and the control weighting matrix, W_θ , is zero, then the result from equation (3) is the same as solving equation (1) directly for the inputs which will give zero responses. The weighting matrix on the responses allows one to place more emphasis on reduction of some of the responses than others. The control weightings allow one to limit the amplitude of controls allowed.

It should be noted that the performance index of equation (1) and the controller of equation (3) are deterministic. If the performance index is assumed to be stochastic, i.e.,

$$J = E \{Z^T W_Z Z + \theta^T W_\theta \theta\} \quad (4)$$

then the controller of equation (3) is modified by terms which are based on the covariance matrix of the Kalman filter. Detailed discussion of these terms is beyond the scope of this paper, but the controller has the form

$$\theta^* = -[\hat{T} W_Z \hat{T} + W_\theta + C_1]^{-1} [\hat{T} W_Z \hat{Z}_0 + C_2] \quad (5)$$

The effect of the added terms C_1 and C_2 is to introduce caution into the controller since these terms account for parameter uncertainties as reflected by the Kalman filter covariance matrix. These first two controllers (eq. (3) and eq. (5)) are adaptive in that the estimates of the parameters used in the model (eq. (1)) are continuously updated through the Kalman filter, and the updated parameter estimates are used to determine the optimal inputs.

Neither the controller of equation (3) nor the controller of equation (5) assume any prior knowledge of the system behavior. If it is assumed that the T -matrix is known, then a constant gain controller is obtained as

$$\theta^* = -[T_0^T W_Z T_0 + W_\theta]^{-1} [T_0^T W_Z \hat{Z}_0] \quad (6)$$

In this case only Z_0 is estimated by the Kalman filter and the T_0 -matrix is preprogrammed based on test or flight conditions.

Since the T -matrix may not be known perfectly at all flight conditions, a perturbation controller was developed which assumes that the model of equation (1) is perturbed about an assumed nominal value of T_0 and Z_0 , i.e.,

$$\begin{aligned} T &= T_0 + \delta T \\ Z_0 &= Z_{00} + \delta Z_0 \end{aligned} \quad (7)$$

The optimum inputs for the perturbation controller are given by

$$\begin{aligned} \theta^* &= \theta_0 + \delta \theta^* \\ \theta_0 &= -[T_0^T W_Z T_0 + W_\theta]^{-1} [T_0^T W_Z Z_{00}] \\ \delta \theta^* &= -[T_0^T W_Z T_0 + W_\theta]^{-1} T_0^T W_Z [\delta \hat{Z}_0 + \delta \hat{T} \theta_0] \end{aligned} \quad (8)$$

The Kalman filter is used in this case to estimate the perturbation quantities δZ_0 and δT .

The Kalman filter used in the estimation portion of each of the above controllers is a recursive algorithm and thus each new measurement of the responses leads to an updated estimate of the parameters in the model of equation (1). With each update of these

parameters, updated "optimum" inputs are calculated and applied to the rotor control system and the cycle begins again. The control algorithms are executed very quickly by the computer and permit updating the optimal control solution every revolution of the rotor. The algorithms would actually permit more rapid updating of the solutions, but it is felt that once-per-revolution updating is sufficient to accommodate the most rapid changes in flight conditions which might be experienced by a helicopter.

DESCRIPTION OF MODEL AND TESTS

The basic wind tunnel model used in this investigation was the Aeroelastic Rotor Experimental System (ARES) shown in figure 2. This model is the successor to the model described in reference 9, and it is used for aeroelastic investigations of model scale rotor systems. These investigations are conducted in the NASA Langley Transonic Dynamics Tunnel (TDT).

The TDT is a continuous-flow tunnel with a slotted test section and is capable of operation over a Mach number range up to 1.20 at stagnation pressures from .01 to 1 atmosphere. The tunnel test section is 4.9 m square with cropped corners and has a cross sectional area of 23 m². Either air or Freon-12 may be used as a test medium in the TDT. For this investigation, Freon-12 at a nominal density of 3.09 Kg/m³ was used as a test medium. The advantages of using Freon-12 as a test medium for aeroelastic model testing have been discussed in references 10 and 11.

The ARES is powered by a 35 kw variable frequency synchronous electric motor connected to the rotor shaft through a belt-driven, two-stage reduction system. The model pitch attitude is changed using a remotely controlled hydraulic actuator and electric servo system. The rotor control system is a conventional swashplate system which is remotely controlled through the use of three electronic servos and hydraulic actuators. The high frequency response characteristics of this control system are necessary for the higher inputs.



Fig. 2. Aeroelastic Rotor Experimental System (ARES) installed in the Langley Transonic Dynamics Tunnel.

Instrumentation provisions on the ARES allow continuous measurement of model control settings, rotor forces and moments, blade loads, and pitch link loads. Model pitch attitude is measured by an accelerometer, and rotor control positions are measured by linear potentiometers connected to the swashplate. Rotor blade flapping and lagging are measured by rotary potentiometers mounted on the rotor hub and geared to the blade

cuff. The rotating blade data are transferred to the fixed system through a 60-channel, horizontal disk slip-ring assembly. Rotor forces and moments are measured by using a six-component strain-gage balance mounted below the drive system. The balance is fixed with respect to the rotor shaft and pitches with the fuselage. Fuselage forces and moments are not sensed by the balance.

The vibratory forces and moments used as response inputs to the higher harmonic control algorithms were taken from the balance. This means that the moment responses used by the control algorithms were made up of the rotor hub moments plus the rotor inplane shears times the offset distance between the rotor hub and the balance center. This offset distance was 51.44 cm.

The rotor system used in this investigation was a four-bladed articulated rotor system. The blades were dynamically scaled to be representative of a current generation rotor system. The blades had swept tips consistent with their full-scale counterpart, but the swept tips were not significant with respect to the higher harmonic control program.

The rotor was tested over a range of advance ratios (tunnel speed/rotor tip speed) consistent with the full-scale flight envelope. Because of tunnel limitations, advance ratios below .2 were not possible. The rotor rotational speed was set so as to achieve a full-scale tip Mach number. At each advance ratio the rotor was trimmed to a condition which represented a 1-g flight condition for the full-scale aircraft. Blade flapping was trimmed with respect to the shaft.

DISCUSSION OF RESULTS

The results to be discussed in this section were obtained using the closed loop active control system discussed earlier. In obtaining these results, the model was trimmed at a given advance ratio, and data were recorded to establish the vibratory responses without higher harmonic control. The automatic control system was then turned on and allowed to stabilize. With the controller still on at its stabilized condition, data were recorded to establish the vibratory responses with higher harmonic control.

Although all the controllers discussed earlier were tested on the model, the results which follow are all based on the controller having the stochastic performance index. It was found during the tests that the caution provided by this controller tended to make it much smoother in minimizing the responses than the other controllers. It should be pointed out that no rate limiting was applied to any of the controllers; however, amplitude limiting was applied to all the controllers with the maximum amplitude being set at 1 degree for most of the testing. The success of the constant gain and perturbation controllers was, as expected, dependent upon the accuracy with which the nominal parameter values were specified. The controller based on the deterministic performance index achieved essentially the same stabilized condition as the stochastic index controller the main difference between the performance of the two being that the deterministic controller tended to be more erratic in its approach to the optimum condition. It is felt that rate limiting may have relieved this problem.

The success of the higher harmonic control in reducing the vibratory responses is shown in figures 3, 4, and 5, where the variation of the responses with advance ratio are shown both with and without higher harmonic control. Figure 3 shows the variation of the vibratory vertical force. As may be seen from this figure, the higher harmonic control was quite successful in reducing this vibratory response. Reductions of from 70 to 90 percent were obtained over the range of advance ratios tested. The vibratory pitching moment shown in figure 4 indicates reductions of from 33 to 68 percent and the vibratory rolling moment shown in figure 5 indicates reductions of from 0 to 46 percent.

The fact that the order of the reductions which could be obtained in the vibratory pitching and rolling moments was much less than the reductions obtained in the vertical force is a result for which no explanation has been established. Mathematically, since three inputs were used to control three responses, it should have been possible to drive each of the responses to near zero values. A considerable amount of testing was done to explore this apparent anomaly, but a satisfactory explanation was not found during the wind tunnel test program.

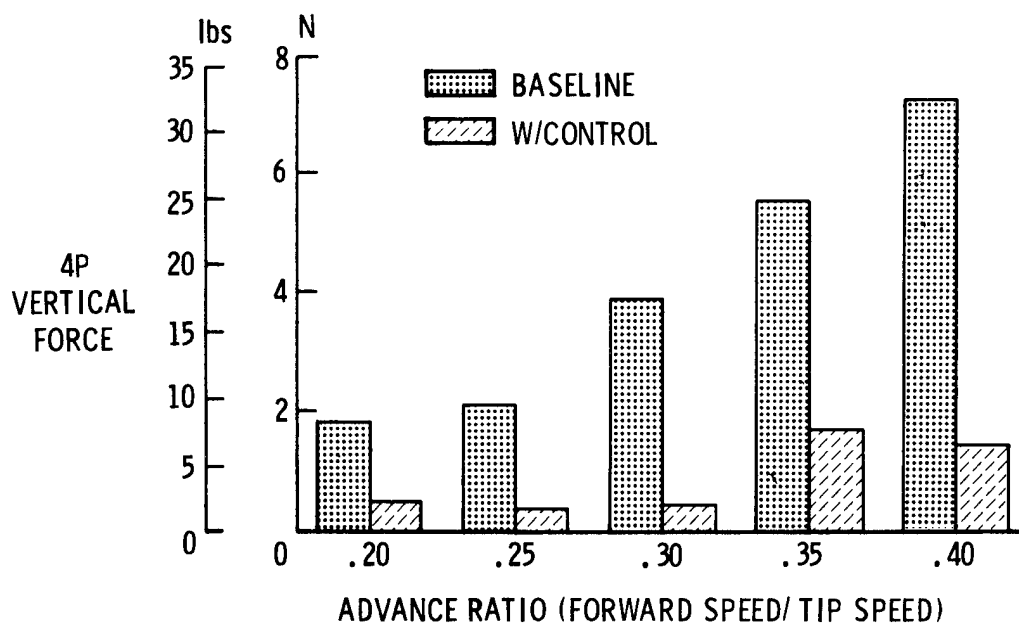


Fig. 3 Variation of vibratory vertical force with advance ratio.

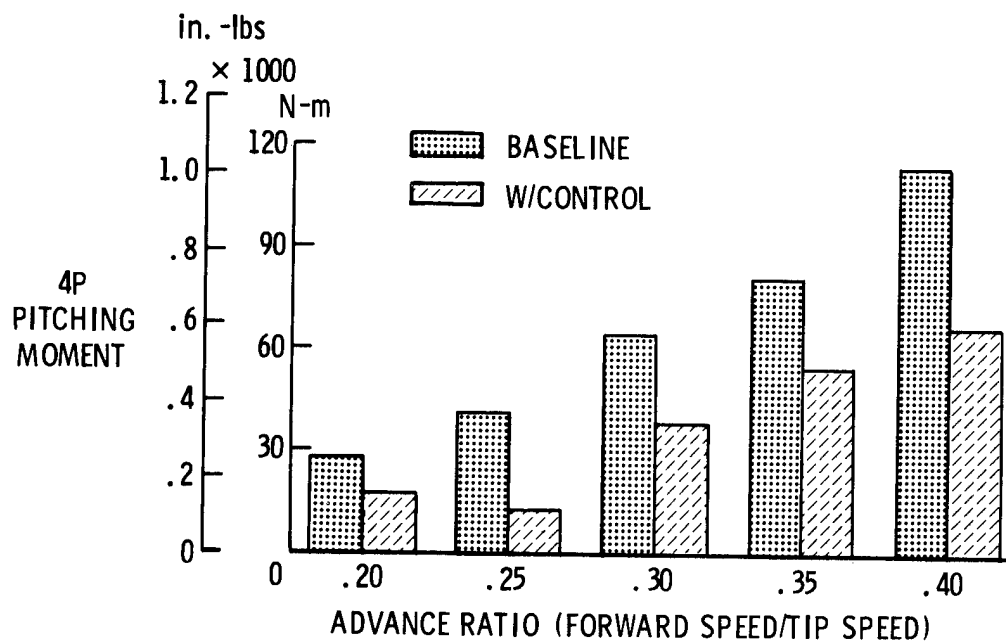


Fig. 4 Variation of vibratory pitching moment with advance ratio.

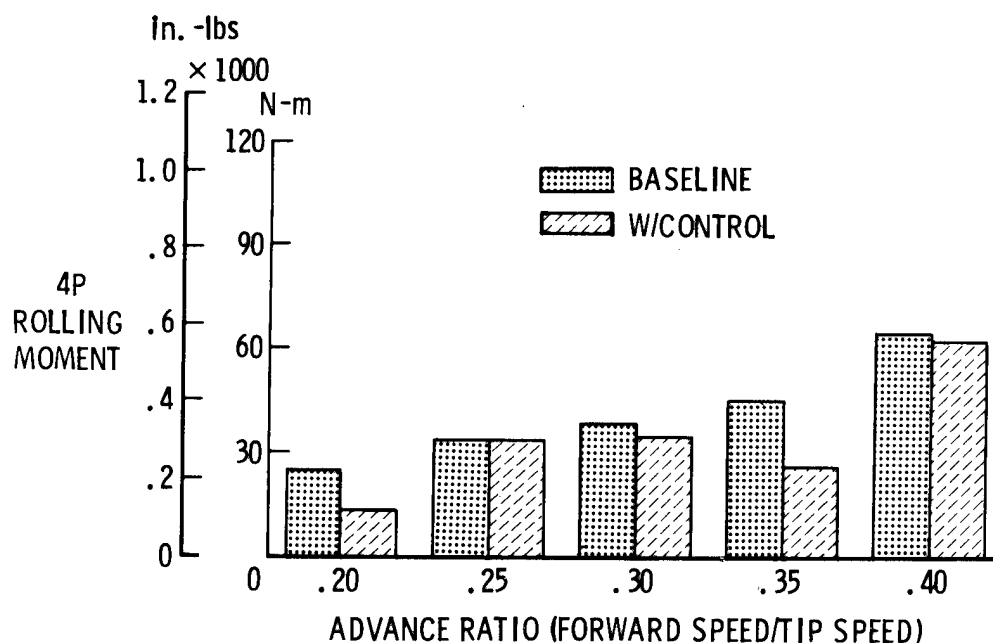


Fig. 5 Variation of vibratory rolling moment with advance ratio.

It should be pointed out that the results presented in figures 3-5 were obtained by weighting the vertical force response more heavily than the moment responses (equations (2), (3)). Numerous combinations of the weightings were explored during the test, and it was found that the weightings play a significant role in the levels of vibration reduction which can be obtained. It was found, for example, that with the proper combination of weights, the moments could be reduced more than is shown in figures 4 and 5, but at the expense of less reduction in vertical force.

Efforts to understand why moment response reductions greater than those shown in figures 4 and 5 could not be obtained in conjunction with large reductions in vertical force response are continuing. Indications are that the problem lies in the sensor location, i.e., the moments being sensed by the balance contained hub moment as well as hub shear contributions. Further tests are being performed to reconcile this issue.

It is imperative when evaluating a system which appears to promise high payoff for low investment, e.g., significant vibration reduction with a low weight penalty, that all avenues of possible side effects be explored. In the case of higher harmonic control, since the concept is based on tailoring the blade aerodynamic loads to achieve reductions in the vibratory responses, an examination of the higher harmonic inputs is appropriate. The results to be shown are from the same test points at an advance ratio of .3 as the vibratory responses shown earlier. The results at other advance ratios were similar.

The radial distribution of blade alternating flapwise bending moment (1/2 peak-to-peak values) is shown in figure 6. Similar distributions for the edgewise moment and torsion are shown in figures 7 and 8, respectively. As may be seen, there is a small reduction in the flapwise bending moment, a significant increase in the edgewise bending moment, and a moderate increase in the torsional moment. With the exception of the edgewise moment, these results are consistent with the open loop results obtained previously.⁶

The cause of the increase in the edgewise moments appears to be associated with placement of the blade's natural frequencies relative to the rotor harmonics. Figure 9 presents a harmonic decomposition of the edgewise bending moment at 53 percent span. As may be seen, there is a strong contribution at 6P without higher harmonic control, and this contribution is aggravated when higher harmonic control is applied. The strong contribution at 6P without higher harmonic control is indicative of a blade natural frequency near 6P. Excitation of this mode by the higher harmonic control comes from

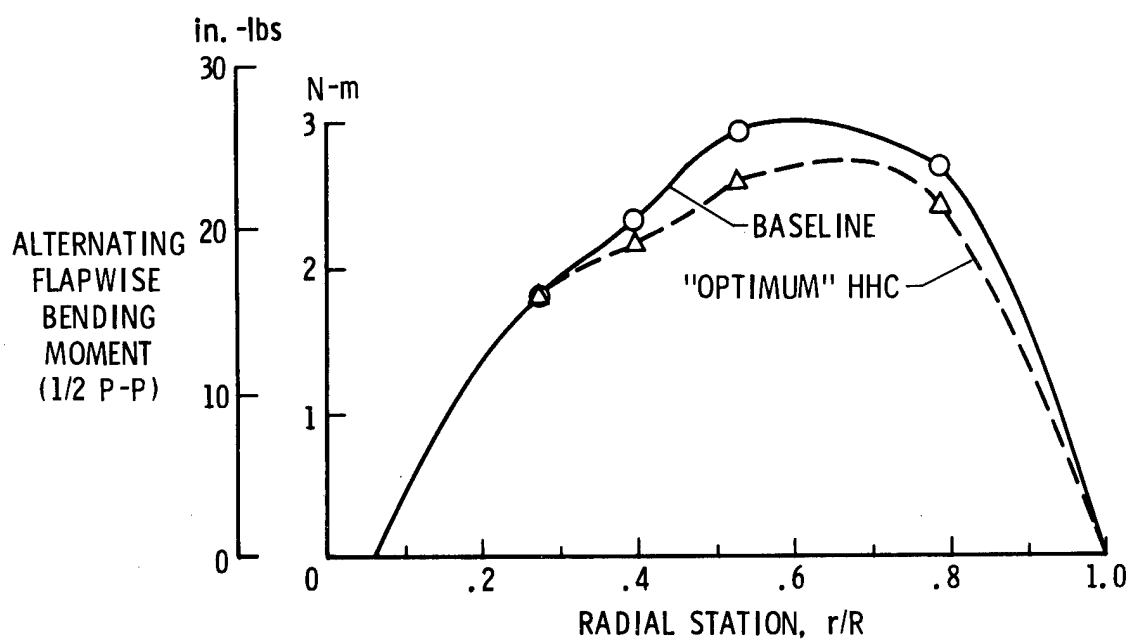


Fig. 6 Radial distribution of blade alternating flapwise bending moment (1/2 peak-to-peak values) at an advance ratio of .3.

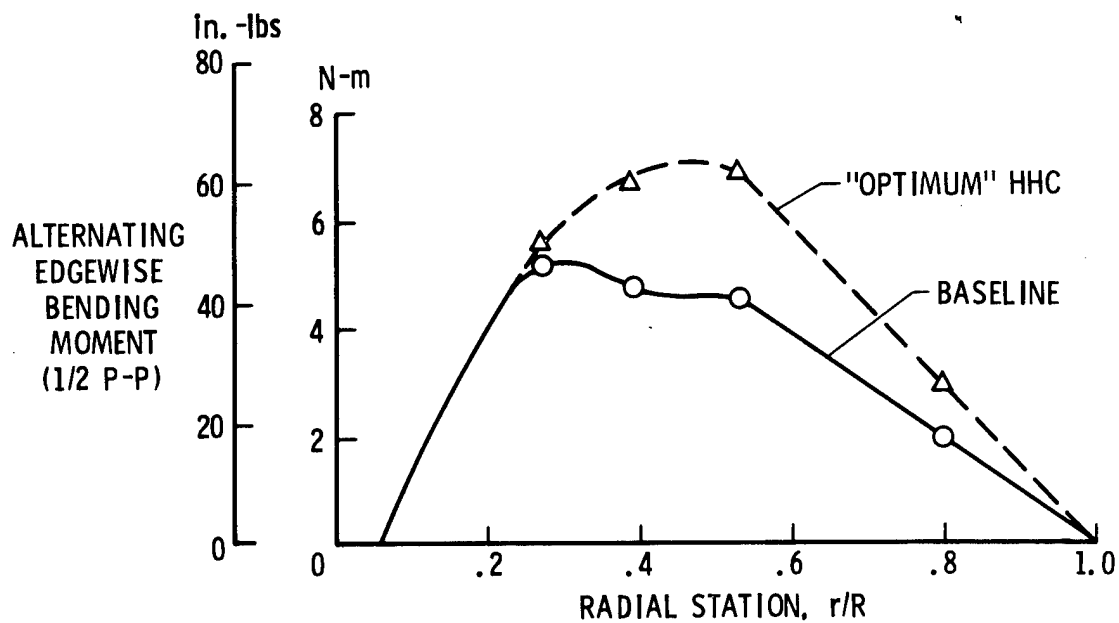


Fig. 7 Radial distribution of blade alternating edgewise bending moment (1/2 peak-to-peak values) at an advance ratio of .3.

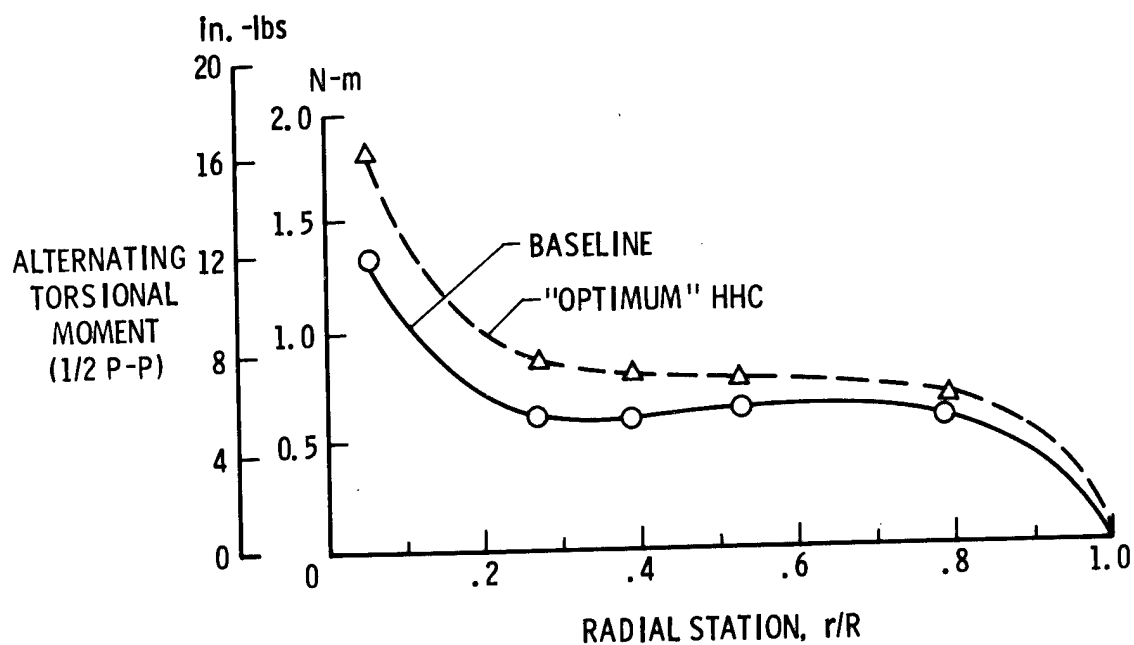


Fig. 8 Radial distribution of blade alternating torsional moment (1/2 peak-to-peak values) at an advance ratio of .3.

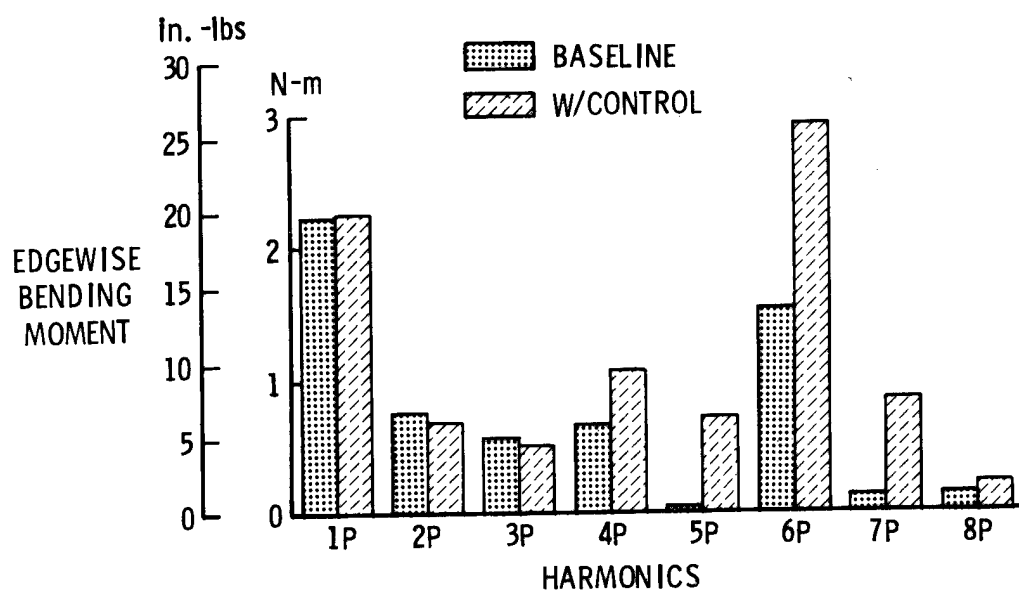


Fig. 9 Harmonic decomposition of edgewise bending moment at 53 percent span, and advance ratio of .3.

the fact that 4P cyclic motion of the non-rotating swashplate results in 3P and 5P motions of blade pitch in the rotating system, whereas 4P collective motion of the swashplate results in 4P blade pitch changes. Any impurity of the 3P blade pitch motions could excite the 6P natural blade mode since it is a second harmonic of the 3P input.

The indication from the edgewise moments is that if a new rotor is designed to incorporate higher harmonic control, blade frequency placements subject to constraints imposed by the higher harmonic control must be a design consideration. Further, for flight testing of higher harmonic control on existing aircraft, the blade loads must be carefully monitored to avoid any excessive stresses. It should be noted that the edgewise loads with higher harmonic control shown in figure 7 are well within the design load envelope for these blades, but the fact that higher harmonic control can produce a significant increase in the loads must be recognized, particularly in flight test programs.

Figure 10 presents the pitch link loads with and without higher harmonic control as a function of advance ratio. As may be seen, and as was expected, there is an increase in the control loads when the higher harmonic control is applied. The source of the increase may be attributed directly to the higher harmonic inputs as may be seen from figure 11. This figure presents a harmonic decomposition of the pitch link load at an advance ratio of .3. Note that the increase in load with higher harmonic input occurs at frequencies of 3P, 4P, and 5P which are the excitation frequencies in the rotating system. These increases in control system loads are consistent with previous findings⁶ and the magnitude of the increases has not caused significant concern among designers. Again, however, these increases must be considered in any flight test program.

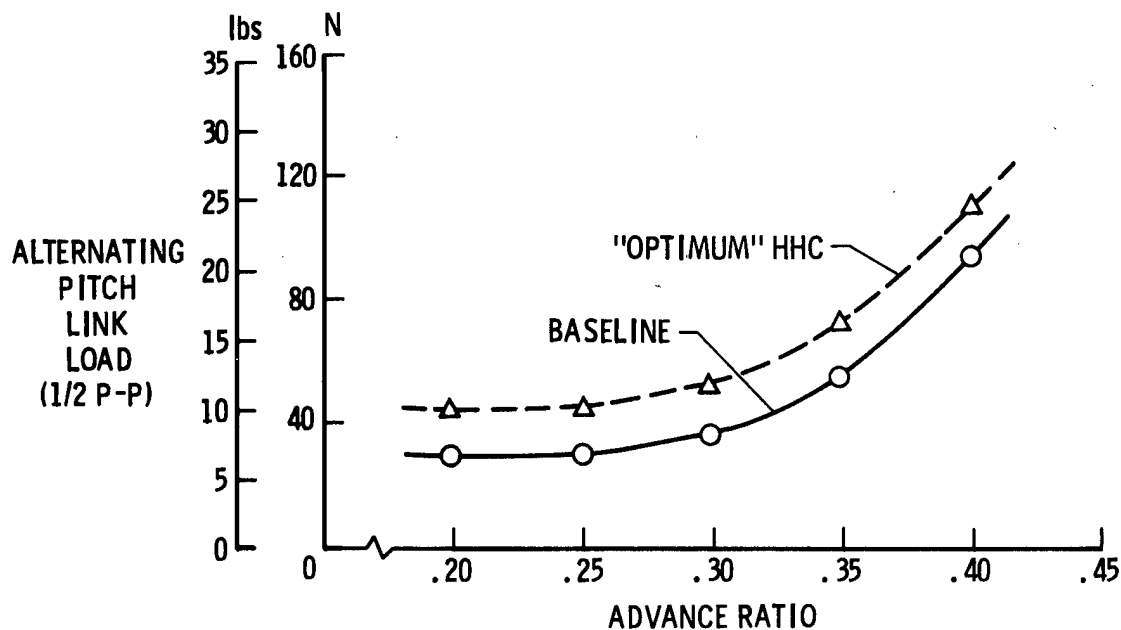


Fig. 10 Variation of alternating pitch link load (1/2 peak-to-peak values) with advance ratio.

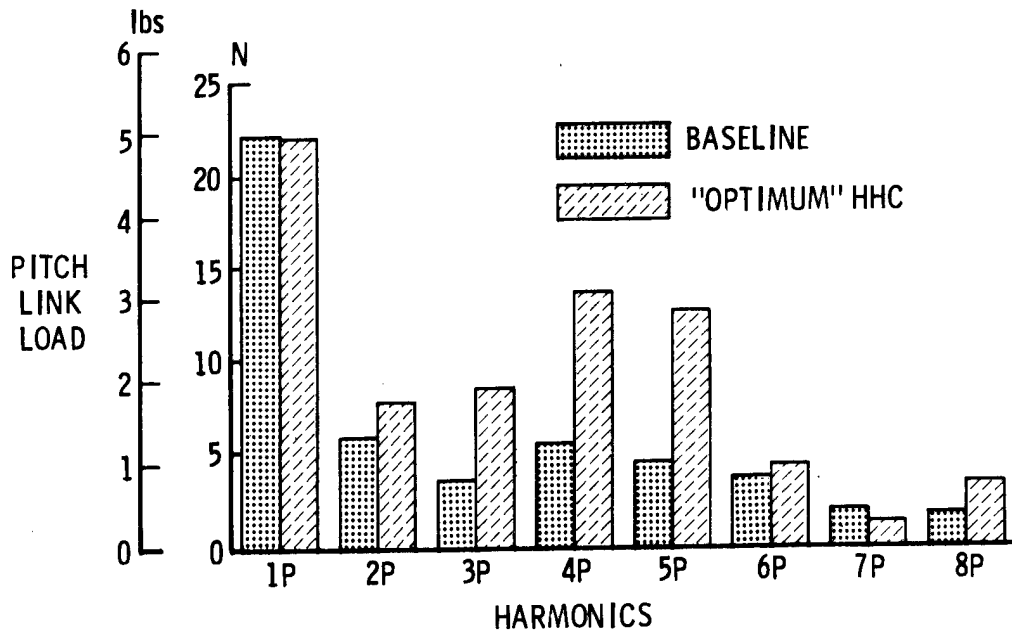


Fig. 11 Harmonic decomposition of pitch link load at an advance ratio of .3.

CONCLUDING REMARKS

Results have been presented from a wind tunnel test of a dynamically-scaled helicopter rotor model in which an active control system employing higher harmonic blade pitch was used for helicopter vibration reduction. This test was the first time that an adaptive control system employing optimal control theory has been used for this purpose. The test was successful in that the control algorithms functioned flawlessly and significant reductions in vibratory responses were achieved. An open issue remains, however, as to why even greater reductions in the vibratory responses were not obtained. Further testing is being conducted with the model to resolve this question.

The test results indicate that higher harmonic control can lead to increases in blade and control system loads. For the model tested, increases were evident in the edgewise bending and torsional moments, as well as the pitch link loads. Although the increased loads were considerably below the design limits for the model tested, the fact that blade and control system loads can increase must be considered in any flight test demonstration of the higher harmonic control concept.

Further wind tunnel testing is planned to more fully explore the characteristics of the control algorithms presented in this paper. Preparations are also underway for a flight test demonstration of the wind-tunnel-developed system. The flight tests will be conducted under contract by Hughes Helicopters using an OH-6A helicopter in the Fall of 1981.

REFERENCES

- ¹Amer, K. B., and Neff, J. R., "Vertical Plane Pendulum Absorbers for Minimizing Helicopter Vibratory Loads," J. American Helicopter Society, Vol. 19, No 4, Oct. 1974, pp. 44-48.
- ²Paul, W. F., "Development and Evaluation of the Main Rotor Bifilar Absorber," Proceedings of the 25th Annual National Forum, American Helicopter Society, May 1969.
- ³Flannely, W. G., "The Dynamic Antiresonant Vibration Isolator," Proceedings of the 22nd Annual National Forum, American Helicopter Society, May 1966.
- ⁴Sissingh, G. J., and Donham, R. E., "Hingeless Rotor Theory and Experiment on Vibration Reduction by Periodic Variation of Conventional Controls, NASA SP-352, Feb. 1974, pp. 261-277.
- ⁵McHugh, F. J., and Shaw, J., Jr., "Benefits of Higher Harmonic Blade Pitch: Vibration Reduction, Blade-Load Reduction and Performance Improvement," Proceedings of the American Helicopter Society Mideast Region Symposium on Rotor Technology, August 1976.
- ⁶Hammond, C. E., "Helicopter Vibration Reduction Via Higher Harmonic Control," Proceedings of the Rotorcraft Vibration Workshop, NASA Ames Research Center, Feb. 22-23, 1978.
- ⁷Bryson, A. E., Jr., and Ho, Y. C., Applied Optimal Control. John Wiley & Sons, 1975.
- ⁸Goodwin, G. C., and Payne, R. L., "Dynamic System Identification: Experiment Design and Data Analysis". Academic Press, 1977.
- ⁹Hammond, C. E., and Weller, W. H., "Wind-Tunnel Testing of Aeroelastically Scaled Helicopter Rotor Models (U)," 1976 Army Science Conference, West Point, NY, June 22-25, 1976.
- ¹⁰vonDoenhoff, A. E., Braslow, A. L., and Swartzberg, M. A., "Studies of the Use of Freon-12 as a Wind Tunnel Testing Medium," NACA TN 3000, 1958.
- ¹¹Hammond, C. E., and Weller, W. H., "Recent Experience in the Testing of a Generalized Rotor Aeroelastic Model at Langley Research Center," Second European Rotorcraft and Powered Lift Aircraft Forum, Paper No. 35, Sept. 1976.

Next page is blank.

ON CONTROL IN PERIODIC SYSTEMS

Leon Kotin
Center for Tactical Computer Systems
CORADCOM, Fort Monmouth, NJ 07703

ABSTRACT

Many control systems can be described mathematically by a system of differential equations, depending on a parameter $p = p(t)$, called the control, which can be chosen to impart a desirable property to the corresponding solutions. The system consists of a set of differential equations $\underline{dx}/dt = \underline{f}(t, \underline{x}; p)$ together with an initial value $\underline{x}(0) = \underline{x}_0$. We consider the special case of the system in which \underline{f} is ω -periodic in t , and we determine values of the control p which yield ω -periodic solutions. One general result which we obtain is an extension of Floquet's theorem to nonlinear systems. Further geometric arguments are used to determine periodicity in the case of a second-order system which arose in a theoretical determination of the onset of oscillations in a laser oscillator.

INTRODUCTION

This paper is devoted to real differential equations of the form

$$\underline{dx}/dt = \underline{f}(t, \underline{x}) \quad (1)$$

where $\underline{x} = \underline{x}(t)$ and $\underline{f}(t, \underline{x})$ are both n -dimensional vectors, the latter being ω -periodic in t ; i.e., $\underline{f}(t, \underline{x}) = \underline{f}(t + \omega, \underline{x})$ identically in t and \underline{x} for some positive constant ω . We shall assume an existence and uniqueness theorem, so that through a point (t_0, \underline{x}_0) in the $(n+1)$ -dimensional (t, \underline{x}) -space there exists a unique solution; moreover this solution is assumed to be defined in the interval $[t_0, \infty]$.

Conforming to the theme of this meeting, the function $\underline{f}(t, \underline{x})$ will depend on a control parameter p which, in our case, is independent of t . We shall show that a proper selection of p will guarantee the existence of a periodic solution of (1) for certain choices of $\underline{f}(t, \underline{x})$.

FLOQUET'S THEOREM FOR CERTAIN NONLINEAR SYSTEMS

In our first result, we generalize one of Floquet's theorems to nonlinear systems.

We recall that Floquet's theorem, applied to a (perhaps complex) linear periodic system

$$\underline{dx}/dt = A(t)\underline{x}, \quad (2)$$

where $A(t)$ is an ω -periodic n by n matrix, affirms the existence of a (quasi-periodic) Floquet solution $\underline{x}(t)$ such that $\underline{x}(t + \omega) = \lambda \underline{x}(t)$ for some scalar constant λ .

It may be, however, that even in the case of a real system (2), λ must be non-real.

For instance, consider the constant coefficient case

$$\underline{x}' = J\underline{x}, \quad J = \begin{pmatrix} 0 & 1 \\ -1 & 0 \end{pmatrix}.$$

Then the solution initially at \underline{x}_0 is

$$\underline{x}(t) = e^{Jt} \underline{x}_0 = (I \cos t + J \sin t) \underline{x}_0,$$

where I is the identity matrix (note the analogy with Euler's formula $e^{it} = \cos t + i \sin t$). If $\underline{x}(t)$ is a Floquet solution then $\underline{x}(t+\omega) = \lambda \underline{x}(t)$ whence $e^{J\omega} \underline{x}_0 = \lambda \underline{x}_0$, so that λ is an eigenvalue of $e^{J\omega}$ for any ω , since J is constant. Thus $\lambda = e^{+i\omega}$, which is real for real ω only of the form $m\pi$ for m an integer.

However, if the dimension n of $A(t)$ is odd and $A(t)$ is real, then there must exist a real Floquet solution. This follows in the usual matrix-theoretic proof of Floquet's theorem since any real odd-dimensional matrix has a real eigenvalue and a corresponding real eigenvector. We now generalize this result, for odd n , to positive-homogeneous nonlinear systems [1, Theorem 1].

THEOREM 1. Suppose that n is odd and that $\underline{f}(t, \alpha \underline{x}) = \alpha \underline{f}(t, \underline{x})$ for any nonnegative scalar α . Then there exists a nontrivial real solution $\underline{x}^1(t)$ of (1), and a positive constant λ , such that $\underline{x}^1(t+\omega) = \lambda \underline{x}^1(t)$.

Proof. Let us associate each point on the unit sphere S^{n-1} with the initial value of a solution of (1). The solution at time $t \geq 0$ then defines a continuous mapping $T_t: \underline{x}(0) \rightarrow \underline{x}(t)/|\underline{x}(t)|$, which takes S^{n-1} into itself, since $|\underline{x}(t)| \neq 0$ from the uniqueness of the (trivial) solution through the origin. Moreover T_ω is homotopic to the identity T_0 in $E^n - 0$. Since n is odd, from the extended Poincaré-Brouwer theorem [2, p. 483], T_ω has a fixed point; i.e., there exists a solution $\underline{x}^1(t)$ such that $\lambda \underline{x}^1(0) = \underline{x}^1(\omega)$, where $\lambda = |\underline{x}^1(\omega)|$. Now clearly $\underline{x}^1(t+\omega)$ and $\lambda \underline{x}^1(t)$ both satisfy (1). Since they are equal at $t = 0$, they are identical.

It seems strange that the proof of this theorem requires the dimension be odd, yet the corresponding result for complex linear systems, i.e., Floquet's theorem, is independent of the parity. It might be hoped therefore that there is a Floquet solution in complex $2k$ -space. However, the Poincaré-Brouwer theorem applies in complex space (as in real space) if and only if the dimension is odd [3].

As in the linear case, we have the following result.

COROLLARY 1. The Floquet solution of Theorem 1 can be expressed as $\underline{x}^1(t) = e^{\rho t} \underline{p}(t)$ where $\rho = (1/\omega) \log \lambda$ and $\underline{p}(t+\omega) = \underline{p}(t)$.

Proof. Define $\underline{p}(t) = e^{-\rho t} \underline{x}^1(t)$. Then

$$\underline{p}(t+\omega) - \underline{p}(t) = e^{-\rho(t+\omega)} \underline{x}^1(t+\omega) - e^{-\rho t} \underline{x}^1(t) = e^{-\rho t} \underline{x}^1(t) (\lambda e^{-\rho \omega} - 1) = 0,$$

whence $\underline{p}(t)$ is ω -periodic as asserted, if ρ assumes the stated value.

Substituting $\underline{x}^1(t) = e^{\rho t} \underline{p}(t)$ into (1), from the homogeneity of \underline{f} we obtain

$$e^{\rho t} (\rho \underline{p} + \underline{p}') = e^{\rho t} \underline{f}(t, \underline{p}(t))$$

whence

$$\underline{p}' = \underline{f}(t, \underline{p}) - \rho \underline{p}. \quad (3)$$

This gives us the next result, in which we may regard ρ as a control, thus justifying the presence of this talk at a meeting on control theory.

COROLLARY 2. Under the hypothesis of Theorem 1, (3) has a nontrivial ω -periodic solution $\underline{p}(t)$ for suitable constant $\rho = (1/\omega) \log \lambda$.

Applying this result to the linear system (2), we immediately conclude that the equation $\underline{x}' = (A(t) - \rho I)\underline{x}$ has a nontrivial periodic real solution for a suitable real constant ρ , if $A(t+\omega) = A(t)$ is real and n is odd.

PERIODIC SOLUTIONS OF A LIÉNARD EQUATION.

The other example which we consider arose in a theoretical study of a laser oscillator [4], namely the question of the existence of periodic solutions of the equation

$$x'' - axx' + \omega^2 x = 0, \quad (4)$$

where ω is a positive constant. When $a = 0$, the answer is immediate. When a is a non-zero real constant, we first assume it to be a positive constant.

We rewrite (4) as the autonomous system

$$\begin{aligned} x' &= y \\ y' &= x(ay - \omega^2) \end{aligned} \quad (5)$$

and observe that the line

$$L: y = \omega^2/a > 0$$

is a trajectory in the phase plane. We now show that all solutions initially below this linear solution is periodic, and the period is independent of a and the initial values.

THEOREM 2. A solution of (5) is periodic if and only if its trajectory lies below L , i.e., if and only if $\omega^2/a > x'(0)$.

Proof. We make two simple geometric observations. First, the mirror image through the y -axis of any trajectory is also a trajectory, for replacing x and t by their negatives preserves (5).

Second, since distinct trajectories of (5) cannot intersect, any trajectory initially above or on L must remain above or on L ; therefore it cannot form a closed path surrounding the origin, which is the only critical point of the system. However, such a closed trajectory is characteristic of periodic solutions.

Now from (5) we find

$$\begin{aligned} dy/dx &= (ay - \omega^2)x/y \\ d^2y/dx^2 &= (ay - \omega^2)(y^2 + \omega^2 x^2)/y^3. \end{aligned}$$

For any nontrivial solution below L , $ay - \omega^2 < 0$, whence $dy/dx < 0$ in the open first and third quadrants and $dy/dx > 0$ in the second and fourth quadrants. Moreover, $d^2y/dx^2 < 0$ when $y > 0$ and $d^2y/dx^2 > 0$ when $y < 0$. Thus, any trajectory initially below L in the second quadrant, say, must travel in a clockwise direction, intersecting the positive y -axis and continuing in the right half-plane until it intersects the negative y -axis. Distinct trajectories cannot intersect; thus from the symmetry of the family of trajectories about the y -axis, the resulting trajectory is itself symmetric about the y -axis and is therefore closed. The corresponding solution is thus periodic.

A similar result, valid for $a < 0$, may be proved similarly.

REFERENCES

1. L. Kotin, "A Floquet theorem for real nonlinear systems," J. Math. Anal. Appl., 21 (1968), pp. 384-388.
2. P. Alexandroff and H. Hopf, "Topologie," Springer, Berlin, 1935.
3. H. Hopf, "Die n-dimensionalen Sphären und projektiven Räume in der Topologie," Proceedings of the International Congress of Mathematicians 1950, Vol. 1, pp. 193-202, American Math. Soc., 1952.
4. I. R. Senitzky, "Radiative damping of a nonlinear oscillator," (to be published).

MIRROR TRACK ANTENNA--AN APPLICATION OF TIME-OPTIMAL CONTROL

Kenneth J. Hintz
Surface Weapons Technology Branch, F14
Naval Surface Weapons Center
Dahlgren, Virginia 22448

ABSTRACT

As an alternative to phased array radar systems, the Multitarget Weapon Control Radar concept is being explored to determine its suitability for multitarget tracking. One component of the Mirror Track Radar is the Mirror Track Antenna consisting of a gimbaled radio frequency (RF) "mirror" which simultaneously reflects the RF signal and rotates its polarization 90°, and a dual-axis hydraulic actuator to rapidly position the mirror, hence the beam, to any position within a hemisphere. The low inertia of the mirror/mount structure allows for more rapid positioning of the radar beam than conventional means would allow. The requirement for rapid positioning of the mirror, and precise pointing accuracy, required the development of a dual-mode, digital controller consisting of a time-optimal scheme (based on switching surfaces) with a transition to a linear controller for final settling. Variational calculus and Pontryagin's minimum principle were applied to solve for the switching boundaries of the third order, type one system. Three-dimensional plots of this switching surface are presented.

INTRODUCTION

Radar systems have taken a jump in the recent past from relatively simple mechanically scanned antennas to complex multielement phased array antennas, and not without good reason. There was every reason to expect that the benefits to be accrued by the electronic scanning made possible by the use of phased arrays with their attendant speed and versatility would outweigh the cost of the many electronically controlled phase shifters, the greater density, and the complexity of the beam control. With ships' topside weight becoming critical and the expected decrease in element costs of phased array antennas not evolving to a satisfactory degree, there is an interest in "filling the gap" in tracking antenna technology. This is leading to the development and application of more complex mechanically scanned antennas.

The increasing density of the electronic warfare (EW) environment adds another impetus to the development of the mirror track antenna (MTA). Whereas a phased array is, by virtue of its design, a single frequency device with limited bandwidth, the MTA can be made, and is being designed, to operate on a pulse-to-pulse basis at two widely differing frequencies. There is also a significant increase in the instantaneous bandwidth to be realized by the implementation of the MTA concept, leading to other forms of electronic countermeasures (ECM), making the system more jam/deception resistant.

The nominal specifications that the Multitarget Weapon Control Radar (MTWCR) is being designed to are necessarily vague since they must be tempered not only with the operational environment and tracking scenario, but also the physical constraints imposed by the mechanical implementation. The design goal is to track a minimum of six targets simultaneously and maintain at least one "hit" per second update rate for the purposes of midcourse guidance. From this general specification, and the requirement for hemispheric coverage, came the more specific minimum required acceleration and velocity. The minimum angular velocity being 15 rad/s and the minimum angular acceleration being 150 rad/s². From these, and an estimated inertia of the mirror/gimbal arrangement of 4.42 slug-ft² (6 kg-m²), required torques could be calculated as approximately 570 ft-# (772.7 n-m).

The MTWCR, with the mirror track antenna as a subsystem, is a distinct departure from current tracking radar systems in that it is being designed not as a single-target, dedicated tracker/illuminator, but rather, as the name implies, a radar able to track several targets simultaneously. But the complexities of the multitarget tracking problem are not the issue at hand, other than that it places constraints on the

mechanical design of the system. Those constraints are of two forms, the first being the time-optimal control (positioning) of the MTA, and the second being the required pointing accuracy to satisfy the constraints of the variable rate sampled data tracking filters. It was soon apparent that the two requirements could not be satisfied by a single control scheme; a linear controller being, by definition, not time-optimal, but yet required for pointing accuracy, and a nonlinear time-optimal controller being unable, in any practical implementation, to have the required pointing accuracy. This necessitated a dual-mode system which was time-optimal for large excursions with a transition to a linear mode for settling. Since the linear mode of operation is a classical case of meeting minimum settling time constraints, its development is not discussed here, nor are the stability considerations resulting from the implementation of a dual-mode control system. The following discussion concerns itself with the conversion of the plant to a linearized equivalent model and the subsequent development of the time-optimal control based on switching surfaces.

MIRROR TRACK ANTENNA PRINCIPLE OF OPERATION

Referring to Figure 1, the feed consists of a conventional linearly polarized monopulse feed. For the purpose of this discussion, it is considered single frequency, although a dual band monopulse feed is being designed and will be included in the final design. The linearly polarized RF signal from the feedhorn illuminates a parabolic transreflector embedded in the protective radome. The transreflector consists of a linear (not a mesh or grid) set of wires that are parallel to the electric field polarization from the linear feedhorn. The parabolic reflector collimates the beam and redirects it towards the feedhorn where it illuminates the twist reflector (mirror). This twist reflector not only reflects the beam, but it also rotates the polarization of the RF signal 90° so that the transreflector is now transparent to the RF signal. The position of the beam can thereby be controlled by a precise positioning of the mirror with a gain of two due to the fact that the angle of reflection equals the angle of incidence. The system is reciprocal on receive which also affords a slight degree of ECM resistance to cross-polarized signals.

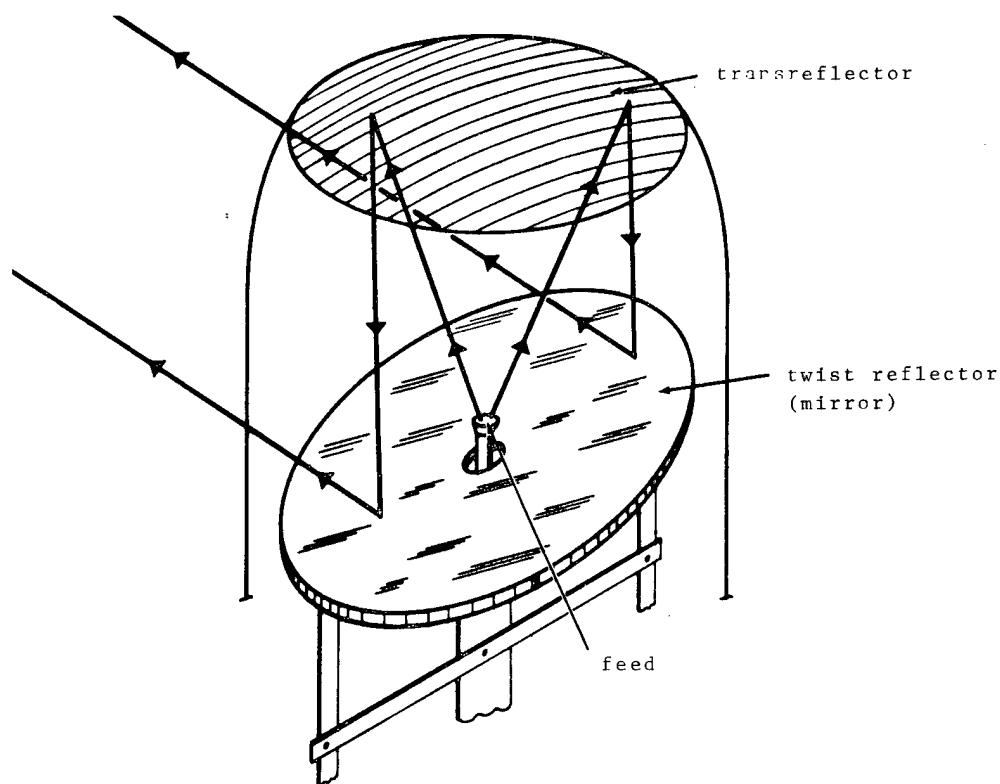


Figure 1. Mirror Track Antenna Principle of Operation

BEAM STEERING MECHANISM

The mirror itself consists of a layer of dielectric material with embedded planar wire grids (to perform the polarization rotation) sandwiched to an aluminum honeycomb support structure. The honeycomb structure was required to dampen any tendency of the mirror to vibrate at its natural frequency when excited by step inputs at the four support points (see Figure 2), and to maintain a "flat" surface since fractional wavelength distortions would result in antenna pattern degradation.

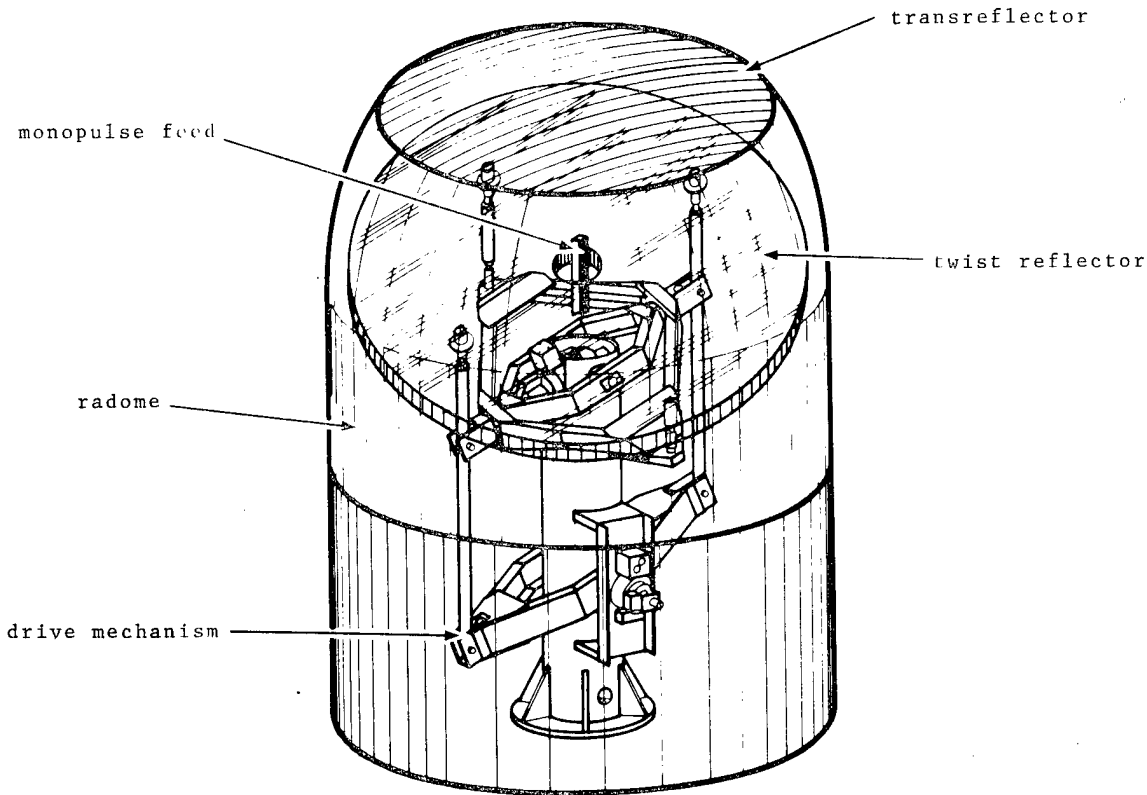


Figure 2. Mirror Track Antenna

The method chosen to position the mirror was a gimballed arrangement with orthogonal single turn hydraulic rotary actuators. The gimballed arrangement was required to allow for hemispheric coverage with the point of rotation of the mirror located at the center and on the surface of the mirror itself to minimize translation motion. Hydraulic actuators were chosen since they have the best torque-to-weight ratio (note that one of the actuators is moving with the upper gimbal and is part of the inertial load for the lower actuator), and require no gearing to achieve sufficient rotational acceleration and velocity.

The majority of the gimbal structure was constructed of 3- and 4-in. aluminum channel for maximum rigidity and minimum inertia without resorting to exotic materials. The aluminum honeycomb of the mirror support structure itself approaches the best weight-to-strength ratio possible. The central supporting column is 10 in. (.25 m) in inside diameter and is made of .25 in. (6.3 mm) thick steel. The approximate overall dimensions of the system are 7 ft (2.1 m) high, 5 ft (1.5 m) in diameter with an estimated weight of 700 lb (318 kg).

THE PLANT

The mechanism and actuating device consist of a servo amplifier, flow control servo valve, a hydraulic actuator, and an inertial load (damping forces are negligible compared to the torque available, and the mechanism is made sufficiently stiff so that there is no appreciable flexure at the frequencies of interest).

The servo amplifier is a voltage-to-current converter with adjustable gain (K_1 amps/volt) and sufficiently high bandwidth such that it can be modeled as a simple gain, K_1 .

The flow control valve can be modeled as a first order lag where

$$\frac{Q}{i}(s) = \frac{K_2}{1 + \tau s}$$

where

K_2 = servo valve static flow gain at zero load pressure drop

τ = apparent servo valve time constant = .008 seconds

Since the mechanism (see Figure 2) is still under development, the inertia will be represented by the variable, J , the anticipated value being from 17.6 to 88.3 #in.-sec² (2 to 10 kg-m²). The mount and mirror are being made sufficiently rigid that spring effects occur at frequencies much higher than those of interest to the control system.

Due to the nonlinearities of the servo valve, the system model requires linearization about an operating point. The drop in pressure resulting from increased flow rate must be accounted for since it is pressure, hence torque, that accelerates the load. Figure 3 is the linear model of the plant chosen to include the effects of changing pressure with flow rate and the states are the angular position, velocity and acceleration--all real, measurable variables. Figure 4 is derived from the valve characteristics and is used to make a linear approximation to K_3 .

STATE SPACE REPRESENTATION

If the state space variables [1] are chosen as shown in Figure 5, the variables are directly related to physical, measurable quantities. That is

$z_1 = \theta$, the output angle

$\dot{z}_1 = z_2$, the angular velocity (1a)

$\dot{z}_2 = z_3$, the angular acceleration (1b)

$\dot{z}_3 = z_3 \left(\frac{-1}{\tau} - \frac{K_5 K_7}{J} \right) + z_2 \left(\frac{-K_5 K_7}{J \tau} \right) + \frac{K_6 K_7}{J \tau} u$ (1c)

the resulting plant can be redrawn, letting

$$K_8 = \frac{-K_5 K_7}{J \tau} \quad (2a)$$

$$K_9 = \frac{-1}{\tau} - \frac{K_5 K_7}{J} \quad (2b)$$

$$K_{10} = \frac{K_6 K_7}{J \tau} \quad (2c)$$

For the linear controller, the same model can be used with a change in K_7 based on a reduced flow rate.

This system (see Figure 6) can be represented in matrix form as

$$\dot{\vec{Z}} = [A] \vec{Z} + \vec{B} u \quad (3)$$

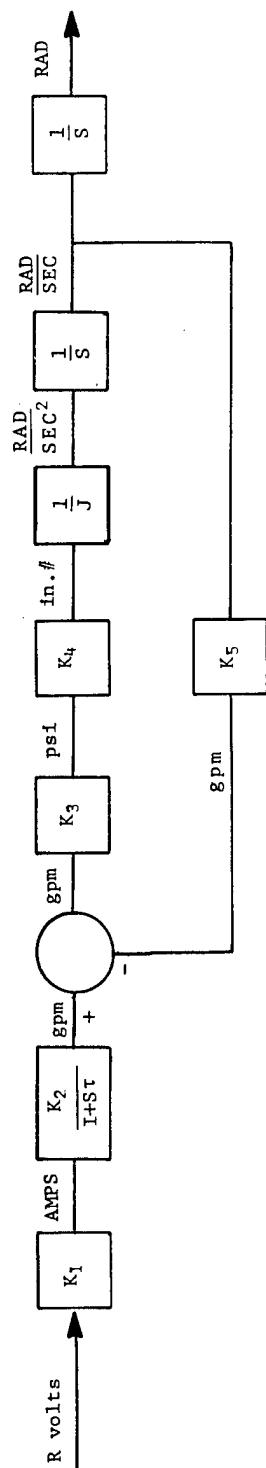
$$[\vec{T}] = \vec{C} \vec{Z} \quad (4)$$

where

$$[A] = \begin{bmatrix} 0 & 1 & 0 \\ 0 & 0 & 1 \\ 0 & K_8 & K_9 \end{bmatrix}$$

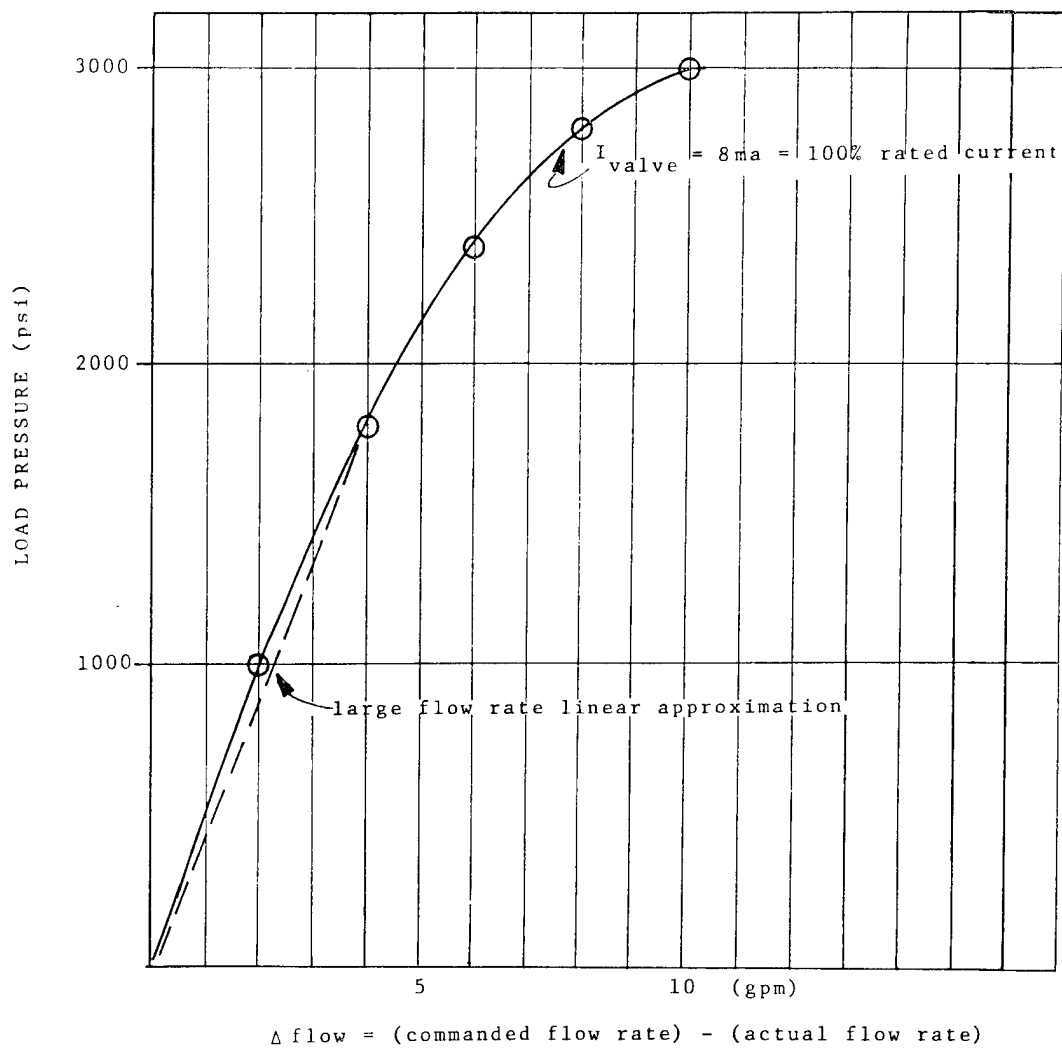
$$\vec{B} = \begin{bmatrix} 0 \\ 0 \\ K_{10} \end{bmatrix}$$

$$\vec{C}^T = \begin{bmatrix} 1 \\ 0 \\ 0 \end{bmatrix}$$



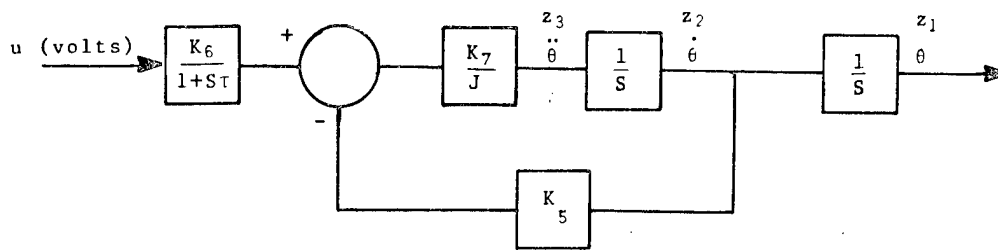
- K_1 = Servo amplifier (voltage to current converter) gain
 K_2 = Servo valve flow gain (gal/min/amp)
 K_3 = Differential flow to pressure linearized gain
 K_4 = Pressure to torque gain
 K_5 = Rad/sec to gal/min conversion (motor constant)
 τ = Servo valve time constant
 J = Inertia of mount/mirror

Figure 3. Block Diagram of Plant Model



FOR LARGE FLOW RATES: $\frac{\text{pressure}}{\Delta \text{flow}} = \frac{1800 \text{ psi}}{4 \text{ gpm}} = 450 \text{ psi/gpm} = K_3$

Figure 4. Load Pressure as a Function of Differential Flow Rate for MOOG Servo Valve #A076-193



$$K_6 = K_1 K_2$$

$$K_7 = K_3 K_4$$

J = inertia of mount/mirror

K_5 = motor constant (gpm/RPS)

Figure 5. Block Diagram of Reduced Plant with Initial State Assignments

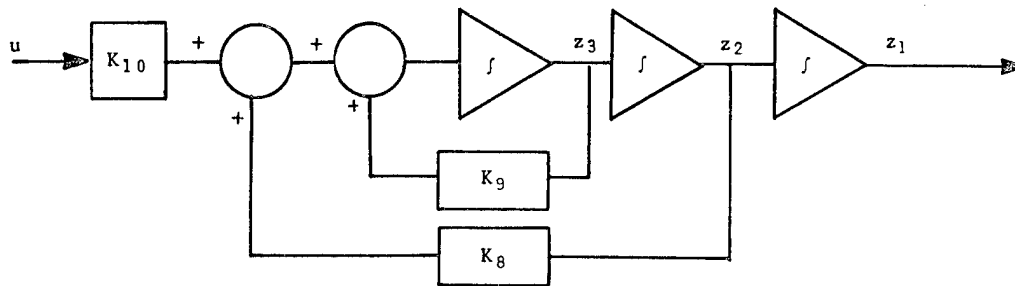


Figure 6. Modified State Space Representation

MODIFICATION OF DESCRIPTION IN ORDER TO MODEL STATES AS ERRORS

Since inputs are restricted to steps, the system can be considered autonomous with various initial conditions [2]. The closed loop system, including the nonlinear controller and plant, $G(s)$, is shown in Figure 7.

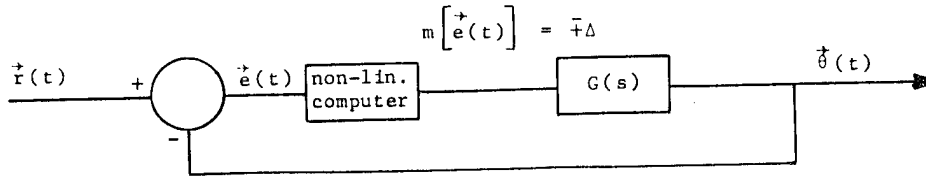


Figure 7. System Block Diagram

The requirement is that after some time t , $\theta(t) = \dot{r}(t)$ and therefore $\dot{e}(t) = \ddot{0}$. This is equivalent to requiring that $e = \dot{e} = \ddot{e} = 0$ at time t . Let the input be zero and the system start with an initial value of $\theta(t)$, then $\dot{e}(t) = -\dot{\theta}(t)$.

From the previous development of the system state equations, $-\dot{e}(t)$ can be substituted for $\dot{\theta}(t)$ leading to the change of variables,

Original System	Error System	
$z_1 = \theta$	$z_1 = -e$	(5a)
$z_2 = \dot{\theta}$	$z_2 = -\dot{e}$	(5b)
$z_3 = \ddot{\theta}$	$z_3 = -\ddot{e}$	(5c)

That is, the analysis is identical, but the definition of the states is changed for the implementation.

So taking the change of variables from (5) and substituting into the models of (3, 4)

$$\begin{aligned} \dot{\vec{z}} &= [A]\vec{z} + \vec{B}u & \vec{T} &= \vec{C}\vec{z} \\ -\dot{\vec{e}} &= [-A]\vec{e} + \vec{B}u & \vec{T} &= -\vec{C}\vec{e} \end{aligned}$$

or, letting the error = \vec{W}

$$\dot{\vec{W}} = [A]\vec{W} - \vec{B}u \quad (6a)$$

and

$$\vec{T} = -\vec{C}\vec{W} \quad (6b)$$

The value of this transformation is that all further analysis can be based on the movement of the initial condition to the origin of the state space.

Another translation will be made to simplify the algebra by finding the diagonal form of the $[A]$ matrix [1]. This is done by finding the Jordan form of the matrix by using the modal matrix, $[P]$, to perform a similarity transformation. Since the eigenvalues will be real, distinct, and nonpositive, the Jordan form is diagonal, and is

$$[J] = \begin{bmatrix} \lambda_1 & 0 & 0 \\ 0 & \lambda_2 & 0 \\ 0 & 0 & \lambda_3 \end{bmatrix} \quad (7)$$

With the modal matrix constructed from the eigenvectors as follows

$$[P] = \begin{bmatrix} 1 & 1 & 1 \\ 0 & -\lambda_1 & -\lambda_2 \\ 0 & \lambda_1^2 & \lambda_2^2 \end{bmatrix} \quad (8)$$

The change of variables can then be made, letting $[PV] = [W]$

$$\dot{\vec{W}} = [A]\vec{W} - \vec{B}u$$

$$[P] \dot{\vec{V}} = [A][P]\vec{V} - \vec{B}u$$

$$[P^{-1}][P]\dot{\vec{V}} = [P^{-1}][A][P]\vec{V} - [P^{-1}]\vec{B}u$$

$$\dot{\vec{V}} = [P^{-1}][A][P]\vec{V} - \vec{g}u \quad (9a)$$

$$\vec{Y} = -\vec{C}\vec{W}$$

$$\vec{Y} = -\vec{C}[P]\vec{V} \quad (9b)$$

The eigenvalues (and hence $[J]$ and $[P]$) are found by finding the roots of the characteristics equation which is the determinant of $(\lambda I - A)$.

$$\det(\lambda[I] - [A]) = \lambda(\lambda^2 - K_9\lambda - K_8) \quad (10)$$

with eigenvalues

$$\lambda_1 = 0 \quad (11a)$$

$$\lambda_{2,3} = \frac{K_9 \pm \sqrt{K_9^2 + 4K_8}}{2} \quad (11b)$$

Let the eigenvalues of the system be 0, λ , $\alpha\lambda$ where $\lambda_2 = \alpha\lambda_3$ then

$$[J] = \begin{bmatrix} 0 & 0 & 0 \\ 0 & \lambda & 0 \\ 0 & 0 & \alpha\lambda \end{bmatrix} \quad (12)$$

$$[P] = \begin{bmatrix} 1 & 1 & 1 \\ 0 & -\lambda & -\alpha\lambda \\ 0 & \lambda^2 & \alpha^2\lambda^2 \end{bmatrix} \quad (13)$$

$$[P^{-1}] = \begin{bmatrix} 1 & \frac{-(\alpha^2 - 1)}{\lambda\alpha(1 - \alpha)} & \frac{1}{\lambda^2\alpha} \\ 0 & \frac{\alpha}{\lambda(1 - \alpha)} & \frac{+1}{\lambda^2(1 - \alpha)} \\ 0 & \frac{-1}{\lambda\alpha(1 - \alpha)} & \frac{-1}{\lambda^2\alpha(1 - \alpha)} \end{bmatrix} \quad (14)$$

From (9) and (3)

$$\vec{g} = [P^{-1}]\vec{B}$$

leading to

$$\dot{\vec{v}} = \begin{bmatrix} 0 & 0 & 0 \\ 0 & \lambda & 0 \\ 0 & 0 & \alpha\lambda \end{bmatrix} \vec{v} - \frac{K_{10}}{\lambda^2} \begin{bmatrix} \frac{1}{\alpha} \\ \frac{-1}{1-\alpha} \\ \frac{1}{\alpha(1-\alpha)} \end{bmatrix} u \quad (15)$$

The solution to this system of linear, time invariant differential equations can be found by using Laplace transforms and letting the control for the time-optimal solution be the scalar

$$u = \frac{\Delta}{s}, \Delta = \pm 1$$

that is

$$\vec{v} = [s[I] - [J]]^{-1} \vec{v}(0) - [s[I] - [J]]^{-1} \frac{g\Delta}{s} \quad (16)$$

The inverse of $[s[I] - [J]]$ is

$$[s[I] - [J]]^{-1} = \begin{bmatrix} \frac{1}{s} & 0 & 0 \\ 0 & \frac{1}{s-\lambda} & 0 \\ 0 & 0 & \frac{1}{s-\alpha\lambda} \end{bmatrix} \quad (17)$$

then

$$\vec{v} = \begin{bmatrix} \frac{1}{s} & 0 & 0 \\ 0 & \frac{1}{s-\lambda} & 0 \\ 0 & 0 & \frac{1}{s-\alpha\lambda} \end{bmatrix} \left[\vec{v}(0) - \frac{g\Delta}{s} \right] \quad (18)$$

$$v_1(s) = \frac{1}{s} v_1(0) - \left(\frac{K_{10}}{\lambda^2 \alpha} \right) \frac{\Delta}{s^2} \quad (19a)$$

$$v_2(s) = \frac{1}{s-\lambda} v_2(0) - \left[\frac{K_{10}}{\lambda^2 (1-\alpha)} \right] \frac{\Delta}{(s)(s-\lambda)} \quad (19b)$$

$$v_3(s) = \frac{1}{s-\alpha\lambda} v_3(0) + \left[\frac{K_{10}}{\lambda^2 \alpha (1-\alpha)} \right] \frac{\Delta}{s(s-\alpha\lambda)} \quad (19c)$$

Taking the inverse Laplace transform to find the time domain solution

$$v_1(t) = v_1(0) - \left(\frac{K_{10}}{\lambda^2 \alpha} \right) \Delta t \quad (20a)$$

$$v_2(t) = v_2(0) e^{\lambda t} - \left[\frac{K_{10} \Delta}{\lambda^3 (1-\alpha)} \right] (e^{\lambda t} - 1) \quad (20b)$$

$$v_3(t) = v_3(0) e^{\alpha\lambda t} + \left[\frac{K_{10} \Delta}{\lambda^3 \alpha^2 (1-\alpha)} \right] (e^{\alpha\lambda t} - 1) \quad (20c)$$

Letting

$$\frac{K_{10}}{\lambda^2 \alpha} = \frac{1}{K_{20}} \quad (21)$$

and

$$\vec{V}K_{20} = \vec{X}$$

to simplify the system representation

$$x_1(t) = x_1(0) - \Delta t \quad (22a)$$

$$x_2(t) = x_2(0)e^{\lambda t} - \frac{\Delta \alpha}{\lambda(1-\alpha)}(e^{\lambda t} - 1) \quad (22b)$$

$$x_3(t) = x_3(0)e^{\alpha \lambda t} + \frac{\Delta}{\lambda \alpha(1-\alpha)}(e^{\alpha \lambda t} - 1) \quad (22c)$$

Equations (22a), (22b), and (22c) represent the step response of the plant in transformed error coordinate. These general solutions will be used to solve for the time-optimal control.

To put the time solution back into standard matrix form, (21) is substituted into (15) yielding

$$\dot{\vec{X}} = \begin{bmatrix} 0 & 0 & 0 \\ 0 & \lambda & 0 \\ 0 & 0 & \alpha \lambda \end{bmatrix} \vec{X} - \begin{bmatrix} 1 \\ \frac{+\alpha}{1-\alpha} \\ \frac{-1}{1-\alpha} \end{bmatrix} u \quad (23)$$

$$\vec{Y} = \left(\frac{-1}{K_{20}} \right) (\vec{C}[P]\vec{X}) \quad (24)$$

VERIFICATION OF THE CONTROLLABILITY AND OBSERVABILITY OF THE SYSTEM

For the system to be completely controllable, the matrix [N] must have rank 3. From (23)

$$[N] = \left[\vec{B} \mid [A]\vec{B} \mid [A^2]\vec{B} \right]$$

$$[N] = \begin{bmatrix} -1 & 0 & 0 \\ \frac{-\alpha}{1-\alpha} & \frac{-\lambda \alpha}{1-\alpha} & \frac{-\lambda^2 \alpha}{1-\alpha} \\ \frac{+1}{1-\alpha} & \frac{+\alpha \lambda}{1-\alpha} & \frac{+\alpha^2 \lambda^2}{1-\alpha} \end{bmatrix}$$

Since no column is a multiple of any other, [N] has rank 3 and is completely controllable.

For complete observability, the matrix [Q] must have rank 3. From (24)

$$\vec{Y} = \frac{-1}{K_{20}} [1 \quad 1 \quad 1] \vec{X}$$

Since the elements of \vec{C} and [A] are real, and [A] is diagonal,

$$[Q] = \left[\vec{C}^T \mid [A^T]\vec{C}^T \mid [A^{T^2}]\vec{C}^T \right]$$

$$[Q] = \frac{-1}{K_{20}} \begin{bmatrix} 1 & 0 & 0 \\ 1 & \lambda & \lambda^2 \\ 1 & \alpha\lambda & \alpha^2\lambda^2 \end{bmatrix}$$

which has rank 3. Hence the system is completely observable.

THE FORM OF THE TIME-OPTIMAL CONTROL

Principles of variational calculus and Pontryagin's minimum principle [3] can be applied to the linear, time invariant system with scalar control, u ,

$$\dot{\vec{X}} = [A]\vec{X} + \vec{B}u$$

where

$$[A] = \begin{bmatrix} 0 & 0 & 0 \\ 0 & \lambda & 0 \\ 0 & 0 & \alpha\lambda \end{bmatrix}$$

and

$$\vec{B} = \begin{bmatrix} -1 \\ \frac{-\alpha}{1-\alpha} \\ \frac{+1}{1-\alpha} \end{bmatrix}$$

The desired performance index for time-optimal control is

$$J = \int_0^t d\tau \quad (25)$$

The optimal control, u , which minimizes the performance index can be found by minimizing the Hamiltonian

$$\begin{aligned} \mathcal{H} &= 1 + \vec{p}^T \dot{\vec{X}} \\ \mathcal{H} &= 1 + \vec{p}^T [A]\vec{X} + \vec{p}^T \vec{B}u \end{aligned} \quad (26)$$

The costate equations can be found from the Hamiltonian

$$\dot{\vec{p}}^* = \frac{-\partial \mathcal{H}}{\partial \vec{X}} = \vec{p}^T [A] = [A^T] \vec{p} \quad (27)$$

$$\dot{\vec{p}}^* = \begin{bmatrix} 0 & 0 & 0 \\ 0 & \lambda & 0 \\ 0 & 0 & \alpha\lambda \end{bmatrix} \vec{p} \quad (28)$$

Using Laplace transform again to find the solution.

$$p_1(t)^* = p_1(0) \quad (29a)$$

$$p_2(t)^* = p_2(0)e^{\alpha\lambda t} \quad (29b)$$

$$p_3(t)^* = p_3(0)e^{\lambda t} \quad (29c)$$

With bounded controls, $-1 < u < +1$, the optimal control, u^* , is the one which minimizes \mathcal{H}

$$\mathcal{H}[\vec{X}^*(t), u^*(t), \vec{p}^*(t)] \leq \mathcal{H}[\vec{X}^*(t), u(t), \vec{p}^*(t)] \quad (30)$$

$$1 + \vec{p}^{*T}[A]\vec{X}^* + \vec{p}^{*T}\vec{B}u^* \leq 1 + \vec{p}^{*T}[A]\vec{X}^* + \vec{p}^{*T}\vec{B}u \quad (31)$$

$$\vec{p}^{*T}\vec{B}u^* \leq \vec{p}^{*T}\vec{B}u \quad (32)$$

Substituting (29) into (32)

$$\left[-p_1^*(0) - p_2^*(0)\left(\frac{\alpha e^{\lambda t}}{1 - \alpha}\right) + p_3^*(0)e^{\lambda t}\left(\frac{1}{1 - \alpha}\right) \right] u^* \leq \vec{p}^{*T}\vec{B}u \quad (33)$$

From this, it can be seen that the control which minimizes (33) is

$$u^* = -\text{sgn} \left\{ -p_1(0) - p_2(0)\left(\frac{\alpha e^{\lambda t}}{1 - \alpha}\right) + \left(p_3(0)e^{\lambda t}\right)\left(\frac{1}{1 - \alpha}\right) \right\} \quad (34)$$

The argument of sgn in (34) has at most two zeros, implying that the sign of u^* can take on three values at most. Candidates for the optimal control are then

$$(+1), (-1), (+1, -1), (-1, +1), (-1, +1, -1), (+1, -1, +1) \quad (35)$$

From (33) it can be seen that the optimal control is also the control of maximum magnitude, so, let

$$u^*(t) = \Delta \quad (36)$$

where

$$\Delta = \pm 1$$

thus, justifying the choice of step input in solving the system (22).

Equations (22a), (22b), and (22c) are the time response of the system to a step input in state variables. Since it is desired to find a control that is independent of time, then (22) can be combined by eliminating time.

First, a few definitions are in order:

$\{V_2\}$ = the set of states from which the origin can be reached under the single control $u^* = \pm 1$.

$\{V_1\}$ = the set of states from which the origin can be reached under a double control of $u^* = (+1, -1)$ or $u^* = (-1, +1)$.

x_{12} = a state variable $\in \{V_2\}$.

METHODOLOGY FOR TIME-OPTIMAL CONTROL DERIVATION

The general sequence of solution [4] for the time-optimal control is to first eliminate time from (22) and find $x_1 = f(x_2)$ and $x_3 = f(x_2)$. These general solutions will be used to first find $\{V_2\}$ by setting the initial conditions, $x_1(0)$, $x_2(0)$, and $x_3(0)$ equal to zero. This is done to find the particular solution that passes through the origin of the state space. Next $\{V_1\}$, a surface, will be found by using as a particular solution to the differential equations, the initial conditions that are $\in \{V_2\}$. And finally, the surface, $\{V_1\}$, will be used as a boundary between the two volumes of state space in which the initial control is either a $+1$ or -1 .

For the general solution, first eliminate time from (22a)

$$t = \frac{x_1(0) - x_1}{\Delta} \quad (37)$$

Substituting (37) into (22b)

$$x_2 = \left[x_2(0) - \frac{\Delta\alpha}{\lambda(1-\alpha)} \right] \exp\left\{ \frac{\lambda}{\Delta} [x_1(0) - x_1] \right\} + \frac{\Delta\alpha}{\lambda(1-\alpha)} \quad (38)$$

Substituting (37) into (22c)

$$x_3 = \exp\left\{ \frac{\lambda\alpha [x_1(0) - x_1]}{\Delta} \right\} \left[x_3(0) + \frac{\Delta}{\lambda\alpha(1-\alpha)} \right] - \frac{\Delta}{\lambda\alpha(1-\alpha)} \quad (39)$$

The trajectory in the x_1, x_2 plane is shown in Figure 8.

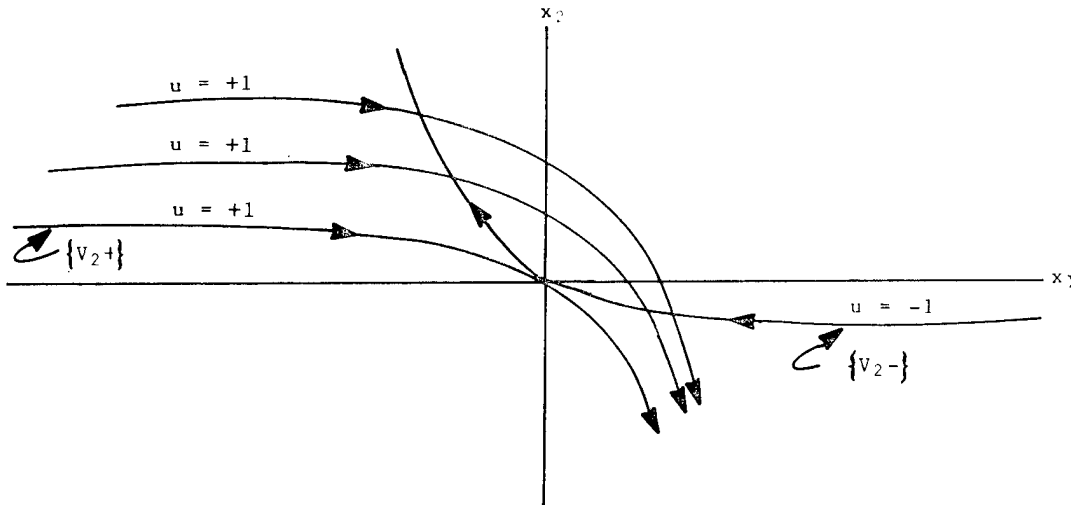


Figure 8. Projection of General Trajectory in x_1, x_2 Plane

The set of states $\{V_2\}$ can be found from (38) and (39) by letting $x_1(0) = x_2(0) = x_3(0) = 0$ since the system is linear and time invariant.

$$x_2 = \left[\frac{-\Delta^*\alpha}{\lambda(1-\alpha)} \right] \exp\left(\frac{-\lambda x_1}{\Delta^*} \right) + \frac{\Delta^*\alpha}{\lambda(1-\alpha)} \quad (40)$$

$$x_3 = \frac{\Delta^*}{\lambda\alpha(1-\alpha)} \exp\left(\frac{-\lambda\alpha x_1}{\Delta^*} \right) - \frac{\Delta^*}{\lambda\alpha(1-\alpha)} \quad (41)$$

Figure 9 shows these particular trajectories, and by inspection, $\Delta^* = -\text{sgn}(x_1)$.

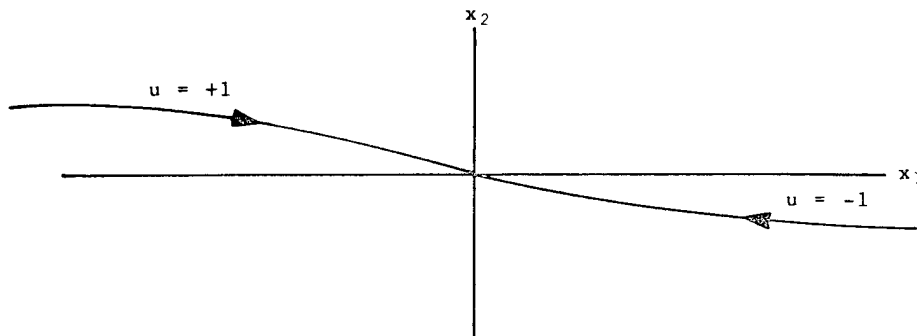


Figure 9. Trajectories in x_1x_2 Plane of $\{V_2\}$

The set of states, $\{V_1\}$, from which the origin can be reached in two controls is sought next. Let $x_{12}, x_{22}, x_{32} \in \{V_2\}$ and $x_1 x_2 x_3 \in \{V_1\}$, then, from (38) and (40)

$$x_{22} = \left[x_2 - \frac{\Delta\alpha}{\lambda(1-\alpha)} \right] \exp \left[\frac{\lambda(x_1 - x_{12})}{\Delta} \right] + \frac{\Delta\alpha}{\lambda(1-\alpha)} \quad (42)$$

$$x_{22} = \frac{-\Delta\alpha}{\lambda(1-\alpha)} \exp \left(\frac{-\lambda x_{12}}{\Delta} \right) - \frac{\Delta\alpha}{\lambda(1-\alpha)} \quad (43)$$

by eliminating x_{22} between (42) and (43)

$$\left[x_2 - \frac{\Delta\alpha}{\lambda(1-\alpha)} \right] \left[\frac{-\lambda(1-\alpha)}{\Delta\alpha} \right] = e^{\frac{-\lambda x_1}{\Delta}} \quad (44)$$

Note that x_{12} drops out. Doing the same for (39) and (41)

$$x_{32} = \exp \left\{ \lambda\alpha \left(\frac{x_1 - x_{12}}{\Delta} \right) \right\} x_3 \left[+ \frac{\Delta}{\lambda\alpha(1-\alpha)} \right] - \frac{\Delta}{\alpha\lambda(1-\alpha)} \quad (45)$$

$$x_{32} = \frac{\Delta}{\lambda\alpha(1-\alpha)} \exp \left(\frac{-\lambda\alpha x_{12}}{\Delta} \right) - \frac{\Delta}{\lambda\alpha(1-\alpha)} \quad (46)$$

equating (45) and (46) leads to

$$\left[x_3 + \frac{\Delta}{\lambda\alpha(1-\alpha)} \right] \left[\frac{\lambda\alpha(1-\alpha)}{\Delta} \right] = e^{\frac{-\lambda\alpha x_1}{\Delta}} \quad (47)$$

To combine these into one equation describing the surface, $\{V_1\}$, divide (44) by (47)

$$x_2 = -x_3 \alpha^2 \exp \left[\frac{x_1 \lambda(\alpha - 1)}{\Delta^*} \right] - \frac{\Delta^* \alpha}{\lambda(1-\alpha)} \exp \left[\frac{x_1 \lambda(\alpha - 1)}{\Delta^*} \right] + \frac{\Delta^* \alpha}{\lambda(1-\alpha)} \quad (48)$$

where

$$\Delta^* = -\text{sgn}(x_{12})$$

It is now necessary to determine the optimal control, Δ^* , as a function of $x_1 x_2 x_3$ rather than x_{12} . From Figure 8, it can be seen that in the $x_1 x_2$ plane, if $x_2 > x_{22}$, then $\Delta^* = +1$ and if $x_2 < x_{22}$, $\Delta^* = -1$. That is

$$u^* = \text{sgn}(x_2 - x_{22})$$

$$u^* = \text{sgn} \left(x_2 - \left\{ \frac{+\text{sgn}(x_1)\alpha}{\lambda(1-\alpha)} \exp \left[\lambda x_1 \text{sgn}(x_1) \right] \frac{-\text{sgn}(x_1)\alpha}{\lambda(1-\alpha)} \right\} \right) \quad (49)$$

this leads to $\{V_1\}$ being

$$\{V_1\} = \left\{ x_1 x_2 x_3 : x_2 = -x_3 \alpha^2 \exp [\Delta^* x_1 \lambda(\alpha - 1)] \right. \\ \left. - \frac{\Delta^* \alpha}{\lambda(1-\alpha)} \exp [\Delta^* x_1 \lambda(\alpha - 1)] + \frac{\Delta^* \alpha}{\lambda(1-\alpha)} \right\} \quad (50)$$

where

$$\Delta^* = \text{sgn} \left\{ x_2 - \frac{\text{sgn}(x_1)\alpha}{\lambda(1-\alpha)} \exp [\lambda x_1 \text{sgn}(x_1)] + \frac{\text{sgn}(x_1)\alpha}{\lambda(1-\alpha)} \right\}$$

To recapitulate, (50) now describes a surface, $\{V_1\}$, in three-dimensional space from which the origin can be reached in one change of control. That is, if $x \in \{V_2\}$, either the control sequence $(+1, -1)$ or $(-1, +1)$ will drive the system to the origin.

It can also be seen that this surface divides the state space into two volumes. Given that the system starts at a state that is not $\in \{V_1\}$, hence not $\{V_2\}$ either, the application of a control, either ± 1 , will drive the system's state toward or away from the surface, $\{V_1\}$. So, the initial control can be found by finding the sign of the difference between the current state and $\{V_1\}$. Let

$$\Sigma = \text{sgn}(x_2 - x_{21})$$

where

$$x_2 = \text{initial condition}$$

$$x_{21} \in \{V_1\} \text{ from (50).}$$

If

$$\Sigma = 0, \text{ then } x_1 \in \{V_1\} \text{ and use } \{V_1\} \text{ test for } \Delta^* \quad (51a)$$

$$\Sigma < 0, \text{ then } \Delta^* = -1 \quad (51b)$$

$$\Sigma > 0, \text{ then } \Delta^* = +1 \quad (51c)$$

$$\begin{aligned} \Sigma = \text{sgn} \left\{ x_2 + x_3 \alpha^2 \exp \left[\Delta^* x_1 \lambda (\alpha - 1) \right] \right. \\ \left. + \frac{\Delta^* \alpha}{\lambda(1 - \alpha)} \exp \left[\frac{\Delta^* \lambda (\alpha - 1)}{\alpha} \right] - \frac{\Delta^* \alpha}{\lambda(1 - \alpha)} \right\} \end{aligned} \quad (52)$$

where

$$\Delta^* = \text{sgn} \left\{ x_2 - \frac{\text{sgn}(x_1) \alpha}{\lambda(1 - \alpha)} \exp \left[\lambda x_1 \text{sgn}(x_1) \right] + \frac{\text{sgn}(x_1) \alpha}{\lambda(1 - \alpha)} \right\}$$

This is the control law for any general state. If $\Sigma = 0$, the Δ^* test for $\{V_1\}$ is performed. If that is zero also, then the final test for $\{V_2\}$ is performed to determine the sign of the control.

SUMMARY OF TIME-OPTIMAL CONTROL LAW FOR $G(S) = \frac{1}{J(s - \lambda)(s - \alpha\lambda)}$

$$\Sigma_1 = \text{sgn} \left[x_2 + x_3 \alpha^2 e^{\left(\Delta^* x_1 \lambda (\alpha - 1) \right)} + \frac{\Delta^* \alpha}{\lambda(1 - \alpha)} e^{\left(\frac{\Delta^* \lambda (\alpha - 1)}{\alpha} \right)} - \frac{\Delta^* \alpha}{\lambda(1 - \alpha)} \right] \quad (53)$$

where

$$\Delta^* = \text{sgn} \left\{ x_2 - \frac{\text{sgn}(x_1) \alpha}{\lambda(1 - \alpha)} \exp \left[\lambda x_1 \text{sgn}(x_1) \right] + \frac{\text{sgn}(x_1) \alpha}{\lambda(1 - \alpha)} \right\}$$

$$\vec{x} = \text{initial state}$$

If

$$\Sigma_1 = 0, \text{ go to } \{V_1\} \text{ since } x \in \{V_1\} \quad (54a)$$

$$\Sigma_1 = > 0, u^* = +1 \quad (54b)$$

$$\Sigma_1 = < 0, u^* = -1 \quad (54c)$$

and continue on this control until $\Sigma_1 = 0$.

When $\Sigma_1 = 0$, change sign of control, or if Σ_1 was initially $= 0$, set control based on

$$u^* = \operatorname{sgn} \left\{ x_2 - \frac{\operatorname{sgn}(x_1)\alpha}{\lambda(1-\alpha)} \exp[\lambda x_1 \operatorname{sgn}(x_1)] + \frac{\operatorname{sgn}(x_1)\alpha}{\lambda(1-\alpha)} \right\} \quad (55)$$

Continue under this control until intersecting $\{V_2\}$. That is, when

$$\Sigma_2 = x_2 + \left[\frac{\Delta^* \alpha}{\lambda(1-\alpha)} \right] \exp\left(\frac{\lambda}{\Delta^*}\right)(-x_1) - \frac{\Delta^* \alpha}{\lambda(1-\alpha)} \quad (56)$$

where

$$\Delta^* = -\operatorname{sgn}(x_1)$$

change the sign of u^* . This final trajectory will terminate in a transition to a linear control based on norm, $\|\vec{x}\| < \delta$ where δ is such that $-1 < u < +1$ (i.e., not saturated) for the final settling.

TRANSFORMATION FROM THE "REAL" STATE OF THE SYSTEM, $\theta, \dot{\theta}, \ddot{\theta}$, TO \vec{x} , THE STATE OF THE MODEL

$$z_1 = \theta$$

$$z_2 = \dot{\theta}$$

$$z_3 = \ddot{\theta}$$

$$y_1 = \theta_C - \theta_R = -e$$

$$y_2 = \dot{\theta}_C - \dot{\theta}_R = -\dot{e}$$

$$\vec{y} = [P]\vec{v}$$

$$\vec{v} = \frac{\vec{x}}{K_{20}}$$

where

$$K_{20} = \frac{\lambda^2 \alpha}{K_{10}}$$

Equation (57) is the transformation from actual system state to the state space model variables and (58) is the reverse.

$$\vec{x} = K_{20}[P]^{-1}(\vec{\theta}_C - \vec{\theta}_R) \quad (57)$$

$$\vec{\theta}_C = \frac{[P]}{K_{20}} + \vec{\theta}_R \quad (58)$$

SWITCHING SURFACE

The complexity of the analytic expression for the switching surface disguises its relatively simple form in three-dimensional state space. Figures 10 through 12 show the shape of the switching surface for various values of eigenvalues. That is, λ_1 was nominally chosen equal to -1 and λ_2 varied from -2 to -3 to -4 in order to show the dynamics of the surface for various ratios of eigenvalues. Most simply stated, the control law means that if the state of the system is above the surface, a positive control of maximum value should be used until intersecting the surface at which time the control is changed and held at a maximum negative value until intersecting the final switching curve. At this final intersection, the sign of the control is again changed until the state of the system approaches within some normed distance of the origin at which time the time optimal control law is no longer used and a linear digital control takes over.

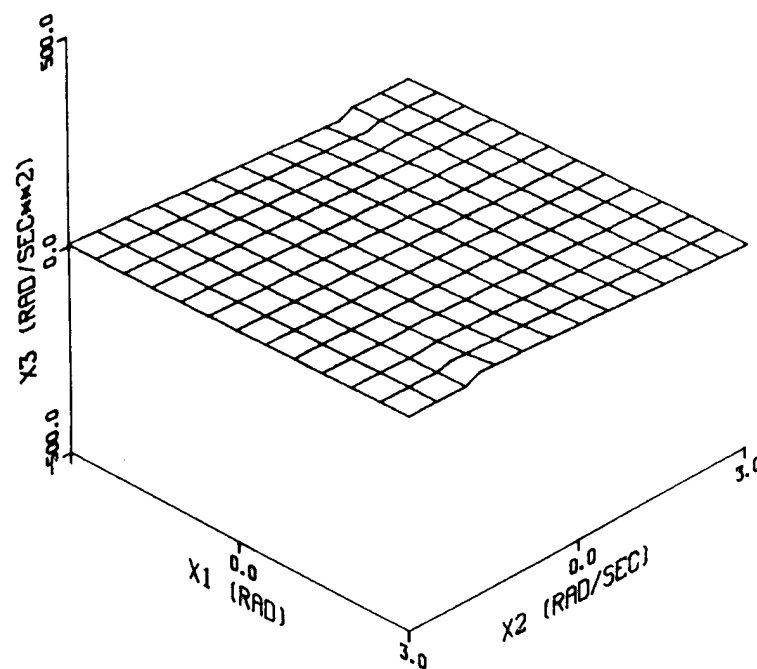


Figure 10. Switching Surface Viewed From Above, $\lambda_1 = -1$, $\lambda_2 = -2$

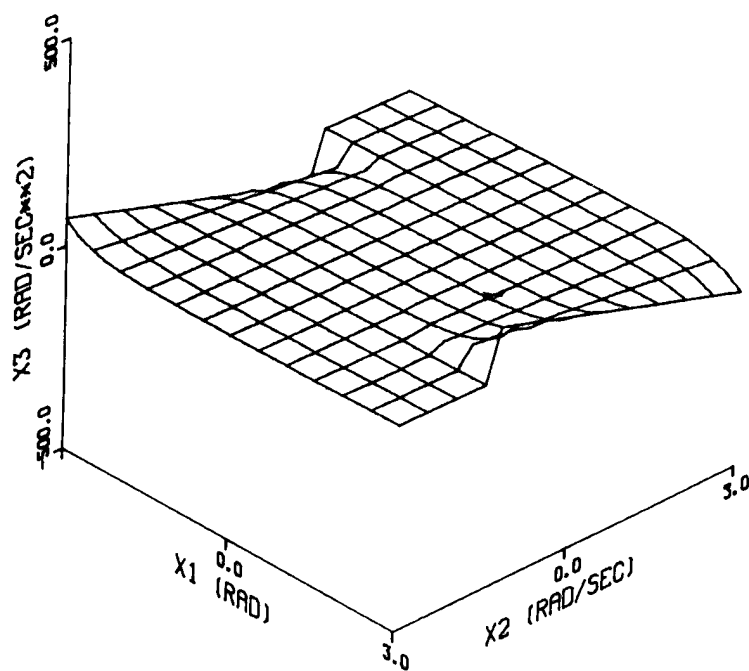


Figure 11. Switching Surface Viewed From Above, $\lambda_1 = -1$, $\lambda_2 = -3$

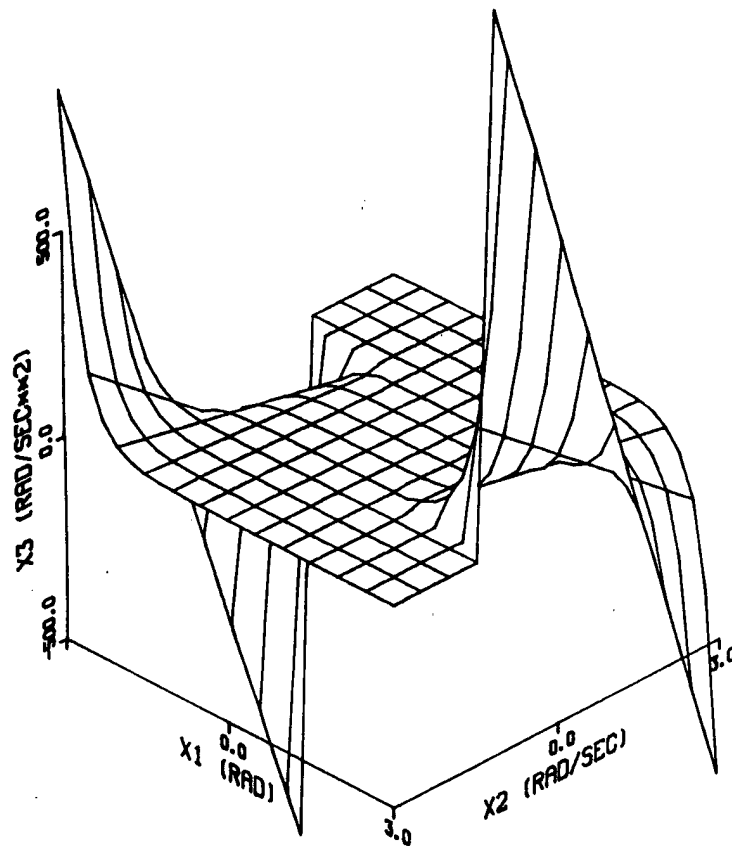


Figure 12. Switching Surface Viewed From Above, $\lambda_1 = -1$, $\lambda_2 = -4$

CONCLUSION

The analytical expression for the switching surface of a type one, third order system has been derived. It is expected that its implementation will not be difficult in a high speed dedicated digital computer. The inherent delay in detecting the switching boundaries, coupled with the random noise of the system will require a linear mode of operation for final settling.

ACKNOWLEDGEMENTS

The invaluable assistance of Dr. E. S. McVey and Dr. G. Cook of the University of Virginia in formulating and modeling the problem is greatly appreciated. Thanks also goes to Mr. Paul Leimer of the Surface Warfare Technology Branch of the Naval Surface Weapons Center, Dahlgren, Virginia, for his invaluable assistance in programming and plotting the three-dimensional graphics of the switching surfaces.

DEFINITION OF SYMBOLS

J	Inertia
$[J]$	Jordan form of matrix
J	Performance index
τ	Servo valve time constant
Δ	Sign of control
u	Control, -1 or +1
\vec{r}	Reference input vector
$\vec{\theta}$	Controlled output vector
$[P]$	Modal matrix
λ	Eigenvalue of $[A]$
α	Multiplier of second eigenvalue $\lambda_2 = \lambda_1 \alpha$
\vec{Y}	Output vector
\mathcal{H}	Hamiltonian
\vec{p}	Costate vector
\vec{X}	State vector
$(\cdot)^*$	Optimal value
$\{V_2\}$	State from which the origin can be reached with two controls, i.e., $u^* = (+1, -1)$ or $(-1, +1)$
(\cdot, \cdot, \cdot)	A sequence of controls
Σ	Switch surface
K_1	Servo amplifier gain (amps/volt)
K_2	Servo valve flow gain (in ³ /sec/amp)
K_3	Differential flow to pressure conversion (psi/gpm)
K_4	Pressure to torque conversion (in#/psi)
K_5	Conversion factor (gpm/RPS)

REFERENCES

1. W. L. Brogan, *Modern Control Theory* (New York: Quantum Publishers, 1974).
2. M. Athanassiades and O. J. M. Smith, "Theory and Design of High-Order Bang-Bang Control Systems," *IRE Trans. On Automatic Control*, May 1961, AC-6, 125-134.
3. D. E. Kirk, *Optimal Control Theory* (Englewood Cliffs, New Jersey: Prentice-Hall, 1970).
4. M. Athans and P. Falb, *Optimal Control* (New York: McGraw Hill, 1966).

OPTIMAL UTILIZATION OF GRAVITY IN A HOMING MISSILE PROBLEM

Dr. William C. Kelly
Guidance and Control Directorate
US Army Missile Laboratory
US Army Missile Command

ABSTRACT

The general theory of disturbance-utilizing control, introduced by Johnson, is applied in this paper to the problem of accommodating gravity in a homing missile guidance problem. While the conventional approach to handling disturbance effects is to attempt to eliminate them, the approach taken here is to formulate the optimal controller that accounts for the waveform properties of the disturbance. Numerical results are given to show the comparison between the performance of the disturbance-utilizing controller and a conventional linear-quadratic controller with respect to gravity effects.

INTRODUCTION

Traditionally, uncontrolled inputs to control systems have been considered to be detrimental to achieving desired control objectives, and design approaches have resulted in elimination schemes such as integral control, feedforward control and the notch filter. However, there are practical problems in which it is wise to consider a way to account for the presence of the disturbance, rather than attempting to remove it. For example, the presence of gravity forces on a homing missile may actually help in driving the missile toward the target. Uncontrolled inputs to control systems may be classified as either noise-type disturbances or disturbances with "waveform structure." Thermal noise in a radar receiver is an example of a noise-type disturbance, while gravity, wind gusts and electronic instrument drift are examples of waveform disturbances. While noise-type disturbances are characterized by their statistical properties (e.g., variance and mean), waveform disturbances can be modeled by giving a differential equation that the disturbances are known to satisfy [1]. Thus, it is useful to view a waveform-type disturbance as having been generated by a dynamic process (not necessarily linear). The state model of the disturbance process can be combined with the typical state model of the plant dynamics [2] to obtain the general expressions:

$$\dot{x} = F(x, t, u(t), W(z, x, t)) \quad (1)$$

$$\dot{z} = D(z, x, t) + \sigma(t) \quad (2)$$

Johnson has shown [2] that the optimal control u^0 , which minimizes

$$J[u; x_0, t_0, T] = G(x(T), T) + \int_{t_0}^T (L(x(t), t, u(t)) dt \quad (3)$$

subject to the combined system Equations (1) and (2), and assuming $\sigma(t) = 0$, can be expressed as

$$u^0 = u^0(x, z, t) \quad (4)$$

That is, the optimal control at time t is a function of the current state $x(t)$ of the plant and the current state $z(t)$ of the disturbance. This result may be contrasted with that obtained by the conventional optimization approach, which gives the optimal control as a function of the plant state $x(t)$ alone. The control Equation (4), which accounts for the presence of disturbances, was derived under the assumption that the impulse sequence $\sigma(t)$ was identically zero. In fact, $\sigma(t)$ is sparsely populated and unknown a priori; and, therefore, its effect could be viewed as a sequence of unknown initial conditions $z(t_0)$ imposed on the model Equation (2). A corollary to this viewpoint (stated as a conjecture in [2]) is that the control $u^0(x, z, t)$ given by Equation (4) is "optimal" also for the case

where the sparsely populated impulsive sequence $\sigma(t)$ is present.

Realization of the control law Equation (4) requires that real-time, current values of the states (x, z) be made available to the controller, through either direct measurements or use of an observer. A discussion of the implementation of plant/disturbance state observers may be found in [1], [3], and in [5].

OPTIMAL CONTROL OF THE LINEAR-QUADRATIC REGULATOR WITH DISTURBANCES

A special case of the optimal control theory discussed in the previous section is the linear-quadratic regulator with disturbances present. Johnson has shown [1], [2], [3], and [4] how the disturbance accommodating theory applies to the set-point regulator and servo-tracking control problems in which the plant dynamics are modeled as:

$$\dot{x} = A(t)x + B(t)u(t) + F(t)w(t) \quad (5)$$

$$y = C(t)x \quad (6)$$

where x , u and w are vectors of dimension n , r and p , respectively, $n \geq r \geq p$. The disturbance process is modeled by the linear system:

$$w(t) = H(t)z + L(t)x \quad (7)$$

$$\dot{z} = D(t)z + M(t)x + \sigma(t) \quad (8)$$

where z is a p -dimensional vector.

The application of modern control theory techniques permits the consideration of three modes of disturbance accommodation [1, 2, 3]:

- (a) exact cancellation of the effect of the disturbance on the control system,
- (b) the "best" approximation to cancellation of the effect of the disturbance (when exact cancellation is not achievable), and
- (c) optimal utilization of the disturbance in accomplishing the control objectives.

This paper considers the third mode, disturbance-utilizing control (DUC) described in [1, 2, 3, 4] and discusses an aerospace application of DUC first addressed in [5]. Reference [6] discussed a homing missile guidance problem with DUC, in which gravity, winds and target maneuvers are considered. The present work considers the more specialized case in which gravity is the most significant disturbance present. The question being considered is: "Is it worthwhile to employ disturbance-utilizing control for a homing missile when the most significant error source is gravity?". The approach here is to go a step beyond the usual procedure of "gravity compensation", which attempts to cancel gravity effects, and show how gravity forces can be optimally utilized to assist in achieving practical control objectives such as minimizing miss distance.

THE DISTURBANCE-UTILIZING OPTIMAL CONTROL PROBLEM

A special case of disturbance-accommodating optimal control theory is the linear-quadratic regulator with disturbances present. Johnson has shown in [1], [2], and [3] how the disturbance accommodating theory applies to the set-point regulator and servo-tracking control problems in which the plant dynamics are modeled as:

$$\dot{x} = A(t)x + B(t)u(t) + F(t)w(t) \quad (9)$$

$$y = C(t)x \quad (10)$$

where x , u and w are vectors of dimension n , r and p , respectively, and $n \geq r \geq p$. The disturbance process is modeled by the linear system:

$$w(t) = H(t)z + L(t)x \quad (11)$$

$$\dot{z} = D(t)z + M(t)x + \sigma(t) \quad (12)$$

where z is a p -dimensional vector.

The key to obtaining maximum utilization of disturbances is to choose a performance index J so that, when J is minimized with respect to the control $u(t)$, the primary control objective is accomplished and maximum use of the disturbance $w(t)$ is achieved. For example, if the primary control objective is to regulate the plant state $x(t)$ to zero, a secondary objective may be to use as little control energy as possible. One may be able to achieve these objectives by choosing a quadratic-type performance index as

$$J = \frac{1}{2} x^T(T) S x(T) + \frac{1}{2} \int_{t_0}^T [x^T(t) Q x(t) + u^T(t) R u(t)] dt \quad (13)$$

where S and Q are given symmetric non-negative definite matrices. $S + Q$ is positive definite, R is a positive-definite matrix, and the terminal time T is specified. The presence of the positive definite matrix R encourages the effective utilization of any "free" energy available in the disturbance.

It is shown in Reference [1], [2], and [3] that the zero set-point disturbance-utilizing problem can be formulated as a linear-quadratic regulator problem by using the augmented vector

$$\tilde{x} = \begin{pmatrix} x \\ z \end{pmatrix} \quad (14)$$

which is a composite of the state vectors of the plant and the disturbance process. The composite system equation may be written by using \tilde{x} and the plant and disturbance dynamic Equations (9), (11) and (12), with $L(t) = 0$ and $M(t) = 0$, as follows:

$$\dot{\tilde{x}} = \begin{pmatrix} \dot{x} \\ \dot{z} \end{pmatrix} = \begin{bmatrix} A & FH \\ 0 & D \end{bmatrix} \tilde{x} + \begin{bmatrix} B \\ 0 \end{bmatrix} u + \begin{pmatrix} 0 \\ \sigma \end{pmatrix} \quad (15)$$

The performance index Equation (13) can be written in the equivalent form

$$J = \frac{1}{2} \tilde{x}^T(T) \bar{S} \tilde{x}(T) + \frac{1}{2} \int_{t_0}^T [\tilde{x}^T(t) \bar{Q} \tilde{x}(t) + u^T(t) R u(t)] dt \quad (16)$$

where $\bar{S} = C^T S C$, $\bar{C} = [-C \mid 0]$ and $\bar{Q} = C^T Q C$.

The sparse sequence of impulses $\sigma(t)$ can be disregarded (for reasons discussed in [1]) and the control which minimizes Equation (16) subject to Equation (15) can be found using standard linear-quadratic methods, resulting in the control

$$u^0 = -R^{-1} B^T [K_X x + K_{XZ} z] \quad (17)$$

which is a function of the states of the plant and of the disturbance process. It has been shown [1], [4], [5] that the time varying gain matrices $K_X(t)$ and $K_{XZ}(t)$ are obtained by solving the matrix differential equations

$$\dot{K}_X = (-A + B R^{-1} B^T K_X)^T K_X - K_X A - C^T Q C; K_X(t) = C^T S C \quad (18)$$

$$\dot{K}_{XZ} = (-A + B R^{-1} B^T K_X)^T K_{XZ} - K_{XZ} F H - K_{XZ} D; K_{XZ}(t) = 0 \quad (19)$$

Although not required for implementation of the control law Equation (17), the equation for $K_Z(t)$

$$\dot{K}_z = - (K_z D + D^T K_z) + K_{xz}^T B R^{-1} B^T K_{xz} - \left[(F H)^T K_{xz} + K_{xz}^T F H \right] ; \quad (20)$$

$$K_z(T) = 0$$

may also be solved for analysis purposes. For the simulation studies of this problem, the matrix functions of time $K_x(t)$, $K_{xz}(t)$ and $K_z(t)$ are obtained by forward-time solution of Equations (18) - (20) on a digital computer as t progresses from $t_0 (=0)$ to T .

The minimum value J^0 of the performance index J obtained under optimal control $u = u^0$ is the solution $V(x, z, t)$ of the Hamilton-Jacobi-Bellman equation corresponding to the composite system (15), (16). This solution may be written [4] as

$$V(x, z, t) = \frac{1}{2} (x^T K_x x) + (x^T K_{xz}) z + \frac{1}{2} z^T K_z z \quad (21)$$

The last term in Equation (21) is due to disturbances alone, and is equal to, or greater than, zero. Since it does nothing but increase the minimum value of J , Johnson has defined it as the "burden" B [4]:

$$B \triangleq \frac{1}{2} z^T K_z z \quad (22)$$

The term $(x^T K_{xz}) z$ in Equation (21) is produced by interactions between the plant state x and the disturbance state z . This term involves bilinear forms which may be negative, zero or positive at any time t . When this term becomes negative, it acts to further reduce the minimum value $J^0(x, z, t)$ of J in Equation (16); that is, negative values of this term actually provide assistance toward the objective of obtaining a minimum value of J . Therefore, Johnson has called the negative of this term [4] the "assistance":

$$A \triangleq -(x^T K_{xz}) z ; \quad (23)$$

$$x(t_0) = x; \quad z(t_0) = z$$

The sign of the assistance in Equation (23) may itself be negative, in which case it has the effect of an additional burden.

The first term in Equation (21) does not involve the disturbance state z at all, and is, in fact, the minimum value of J that would be obtained when no disturbance is present. Therefore, any constructive action by the disturbance will be reflected in the difference between the V expression when the disturbance is present and that same V when the disturbance is absent. Johnson has defined this latter difference as "utility" [4]:

$$U \triangleq V \Big|_{w(t) \equiv 0} - V \Big|_{w(t) \neq 0} \quad (24)$$

Thus, utility can be written as

$$U = -(x^T K_{xz}) z - \frac{1}{2} z^T K_z z \quad (25)$$

or, symbolically,

$$U = A - B \quad (26)$$

Positive utility results when the assistance A is greater than the burden B .

APPLICATION TO HOMING MISSILE GUIDANCE

MATHEMATICAL MODEL

In this section we consider a homing intercept problem in which a missile is to be controlled during the final phase of its flight so that its position coincides with

that of a target at a specified terminal time, even in the face of disturbances which may, or may not, be detrimental to the control objective. The planar geometry for this problem is shown in Figure 1, where the origin is located at the fixed ground target position and the position of the missile is defined by the coordinates (x_M, y_M) , where x_M is horizontal and y_M is vertical.

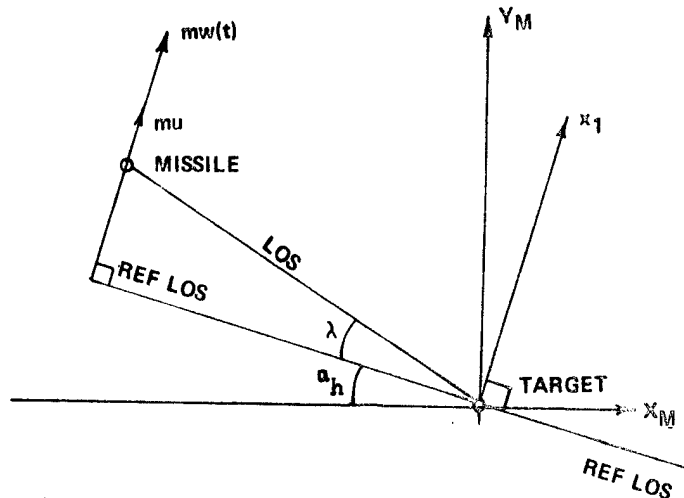


Figure 1. Coordinate system for small line-of-sight angle homing intercept model.

It is convenient to consider a reference line-of-sight (REF LOS) passing through the target and oriented at a known angle α_h relative to the horizontal line x_M . The REF LOS is established a priori, and may correspond to a desired orientation of the line-of-sight. A coordinate x_1 is established normal to the REF LOS (Figure 1) and it is assumed that the missile begins the homing phase of the problem with a certain displacement $x_1(0)$ and velocity $x_2(0)$ (where $x_2 = \dot{x}_1$) normal to the REF LOS. It is assumed that a previous "midcourse" guidance phase has delivered the missile to the beginning of the homing phase at $t = t_0$; thus, non-zero values of $x_1(0)$ and $x_2(0)$ characterize the extent to which the midcourse phase has failed to enable the missile to start the homing phase under ideal conditions. The initial range to the target and the closing velocity are assumed given. The problem at hand uses the "small LOS" assumptions as in [5] and [6] and considers that the disturbance forces of primary interest are those acting normal to REF LOS. Errors in estimating time-to-go to intercept are not considered here.

The "small LOS angle" model is used in the present work in a unique way - disturbances normal to the REF LOS are utilized in an optimal manner. Former approaches either ignored these disturbances, or modeled them as gaussian noise and used stochastic control approaches to cope with them. The application of the "small LOS angle" model to the missile homing problem where disturbances are present results in a particularly straight-forward implementation of the linear-quadratic disturbance-utilizing control theory.

The equations describing the motion of the missile normal to the REF LOS are

$$\dot{x}_1 = x_2 \quad (27)$$

$$\dot{x}_2 = u + w(t) \quad (28)$$

$$y = [x_1, x_2]^T \quad (29)$$

where the output vector y has x_1 and x_2 as its elements. These equations may be written in the form

$$\dot{x} = Ax + Bu + Fw \quad (30)$$

$$y = Cx \quad (31)$$

where

$$A = \begin{bmatrix} 0 & 1 \\ 0 & 0 \end{bmatrix} \quad (32)$$

$$F = \begin{pmatrix} 0 \\ 1 \end{pmatrix} \quad (33)$$

$$B = \begin{pmatrix} 0 \\ 1 \end{pmatrix} \quad (34)$$

$$C = \begin{bmatrix} 1 & 0 \\ 0 & 1 \end{bmatrix} \quad (35)$$

It is assumed in the example to follow that the disturbance $w(t)$ is described by

$$w(t) = C_1 \quad (36)$$

where C_1 is an unknown constant. The disturbance process is written in state-variable form as

$$z_1 = w \quad (37)$$

$$\dot{z}_1 = z_2 + \sigma_1(t) \quad (38)$$

$$\dot{z}_2 = 0 + \sigma_2(t) \quad (39)$$

or in the form

$$\dot{z} = Dz + \sigma(t) \quad (40)$$

$$w = Hz \quad (41)$$

where

$$D = \begin{bmatrix} 0 & 1 \\ 0 & 0 \end{bmatrix} \quad (42)$$

$$H = \begin{bmatrix} 1 & 0 \end{bmatrix} \quad (43)$$

and $\sigma(t) = [\sigma_1, \sigma_2]$ a sparse vector-impulse sequence occurring at unknown instants. Note that a simpler model $\dot{z} = \sigma(t)$, where z is a scalar, would also suffice for modeling the piecewise constant disturbance dynamics. The second-order model used here will also model the dynamics of disturbances that include piecewise continuous ramp functions, and has been used for that in other problems [5].

The disturbance considered in this problem is gravity. The gravity component acting normal to the REF LOS is

$$-32.2 \cos \alpha_h .$$

CONTROL OBJECTIVE

The primary control objective for the class of problems considered here is to drive the displacement of the missile (normal to the REF LOS) to zero at a specified terminal time T ; that is, to regulate the state x_1 to zero at $t = T$. The secondary objective is to achieve the primary objective while effectively utilizing the "free" energy of the disturbance $w(t)$.

The control objectives are to be achieved by minimizing the quadratic performance index

$$J = \frac{1}{2} e^T(T) S e(T) + \frac{1}{2} \int_{t_0}^T [e^T(t) Q e(t) + u^2(t)] dt \quad (44)$$

where $e = x_{sp} - x$, subject to the plant Equations (30) and (31) and the disturbance process Equations (40) and (41).

DISCUSSION OF RESULTS

The homing intercept problem is solved by applying the theory already described which leads to the composite state vector (14), the composite system (15) and the performance index (16). The optimal control is computed by (17) after computing the time-varying gains $K_x(t)$ and $K_{xz}(t)$ as the solutions of Equations (18) and (19). The time-varying gain $K_z(t)$ is also computed (by solving Equation (20)) for use in computing the disturbance utility U for analysis purposes. The problem is solved on a CDC-6600 computer, using backward-time integration to find the initial conditions for K_x , K_{xz} and K_z .

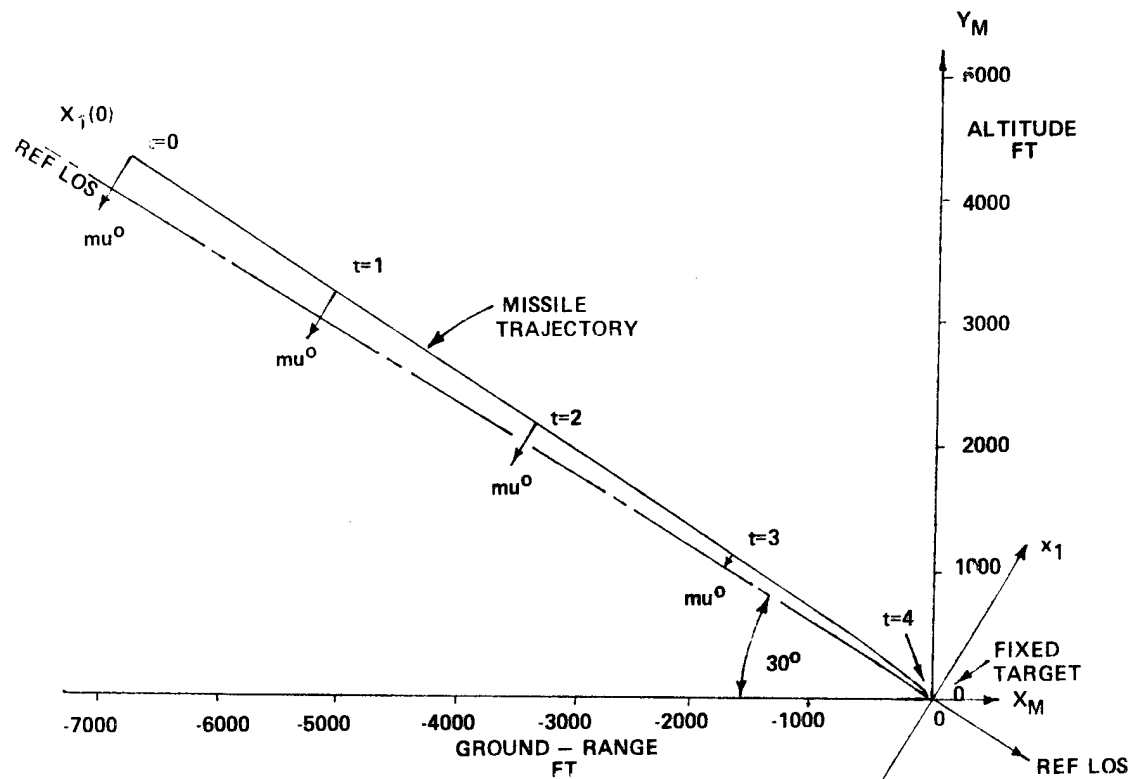
The plant state x for the optimal control Equation (17) is assumed to be available from position and velocity data (as from high-quality radar tracking measurements, for example). In general problems employing DUC, an estimator [1,3,5] will be employed to provide real-time estimates of states x and z . In the special case considered here, estimation of z can be avoided if missile attitude angle information is available for determining the lateral gravity component.

NUMERICAL EXAMPLES

Case 1 - Planar Homing Intercept. Disturbance Input: Gravity (helpful).

In this case we consider the performance of a missile with disturbance-utilizing control in a planar homing intercept having the missile-target geometry as shown in Figure 2. The parameter values are:

- | | |
|---|---------------|
| a) Fixed target at 0. ft down-range, altitude. | 0. ft |
| b) Initial missile ground-range | -6778. ft |
| c) Initial missile altitude | 4260. ft |
| d) Initial missile offset normal to REF LOS, $x_1(0)$ | 300. ft |
| e) Initial missile range along REF LOS | -8000. ft |
| f) Initial missile velocity normal to REF LOS, $x_2(0)$ | 0. ft/sec |
| g) Missile velocity along REF LOS (constant, toward target) | -2000. ft/sec |
| h) Angle of REF LOS from horizontal | 30. deg |
| i) Specified terminal time T | 4.0 sec |
| j) Disturbance: gravity, helpful | |
| k) Control weighting parameter | 1.0 |
| l) $S = \begin{bmatrix} 10 & 0 \\ 0 & 0 \end{bmatrix}$ | |
| m) $Q = \begin{bmatrix} 0 & 0 \\ 0 & 0 \end{bmatrix}$ | |



NOTE: μ^0 scale is 1.cm = 1000 lb.

Figure 2. Missile trajectory for Case 1, showing control force μ^0 ; disturbance-utilizing control. Disturbance present: gravity.

This homing-intercept problem was solved and the resulting optimally controlled missile trajectory is shown in Figure 2, with the associated disturbance-utilizing control force μ^0 displayed at 1 second intervals. The optimal control u^0 is computed as a function of the time-varying gain matrices K_X and K_{XZ} . The missile is able to apply the control force in a direction approximately normal to the missile trajectory (assuming small angle of attack) rather than normal to the REF LOS as desired. The missile trajectory angle relative to the horizontal goes from 30 degrees at $t = 0$ to 34 degrees at $t = 4.0$. Therefore, the maximum error in the angle of application of the control force is 4 degrees, which results in the application of 99.8% of the control force μ^0 normal to the REF LOS. The time-history of the control force requirement is shown in Figure 3, which is seen to be nearly a linear function of time.

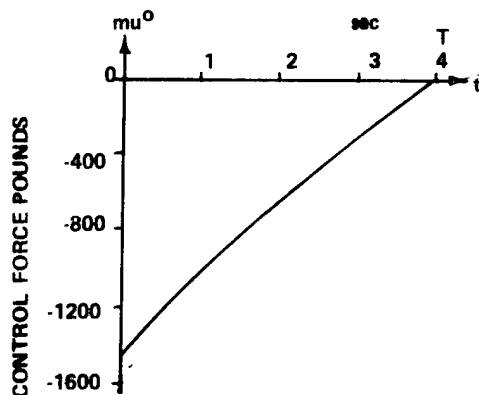


Figure 3. Disturbance-utilizing control force for Case 1.

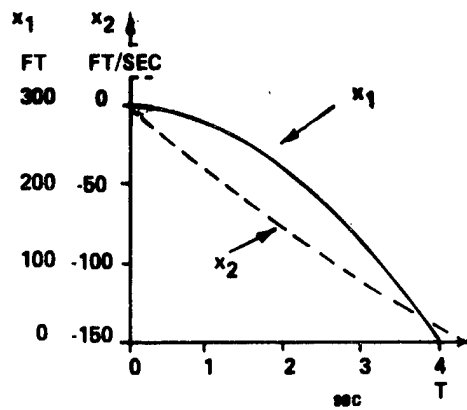


Figure 4. State histories: x_1 and x_2 for Case 1 with disturbance-utilizing control.

The time-histories of the states x_1 and x_2 are shown in Figure 4. Note that, since no penalty has been placed on $x_2(T)$, it has a relatively large value of -140 ft/sec, corresponding to the missile trajectory angle which is about 4 degrees greater than the 30 degree angle of the REF LOS. The disturbance for this case (Figure 5) is the projection of gravity normal to the REF LOS. The utility (Figure 6) is non-negative for the whole flight, as the result of the helpful action of the disturbance in this case.

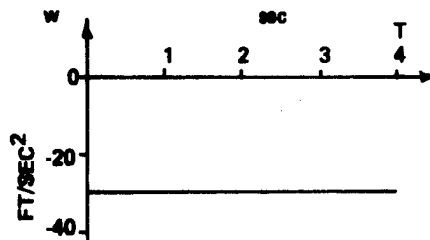


Figure 5. Disturbance acceleration w , for Case 1.

The performance of the missile with disturbance-utilizing control for this case is compared with that of the conventional linear-quadratic controller in Table 1, showing superior performance for the disturbance-utilizing controller in terms of J , E_T , EU , EAU , $x_1(T)$ and E_{MD} .

$$E_T = \frac{J_{LQ} - J_{DUC}}{J_{LQ}} \times 100\% \quad (45)$$

$$EU = \frac{1}{2} \int_{t_0}^T u^2(t) dt \quad (46)$$

$$EAU = \frac{1}{2} \int_{t_0}^T |u(t)| dt \quad (47)$$

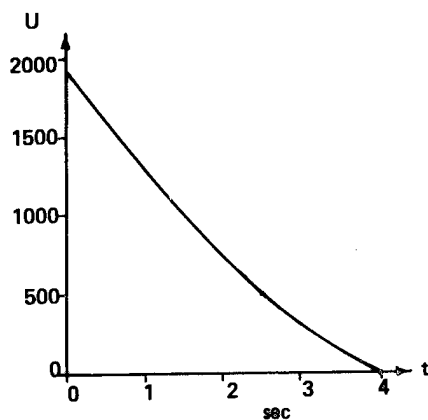


Figure 6. Disturbance utility for Case 1.

TABLE 1. PERFORMANCE OF DISTURBANCE-UTILIZING CONTROLLER COMPARED WITH CONVENTIONAL LINEAR-QUADRATIC CONTROLLER FOR CASE 1.

	PERFORM- ANCE INDEX J	E_T %	CONTROL ENERGY EU	CONTROL FUEL EAU	MISS- DISTANCE NORMAL TO REF LOS $x_1(T)$ (FT)	E_{MD} %
DUC	138.0	94.9	137.0	29.0	0.4	96.6
LQ	2722.0	X	2047.0	113.0	-11.6	X

NOTE: SEE PAGES 202 AND 205 FOR DEFINITIONS OF J, E_T , EU, EAU AND E_{MD}

$$E_{MD} = \frac{\left| \frac{x_1(T)}{x_1(T)} \right|_{LQ} - \left| \frac{x_1(T)}{x_1(T)} \right|_{DUC}}{\left| \frac{x_1(T)}{x_1(T)} \right|_{LQ}} \times 100\% \quad (48)$$

All effectiveness measures show a sizeable margin at $T = 4.0$. Values of total effectiveness E_T versus terminal time values are plotted in Figure 7, which indicates a continuing increase in E_T as T increases.

Case 2 - Planar Homing Intercept. Disturbance Input: Gravity (non-helpful).

Case 2, considered in this section, examines the performance of a missile with disturbance-utilizing control in a planar homing intercept configuration where the missile-target geometry (Figure 8) is such that gravity is a non-helpful disturbance, and the missile's offset from the REF LOS at $t = 0$, $x_1(0)$, is twice what it was in Case 1. The parameters for Case 2 are as follows:

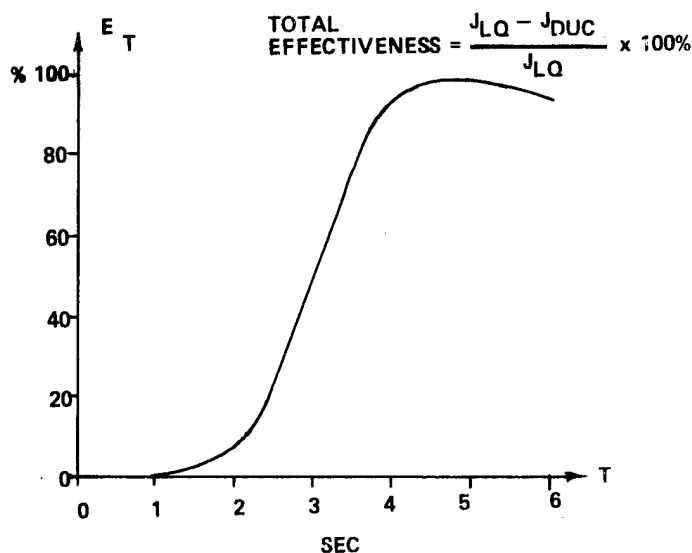


Figure 7. Total effectiveness E_T versus specified terminal time values T for Case 1.

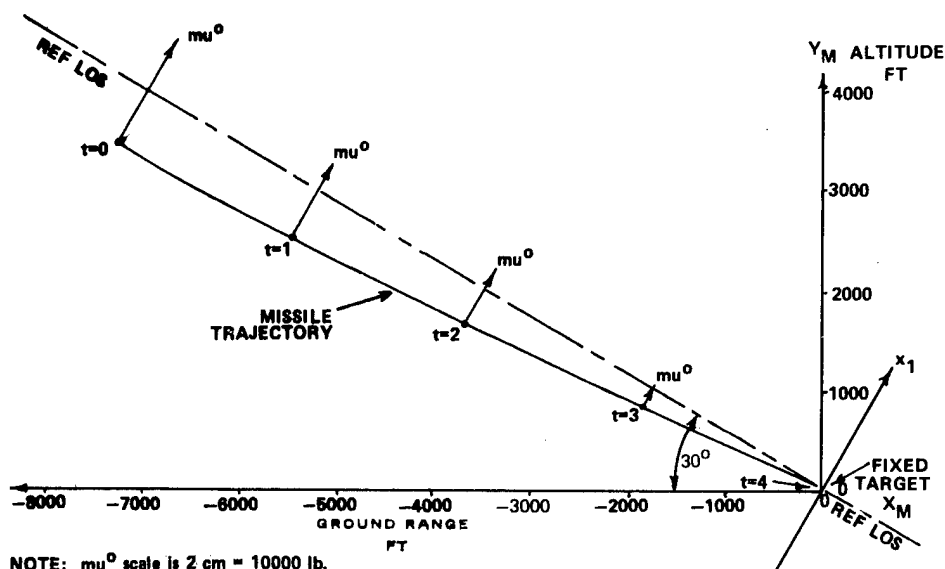


Figure 8. Missile trajectory for Case 2, showing control force μ^0 ; disturbance-utilizing control. Disturbance present: gravity.

- | | |
|---|-----------|
| a) Fixed target at 0. ft down-range, altitude. | 0. ft |
| b) Initial missile ground-range | -7228. ft |
| c) Initial missile altitude | 3480. ft |
| d) Initial missile offset normal to REF LOS, $x_1(0)$ | -600. ft |
| e) Initial missile range along REF LOS | -8000. ft |
| f) Initial missile velocity normal to REF LOS, $x_2(0)$ | 0. ft/sec |

- g) Missile velocity along REF LOS -2000. ft/sec
(constant, toward target)
- h) Angle of REF LOS from horizontal 30. deg
- i) Specified terminal time T 4.0 sec
- j) Disturbance: gravity, nonhelpful
- k) Control weighting parameter r 1.0

l) $S = \begin{bmatrix} 10 & 0 \\ 0 & 0 \end{bmatrix}$

m) $Q = \begin{bmatrix} 0 & 0 \\ 0 & 0 \end{bmatrix}$

The computer results were obtained for Case 2, and the final optimally controlled missile trajectory is shown in Figure 8, with the associated disturbance-utilizing control force μ^0 displayed at 1 sec intervals. This case has a 600 ft initial off-set from the REF LOS (twice that of Case 1) and the geometry of this problem makes the gravity disturbance non-helpful, in contrast with Case 1. As a result, the control force magnitudes for this sub-case are considerably larger than for Case 1 (Figure 9). The missile trajectory angle for Case 2 goes from 30 degrees at $t = 0$ to about 24 degrees at $t \rightarrow T$; the maximum error in the angle of application of the control force is -6 degrees, which results in the application of 99.5% of the control force μ^0 normal to the REF LOS. As in Case 1, the control force for this case (Figure 9) is almost a linear function of time.

The time-histories of the states x_1 and x_2 are plotted in Figure 10. As in Case 1, no terminal penalty is placed on x_2 , and a relatively large value of $x_2(T)$ results. The disturbance in this case (Figure 11), which is the projection of the gravity acceleration normal to the REF LOS, is non-helpful, since it acts to hinder the missile from the intercept objective. As a result, the disturbance utility (Figure 12) is either negative or zero for the whole flight.

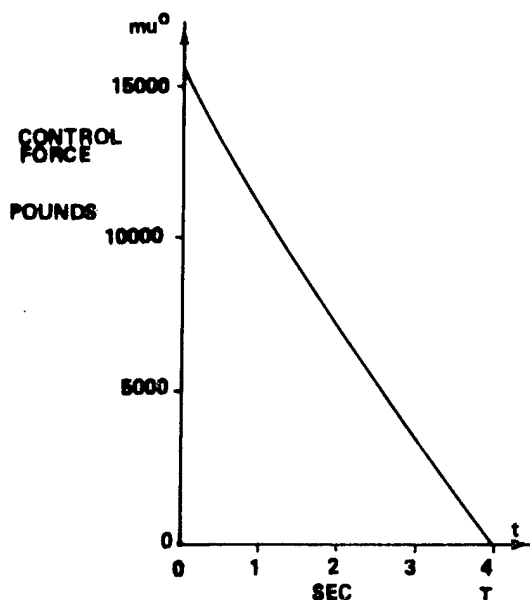


Figure 9. Control force for Case 2; disturbance-utilizing control.

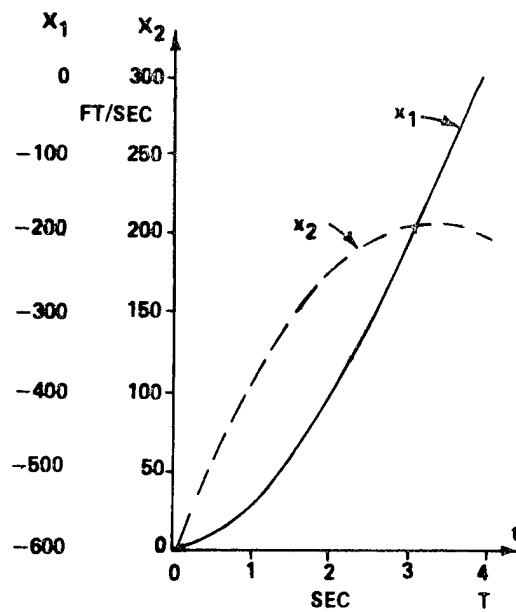


Figure 10. State histories: x_1 and x_2 for Case 2; disturbance-utilizing control.

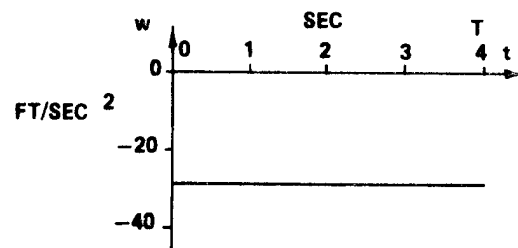


Figure 11. Disturbance acceleration w for Case 2.

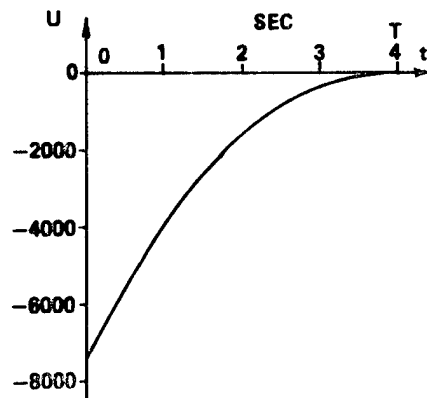

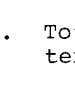


Figure 12. Disturbance utility for Case 2.

The disturbance-utilizing controller for Case 2 performs better than the conventional linear-quadratic controller (see Table 2) even in the face of the totally detrimental disturbance, which indicates that, even though positive utility is never available, the disturbance-utilizing control law still does better in managing the states of the plant relative to the disturbance states.

TABLE 2. PERFORMANCE OF DISTURBANCE-UTILIZING CONTROLLER COMPARED WITH CONVENTIONAL LINEAR-QUADRATIC CONTROLLER FOR CASE 2.

	PERFORMANCE INDEX J	E_T %	CONTROL ENERGY EU	CONTROL FUEL EAU	MISS-DISTANCE NORMAL TO REF LOS $x_1(T)$ (FT)	E_{MD} %
DUC	0.158 $\times 10^5$	14.2	0.167 $\times 10^5$	306.0	-3.8	75.8
LQ	0.183 $\times 10^5$		0.171 $\times 10^5$	358.0	-15.7	

The effectiveness (Figure 13) for Case 2 shows that the disturbance-accommodating controller continues to achieve a lower J as the specified terminal time is increased.

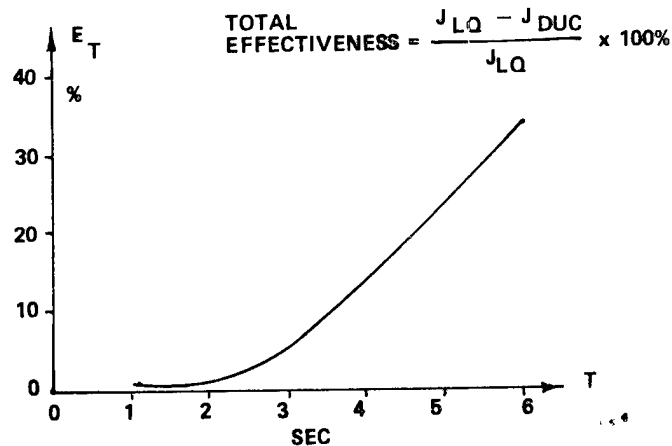


Figure 13. Total effectiveness E_T versus specified terminal time T for Case 2.

CONCLUSIONS

The theory of disturbance-utilizing control, developed by Johnson [1-4], is applied in this paper to the optimal utilization of gravity in a homing missile problem. Whereas an earlier paper considered disturbance-utilizing control in the context of gravity, winds and target maneuvers, this paper considers the homing missile problem in which the most significant disturbance present is gravity alone. A disturbance-utilizing controller is formulated as a linear-quadratic regulator by using an augmented state vector which is the composite of the plant state vector and the state vector of the dynamic system of the disturbance process. Numerical examples are given for the case where gravity is "helpful" and for the case where it is not. In both cases, the disturbance-utilizing controller is seen to provide better guidance performance than a conventional linear-quadratic controller that does not account for waveform properties of the disturbance.

REFERENCES

1. Johnson, C.D., "Theory of Disturbance-Accommodating Control", Control and Dynamic Systems, Advances in Theory and Applications, Vol. 12, Academic Press, New York, 1976.
2. Johnson, C.D., "Accommodation of Disturbances in Optimal Control Problems", International Journal of Control, Vol. 15, No. 2, 1972, pp. 209-231.
3. Johnson, C.D., "Accommodation of External Disturbances in Linear Regulator and Servomechanism Problems", IEEE Transactions on Automatic Control, Vol. AC-16, No. 6, December 1971, pp. 635-644.
4. Johnson, C.D., "Utility of Disturbances in Disturbance-Accommodating Control Problems", Proceedings 15th Annual Meeting of the Society for Engineering Science; Gainesville, Florida, December, 1978.
5. Kelly, W.C., "Theory of Disturbance-Utilizing Control with Application to Missile Intercept Problems", Technical Report RG-80-11, US Army Missile Command, Redstone Arsenal, Alabama, 12 December 1979.
6. Kelly, W.C., "Homing Missile Guidance with Disturbance-Utilizing Control", Proceedings of the 12th Southeastern Symposium on System Theory, Virginia Beach, Virginia, May 1980.

Next page is blank.

EVALUATION OF GUNNER STATION CONFIGURATIONS
FOR FIRING-ON-THE-MOVE

Richard A. Lee
Tank-Automotive System Laboratory
U.S. Army Tank-Automotive
Research and Development Command
Warren, Michigan 48090

William D. West
U.S. Army Armor and Engineer Board
Fort Knox, Kentucky 40121

Monica Glumm
U.S. Army Human Engineering Laboratory
Aberdeen Proving Grounds, Maryland 21105

ABSTRACT

This study evaluated the effect on gunner performance for firing on-the-move. Four different gunner station configurations were evaluated, i.e. isometric tracker, yoke handles, monocular eyepiece with brow pad, and TV type display. Five different ride levels and four different target motions were used. Gunner lay and rate errors at firing and tracking accuracy were measured for use in evaluating gunner performance. Ride level was determined from the absorbed power at the base of the gunner's seat.

OBJECTIVE

The objective of this study was to evaluate the effect of ride on gunner performance for firing-on-the-move. Four different gunner station configurations were evaluated, consisting of isometric and yoke tracking controllers in combination with monocular and video gunner displays.

INTRODUCTION

The study originated because of the difficulty in attempting to evaluate several different gunner station configurations and the difficulty in attempting to evaluate the effect of the ride on gunner performance in a fielded vehicle. It became apparent that it would be too time consuming and costly to evaluate even simple hardware changes in the gunner's station configuration. The cost was not limited to making the hardware changes in the vehicle, but included costs to develop data to evaluate the changes. When one considers the possible different combinations of handles, viewing devices, and seating arrangements, and the effects of different types of rides on performance, the time and cost associated with an evaluation of this type is prohibitive. There is also the possibility that test conditions such as temperature and wind as well as the actual terrain the vehicle traverses may change between evaluations of the different combinations. This, coupled with the possibility that changes in gunner performance could be meshed with errors caused by the rest of the system, made field evaluation virtually impossible.

Another approach had to be devised. The approach had to distinguish between small changes in performance in a timely, cost-effective manner. It was decided to use the ride simulator at TARADCOM to simulate vehicle ride. A Chrysler fire control combat simulator would be modified and mounted on the seat. This would allow the gunner to ride the vehicle and fire the gun at simulated targets. The computer would automatically measure and store gunner tracking error as well as error at

trigger pull. The error at trigger pull would be the horizontal and vertical lay and rate errors. These errors could then be analyzed to determine gunner performance. Recoil was also supplied when the gunner pulled the trigger.

The ride simulator has some shortcomings. It has four degrees of freedom but only three were used in this study--vertical, pitch, and roll. In reality a vehicle has some lateral and fore and aft accelerations. Some of these accelerations were accounted for by pitch and roll motions in the seat, but these were limited to short-duration accelerations.

All errors and analysis presented in this report are gunner errors only. All other errors that normally occur in a vehicle are zero. This is extremely important. When one encounters terms in this report such as hits, hit probability, errors, etc. these are considering gunner errors only. They are the hits and hit probability that would be achieved if all other errors are zero.

TEST PLAN DESCRIPTION

Test Description

The test was structured to present gunner test subjects with simulated target engagements from a moving platform. The simulation allowed a gunner, seated in a gunner station mock-up, to visually acquire, track and "fire" (pull the control handle trigger) at targets while being subjected to motions encountered in the gunner's station of a moving, tracked vehicle. Data were collected to evaluate task performance of six gunners using four combinations of control handle and sight presentation configurations. Simulated vehicle motions, or rides, ranged from stationary to severe cross-country. The simulated target was capable of performing maneuvers and evasive actions at various speeds as well as remaining stationary. Each simulation run, lasting 45 seconds, required the gunner to engage the target, experience the gun recoil at trigger pull, reacquire the target and repeat the process. Descriptions of the test hardware configuration, rides, target scenarios and data collected are presented in the following sections.

Test Configuration

The test set-up consisted of the TARADCOM ride simulator fitted with a M-60 tank gunner's station mock-up and a sight presentation device, the TARADCOM HYSHARE computer system, a modified Chrysler Corporation Fire Control Combat Simulator, an analog computer and a voice communications network. An overall block diagram of the hardware configuration and the associated control and data channels is shown as Fig. 1. A brief description of the major test components is contained in the following paragraphs.

Ride Simulator

The TARADCOM ride simulator, a hydro-pneumatically actuated simulator, is capable of providing motions about the pitch, roll, yaw and vertical axes. The basic, four degrees of freedom test bed was fitted with a standard M-60 tank gunner station mock-up. This baseline test configuration consisted of the gunner's seat, yoke control handles and monocular sight. The fittings allowed rapid changing between the yoke and isometric handles, and the monocular and video display sights undergoing evaluation. The ride simulator accommodated the gunner and imparted rides typical of the type experienced at the gunner's station of a moving tank.

Fire Control Combat Simulator

The basic fire control combat simulator consists of a microprocess, monocular display, gunner's handles, and operator's console. The simulator generated a slight picture consisting of a converging grid pattern, which represents a terrain, a super-imposed, moving rectangle, signifying a target and a sight reticle pattern.

The fire control combat simulator presented the gunner with the sight picture and moved the reticle in response to signals generated by the gunner's movement of the control handles. The microprocessor calculated tracking and firing errors based on the position of the target and the gunner's positioning of the control handles.

HYSHARE System

The HYSHARE system is a high speed digital/analog computer system. Through hardware and software interfaces the system provides mass storage, digital and analog conversions, and responds to external interrupts which provide program controls and sequencing. The HYSHARE system provided storage for ride and recoil programs and, using the interrupts, controlled consistent output of the signals used to excite the seat simulator. The HYSHARE system also managed all data collection from the seat simulator and the fire control combat simulator. The system monitored program status and indicated if any errors in terrain output or data collection were occurring during a test run.

Analog Computer

The analog computer in the test set-up was used as an interface between the ride simulator and the HYSHARE system. The computer provided electrical isolation between the ride simulator and HYSHARE, imposed an additional voltage limitation on the terrain and recoil signals for added safety, and served as a termination for signal bus lines.

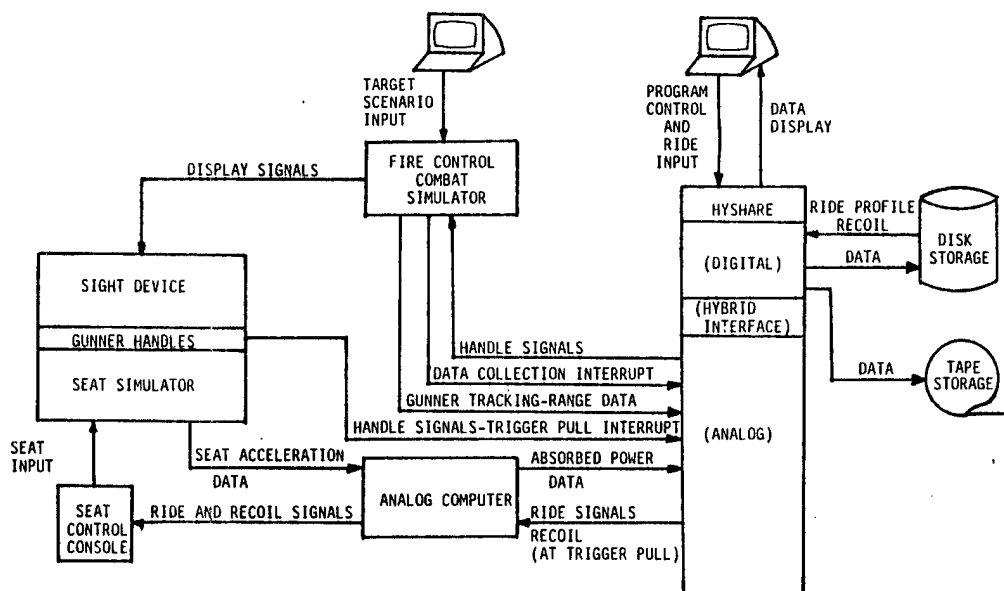


FIGURE 1 TEST CONFIGURATION BLOCK DIAGRAM

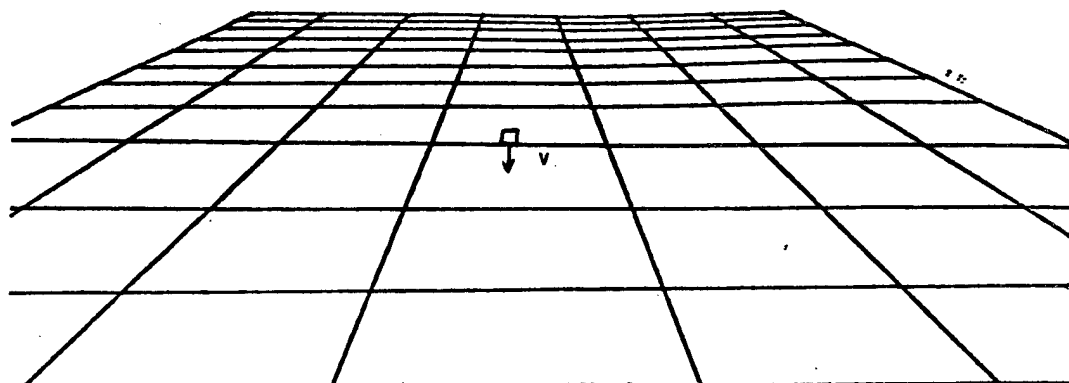
Rides

The terrain profiles, or rides, used to simulate the motions encountered at gunner's station of a moving vehicle were obtained from an instrumented High Mobility and Agility (HIMAG) vehicle run at Ft. Knox, Kentucky. Acceleration data for vertical, pitch, and roll about the vehicle center of gravity (CG) were collected at 100 samples per second on magnetic tape. The acceleration data were double integrated to generate displacement values, detrended to fit the travel constraints of the seat, and translated from the CG to the gunner's station. The displacement values were stored on the HYSHARE disk from which they were recalled and sent to the seat simulator.

Target Scenarios

A modified fire control combat simulator was used to generate and control the behavior of the target engaged by the gunners. Four different target motions, or scenarios, were used during the test. The scenarios ranged from a stationary target to a closing, evasive target. Figures 2-5 are plots of the target paths for each of the four scenarios. Target speeds and evasiveness period and amplitudes are given on the plots. The target always presented a head on aspect angle to the gunner and steadily increased in size as the target range decreased. Test runs began with the target at 1500 meters range. The initial sight picture presented to the gunner at the beginning of each run caused the 1500-meter range target to appear at random locations in or near the field of view, preventing gunner anticipation of the target location. The target was capable of closing with the gunner to within 750 meters.

FIGURE 2

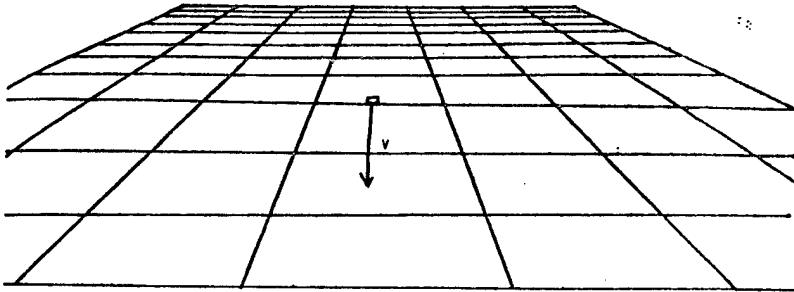


SCENARIO 1

Moving Vehicle/Stationary Target

<u>Power Level</u>	<u>Target Velocity (v)</u>	<u>Horizontal Drift</u>	<u>Vertical Drift</u>
1	0 mph	0 mils/sec	0 mils/sec
2	9	.5	4.2
3	6	0	3.4
4	22	8.2	6.9
5	13	2.9	5.1

FIGURE 3

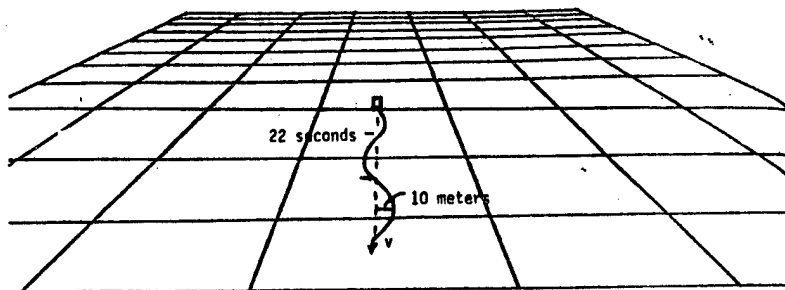


SCENARIO 2

Moving Vehicle/Moving Target

<u>Power Level</u>	<u>Target Velocity (v)</u>	<u>Horizontal Drift</u>	<u>Vertical Drift</u>
1	15 mph	0 mls/sec	0 mls/sec
2	24	.5	4.2
3	22	0	3.4
4	37	8.2	6.9
5	29	2.9	5.1

FIGURE 4

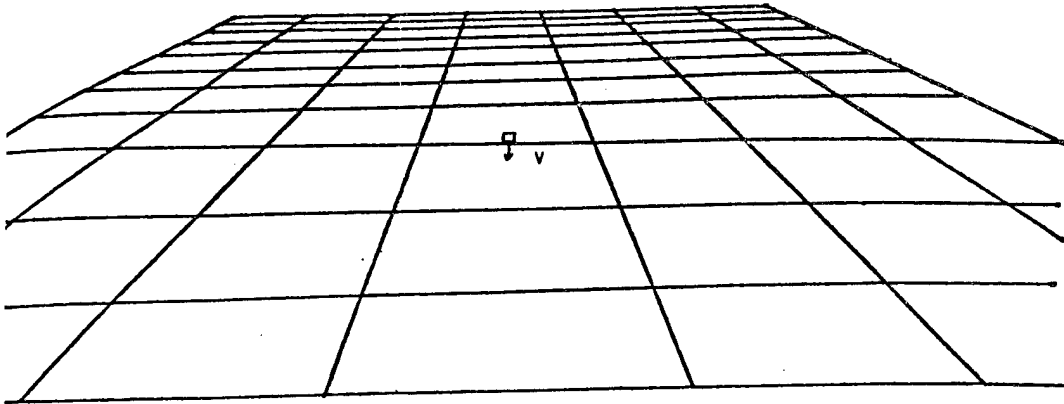


SCENARIO 3

Moving Vehicle/Evasive Target

<u>Power Level</u>	<u>Target Velocity (v)</u>	<u>Horizontal Drift</u>	<u>Vertical Drift</u>
1	15 mph	0 mls/sec	0 mls/sec
2	24	.5	4.2
3	22	0	3.4
4	37	8.2	6.9
5	29	2.9	5.1

FIGURE 5



SCENARIO 4

Evasive Vehicle/Stationary Target

<u>Power Level</u>	<u>Target Velocity (v)</u>	<u>Horizontal Drift</u>	<u>Vertical Drift</u>
2	10 mph	0	4.6
3	7	0	3.6
4	25	$.7 \sin (.4681 t)$	7.5
5	15	0	5.7

DATA

Data collected during each of the 2,400 test runs consisted of the following:

Test Identification Accounting data of an informational nature describing the type of ride, time of the test run, test subject, handle and sight configuration, and target scenario.

Absorbed Power The averaged value of power imparted to the test subject at each trigger pull.

Tracking Error Tracking errors were collected on two channels, vertical and horizontal error. The errors were collected at rates of 100 samples per second for the total duration of each test run.

Firing Errors For each of over 22,000 trigger pulls during the test runs, data for the absorbed power, horizontal and vertical firing lay error, and horizontal and vertical tracking rate errors were collected*

DATA SUMMARY

Introduction

This section will present a summary of the data. The data will not be separated or analyzed according to scenario, gunner or individual errors. An in-depth analysis of the individual errors for different rides and scenarios will be presented in the section titled Configuration and Power Analysis. Some data will be presented that discriminates gunner performance versus ride level but when this is done the total or cumulative data will also be presented. All data presented in this section will discriminate between gunner station configurations and their components. A variety of different indicators in the data will be analyzed and presented to determine which configuration had the best overall performance. The separation and evaluation of this performance according to ride, scenario, etc. will be presented in the previously mentioned section of this report.

Error Indicators

Several different indicators of performance can be extracted from the data. When a scenario starts, the target appears on the visual display in a random circular pattern displaced from the cross hairs. The gunner then traverses, elevates/depresses to acquire the target. One indicator of performance is then the time from the start of the scenario to the first shot.

The horizontal and vertical lay and rate errors at trigger pull are measured. The lay error is the distance from the center of the target to the cross hairs calculated in mils. The rate error is the difference between the target velocity and the gunner tracking rate, also calculated in mils per second. The standard deviation of the errors supplied additional performance indicators. The mean of these errors was calculated and found to be essentially zero. Consequently, the standard deviation is equal to the RMS (Root Mean Square) of the error. One thing these indicators do not include is the difference in total number of shots or trigger pulls for each configuration. Some configurations allow the gunner to be on target more and consequently get more trigger pulls for the same target exposure time. Thus, another indicator is the total number, or average time between trigger pulls for each configuration.

One indicator that includes the lay and rate error as well as the number of trigger pulls is the total number of hits on a 2.3 meter target. The hits are calculated by adding the lay error and the rate error multiplied by the projectile time of flight. The time of flight varies with range for this calculation. The projectile velocity used was 1500 meters/second. To use this parameter the

*Refer to TARADCOM Technical Report No. 12520 for complete detail.

total target exposure time must be the same for each configuration. When hits on target are used in this section to compare different configurations, the target exposure time is identical for each condition.

Another indicator that is frequently used is tracking error. This section will present the RMS tracking error for each configuration from the time of the first trigger pull until the end of the scenario. When the RMS's are averaged for all ride levels they are squared, averaged, and then the square root taken. When the vertical and horizontal RMS's are added, they are added as the square root of the sum of the squares. The tracking error is not a universally accepted measure of performance. The major reason for this is the gunner has a tendency to pull the trigger when he is on target, and his error prior to trigger pull does not have a large influence on his ability to hit the target. This question will be addressed in the subsequent section of this report.

Discussion

The file that stored the gunner trigger pull data can be interrogated in several different ways. It can be interrogated according to ride level, gunner, scenario, and configuration. This section will only consider configuration and ride level.

Table 1 presents the data according to configuration and ride level. Several observations are immediately apparent from this data.

- (i) There is a considerable decrease in performance for all configurations with increasing ride level.
- (ii) Ride has more effect on the video display than the monocular eyepiece.
- (iii) Ride not only affects hit probability but also the time required for the gunner to acquire the target.
- (iv) The tracking error increases with ride but it does not appear to be affected as much as target hits.

Table 2 combines the ride data of Table 1 but eliminates the stationary firing or zero ride level. The best performing configuration was the Yoke Handle Monocular Display. However, the isometric handle acquired the target faster and has more trigger pulls than the yoke.

The difference between the handles and viewing devices eliminating stationary firing is presented in Table 3. The monocular display significantly outperformed the video display in all categories except tracking error. If tracking error had been the only error measurement used to evaluate the different displays, an erroneous conclusion would have been made.

The isometric handle allowed the gunner to acquire the target faster and get more shots off, but its percent hits were lower than the yoke. However, because it allowed the gunner to fire sooner and faster, it had more hits on target than the yoke. The isometric handle had a larger tracking error than the yoke.

TABLE 1
CONFIGURATION PERFORMANCE COMPARISON

RIDE LEVEL WATTS AVG.	SECONDS TO FIRST TRIGGER PULL AVG.	TRIGGER PULLS	SECONDS BETWEEN PULLS AVG.	TARGET HITS	PERCENT HITS	RADIAL TRACKING ERROR RMS
ISOMETRIC HANDLE - MONOCULAR DISPLAY						
0	5.04	888	3.37	841	94.71	.2956
.744	5.31	768	3.90	601	78.26	1.014
.840	5.67	751	3.94	526	70.04	.6176
1.64	6.65	691	4.22	472	68.31	.9770
3.73	6.97	610	4.79	334	54.75	1.022
TOTALS	5.928	3708	4.044	2774	73.214	.7892
YOKE HANDLE - MONOCULAR DISPLAY						
0	5.45	849	3.47	833	98.12	.2914
.744	5.66	721	4.08	596	82.66	.5514
.840	5.25	694	4.33	561	80.84	.5921
1.64	7.22	628	4.57	454	72.29	.9097
3.73	6.94	606	4.81	418	68.98	.7942
TOTALS	6.104	3528	4.252	2862	80.58	.6630
ISOMETRIC HANDLE - VIDEO DISPLAY						
0	5.00	903	3.31	868	96.12	.2225
.744	6.09	746	3.92	578	77.48	.4745
.840	6.71	689	4.22	446	64.73	.5508
1.64	7.53	646	4.42	401	62.07	.8874
3.73	8.28	542	5.17	265	48.89	1.006
TOTALS	6.722	3526	4.208	2558	69.858	.6886
YOKE HANDLE - VIDEO DISPLAY						
0	5.89	854	3.44	841	98.48	.2860
.744	7.24	601	4.75	456	75.87	.6590
.840	7.33	591	4.85	451	76.31	.6858
1.64	9.42	533	5.13	355	66.60	1.050
3.73	8.70	503	5.56	255	50.70	1.049
TOTALS	7.716	3082	4.746	2358	73.592	.7986

TABLE 2
CONFIGURATION DATA SUMMARY - STATIONARY FIRING REMOVED

	SECONDS TO FIRST TRIGGER PULL AVG.	TRIGGER PULLS	SECONDS BETWEEN PULLS AVG.	TARGET HITS	PERCENT HITS	RADIAL TRACKING ERROR RMS
ISOMETRIC HANDLE MONOCULAR DISPLAY	6.15	2820	4.21	1933	68.54	.9231
YOKE HANDLE MONOCULAR DISPLAY	6.26	2649	4.44	2029	75.59	.7268
ISOMETRIC HANDLE VIDEO DISPLAY	7.15	2623	4.43	1690	64.43	.7629
YOKE HANDLE VIDEO DISPLAY	8.17	2228	5.07	1517	68.08	.8814

TABLE 3
COMPONENT DATA SUMMARY - STATIONARY FIRING REMOVED

	SECONDS TO FIRST TRIGGER PULL AVG.	TRIGGER PULLS	SECONDS BETWEEN PULLS AVG.	TARGET HITS	PERCENT HITS	RADIAL TRACKING ERROR RMS
VIDEO DISPLAY	7.66	4851	4.75	3207	66.25	.8243
MONOCULAR DISPLAY	6.20	5469	4.32	3962	72.06	.8307
ISOMETRIC HANDLE	6.65	5443	4.32	3623	66.48	.8468
YOKE HANDLE	7.21	4877	4.75	3546	71.83	.8078

CONFIGURATION AND POWER ANALYSIS

Introduction

The evaluation of visionics and gunners controls used during this test will be based on several gunner measures of performance (MOP). During the test, the gunners were required to accurately track a target in both azimuth and elevation. The MOP used to characterize their ability to accomplish this consists of: lay errors at trigger pull, rate errors for a period of 1/4 second prior to trigger pull, and the resultant total error based on the vector addition of the lay error and the rate error propagated over a 1.0 second round flight time. These errors were expressed in the angular measurement of mils and mils/second and reflect the requirement for inputting angular rates to linear lead fire control systems.

The gunners were instructed to fire as soon as they could after achieving a good "lay" and a good "rate" match with the target. Another MOP is thus the time required for first trigger-pull (TP) and the time between subsequent trigger pulls. The minimum allowable time between trigger pulls was set at 3 seconds. The combination of azimuth and elevation errors were also expressed as a radial miss distance, reflecting the absolute distance of each "impact" from the target center-of-mass, and the ability of the gunner to control errors in azimuth and elevation simultaneously.

The tracking performance of each configuration for the M/S scenario is as shown in Figure 6. (See*Appendix A). The following notation will be used to discuss the comparisons: the isometric tracker = I, the yoke tracker = Y, the monocular display = M, and the video display = V. Thus, IM designates the isometric-monocular configuration.

As a final introductory note, the values displayed in Figure 6 represent the standard deviations for azimuth and elevation and the average radial errors experienced during the test. Because of the greater number of trigger pulls experienced at lower power levels, these values are lower than would be the case if equal weighting were applied to the values at each power level. Each value displayed represents between 700 and 900 trigger pulls.

Configuration Comparison

Considering only the total errors in azimuth, elevation and radial, it is clear that under the conditions of the current test the yoke controller is better than the isometric and that the monocular display is superior to the video. These statements are true at the 99+% statistical confidence level. In looking at the components of these errors, the lay error shows no difference between the isometric and the yoke, but for each, the monocular display is significantly better than the video. The difference between the isometric and the yoke controller is clearly associated with the larger rate errors for the isometric.

This may be explained by the highly responsive nature of the isometric controller. Where the yoke has a definite "dead" or neutral zone in both azimuth and elevation, the isometric unit tested, has immediate, uniform sensitivity in all directions. Thus, it appears to be more difficult to keep unwanted rate changes from occurring while tracking the target with the isometric than with the yoke. This appears to be the case, in spite of the fact that the gunners unanimously liked the isometric control better, and felt that they had much better control with it than the yoke.

The time to fire MOP, shown in Figure 7, both for first and subsequent rounds, shows consistent relationships between configurations. The monocular configurations have 30 first trigger pulls and between 1300 and 1500 subsequent trigger pulls, while the video configurations are characterized by 18 first trigger pulls and from 700 to 900 subsequent trigger pulls. In time to first trigger pull, the only statistically significant difference between configurations ($\alpha = .05$) occur between YM and YV. However, in comparing IM to IV, there is a consistently short-

*Only data of the M/S scenario is listed in Appendix A. For complete detail, see TARADCOM Technical report No. 12520.

er time for the monocular configuration. Time between subsequent trigger pulls show consistent trends with small differences between configurations. The isometric has a shorter time than the yoke, and the monocular has a shorter time than the video. Although the differences between configurations mentioned above are small in absolute terms, the large number of trigger pulls on which these means are based allows a statistically significant difference to exist ($\alpha = .05$), between the isometric and yoke tracking controllers and between the monocular and video displays.

Absorbed Power Effect on MOP

One of the major goals of this test was to develop a relationship between gunner performance and ride quality, expressed in watts absorbed power at the gunner's station. Mathematical models of the hardware performance for combat vehicles exist which will predict system response as a function of the vehicle parameters and speed, and the characteristics of the terrain it is traversing. By combining hardware performance characteristics with gunner input performance, the overall system capability to engage a target from a moving combat vehicle can be predicted.

Figures 8 through 11 illustrate the components of gunner tracking performance for each of the five ride quality levels used in the test. Each figure is for the M/S scenario and a single configuration. An examination of these figures reveals the following trends*:

- a. Both lay errors and rate errors increase with increasing levels of absorbed power, which thus results in total errors increasing with power.
- b. The rate of increase in gunner error with increasing power (slope) is larger for isometric tracking controllers than for yoke tracking controllers.
- c. The slope is larger for video systems than for monocular systems.

The relationships between gunner tracking performance and ride quality is illustrated analytically in Table 4. This table shows the results from a multiple linear regression analysis of the dependent variables of gunner tracking error and time-to-fire and the independent variables of average and peak watts absorbed power at the gunner's station. The coefficient of determination (R^2) is defined as the 100 R^2 percentage of the relationship that is "explained" by the regression equation. In general* the performance of the isometric tracker is highly predictable, with all R^2 values greater than .739 and the majority greater than .9. Looking only at total radial error, the gunner tracking error "bottom line" and the "average" R^2 for the isometric configurations, was .927.

The performance of the yoke controller was not as predictable as the isometric controller. The average R^2 for the yoke was .888, still a good value however. The ability to predict X and Y errors and their components was better for the isometric than the yoke. Radial errors were more predictable than X and Y errors.

Time to fire as a function of absorbed power for the M/S scenario and each combination of gunner station configuration is as shown in Figures 12-15. The mathematical relationship between time to fire and absorbed power is shown in Table 4. As with tracking performance, time to fire is highly predictable based on average and peak power.

Gunner Comparisons

Each of the six gunners has lower overall tracking errors with the yoke than with the isometric control. The standard deviations of gunner tracking error for each gunner are shown in Table 5. Some gunners tracked almost as well with the isometric as the yoke, while other gunners did much worse. The average difference between the standard deviation of the isometric and the yoke is shown in Table 7 for total X and total Y errors. Configuration comparisons are shown in Table 6.

*Refer to TARADCOM Technical Report No. 12520 for complete detail.

TABLE 4
MULTIPLE REGRESSION RESULTS

$$D.V. = A_0 + A_1 W_{avg} + A_2 W_{pk}$$

6 GUNNERS CONFIGURATION	SCENARIO	D.V. DEP.VAR.	A ₀	A ₁	A ₂	R ²
A-ISO-MONO	1 M/S	σX TOT	.309	-.159	.185	.897
	"	σX LAY	.128	-.033	.039	.790
	"	σX RATE	.240	-.128	.153	.922
	"	σY TOT	.346	.059	.113	.890
	"	RADIAL ERR	.362	-.021	.144	.912
	"	T IST	4.91	.243	.197	.995
	"	T SUB	3.47	.321	.042	.960
C-YOKE-MONO	1 M/S	σX TOT	.341	.113	-.0227	.461
	"	σX LAY	.147	.0243	-.00150	.797
	"	σX RATE	.260	.0694	-.00479	.439
	"	σY TOT	.277	-.218	.194	.911
	"	RADIAL ERR	.355	-.0899	.114	.854
	"	T IST	4.91	.116	.223	.952
	"	T SUB	3.51	.0435	.226	.876
E-ISO-VIDEO	1 M/S	σX TOT	.446	-.0464	.203	.880
	"	σX LAY	.160	-.0158	.2092	.812
	"	σX RATE	.337	-.0388	.175	.904
	"	σY TOT	.344	.260	.125	.943
	"	RADIAL ERR	.418	.0890	.176	.923
	"	T IST	5.28	-1.17	1.07	.896
	"	T SUB	3.46	.446	.0489	.910
F-YOKE VIDEO	1 M/S	σX TOT	.282	.435	-.0557	.906
	"	σX LAY	.155	.0660	.000560	.839
	"	σX RATE	.208	.381	-.0594	.898
	"	σY TOT	.305	-.0973	.142	.870
	"	RADIAL ERR	.336	.163	.0596	.938
	"	T IST	6.29	-.824	.816	.637
	"	T SUB	3.79	.327	.0823	.712

TABLE 5
GUNNER COMPARISONS

SCENARIO	CONFIGURATION	VARIABLE	GUNNER						TOT
			1	2	3	4	5	6	
M/S	ISO-MONO	σ X TOT	.472	.291	.558	.510	.722	.974	.558
	YOKE-MONO	σ X TOT	.304	.227	.367	.542	.359	.491	.479
	ISO-MONO	σ Y TOT	.377	.631	.873	.707	.958	.724	.745
	YOKE-MONO	σ Y TOT	.368	.352	.559	.542	.446	.606	.589

TABLE 6
CONFIGURATION COMPARISONS

SCENARIO	VARIABLE	ISO	ISO	YOKE	YOKE	σ IV	σ YV	σ IM	APPROX
		MONO	VIDEO	MONO	VIDEO	σ IM	σ YM	σ YM	
M/S	σ X TOT	.687	.936	.499	.798	1.36	1.607	1.387	900
	σ X LAY	.208	.260	.193	.248	1.250	1.29	1.08	
	σ X RATE	.557	.763	.393	.636	1.37	1.62	1.42	
	σ Y TOT	.822	1.099	.537	.554	1.34	1.03	1.53	
	σ RAD TOT	.781	1.130	.484	.722	1.45	1.49	1.61	

TABLE 7
DIFFERENCES IN STANDARD DEVIATIONS

GUNNER						
AVG DIFF IN σ X	1	2	3	4	5	6
ISO VS YOKE	.063	.202	.058	.074	.214	.380
AVG DIFF IN σ Y	.014	.115	.268	.121	.414	.058

CONCLUSIONS

For the conditions of this test, the data indicate the following:

1. Simulators can be effectively used to determine optimum gunner configurations for firing-on-the-move. Over 22,000 simulated firings were achieved during this test, giving excellent statistical significance to the results.
2. Absorbed power can be used to determine gunner performance for firing-on-the-move, but values change with configuration.
3. The monocular eyepiece with brow pad was superior to the video-type display for all measured parameters.
4. The yoke handle was superior to the isometric for hit probability, but the isometric handle had more trigger pulls and target hits.
5. The rate error was considerably larger than the lay error for all the tested scenarios and configurations.
6. Tracking error is not a good indicator of system performance when firing from a moving vehicle.
7. For the ride used in this test the video display was more affected by ride than the monocular eyepiece with brow pad.
8. Ride affects both hit probability and the time required for the gunner to acquire the target.
9. There is a decrease in performance for all configurations with increasing ride level.

ACKNOWLEDGEMENTS

This study was made possible by the contributions of many people. The gunners from Ft. Knox spent many long hours riding the seat. The seat operators, Messrs. Martin Agnetti and David Clinton, operated and maintained the seat during the test. The personnel from the Computer Simulation and Test Methodology Sub-Function, Messrs. Conaley Flanagan, Alan Havrilla, Ullrich Heym, Jonathan Kring, James Thero and 1LT Dana Charles, wrote the software and operated the computer during the test. Mr. James Cumbow aided with the patching of the analog computers and operated them during the test. Messrs. Andrew Eckles, Thomas Garry, and Mohsin Ingapore from the Human Engineering Laboratory (HEL) coordinated the study with other agencies. Mr. Leonard Buchner of BDM worked with Mr. William West in formulating the final test plan. Appreciated are personnel from USENBEND at Ft. Knox whose support and technical assistance made the study possible and Miss Bonnie Hunter who organized and typed the report.

APPENDIX A

FIGURES 6 through 15

GUNNER ERROR
SCENARIO M/S

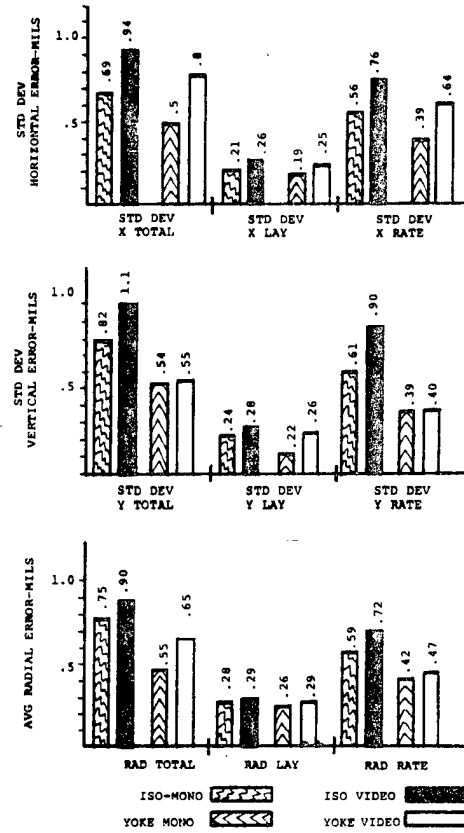


FIGURE 6

TIME-TO-FIRE
SCENARIO M/S

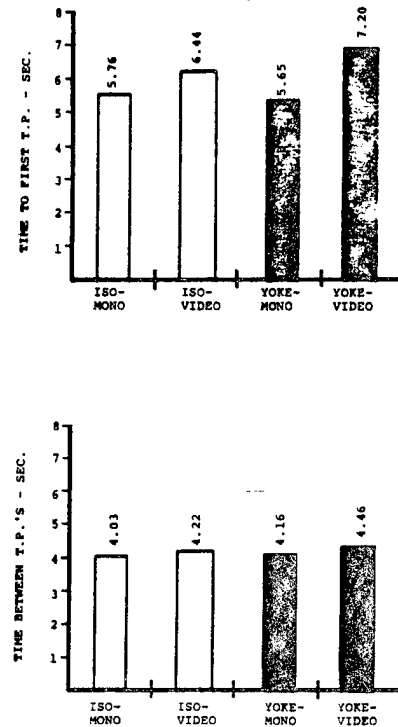


FIGURE 7

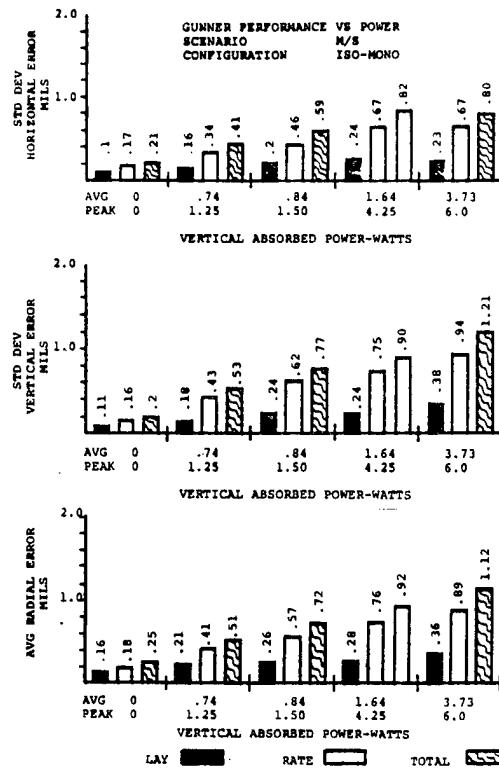


FIGURE 8

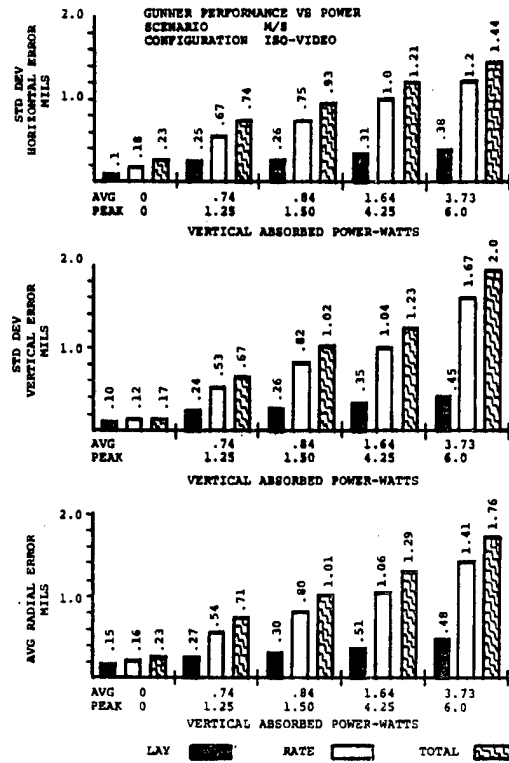


FIGURE 9

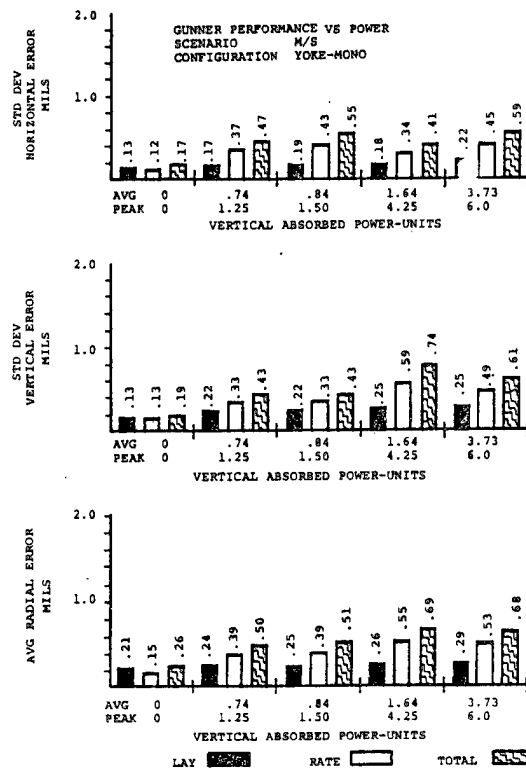


FIGURE 10

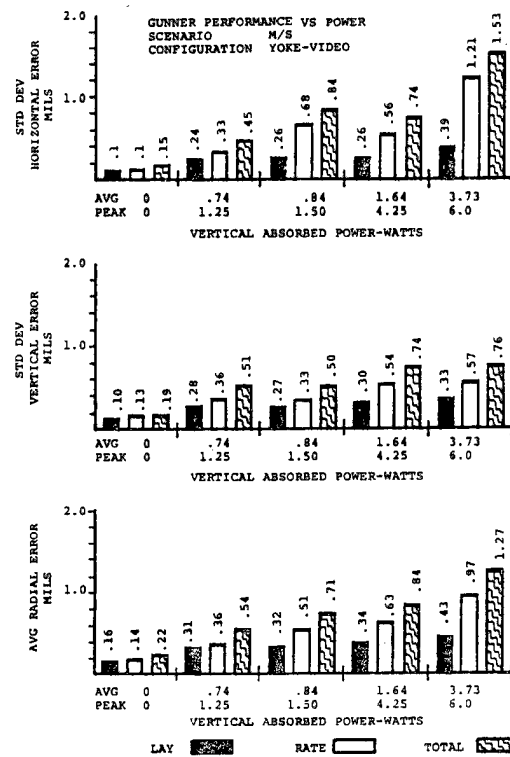


FIGURE 11

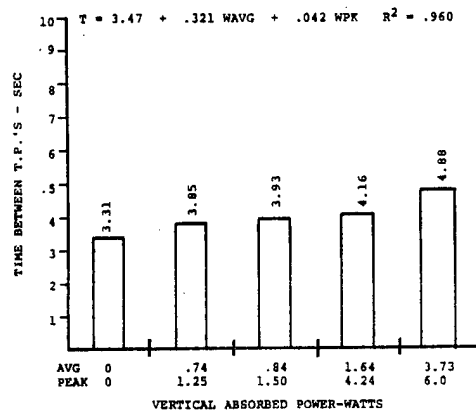
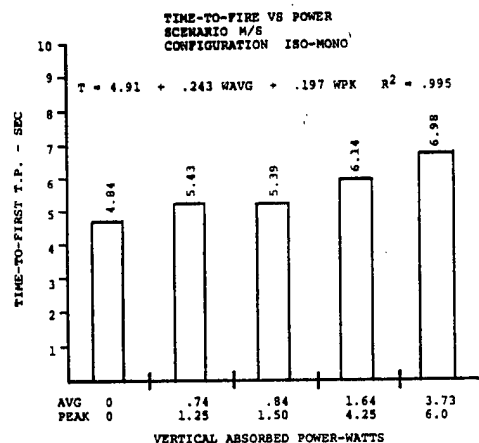


FIGURE 12

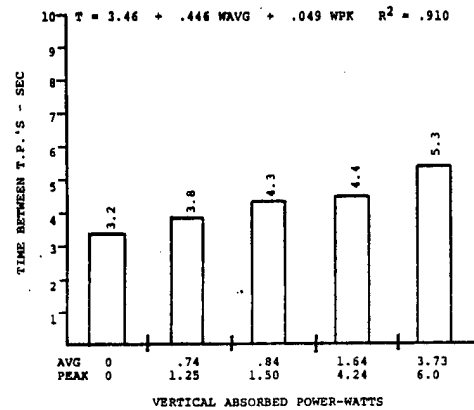
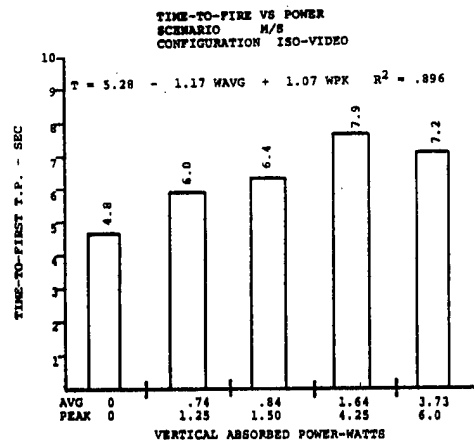


FIGURE 13

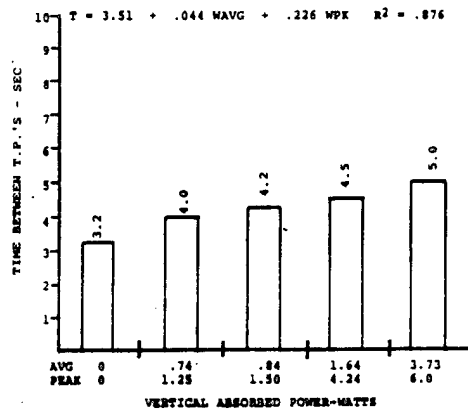
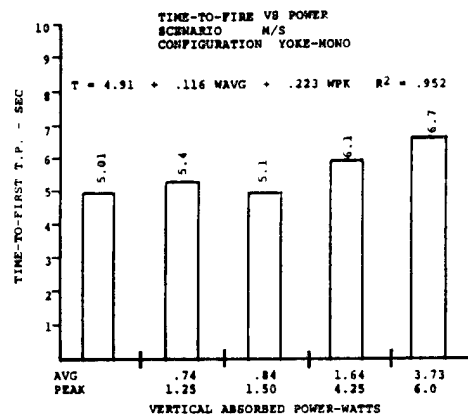


FIGURE 14

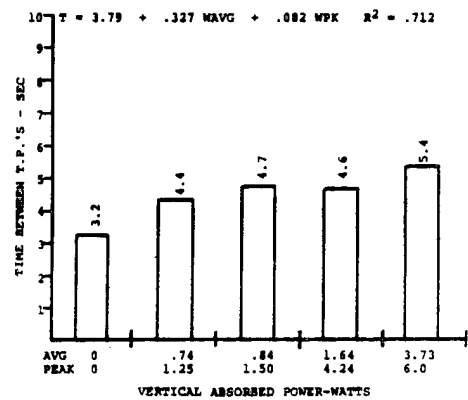
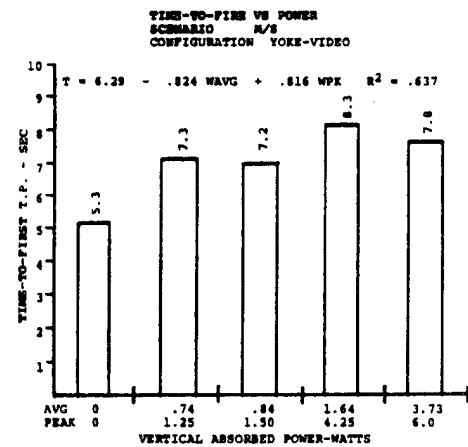


FIGURE 15

DYNAMIC GUN TUBE BENDING ANALYSIS

Richard A. Lee
1LT Dana S. Charles
Jonathan F. Kring
U.S. Army Tank-Automotive
Research and Development Command
Warren, Michigan 48090

ABSTRACT

A simulation is presented of the 75-MM gun barrel (HIMAG) and its support at the trunnion. The simulation was programmed on the new TARADCOM hybrid computer. Bending analysis of the gun was conducted using dynamic inputs at the trunnion from a HIMAG (Configuration No. 2) magnetic field test tape. Errors due to dynamic gun tube bending are presented in graphic and tabular form.

OBJECTIVE

Evaluate the error due to gun tube flexure introduced from vehicle motions while firing-on-the-move.

INTRODUCTION

In recent years there has been an increased emphasis on firing a combat vehicle's main weapon while the vehicle was moving. This has commonly been called "firing-on-the move" (FOM). Stabilization systems were added to vehicles that were designed to perform accurate stationary firing with the idea that stabilizing the gun in elevation and azimuth would allow the vehicle to perform accurate firing while moving. However, this was not the case. Errors occurred while firing-on-the-move that are not significant when firing from a stationary vehicle. Some of these errors are the horizontal and vertical vehicle velocities, stabilization errors, combined pitching and rolling motions, and gun tube flexure. This report is concerned with evaluating the error due to gun tube flexures that are introduced from vehicle motions.

A gun tube can bend or take non-uniform shape due to disturbances or phenomena that are not vehicle introduced. These can be caused from firing the gun or from sunlight heating one side of the gun tube. These errors are not included in this simulation. The static or quasi-static error caused from thermal gradients in the tube is corrected for in current vehicles with a muzzle reference system. This system has a small mirror mounted on the muzzle end of the tube. A light beam is reflected off the mirror to align the sight with the tube muzzle. This system performs very well for these quasi-static corrections but cannot be used for dynamic tube leveling on the moving vehicle.

It is extremely difficult to measure the dynamic bending of a gun tube in a vehicle traversing cross-country terrain. A one-mil angular bending error in a tube will produce approximately a five-foot error firing at a target 1600 meters away. This is a significant error and one must measure the tube bending to considerably less than one mil. To give some indication of the angular size this corresponds, i.e.,

the angle a golf ball subtends a football field away is about 0.3 mils.

The derivation of the equations that were programmed on the computer is given in Appendix A. The equations and computer programs are in a general form and are applicable to any symmetrical gun tube. The data presented in this report are for a 75-MM gun. The gun tube is separated into eighteen uniform elements. Each finite element is considered to have uniform characteristics over its length. One thing to note in the equations is that the gun tube rigidity increases as the fourth power of the diameter. Thus, larger caliber gun tubes are considerably more rigid than small ones.

The model was implemented and solved on a hybrid computer. The gun was modeled on an analog computer and forcing functions were supplied by the digital computer via D/A. The vehicle ride was obtained from magnetic tape recordings of the HIMAG vehicle. These rides were digitized and stored in the digital computer for use as the gun forcing functions. The input into the gun was only in the vertical direction; consequently, the error data presented are for the gun tube flexure in a vertical plane. In reality, there is some flexing in the horizontal direction but that is not considered here.

DISCUSSION

The purpose of this study was to measure by computer techniques the muzzle error at a mile range of the 75-MM gun barrel (HIMAG) subjected to dynamic inputs at the trunnion. A schematic of the gun barrel and its support is shown in Fig. 1. To simulate the gun tube, it was divided into sections to analyze its response using Euler's equation for the flexure of a beam. Figure 2 shows a sketch of the gun and the accompanying design data.

The equations of motion as applied to Fig. 2 are as follows:

1. Basic equation for gun barrel without support:

$$M_L \ddot{Y}_L = \frac{2(EI)_L}{X_L^3} [Y_{L+1} - 2Y_L + Y_{L-1}] - \frac{(EI)_{L+1}}{X_L X_{L+1}^2} [Y_{L+2} - 2Y_{L+1} + Y_L] \\ - \frac{(EI)_{L-1}}{X_L X_{L-1}^2} [Y_L - 2Y_{L-1} + Y_{L-2}]$$

Where:

L = Subscript to designate the section
M = Mass
E = Modulus of elasticity
I = Moment of inertia
X = Length
Y = Vertical displacement
 \ddot{Y} = Vertical acceleration

2. Basic equations for gun barrel with support acting on 1st, 2nd, and 11th sections:

- a. 1st Section

$$M_1 \ddot{Y}_1 = \frac{(EI)_2}{X_1 X_2^2} [Y_3 - 2Y_2 + Y_1] - K_s [Y_1]$$

where: K_s = Spring constant of support (12,200 lbs/in)

- b. 2nd Section

$$M_2 \ddot{Y}_2 = \frac{2(EI)_2}{X_2^3} [Y_3 - 2Y_2 + Y_1] - \frac{(EI)_3}{X_2 X_3^2} [Y_4 - 2Y_3 + Y_2] - K_s [Y_2]$$

c. 11th Section

$$M_{11} \ddot{Y}_{11} = \frac{2(EI)_{11}}{x_{11}^3} [Y_{12} - 2Y_{11} + Y_{10}] - \frac{(EI)_{12}}{x_{11}x_{12}^2} [Y_{13} - 2Y_{12} + Y_{11}] \\ - \frac{(EI)_{10}}{x_{11}x_{10}^2} [Y_{11} - 2Y_{10} + Y_9] - K_s Y_{11}$$

NOTE: A detailed description in the development of the equations of motion is noted in APPENDIX A.

The equations of motion were simulated on the analog portion of the hybrid computer. A typical analog circuit that generates sections 1,2, and 3 is shown in Fig. 3.

The muzzle error due to the flexure of the gun tube has two components, one based on the bending displacement and one based on the rate of change of that bending. We refer to these as angular error and velocity error and their sum as total error. If the tube were completely rigid, this error would be zero. Bending from gravity occurs, but since the error from this is well-known and compensated for, it is removed prior to a simulation run. The effects of gravity for various loads are noted in Fig. 4.

At the start of a simulation run, the static error due to analog noise was measured and removed. The model was run 100 times slower than real time and 20 sample measurements of the error each second were taken to avoid interference from the natural frequency of the tube, which was approximately 500 Hz. Seven and one-half seconds of each ride was studied to obtain a representative sampling of the error. The vertical displacements of the trunnion were inputted dynamically, and the resulting error measurements saved in computer storage for processing after the run*

Six different vehicle rides were studied, each with and without the additional support. For each of the types of error collected, distributions were determined with regard to the gun aiming at a target 1600 meters distant. The range of error was divided into classes and histograms of the frequency that the error fell into each class were made. Time histories of the total error were also plotted*

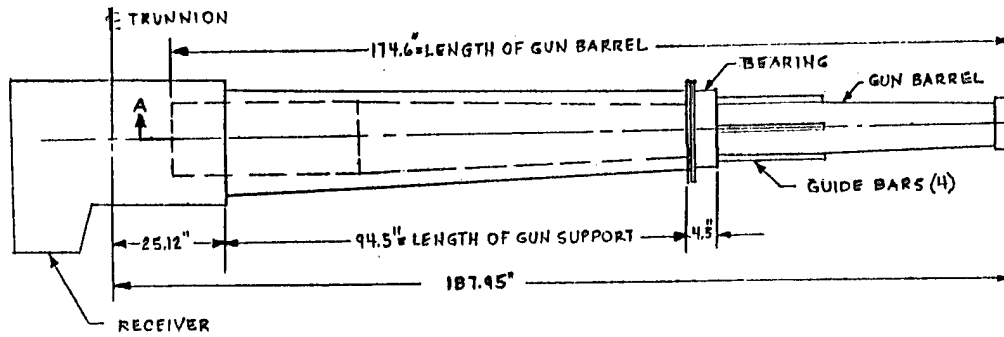
Hit probability curves were generated based on each type of error. For ten selected target sizes the percentage of hits given the measured errors were calculated. Figures 5 through 8 show these curves for each vehicle ride and support condition studied. A smooth curve was fit through the ten target size points. Since an enemy tank would be approximately 2.5 meters high, hit probabilities for this particular target size are displayed in Fig. 9.

A major concern was the relative contribution of the velocity error, as a compensating system for this does not yet exist. For all the rides studied, the velocity error averaged 3.2 percent of the total error without the support and 15.6 percent with the support. In the latter case, the increase is probably due to the higher total accuracy of the system with the extra support. However, in both cases, the contribution is minor. These results are displayed in Fig. 10.

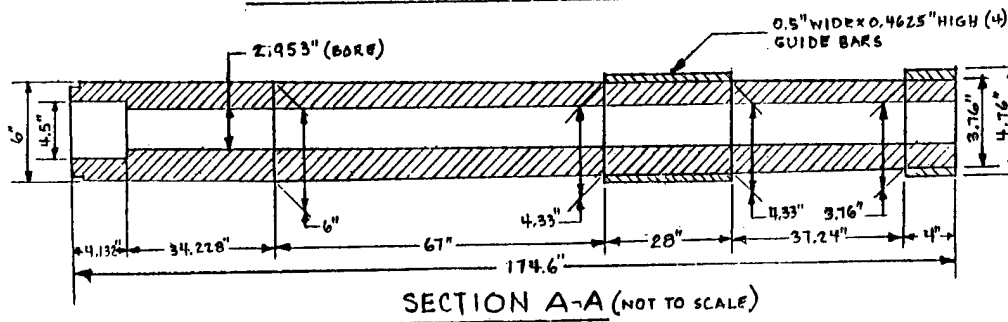
By referring to Fig. 9, the effect of the additional support can be easily seen. For the 2.5 meter target hit probability increased from an average of 12.9 percent to an average of 79.3 percent*. This large improvement in performance shows that if firing on the move is desired, additional rigidity of the gun barrel will greatly reduce the error caused by the dynamic motion of the vehicle.

*Refer to TARADCOM Technical Report No. 12482 for complete detail.

FIGURE 1

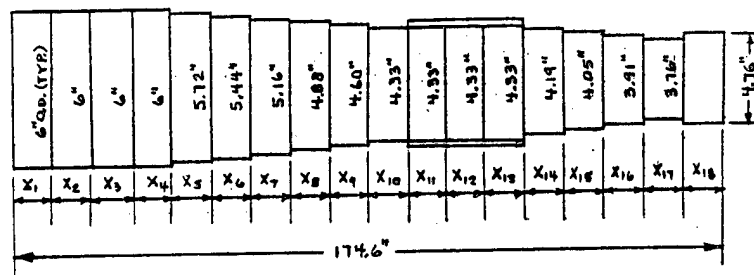


GUN BARREL, SUPPORT AND RECEIVER ASSEMBLY



SECTION A-A (NOT TO SCALE)

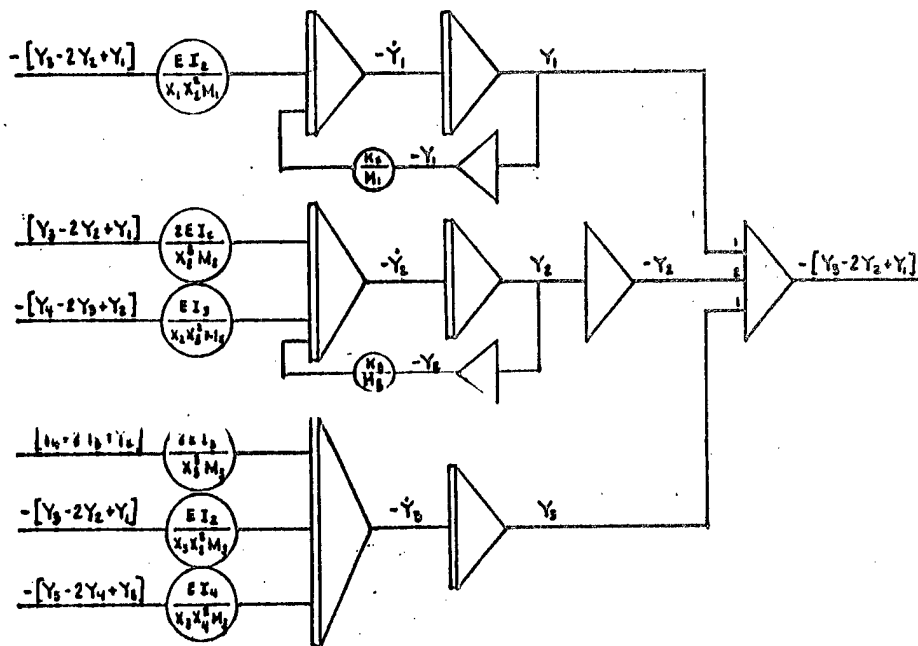
FIGURE 2



75 MM SIMULATED GUN BARREL

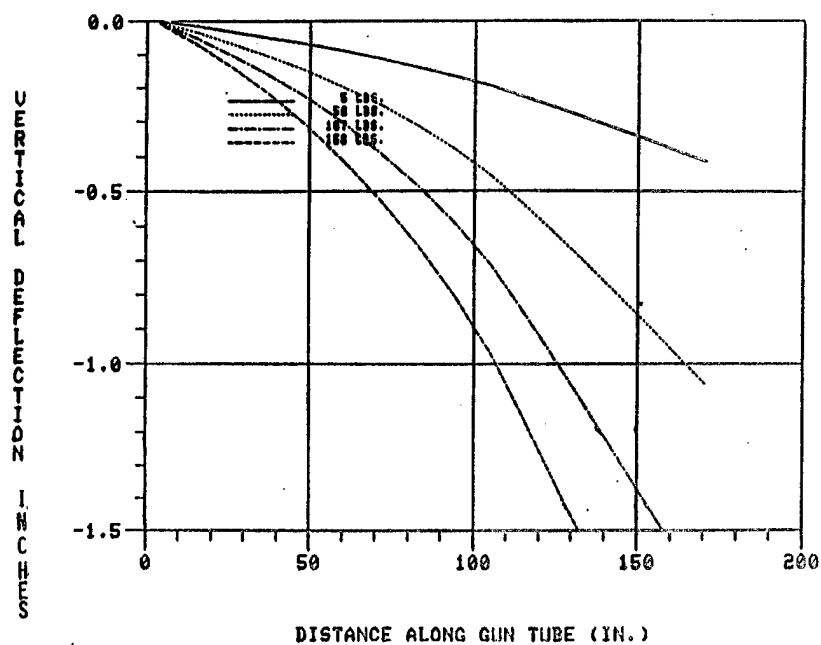
75 MM GUN BARREL DESIGN DATA				
SECTION NO.	SECTION LENGTH (IN.)	MOMENT OF INERTIA (IN. ⁴)	WEIGHT (LBS.)	MASS (LBS-SEC ² /IN.)
X ₁	4.132	63.62	33.06	0.08565
X ₂	11.4	59.88	69.12	0.17407
X ₃	11.4	59.88	69.12	0.17407
X ₄	11.428	59.88	69.29	0.17451
X ₅	11.2	48.81	59.79	0.15479
X ₆	11.2	39.26	51.95	0.13459
X ₇	11.2	31.07	44.69	0.11552
X ₈	11.2	24.11	37.57	0.09733
X ₉	11.2	18.25	30.97	0.08023
X ₁₀	11.0	13.52	24.52	0.06352
X ₁₁	9.4	16.44	23.42	0.06067
X ₁₂	9.3	16.44	23.16	0.06000
X ₁₃	9.3	16.44	23.16	0.06000
X ₁₄	9.34	11.40	18.35	0.04754
X ₁₅	9.3	9.47	15.87	0.04111
X ₁₆	9.3	7.74	13.58	0.03518
X ₁₇	4.3	6.08	11.40	0.02902
X ₁₈	4.0	21.47	12.39	0.03211
BORE = 2.933"				
MODULUS OF ELASTICITY (E) = 30 x 10 ⁶ LBS/IN ²				

FIGURE 3



TYPICAL ANALOG CIRCUIT (SECTIONS 1, 2 AND 3)

FIGURE 4
GUN TUBE BENDING W/O SUPPORT



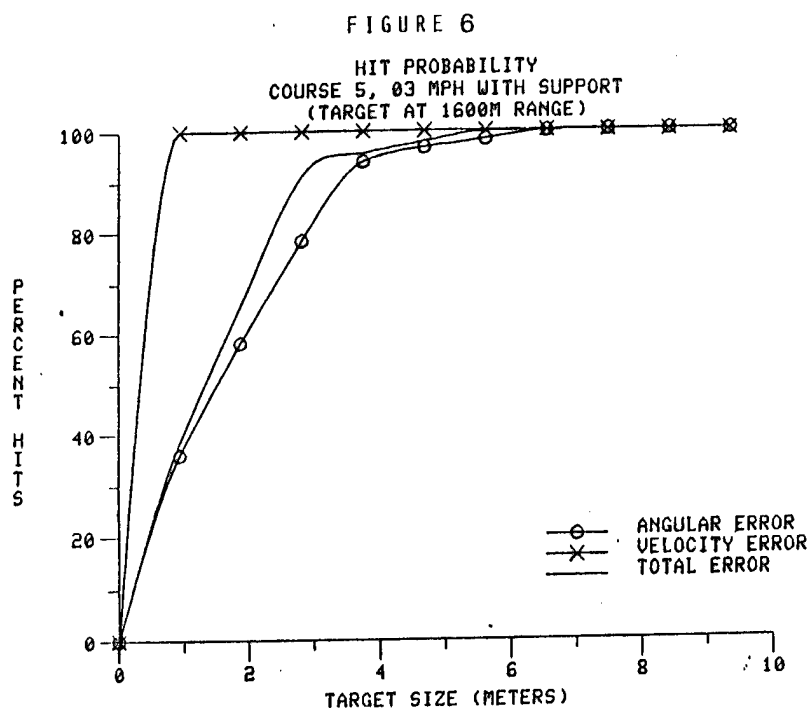
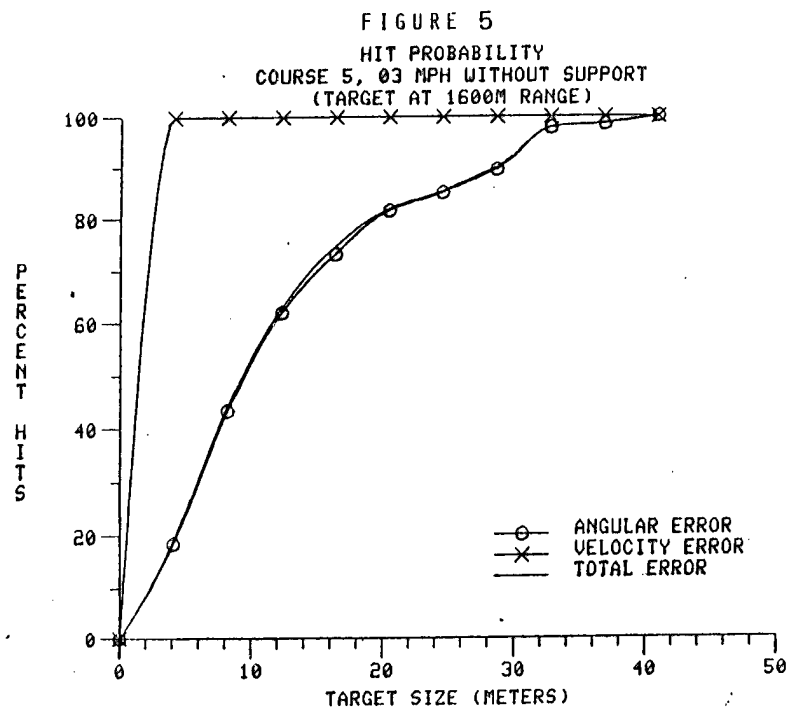


FIGURE 7

HIT PROBABILITY
COURSE 4, 07 MPH WITHOUT SUPPORT
(TARGET AT 1600M RANGE)

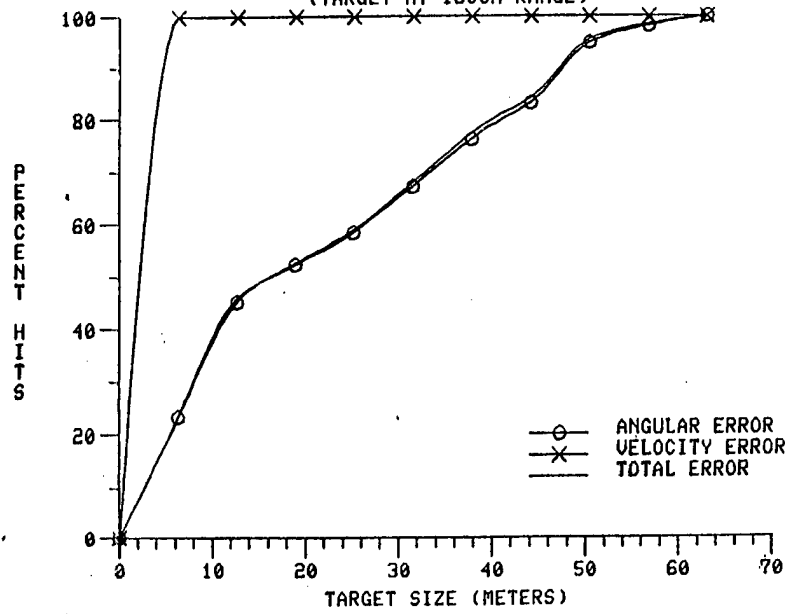


FIGURE 8

HIT PROBABILITY
COURSE 4, 07 MPH WITH SUPPORT
(TARGET AT 1600M RANGE)

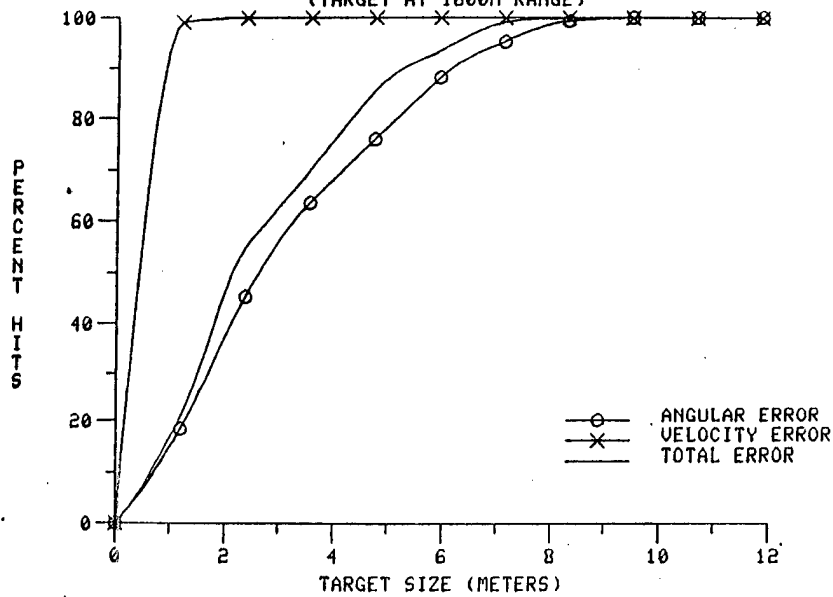


Fig. 9

Hit Probability for 2.5 Meter Target

Course 5, 03 MPH Without Support	11.5 Percent
Course 5, 03 MPH With Support	81.6 Percent
Course 4, 07 MPH Without Support	7.9 Percent
Course 4, 07 MPH With Support	57.5 Percent
Course 3, 15 MPH Without Support	8.9 Percent
Course 3, 15 MPH With Support	66.9 Percent
Course 2, 30 MPH Without Support	21.4 Percent
Course 2, 30 MPH With Support	85.4 Percent
Course 2, 25 MPH Without Support	14.2 Percent
Course 2, 25 MPH With Support	92.1 Percent
Course 2, 10 MPH Without Support	13.5 Percent
Course 2, 10 MPH With Support	92.0 Percent

Fig. 10

Contribution of Velocity Error

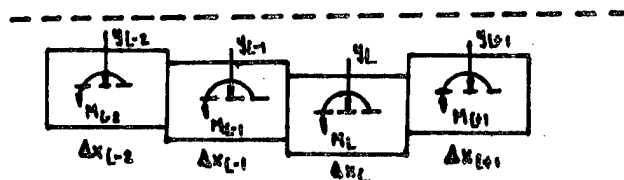
Course 5, 03 MPH Without Support	2.7 Percent
Course 5, 03 MPH With Support	15.5 Percent
Course 4, 07 MPH Without Support	2.7 Percent
Course 4, 07 MPH With Support	13.3 Percent
Course 3, 15 MPH Without Support	3.2 Percent
Course 3, 15 MPH With Support	16.5 Percent
Course 2, 30 MPH Without Support	3.9 Percent
Course 2, 30 MPH With Support	15.1 Percent
Course 2, 25 MPH Without Support	3.4 Percent
Course 2, 25 MPH With Support	15.5 Percent
Course 2, 10 MPH Without Support	3.1 Percent
Course 2, 10 MPH With Support	18.0 Percent

CONCLUSIONS

1. To perform accurate firing on the move, the gun tube flexure due to vehicle motion must be considered.
2. For the HIMAG ride and 75-MM gun used in this simulation, traversing Course 4 at 7 MPH resulted in the gun being on a 2.5 meter target 1600 meters away less than 10% of the time. This error was due only to gun tube bending--the sight and breech end of the gun were pointing at the center of the target.
3. Providing a rigid support for the gun tube resulted in an increase in the hit probability for the "bending" condition of a factor greater than 7.
4. Providing a rigid support for a gun tube will significantly decrease the bending error.
5. The tube bending error is due almost entirely to tube's angular position. The error due to muzzle velocity was insignificant.
6. For some conditions the gun tube bending error can be the most significant error occurring while firing on the move.

APPENDIX A

Equations of Motion Derivation



Euler's equation for the flexure of a beam:

$$\frac{d^2}{dX^2} [EI \frac{d^2 Y}{dX^2}] = \frac{w}{g} \frac{d^2 Y}{dt^2} \quad (A-1)$$

The slope across on element L is given by:

$$\frac{dY_L}{dX_L} = \frac{(Y_{L-1} - Y_L)}{\Delta X_L} \quad (A-2)$$

Y_L is the vertical distance moved for element L from an arbitrary reference line.

The second derivative or rate of change of slope is the difference between the left and right faces of the element.

i.e.

$$\frac{d^2 Y_L}{dX_L^2} = \frac{Y'_{L-1} - Y'_{L+1}}{\Delta X_L} \quad (A-3)$$

Where the prime denotes derivative

Then:

$$\frac{d^2 Y_L}{dX_L^2} = \frac{Y_{L-1} - 2Y_L + Y_{L+1}}{\Delta X_L^2} \quad (A-4)$$

The bending moment at each element is given by:

$$M_L = (EI)_L \frac{d^2 Y_L}{dX_L^2} \quad (A-5)$$

Then for EI constant over element L the bending moment of element L is given by:

$$M_L = \frac{(EI)_L (Y_{L-1} - 2Y_L + Y_{L+1})}{\Delta X_L^2} \quad (A-6)$$

Euler's equation states:

$$\frac{d^2 M}{dX^2} = \frac{w}{g} \frac{d^2 Y}{dt^2} \quad (A-7)$$

To take the derivative of the bending moment EI must be constant over the element.

The rate of change of bending movement over the element is given by:

$$\frac{dM_L}{dX_L} = \frac{M_{L-1} - M_L}{\Delta X_L} \quad (A-8)$$

The second derivative is then given by:

$$\frac{d^2 M_L}{dX_L^2} = \frac{M'_{L-1} - M'_{L+1}}{\Delta X_L} \quad (A-9)$$

Then:

$$\frac{d^2 M_L}{dX_L^2} = \frac{M_{L-1} - 2M_L + M_{L+1}}{\Delta X_L^2} \quad (A-10)$$

Writing each moment equation

$$M_{L-1} = \frac{(EI)_{L-1} (Y_{L-2} - 2Y_{L-1} + Y_L)}{\Delta X_{L-1}^2} \quad (A-11)$$

$$M_L = \frac{(EI)_L (Y_{L-1} - 2Y_L + Y_{L+1})}{\Delta X_L^2} \quad (A-12)$$

$$M_{L+1} = \frac{(EI)_{L+1} (Y_L - 2Y_{L+1} + Y_{L+2})}{\Delta X_{L+1}^2} \quad (A-13)$$

The mass of each element is the mass per unit length times the length of the element.

$$M_L = \left(\frac{w}{g}\right)_L \Delta X_L \quad (A-14)$$

Euler's equation is then written as:

$$\begin{aligned} M_L \frac{d^2 Y_L}{dt^2} &= \frac{(EI)_{L-1} (Y_{L-2} - 2Y_{L-1} + Y_L)}{\Delta X_L \Delta X_{L-1}^2} \\ &\quad - \frac{2(EI)_L (Y_{L-1} - 2Y_L + Y_{L+1})}{\Delta X_L^3} \\ &\quad + \frac{(EI)_{L+1} (Y_L - 2Y_{L+1} + Y_{L+2})}{\Delta X_L \Delta X_{L+1}^2} \end{aligned} \quad (A-15)$$

Evaluating the end conditions:

There is no bending moment on the end element

$$\frac{d^2 M_{\text{end}}}{dX_{\text{end}}^2} = \frac{M_{L+1}}{\Delta X_L^2} \quad (A-16)$$

Second from end

$$\frac{d^2 M_{\text{end}+1}}{dX_{\text{end}+1}^2} = \frac{-2M_L + M_{L+1}}{\Delta X_L^2} \quad (A-17)$$

The opposite end

$$\frac{d^2 M_{\text{end}}}{dX_{\text{end}}^2} = \frac{M_{L-1}}{\Delta X_L^2} \quad (A-18)$$

and

$$\frac{d^2 M_{\text{end-1}}}{dx_{\text{end-1}}^2} = \frac{M_{L-1} - 2M_L}{\Delta X_L^2} \quad (\text{A-19})$$

Next page is blank.

ANALYSIS OF THE UNIVERSAL TURRET SUBSYSTEM (UTS) IN THE AH-1S MODERNIZED COBRA

T. Hutchings
DRDAR-SCS-M
FC&SCWSL

Abstract

This paper describes a dynamic analysis of the UTS in the 20mm AH-1S gun system configuration. The response of the turret to step, ramp and sinusoidal control inputs is predicted from a state space computer model of the azimuth and elevation servocontrol systems. These results are compared to Bell Helicopter Textron (BHT) specifications. Also, the coupled dynamical motions of the UTS and AH-1S airframe during gun fire are determined for a set of initial pointing positions. In this study, the flexural characteristics of the AH-1S airframe are determined by a ASTRAN model. Results of this analysis show that the UTS meets all specifications.

Introduction

The analysis of the UTS was conducted in support of TECOM's Independent Evaluation Report (IER) for Development Test IIa of the UTS and critical issues demonstration of the AH-1S Fire Control Subsystem (FCS). Objectives of the evaluation, in regard to the UTS, were to assess the technical performance and functional accuracy of the system and the degree to which the UTS meets the specifications and operational capabilities.

The UTS was developed as a replacement for the current M28 turret on the Cobra helicopter. It can accommodate the 20mm M197 gattling gun. Presently, the AH-1S Modernized Cobra helicopters are being equipped with the 20mm M197 gun. The AH-1S gun system consists of the TOW sight (which is a stabilized optical sight), a laser rangefinder, a fire control computer, an air data subsystem, aircraft attitude sensors, a navigation system, the UTS and weapon. When the primary gun system is activated the UTS is slaved to the TOW sight. That is, the position of the azimuth and elevation gear drives in the UTS, which are measured by two resolvers, are compared to gyro signals from the TOW sight. Errors in the relative angular positions provide the control input to the independent azimuth and elevation turret controllers. In addition, ballistic lead angles, determined by the fire control computer, are added to the relative error signals between the UTS resolvers and TOW sight gyros. Thus the UTS

functions as two independent servocontrol systems (one controlling azimuth motions, the other controlling elevation motion) based on classical, positional feedback control. The M197 gattling gun is externally powered and fires at a nominal rate of 725 shots per minute (spin).

UTS Model Description

Modeling information for the UTS was provided by General Electric Company, the primary developer of the turret. The data, which is considered proprietary information by General Electric, was provided in the form of a functional block diagram of the servocontrol system and a computer program (model UTSIM) that determines the dynamics of the control system. A simplified block diagram of the UTS model is shown in Figure 1. Not shown in the diagram are various non-linear terms such as current and voltage saturation levels, deadbands, gear backlash and coulumb friction of the motor and load. The feedback error signal after being demodulated, is passed through a band reject or notch filter. This filter effectively removes signal components at the fundamental mechanical resonance frequency of about 9 Hz., which is caused by motor shaft windup. In the model, the notch filter is represented by a third order system whose frequency response function is given by:

$$H(w) = \frac{(1 - a_2 w^2) + i a_1 w}{(1 - b_2 w^2) + i w (b_1 - b_3 w^2)} \quad (1)$$

where a_1 , a_2 , b_1 , b_2 , and b_3 are constant coefficients. Amplitude and phase diagrams of $H(w)$ are shown in Figures 2 and 3, respectively. The signal, after it is amplified, drives an electric motor. A clutch model differentiates between motor speed and the speed of the drive shaft. It allows for slippage to occur when a friction limit is exceeded. The motor torque is stepped-up through a gear transmission to drive the load. Besides the control input, external torques induced by helicopter platform vibrations and weapon recoil loads influence the dynamics of the turret.

The complete model is represented by a set of 12 state variable equations which are expressible in vector notation by

$$\dot{\underline{x}}(t) = \underline{A} \underline{x}(t) + \underline{B} \underline{u}(t) + \underline{F} \underline{w}(t)$$

where

$\underline{x}(t)$ is the vector of state variables,

$\underline{u}(t)$ is the vector of control inputs,

$\underline{w}(t)$ is the vector of disturbances,

\underline{A} , \underline{B} , and \underline{F} are constant coefficient matrices

The integration routine used to solve equation (2) is a modified Euler technique which includes a turnable parameter to compensate for phase lag. This routine runs quickly and has good phase characteristics.

UTS Responses to Step and Ramp Control Inputs

Performance specifications for the UTS are cited in Reference 1. Figure 4 contains a list of the specifications considered in this investigation. The first analytical investigation conducted was the response of the UTS to step control inputs of

0.005, 0.01, 0.02, and 0.2 radians. The characteristic response of the turret is shown in Figure 5 for a command input of 0.01 radians. Basically the turret responds in a manner similar to that of an underdamped second order mechanical system. The flattening of the overshoot portion of the response curve results from Coulomb frictions in the motor and load. After 0.5 seconds the response settles to within about 0.3 milliradians of the command input value. Residual error in the system is caused by a gear deadband and by amplifier voltage deadbands. Table I contains summary information for the step response case. Overshoots ranged from 23.7% to 50.4% in azimuth and from 31.5% to 44.8% in elevation. Steady state track errors were all well below the accuracy specification of 3.0 mrad; however, the results presented do not include resolver error, which is estimated to be about 1.0 mrad. Other performance data presented in Table I are the settling time and the maximum slew rate. Settling time is defined as the time it takes for the error signal to settle within 2.0 mrad of the command input. Peak slew rates of 71.3 deg/sec and 91.0 deg/sec were achieved in elevation and azimuth, respectively. These values exceed the desired peak slew rates listed in the specification sheet.

A typical response to a range control input is shown in Figure 6 for a 50 deg/sec rate input. The response curve is for the azimuth controller. It shows the characteristic initial log, followed by an overshoot and settling period. A summary of results for ramp inputs is shown in Table II for slew command rates of 5, 50, 60, 70 and 85 degrees per second. On the basis of model simulations, the specification on minimum slew acceleration of 120 deg/sec is easily satisfied; furthermore, the steady state error for a 5 deg/sec slew is well below the specification bound of 2 mrad. In regard to slew rate, the model simulations show that the desired 60 deg/sec elevation rate is achieved in about 0.69 sec. In azimuth a steady state slew rate of 70 deg/sec is arrived at in about 0.41 seconds. Peak slew rates of 72.8 deg/sec in elevation and 94.3 deg/sec in azimuth were obtained in the simulation.

UTS Response to Weapon Recoil Forces

The procedure used to analyze the effects of weapon recoil forces on dynamic gunpointing accuracy is illustrated in Figure 7. In the model simulations constant reference angles are specified for the control input. Initially, the turret is assumed to be pointing in the proper direction; however, the turret is subsequently disturbed by torques generated by weapon recoil eccentricities and helicopter platform vibrations. To determine the dynamics of the turret support platform a model was developed to solve the forced vibration problem for the AH-1S helicopter. Dynamical characteristics of the AH-1S Cobra structural frame have been modeled in NASTRAN by Bell Helicopter Textron (BHT). The AH-1S Nastran Model is a modification of the original AH-1G model described in Reference 2. As the first step in the analysis, the natural frequencies and modeshapes of the AH-1S Cobra are determined by the NASTRAN Rigid Format 3 analysis and the model data is saved on an output file. The model is accurate for frequencies up to about 30 Hz. Table III contains a list of the first twelve modeshapes used in the analysis.

Modal data is used by the helicopter vibration model to solve the forced vibration problem. In the present analysis the forcing function is composed of the generalized vector of transmitted weapon recoil force components. Primary outputs of the helicopter vibration model are the platform rotation and accelerations. Platform accelerations induce torque disturbances that affect the dynamics of the UTS. The torques depend on the initial pointing direction (See Figure 8) and on various turret parameters (illustrated in Figure 9). In Figure 8 angles α and ϕ locate the gun line orientation in the helicopter coordinate frame. An expression for the recoil torque disturbance in azimuth is given by

$$T_a = -F_R d_3 \cos \alpha - I_a \ddot{\Theta}_y + m_a a_1 (\ddot{x} \sin \phi + \ddot{z} \cos \phi) \quad (2)$$

and in elevation the torque disturbance is

$$T_e = F_R d_2 - I_e (\ddot{\Theta}_x \sin \phi + \ddot{\Theta}_z \cos \phi) - m_e [(a_2 + a_3 \cos \alpha) \ddot{y} - (\ddot{x} \cos \phi - \ddot{z} \sin \phi) (-b_2 + a_3 \sin \alpha)]$$

where F_R = recoil force,
 d_2, d_3 = recoil eccentricities,
 m_a, m_e = masses of turret components (azimuth and elevation)
 I_a, I_e = inertias of turret components (azimuth and elevation)
 $\ddot{x}, \ddot{y}, \ddot{z}$ = platform linear acceleration components
 $\ddot{\Theta}_x, \ddot{\Theta}_y, \ddot{\Theta}_z$ = platform angular acceleration components

In the model simulation disturbance torques were generated for several different initial turret orientations and for two sets of recoil data corresponding to the 20mm M197 and 30mm XM230 guns. At each initial orientation the platform acceleration data generated by the helicopter vibrations model is stored on a permanent file, which is later used by the UTS model to calculate torque disturbances.

Weapon recoil data for the 20mm M197 and 30mm XM230 guns were provided in Reference 3. These data represent the steady state recoil force measured from burst firings. To simulate burst firings the single shot recoil data was repeated as shown in Figure 10 for the 20mm weapon. Elevation torque disturbance for the case of 25 degrees depression angle and 90 degrees azimuth is shown in Figure 11, and the corresponding turret position error is shown in Figure 12. In this case the maximum error in the turret feedback angle is about 1.2 mrad.

Simulation results for the 20mm recoil analysis are summarized in Table IV. The table lists the initial turret angles and statistical means and standard deviations of the elevational vibration responses. No significant errors were obtained in the azimuth angle. Table IV lists the total gun pointing error as well as the separate contributions from helicopter platform rotation and UTS servocontrols. In most cases the statistical errors are less than 1.0 mrad, which is smaller than expected. Since the recoil force used in the simulation does not include transients

actual turret dynamic errors are expected to be somewhat larger than the values obtained in the simulations.

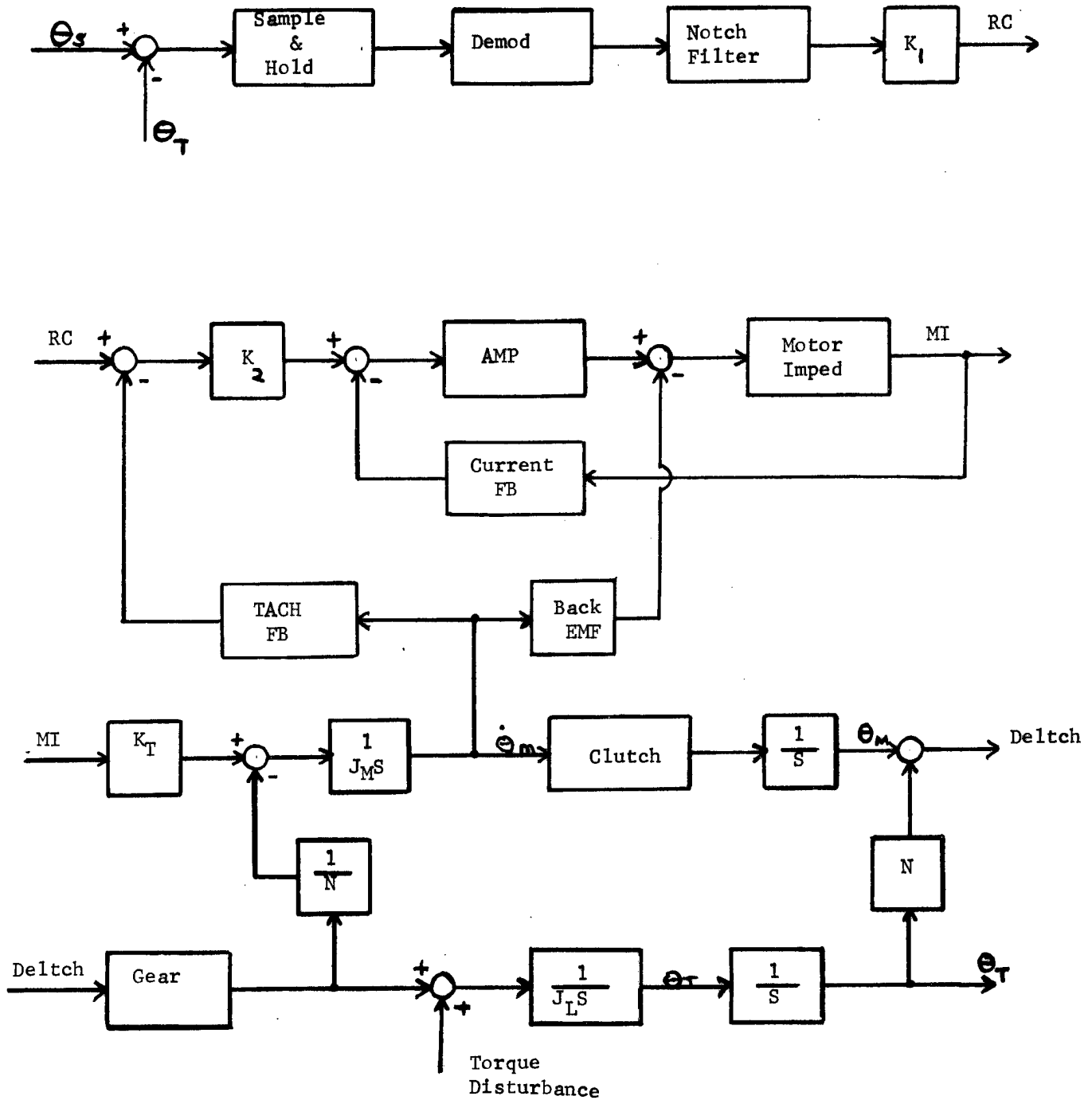
A similar analysis was conducted for the 30mm Hughes Chain gun. The gun recoil force, again obtained from Reference 3, is illustrated in Figure 13. Simulation results for the elevation motions are presented in Figures 14 and 15 for the case of forward firing with a depression angle of 5 degrees. The torque disturbance (shown in Figure 14) has a peak value less than 100 ft-lb and the turret position error (shown in Figure 15) has a peak value of 1.43 mrad. A complete set of results for the 30mm gun are presented in Table V. In all cases simulated, the elevation angle errors were below 3.0 mrad, and the azimuth angle error were about 0.25 mrad.

Conclusions

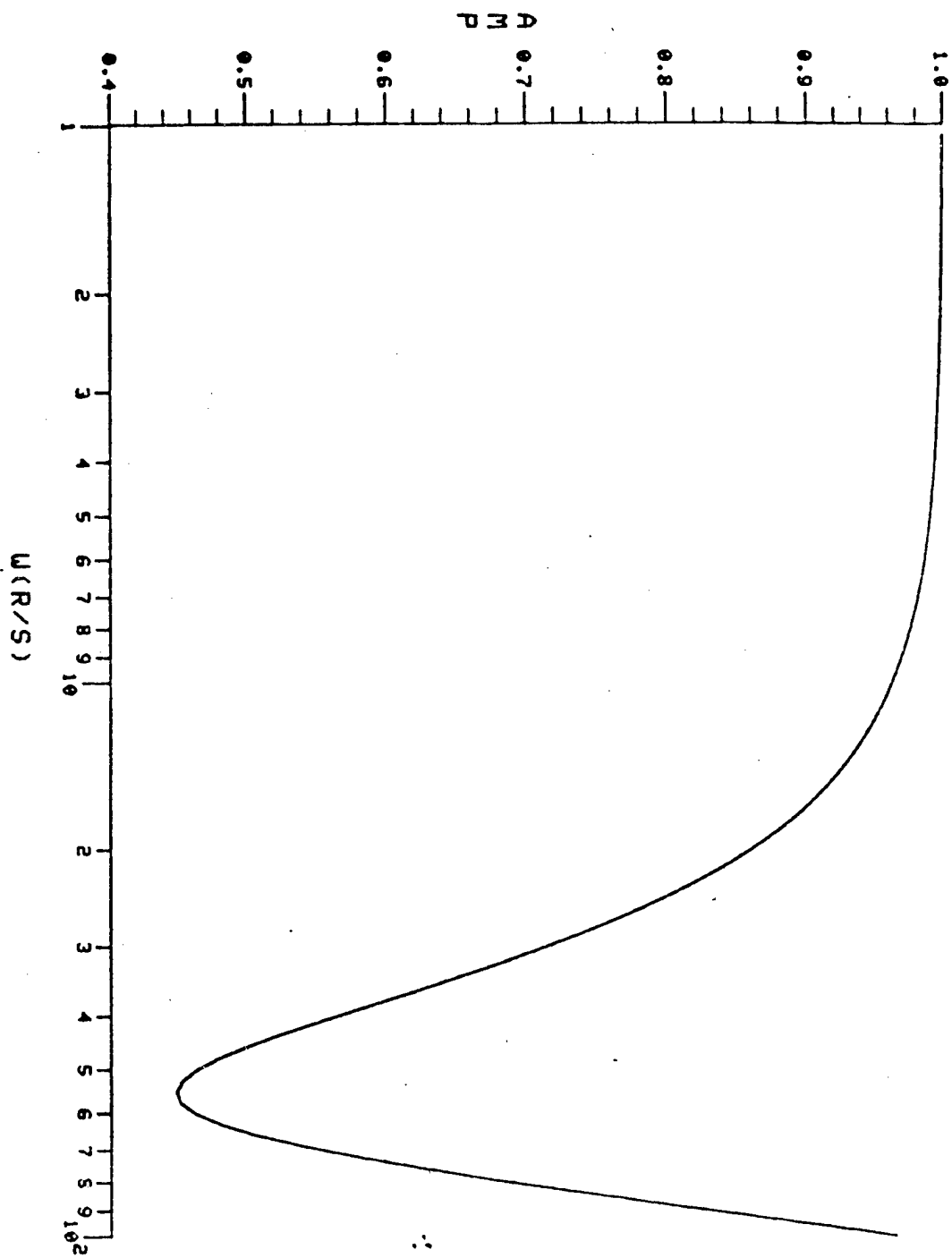
An analysis of the UTS was conducted to support TECOM's Independent Evaluation Report (IER) of the AH-1S Modernized Cobra. The main purpose of the analysis was to determine whether performance specifications were met and to estimate dynamic accuracy levels for 20mm and 30mm weapons. Model simulations for step and ramp control inputs resulted in good performance predictions that exceeded desired specification requirements on slew acceleration, slew rate, and positional accuracy.

To assess the dynamic performance of the UTS from weapon recoil loads, a model was developed to analyze the coupled interaction of the UTS with the AH-1S structural airframe. Disturbance-torques applied to the UTS from recoil induced platform dynamics were determined from transmitted recoil forces for both the 20mm M197 and 30mm XM230 guns. Statistical representations of the gun pointing errors obtained from the mathematical simulations were on the order of 1.0 mrad for the 20mm weapon and 2.0 mrad for the 30mm weapon. On the basis of mathematical simulations the accuracy of either the 20mm or 30mm guns is expected to meet or exceed specifications of the UTS during firings

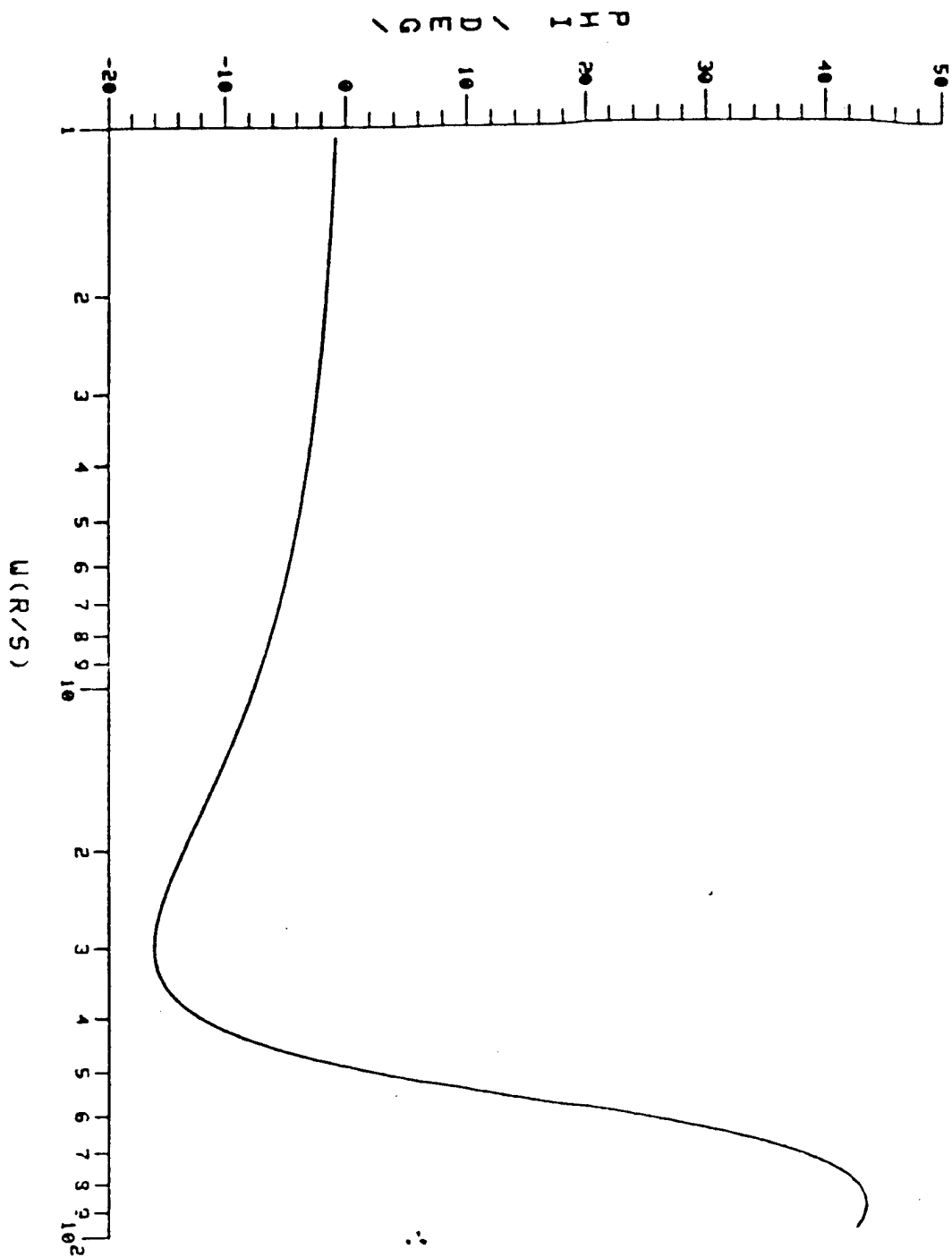
FIGURE 1: UTS BLOCK DIAGRAM



UTS NOTCH FILTER
 FIGURE 2: AMPLITUDE VS. FREQUENCY



UTS NOTCH FILTER
FIGURE 3: PHASE ANGLE VS. FREQUENCY



UTS SPECIFICATION SHEET

FIGURE 4: (FROM BHT SPEC NO 209-947-281)

- 1) PEAK RECOIL: 2100 LBS -- 20MM
 2700 LBS -- 30MM
 - 2) HARD STAND FIRING:
 80% CIRCLE DIA ≤ 12 MRD
 - 3) STATIC POSITION ACCURACY ≤ 3 MRAD
 - 4) SLEW ACCELERATION: 120 DEG/SEC ² MINIMUM
 - 5) POSITION ERROR FOR 5 DEG/SEC SLEW ≤ 2 MRAD
 - 6) SLEW RATE: AZIMUTH ELEVATION
 - a) PEAK RATE: MIN: 60 DEG/SEC 50 DEG/SEC
 DESIRED 80 DEG/SEC 60 DEG/SEC
 - b) FULL SLEW * MIN 4.2 SEC 1.8 SEC
 DESIRED 3.3 SEC 1.6 SEC
- * 220 DEG AZIMUTH; 65 DEG ELEVATION

X10⁻¹

FIGURE 5: Y(10) -- TURRET POSITION

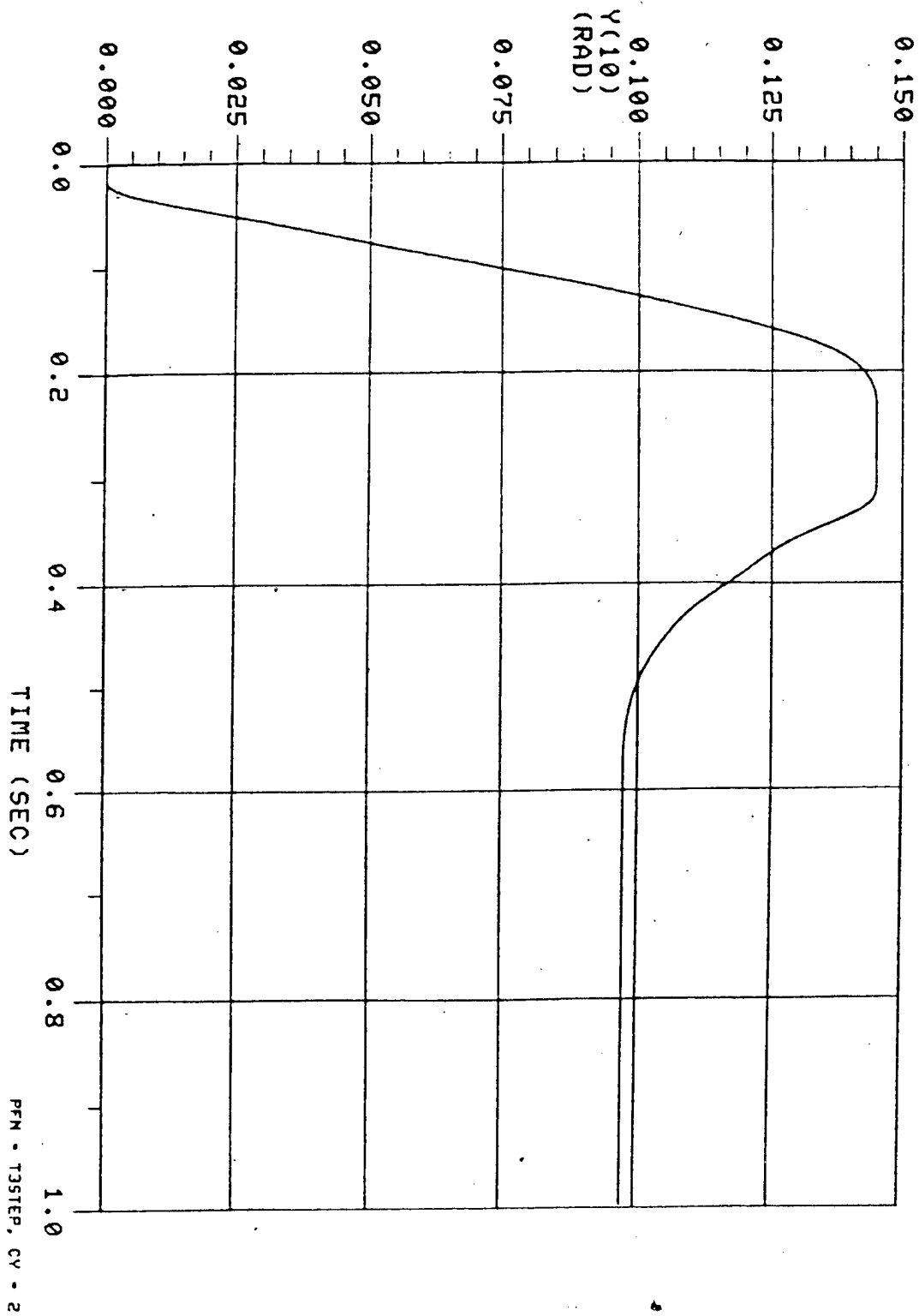


FIGURE 6: $\gamma(9)$ -- TURRET ANGULAR RATE

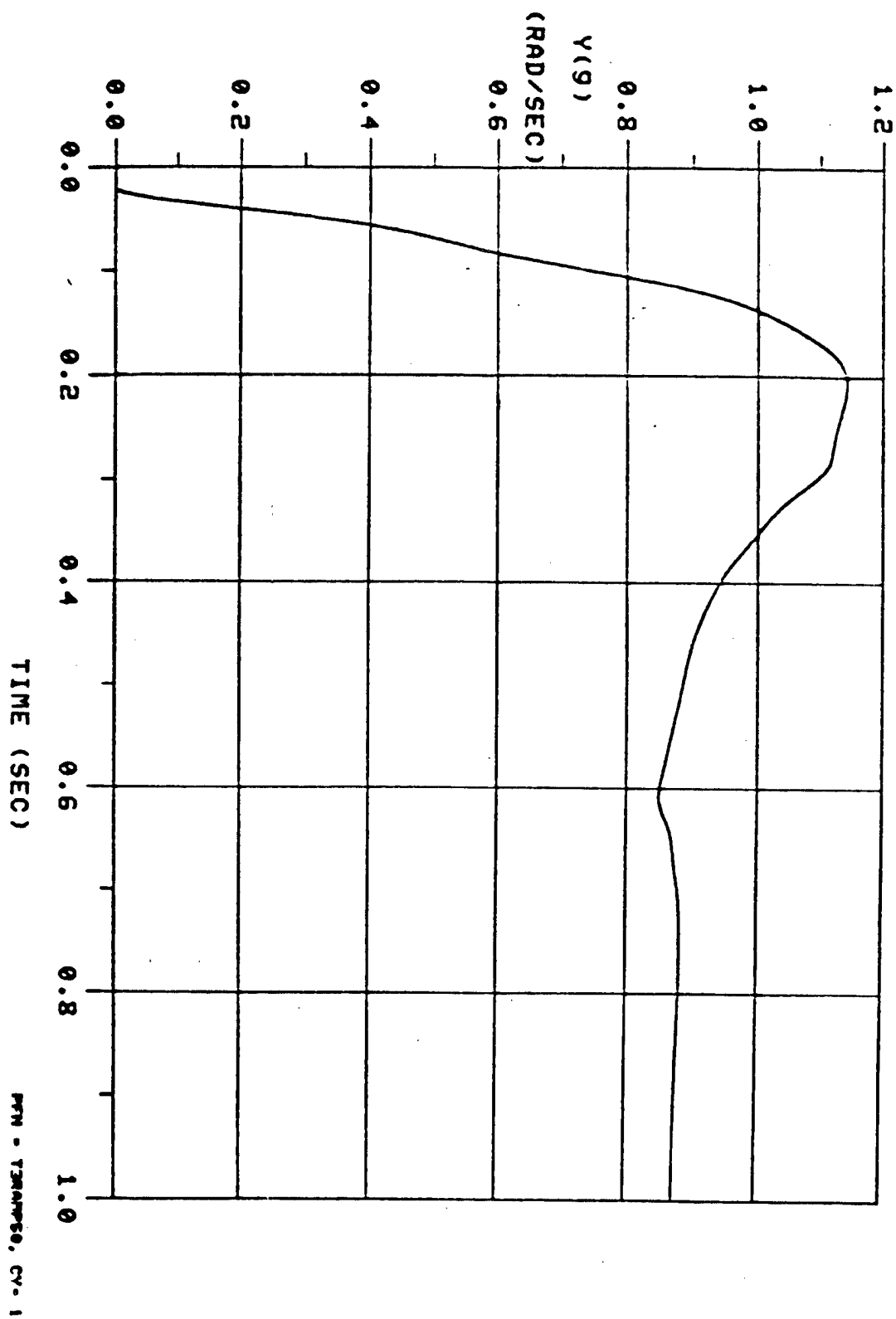


FIGURE 7: HELICOPTER-TURRET DYNAMIC ANALYSIS
BLOCK DIAGRAM

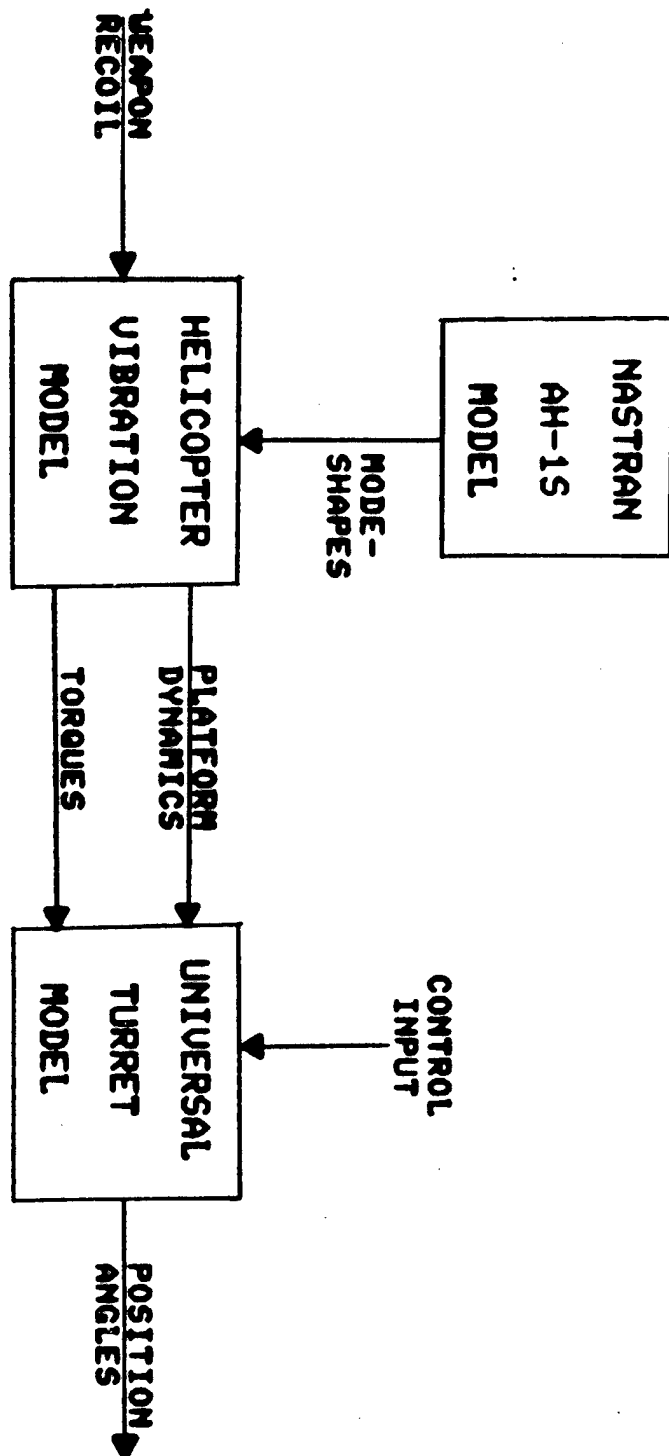
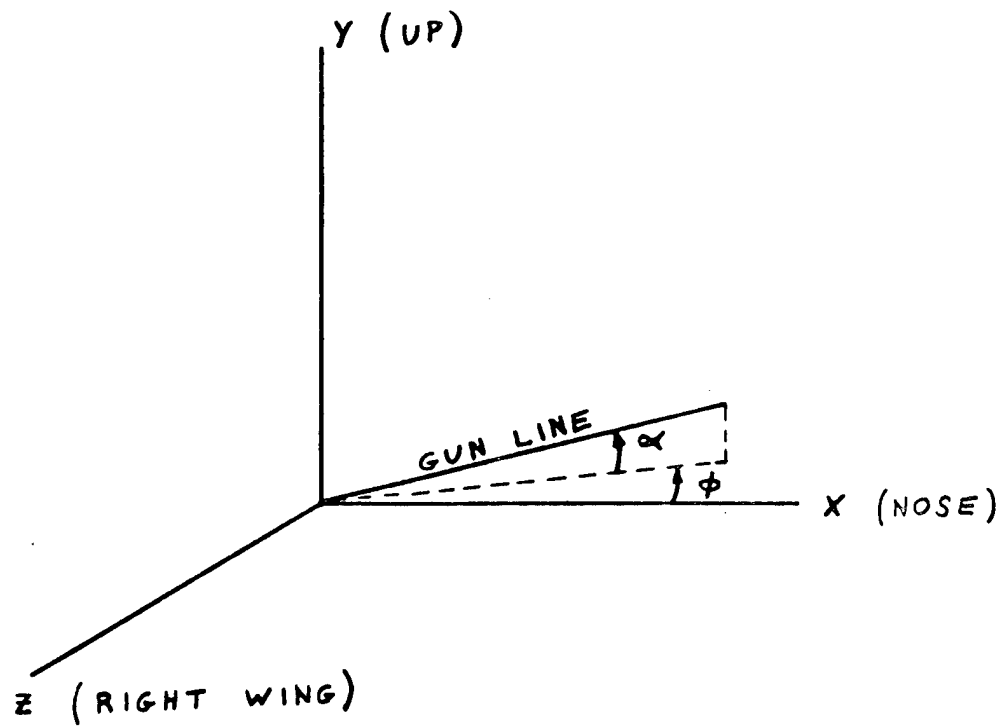


FIGURE 8: GUN LINE COORDINATE SYSTEM



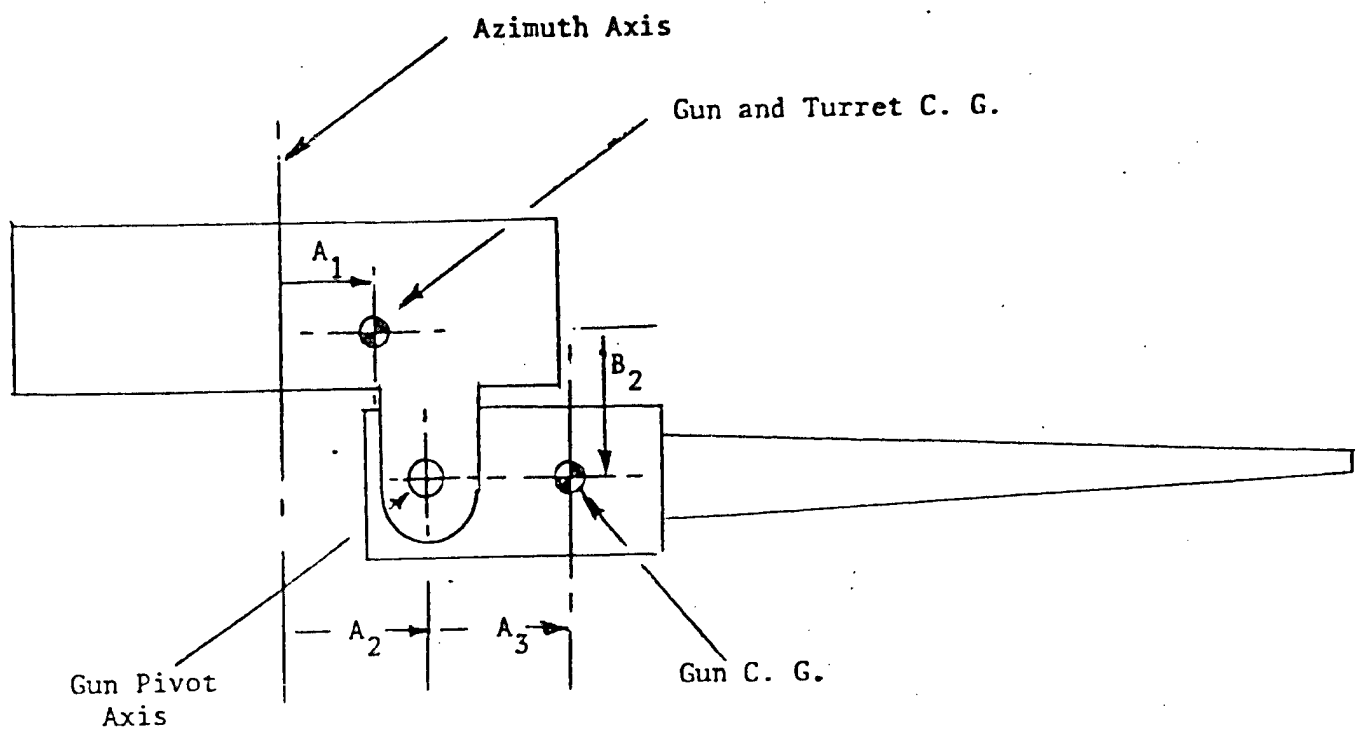


Figure 9. Turret and Gun Pivot and Center of Gravity Distance Parameters

FIGURE 10: F -- RECOIL FORCE

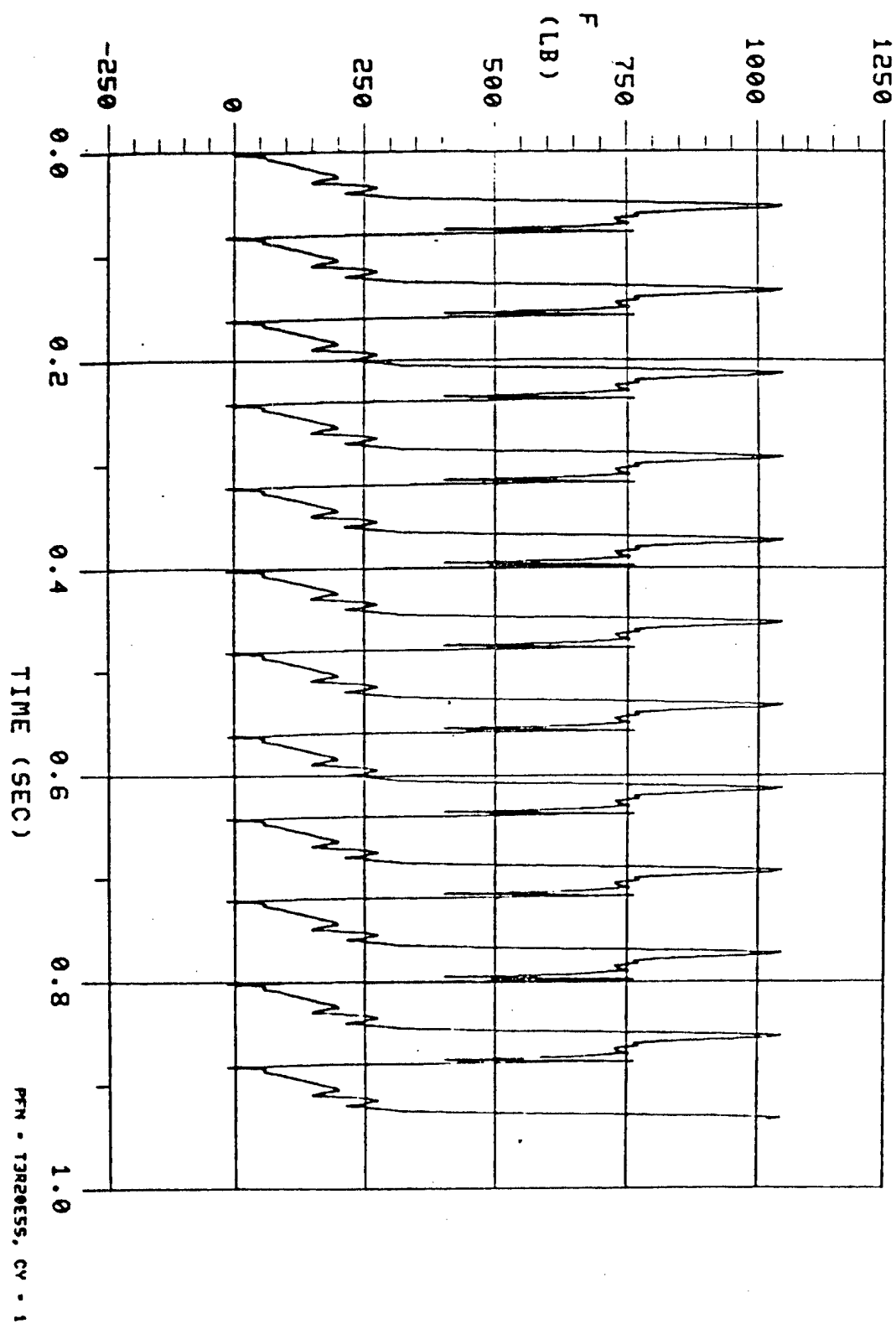
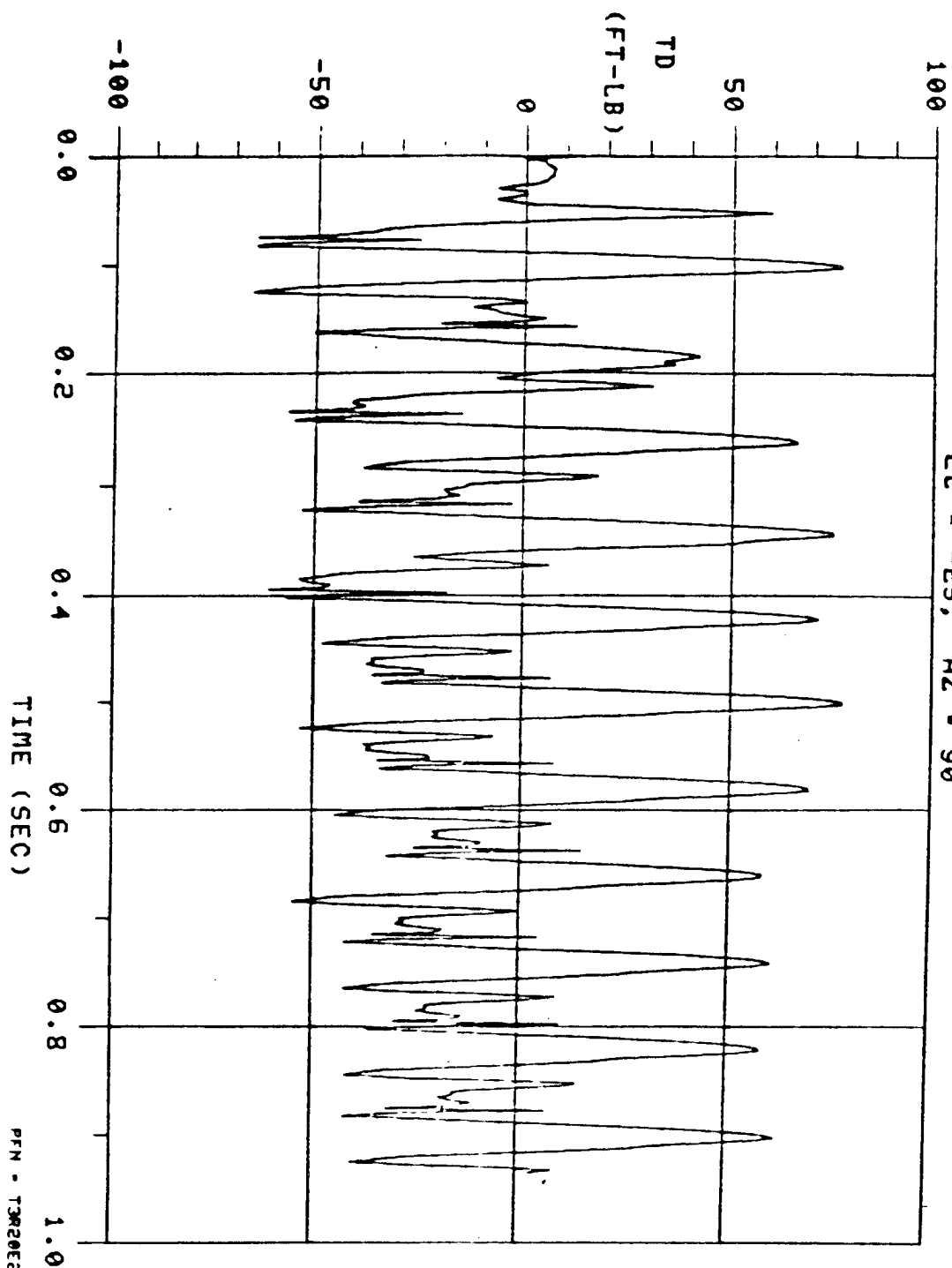


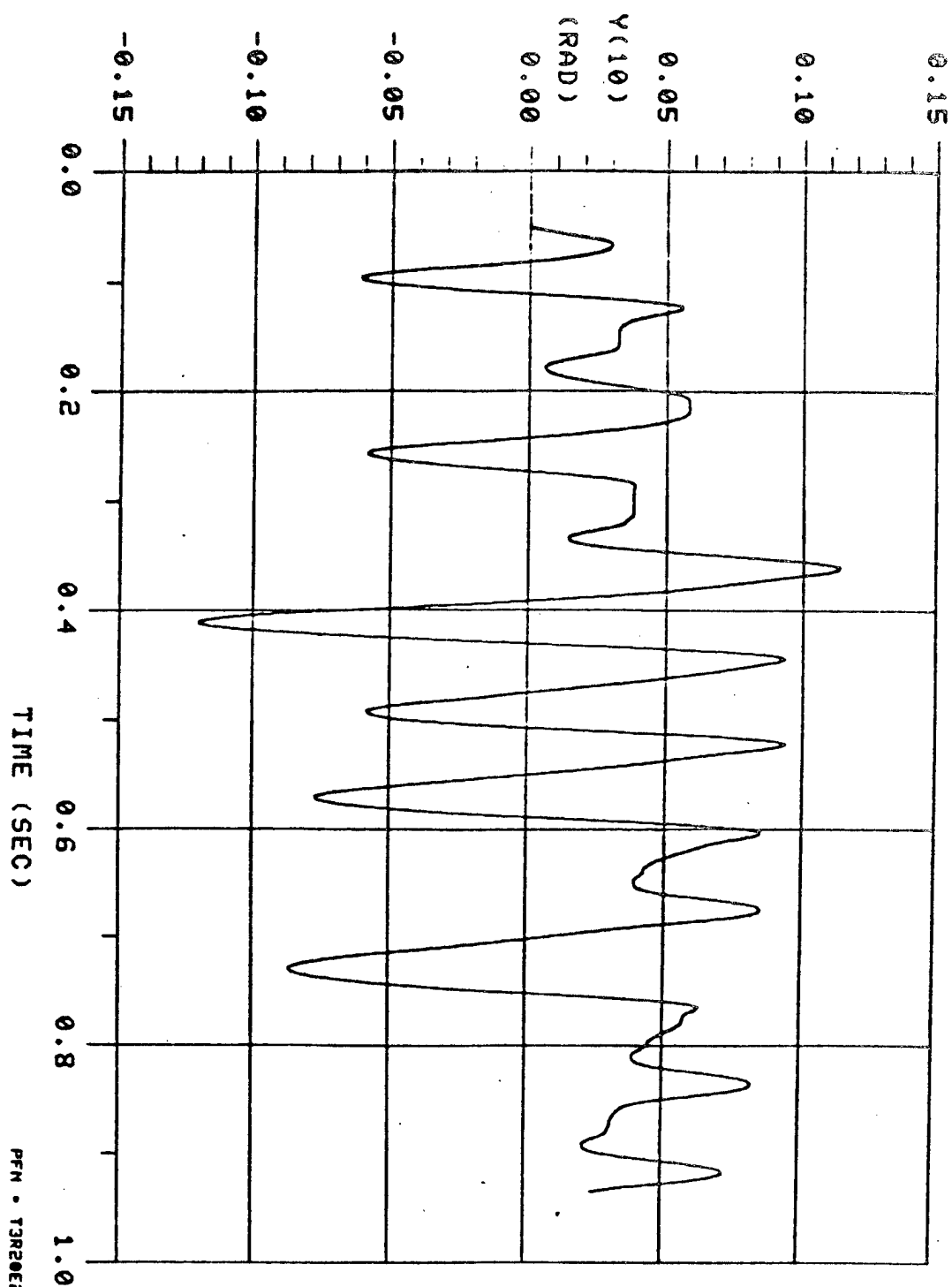
FIGURE 11: TD -- TORQUE DISTURBANCE
EL - -25, AZ - 90



PFN - T3R20E255, CV - 3

X10⁻²

FIGURE 12: $\gamma(10)$ -- TURRET POSITION



PFM • T3R20E55, CV • 3

FIGURE 13: F -- RECOIL FORCE

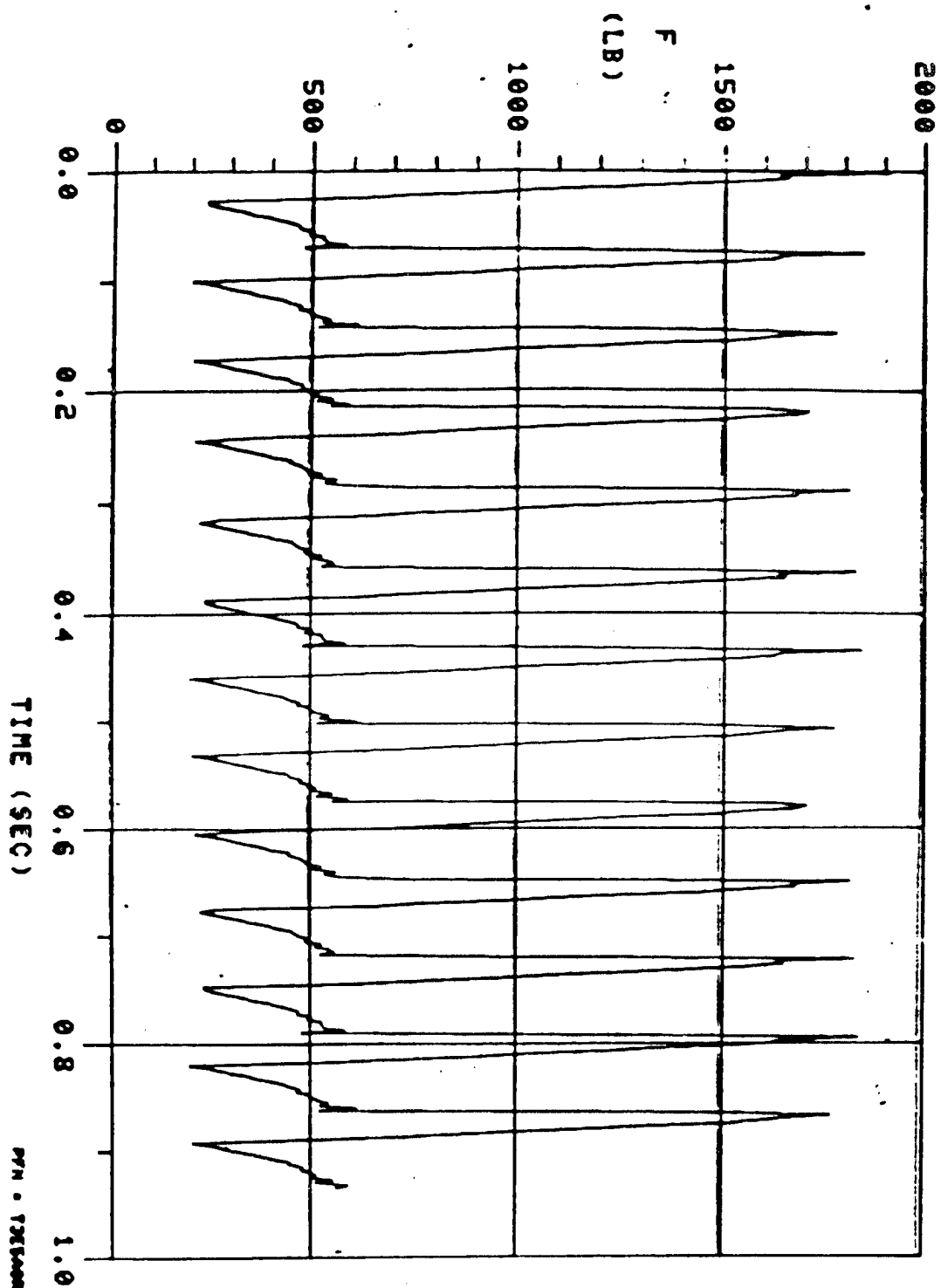
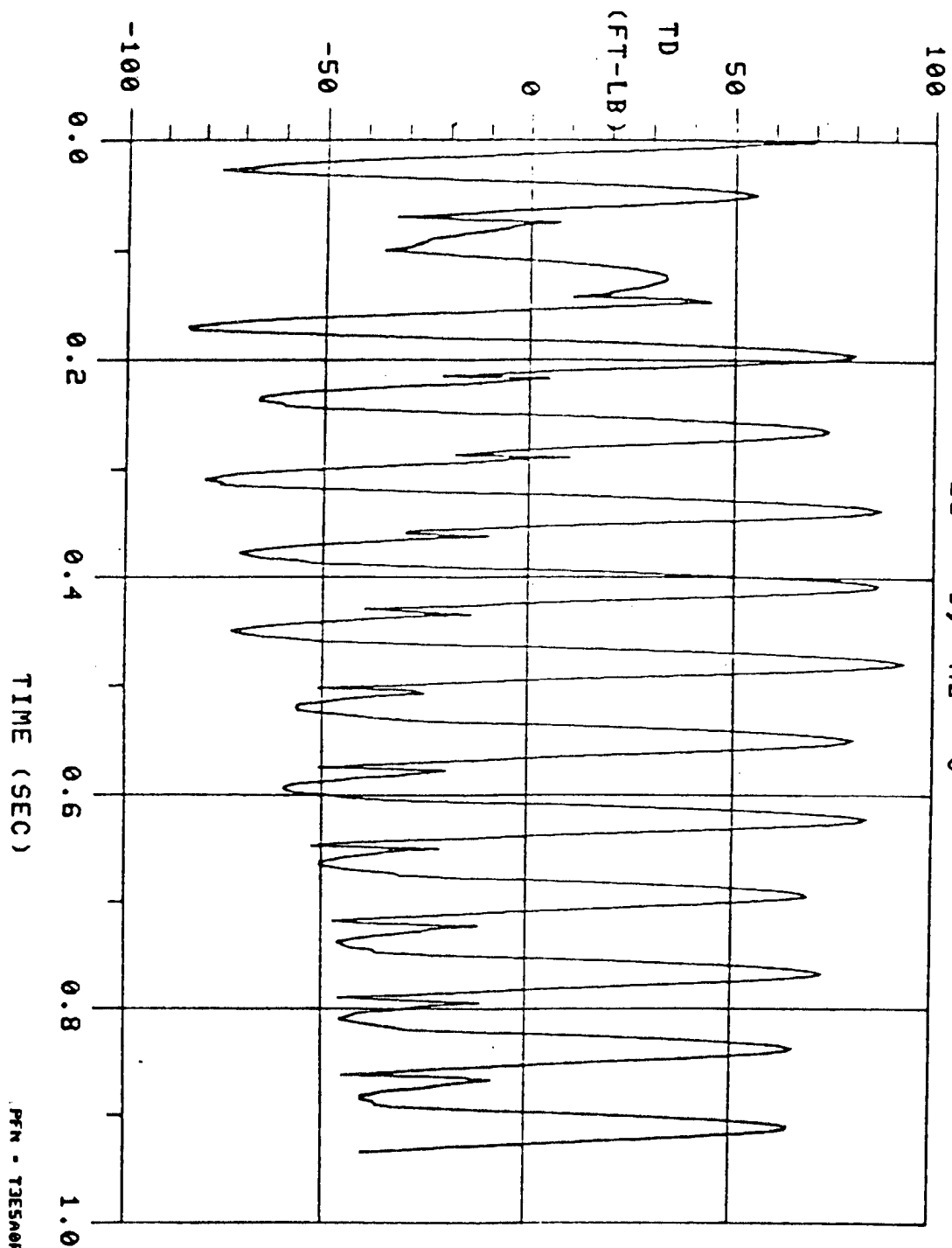


FIGURE 14: TD -- TORQUE DISTURBANCE
EL - -5, A2 - 0



PTN - T3E5A0R30, CY - 1

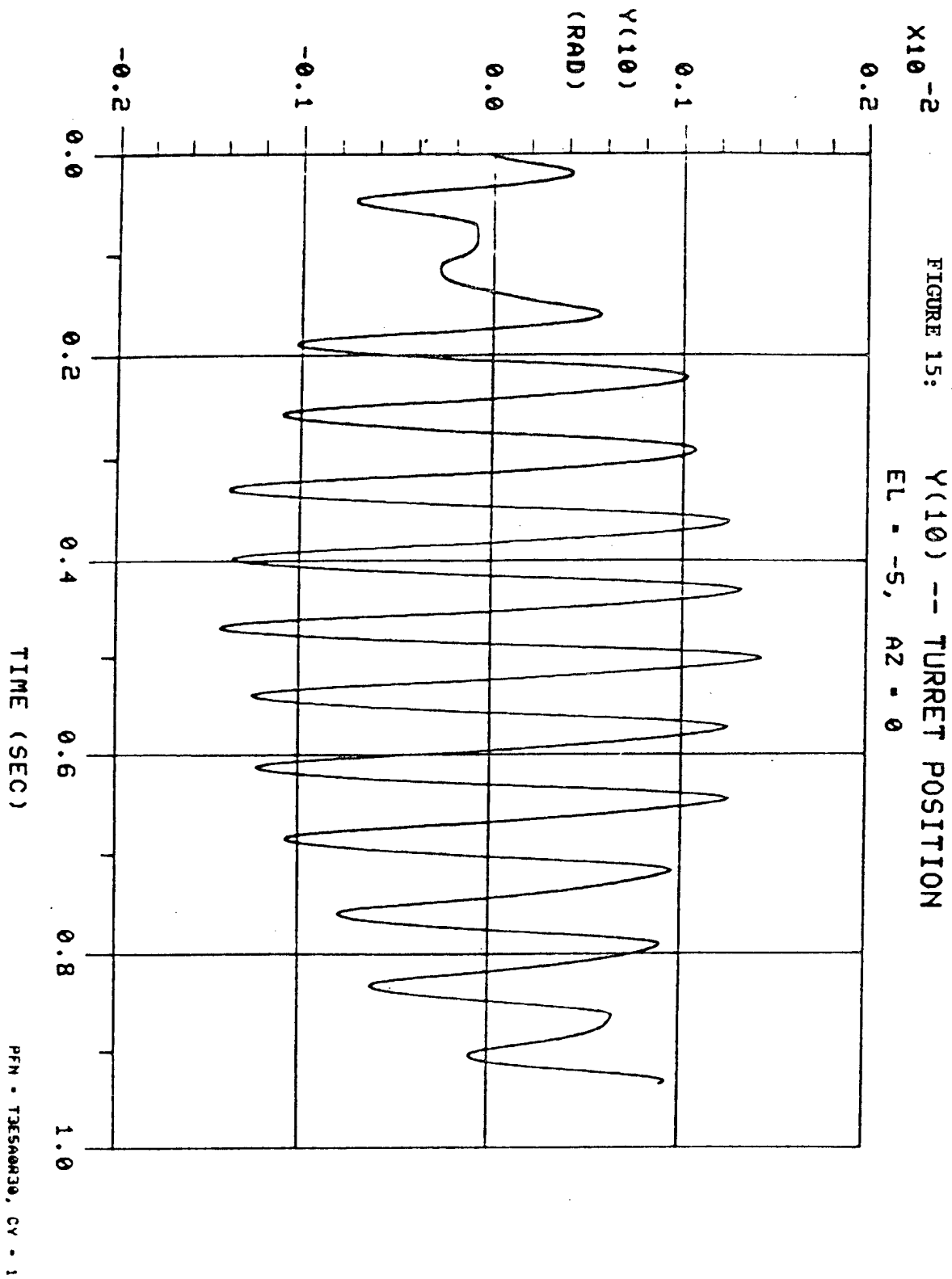


TABLE I

UNIVERSAL TURRET ANALYSIS

RESPONSE TO A STEP COMMAND

	STEP COMMAND (RAD)	% OVERSHOOT	STEADY STATE ERROR (MRAD)	TIME TO ERR < 2 MR (SEC)	MAX. SLEW RATE (DEG/SEC)
ELEVATION	0.005	32.2	0.40	0.10	3.44
	0.010	44.85	0.26	0.39	5.82
	0.020	37.53	0.14	0.40	13.05
	0.200	31.49	-0.23	0.52	71.33
AZIMUTH	0.005	23.72	0.35	0.10	4.44
	0.010	50.36	0.28	0.39	7.77
	0.020	45.79	0.03	0.39	15.20
	0.200	48.57	0.05	0.72	90.97

TABLE II

UNIVERSAL TURRET ANALYSIS RESPONSE TO A SLEW COMMAND

MOTION	COMMAND RATE (DEG/SEC)	RATE AT $T=1.0$ SEC (DEG/SEC)	TIME TO $ ERROR < 2$ MR (SEC)	STEADY STATE ERROR (MRAD)	PEAK SLEW RATE (DEG/SEC)	TIME TO PEAK RATE (SEC)	MAX. TRACK ERROR (DEG)
ELEVATION	5	5.00	0.29	0.12	7.09	0.17	0.41
	50	50.00	0.43	0.18	65.44	0.21	3.29
	60	60.15	0.69	0.47	72.75	0.45	3.96
	70	72.77	-	-	72.77	0.65	5.03
	85	72.77	-	-	72.77	0.64	17.39
AZIMUTH	5	5.00	0.28	0.16	7.45	0.14	0.49
	50	49.96	0.60	0.22	66.90	0.20	3.40
	60	59.95	0.59	0.26	80.16	0.20	4.06
	70	69.96	0.41	0.33	93.18	0.34	4.87
	85	92.99	-	-	94.34	0.82	6.64

TABLE III: AH-1S NASTRAN MODE

SHAPE DATA

<u>No.</u>	<u>Frequency (Hz)</u>	<u>Mode</u>
1	2.986	Main Rotor Pylon Pitch
2	3.613	Main Rotor Pylon Roll
3	6.546	First Fuselage Lateral Bending
4	7.588	First Fuselage Vertical Bending
5	13.69	Second Fuselage Lateral Bending
6	14.68	Skid Gear
7	14.98	Second Fuselage Vertical Bending
8	15.95	Fuselage Torsion/Engine Roll
9	18.71	Skid Gear
10	19.69	Third Fuselage Lateral Bending/Torsi
11	19.34	Skid Gear
12	20.57	Third Fuselage Vertical Bending

TABLE IV

GE UNIVERSAL TURRET ANALYSIS
DYNAMIC RESPONSE TO THE 20mm XM197

WEAPON -- STATISTICAL ERRORS

ELEVATION MOTION

ELEV (DEG)	AZIM (DEG)	\bar{Y}_{10} (MRAD)	$\sigma_{Y_{10}}$ (MRAD)	$\bar{\Theta}_B$ (MRAD)	σ_{Θ_B} (MRAD)	$\bar{\Theta}_T$ (MRAD)	σ_{Θ_T} (MRAD)	PEAK $ Y_{10} $ (MRAD)
-5	0	0.20	0.23	-0.04	0.12	0.17	0.29	0.52
	45	0.20	0.30	-0.30	0.38	-0.32	0.35	0.85
	90	0.08	0.29	-1.07	0.69	-0.99	0.73	0.95
-25	0	0	0	0.07	0.08	0.07	0.08	0
	45	0.20	0.26	-0.38	0.31	-0.18	0.29	0.82
	90	0.21	0.47	-0.84	0.62	-0.63	0.79	1.20
-45	0	0	0	0.17	0.10	0.17	0.10	0
	45	0.21	0.21	-0.20	0.22	0.01	0.24	0.66
	90	0.21	0.42	-0.61	0.46	-0.39	0.66	1.16
0	0	0.20	0.21	-0.07	0.13	0.13	0.27	0.57

 Y_{10} = TURRET POSITION Θ_B = HELICOPTER-TURRET PLATFORM POSITION Θ_T = GUN LINE POSITION

NO SIGNIFICANT ERROR IN AZIMUTH MOTION

TABLE V

GE UNIVERSAL TURRET ANALYSIS
DYNAMIC RESPONSE TO THE 30mm ADEN/DEFA

WEAPON -- STATISTICAL ERRORS

ELEVATION MOTION

ELEV (DEG)	AZIM (DEG)	\bar{Y}_{10} (MRAD)	$\sigma_{Y_{10}}$ (MRAD)	$\bar{\Theta}_B$ (MRAD)	σ_{Θ_B} (MRAD)	$\bar{\Theta}_T$ (MRAD)	σ_{Θ_T} (MRAD)	PEAK $ Y_{10} $ (MRAD)
-5	0	0.05	0.72	-0.07	0.27	-0.02	0.77	1.43
	30	0	0.95	-0.58	0.45	-0.58	1.06	1.83
	60	0.01	1.03	-1.50	0.85	-1.50	1.33	1.78
	90	0	1.16	-1.94	1.06	-1.94	1.60	1.89
-25	0	0.23	0.22	0.13	0.15	0.35	0.32	0.74
	30	0.18	0.38	-0.34	0.29	-0.16	0.50	0.86
	60	-0.07	0.82	-1.20	0.69	-1.28	1.05	1.50
	90	0	1.26	-1.67	0.92	-1.67	1.61	2.26
-45	0	0.22	0.23	0.31	0.15	0.53	0.29	0.46
	30	0.17	0.16	-0.06	0.15	0.11	0.27	0.70
	60	-0.06	0.74	-0.76	0.47	-0.82	0.89	1.42
	90	-0.02	1.25	-1.20	0.68	-1.22	1.42	2.30

 Y_{10} = TURRET POSITION Θ_B = HELICOPTER-TURRET PLATFORM POSITION Θ_T = GUN LINE POSITION

STATISTICAL ERRORS FOR THE AZIMUTH MOTION ARE

LESS THAN 0.25 MRAD (1σ)

References

1. Development Specifications--Universal Turret Subsystem, BHT Report No. 209-947-281, July 1976.
2. A NASTRAN Vibration Model of the AH-1G Helicopter Airframe, Vol. I, BHT Final Report, June 1974, AD A 009482.
3. AH-1S/Universal Turret Simulated Recoil Force Test, Vols I and II, BHT Report 209-909-001, Jan 1978.

DISTRIBUTION LIST

<u>NO. OF COPIES</u>	<u>ORGANIZATION</u>
12	Commander Defense Technical Information Center ATTN: TCA Cameron Station Alexandria, VA 22314
1	Commander US Army Materiel Development & Readiness Command ATTN: DRCCP DRCPA-S DRCDE-R DRCDE-D DRCBSI-L DRCBSI-D 5001 Eisenhower Avenue Alexandria, VA 22333
2	Commander US Army Armament Research & Development Command ATTN: DRDAR-SEA Technical Library
1	ATTN: DRDAR-SCF-DD (W. J. Dzwiak)
1	DRDAR-SCF-CC (Doo J. Lee)
1	DRDAR-SCF-CC (J. Schmitz)
1	DRDAR-SEA (Richard Moore)
1	DRDAR-SCF-C (Dr. Norman Coleman)
1	DRDAR-SCS-M (Dr. T. Hutchings)
1	DRDAR-SCF-C (Mr. Pak T. Yip)
	Dover, NJ 07801
1	Commander Rock Island Arsenal ATTN: Tech Lib Rock Island, IL 61299
1	Commander Harry Diamond Laboratories ATTN: DELHD-SAB 2800 Powder Mill Road Adelphi, MD 20783
1	Commander US Army Test & Evaluation Command ATTN: STEDP-MT-L Dugway Proving Ground, UT 84222
1	Commander US Army Aviation R&D Command ATTN: DRDAV-BC PO Box 209 St Louis, MO 63166

NO. OF
COPIES

ORGANIZATION

1	Commander US Army Concepts Analysis Agency 8120 Woodmont Avenue Bethesda, MD 20014
1	Commander David W. Taylor Ship R&D Center ATTN: Code 1576 (Mr. William E. Smith)
1	Code 1576 (Mr. T. L. Moran) Bethesda, MD 20084
1	Reliability Analysis Center ATTN: Mr. I. L. Krulac Griffiss AFB, NY 13441
1	Commander Applied Technology Laboratory US Army Research & Technology Laboratories ATTN: DAVDL-ATL-ATA (Dr. C. E. Hammond) Ft Eustis, VA 23604
1	Commander US Air Force Armament Laboratory (AFSC) ATTN: DLM (1LT McClendon) Eglin Air Force Base, Florida 32542
1	Commander US Air Force Wright Aeronautical Laboratories (AFSC) ATTN: FIGC (Dr. David K. Bowser) Wright-Patterson AFB, Ohio 45433
1	Commander US Naval Surface Weapons Center ATTN: Code F14 (Kenneth J. Hintz) Code F14 (Richard A. Holden) Dahlgren, VA 22448
1	Commander US Naval Research Laboratory ATTN: Code 7931 (Dr. Warren William) Washington, DC 20375
1	Commander US Naval Weapons Center ATTN: Code 3911 (Dr. Robert D. Smith) China Lake, CA 93555
1	President USAARENBD ATTN: ATZK-AE-CV (Mr. William West) Ft Knox, KY 42101
1	General Electric Company Ordnance Engineering ATTN: Paul Cushman 100 Plastics Ave Pittsfield, MASS 01201

NO. OF
COPIES

ORGANIZATION

1	Commander US Army Electronics R&D Command ATTN: DRDEL-SA Fort Monmouth, NJ 07703
1	Commander US Army Communications R&D Command ATTN: DRDCO-TCS-BS (Dr. Leon Kotin) Fort Monmouth, NJ 07703
1	Commander US Army Electronics R&D Command ATTN: DRDEL-AP-OA 2800 Powder Mill Road Adelphi, MD 20783
2	Director US Army TRADOC Systems Analysis Activity ATTN: ATAA-SL ATTA-T White Sands Missile Range, NM 88002
1	Commander US Army Missile Command ATTN: DRSMI-C (R&D)
1	DRSMI-RGN (Dr. H. L. Pastrick)
1	DRSMI-RGN (Dr. William C. Kelly)
1	Redstone Arsenal, AL 35809
1	Commander US Army Troop Support & Aviation Materiel Readiness Command ATTN: DRSTS-BA 4300 Goodfellow Blvd St Louis, MO 63120
1	Commander US Army Tank-Automotive Research & Development Command
1	ATTN: DRDTA-UL (Tech Lib)
1	DRDTA-V
1	DRDTA-ZSA (Dr. Ronald R. Beck)
1	DRDTA-RCKS (Dr. Richard Lee)
1	Commander US Army Mobility Equipment R&D Command ATTN: DRDME-O Fort Belvoir, VA 22060
1	Commander US Army Natick R&D Command ATTN: DRDNA-O Natick, MA 01760
2	Chief Defense Logistics Studies Information Exchange US Army Logistics Management Center ATTN: DRXMC-D Fort Lee, VA 23801

NO. OF
COPIES

ORGANIZATION

1	Commander US Army Tank-Automotive Research & Development Command ATTN: DRDTA-RCKS (1LT Dana S. Charles) (Johnthan F. Kring)
1	Warren, MI 48090
1	Commander US Naval Weapons Center ATTN: Code 3911 (T. L. Moran) China Lake, CA 93555
1	Commander US Army Armament Research & Development Command ATTN: Stanley A. Goodman Dover, NJ 07801
1	Commander US Air Force Armament Laboratory (AFSC) ATTN: DLM (1 LT P. L. Vergez) Eglin Air Force Base, Florida 32542
1	Commander US Army Missile Command ATTN: DRSMI-RGN (D. W. Sutherlin) Redstone Arsenal, AL 35809
	<u>Aberdeen Proving Ground</u>
2	Cdr, USATECOM ATTN: DRSTE DRSTE-CS-A Bldg 314
1	Dir, BRL, Bldg 328
1	Dir, BRL ATTN: DRDAR-TSB-S (SINTFO BRANCH) Bldg 305 Dir, HEL ATTN: Monica Glumm
1	Dir, HEL, Bldg 420 ATTN: DRXHE-AM (Seymour Steinberg)
1	Cdr, USATECOM ATTN: Huber Cole Bldg 314
1	Dir, USAMSAA Bldg 392
1	Dir, USAMSAA ATTN: DRXSY-MP (Herbert E. Cohen)
1	DRXSY-A (D. Nuzman)
1	DRXSY-F (Harry Harris)
1	DRXSY-G (Bob Conroy)
1	DRXSY-A (Larry Cohen)
1	DRXSY-A (Gary Drake)
1	DRXSY-A (John Meredith)
1	DRXSY-A (Joseph Wald)
1	DRXSY-CS (Toney R. Perkins)
1	DRXSY-CS (Partick E. Cororan)
1	DRXSY-G (John Groff)
1	DRXSY-C (Keith A. Myers)

NO. OF
COPIES

ORGANIZATION

UNCLASSIFIED PORTION ONLY

1	Dr. N. Loh School of Engineering Oakland University Rochester, MI 48063
1	Dr. James F. Leathrum Dept of Electrical & Computer Engineering Clemson University Clemson, SC 29631
1	Dr. Max Mintz Dept of Systems Engineering University of Pennsylvania Philadelphia, Pa 19104
1	Mr. E. B. Pate Dept of Systems Engineering University of Pennsylvania Philadelphia, PA 19104
1	Mr. D. H. Chyung Division of Information Engineering University of Iowa Iowa City, Iowa 52242
1	Professor Naim A. Kheir University of Alabama Huntsville, AL 35899